Investigations of Suction Caissons in Dense Sand

by

Byron Walter Byrne

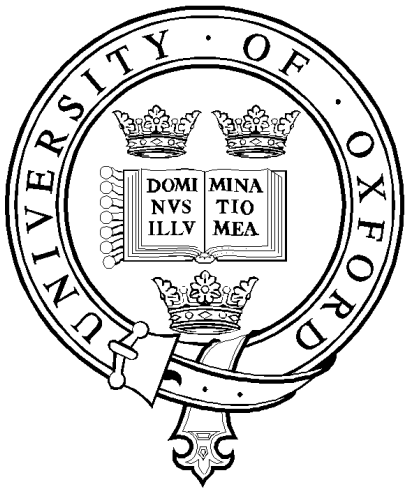

A thesis submitted for the degree of
Doctor of Philosophy
at the University of Oxford

Magdalen College
Trinity Term 2000

Abstract

INVESTIGATIONS OF SUCTION CAISSONS IN DENSE SAND

A thesis submitted for the degree of Doctor of Philosophy

Byron Walter Byrne
Magdalen College, Oxford
Trinity Term 2000

Offshore structures are used in a variety of applications ranging from the traditional oil and gas extraction facilities to emerging renewable energy concepts. These structures must be secured to the seabed in an efficient and cost effective manner. A novel approach is to use shallow inverted buckets as foundations, installed by suction, in place of the more usual piles. These foundations lead to cost savings through reduction in materials and in time required for installation. It is necessary to determine how these foundations perform under typical offshore loading conditions so that design calculations may be developed. This thesis presents experimental data from a comprehensive series of investigations aimed at determining the important mechanisms to consider in the design of these shallow foundations for dense sand.

Initially the long term loading behaviour (e.g. wind and current) was investigated by conducting three degree of freedom loading $\{V{:}M/2R{:}H\}$ tests on a foundation embedded in dry sand. The results were interpreted through existing work-hardening plasticity theories. The analysis of the data has suggested a number of improved modelling features. Cyclic and transient tests, representing wave loading, were carried out on a foundation embedded in an oil saturated sand. The novel feature of the cyclic loading was that a 'pseudo-random' load history (based on the 'NewWave' theory) was used to represent realistic loading paths. Of particular interest was the tensile load capacity of the foundation. The results observed suggested that for tensile loading serviceability requirements rather than capacity may govern design. Under combined-load cyclic conditions the results indicated that conventional plasticity theory would not provide a sufficient description of response. A new theory, termed 'continuous hyperplasticity' was used, reproducing the results with impressive accuracy. Surprisingly, under the conditions investigated, loading rate was found to have a negligible effect on response.

Acknowledgements

A piece of research is only possible with the support of many people whom it is appropriate to acknowledge and thank.

The research presented in this thesis would not have been possible without the stimulating supervision, wonderful insight and constructive advice, offered by Professor Guy Houlsby. He possesses an outstanding ability of redefining intractable problems into manageable ones. Most importantly he has fostered a very friendly and relaxed atmosphere within the Civil Engineering research group. The support staff, Nicola, Bob and Clive, whilst helping when needed, have also ensured that my time in the laboratory has been very enjoyable. During an early stage of the research important funding, for equipment and technician time, was obtained from the Engineering and Physical Sciences Research Council (grant number GR/L/67547). I would also like to acknowledge Rob Ellis and Bobby Bazalgette from Offshore Data Limited who allowed access to their field trials. It is appropriate to also thank Tor-Inge Tjelta of Statoil who has allowed the use of data from the Statoil sponsored tests performed at Oxford University for the Sleipner T project.

I would not have come to Oxford if it had not been for the support of the Rhodes Trust. The experience has been a thoroughly enjoyable one and to be recommended to anyone lucky enough to have such an opportunity. I am also very grateful to the Royal Commission for the Exhibition of 1851 and Magdalen College for providing me with the opportunity for further post-doctoral research at Oxford University.

Over the course of my doctorate I have made many friends throughout the University and in particular in Holywell Manor and of course engineering. Andrew Fry has always been quick to engage in argument (or philosophical discussion?) on many issues, always important at the time, including research, education, sport and quick-rich internet schemes. One of our most favourite past-times, along with Mark Cassidy, has been discovering the finer eating establishments around Oxford. Irrefutable evidence collected over many years leads to the luncheon DimSum at the Liaison Restaurant.

Cricket has always offered me a convenient excuse to be out of the laboratory for a day, or three. I have always enjoyed the experience of playing fixtures at The Parks and Lord's for Oxford or for Sir Paul Getty at the Wormsley ground. These are memories which will be everlasting, and the experiences were very therapeutic at the time. As was travelling down to London on the odd occasion to visit friends and family. It always surprised me how many of my UWA friends were there to help me relax, particularly Andrew Hinchliff and Ben McInnes – there was never a shortage of a spare bed and fully stocked fridge.

Finally I would like to thank my parents, family and friends for supporting me throughout my time in the United Kingdom.

Table of Contents

Notation

Soil parameters

f	Friction angle of sand (degrees)
d	Interface friction angle (degrees)
K_a	Active earth pressure coefficient
K_p	Passive earth pressure coefficient
K	Earth pressure coefficient (K_p-K_a)
m	Sliding friction coefficient
g	Unit weight of soil (F/L^3)
g'	Effective unit weight of soil (F/L^3)
g_w	Unit weight of water (F/L^3)
c	Cohesion of soil (F/L^2)
q	Overburden pressure (F/L^2)
q_c	Cone pressure (F/L^2)
R_D	Relative density
G	Shear modulus of soil (F/L^2)
c_v	Coefficient of consolidation (L^2/T)
t_{50}	Time for 50% consolidation (T)

Bearing capacity parameters

N_g	Bearing capacity factor self weight
N_g^*	Bearing capacity factor self weight (circular footing)
N_q	Bearing capacity factor overburden
N_q^*	Bearing capacity factor overburden (circular footing)
N_c	Bearing capacity factor cohesion

Footing parameters

A	Area of footing (L^2)
B	Strip footing width (L)
e	Eccentricity of moment load (L) ($=M/V$)
R	Radius of footing (L)
D	Diameter of footing (L)
h	Current embedded depth of caisson skirt (L)
t	Wall thickness of caisson skirt (L)
L	Total depth of caisson skirt (L)
y	Embedment ratio ($=L/D$)
l	Rotation point (L)
x	Non-dimensional transition depth (L)

Load parameters

V	Vertical load (F)
V'	Effective vertical load (F)
H	Horizontal load (F)
H_{peak}	Peak horizontal load during swipe (F)
M	Moment load (FL)
V_{peak}	Peak vertical bearing capacity (F)
$V_{peak(skirted)}$	Peak bearing capacity for a skirted footing (F)
V_o	Maximum previous vertical load (F)
V_{oN}	New V_o during swipe test (F)
V_{oI}	V_o before swipe test (F)
i_g	Inclination factor for horizontal and vertical loads
W	Load inclination angle (degrees)
s	Stress (F/L^2)
s'	Effective stress (F/L^2)
u_w	Water pressure (F/L^2)

Displacement parameters

w	Vertical displacement (L)
q	Rotation (degrees)
u	Horizontal displacement (L)
k	Stiffness (F/L)
v_n	Non-dimensional footing velocity
v	Footing velocity (L/T)

Installation parameters

u_o	Suction pressure for installation (F/L^2)
a	Variation of suction pressure with installation depth
f	Cavitation factor
p_a	Atmospheric pressure (F/L^2)
d	Water depth (L)

PID control parameters

u	Control signal (Volt)
e	Error between set point and actual signal (Volt)
k	Gain
T_d	Derivative time
T_i	Integral time

Wave mechanics parameters

$S_{nn}(f)$	Wave energy power spectrum (L^2/T)
H_s	Significant wave height (L)
T_z	Zero crossing period (T)
f	Frequency ($1/T$)
A	Spectral density parameters
B	Spectral density parameters
H_{max}	Maximum wave height (L)
T_{zv}	Zero crossing period for vertical loading (T)
V_s	Significant vertical load (F)

Plasticity modelling parameters

h_o	Horizontal dimension of yield surface
m_o	Moment dimension of yield surface
a	Parameter controlling ellipse of yield surface
b_1	Parameter controlling shape of yield surface at low stress

b_2	Parameter controlling shape of yield surface at high stress
q	Normalised deviatoric loads
m_n	Normalised moment load
h_n	Normalised horizontal load
h_{opeak}	Horizontal dimension of yield surface at peak bearing capacity
m_{opeak}	Moment dimension of yield surface at peak bearing capacity
C_1	Hardening law parameter
C_2	Hardening law parameter
k_v	Elastic vertical stiffness coefficient
k_m	Elastic moment stiffness coefficient
k_h	Elastic horizontal stiffness coefficient

Scaling parameters

N	Geometric scaling factor
d	Small displacements (L^*)
V_m	Mean vertical load (F)
V_p	Peak vertical load (F)
n	Number of dimensional parameters
k	Number of fundamental dimensions
V_{norm}	Normalised vertical load
d_{norm}	Normalised displacements

Hyperplasticity modelling

c_{ult}, c	Ultimate load in hyperbolic relationship (F)
s	Shaping factor in hyperbolic relationship
M_{ult}	Ultimate moment load at constant vertical load ($=2Rm_oV_m$) (F)
H_{ult}	Ultimate horizontal load at constant vertical load ($=h_oV_m$) (F)
P	Load (F)
k	Initial stiffness (F/L)
k_1	Secondary stiffness (F/L)
a	Plastic displacement (L)
g	Gibbs free energy function (FL)
d	Dissipation function (FL)
$\overline{c}$	Generalised load (F)
χ	Generalised dissipative load (F)
l	Non-negative multiplier which determines the magnitudes of the plastic displacements (L/F)
h	Number of yield surfaces

Subscripts

e	Elastic component
p	Plastic component

CHAPTER ONE
FOUNDATIONS FOR OFFSHORE STRUCTURES

1.1 INTRODUCTION

The research presented in this thesis is focussed on the development of novel foundation systems for offshore structures, which may typically be used for oil and gas extraction. The foundation provides the direct connection with the sea floor, transferring any forces applied to it, from the structure, to the surrounding soil. Clearer understanding of these mechanisms of load transfer, from foundation to the soil, will lead to increased confidence in the overall design. It is critical that the foundation can sustain all loads that may be applied, particularly during extreme environmental conditions, as loss of life and financial investment may result.

Shallow foundation systems are becoming increasingly viable options, particularly in the development of marginal offshore oil-fields, and, for structures in the emerging offshore renewable energy sector. Whilst pile design procedures evolved smoothly from onshore experience and theory, design guidelines for shallow systems have had to be re-examined in light of the intense offshore loading conditions. To develop these design guidelines it is necessary to conduct laboratory experiments so that critical mechanisms may be defined and explored. This thesis discusses and analyses experiments undertaken to examine the various aspects of behaviour of shallow foundations installed in sand.

This chapter examines the use and design of shallow foundations for offshore structures, from traditional theories to the current state-of-the-art. The chapter details trials and projects, which have used the novel suction installed skirted foundations, and highlights perceived problematic areas. Calculations that can be readily made for the foundation performance in sand are then presented. The chapter concludes by giving an overview of the thesis work and highlights a potential application for novel shallow foundations once a design framework is fully functional.

1.2 OFFSHORE STRUCTURES

The natural energy resources of the Earth (for example fossil fuels and renewables) are often located offshore, and most likely in remote harsh environments. Structures are required to be placed in these environments so that the resources may be extracted. These structures are often subjected to very extreme loads from a variety of sources including hurricanes, tornadoes, large winds, large waves, high currents and perhaps ice flow. The

ever increasing social need to extract these vital energy resources, in these harsh environments, has led to the development of large structures, which are often located in deep water. The price of oil over the past few years has been steadily decreasing, which has driven the need for increasingly more economical structures. During periods of comparatively high oil prices, companies could afford higher conservatism, however the recent climate of low oil prices has led to the development of improved design procedures for existing technologies, as well as new and novel design solutions.

A typical fixed offshore facility consists of a four legged, steel lattice, structure resting on foundations at the corners, as shown in Figure 1.1. The loads applied to the structure, from the environmental conditions, are transferred to the foundations, and thus must be resisted by the interaction between the foundation and surrounding soil. More recently floating facilities have become more preferable, as oil companies move extraction into deeper and deeper water. As well subsea production is becoming more commonplace where there maybe several subsea wells connected back to one centralised production facility.

1.2.1 Deep Foundations

Historically, these offshore structures (such as in Figure 1.1) have been anchored to the sea floor by large diameter piles, which maybe up to 2.5m diameter and 150m long. The piles are arranged in groups at each corner of the base of the structure. The piles are installed with the use of large hammers (shown in Figure 1.2), and may take several weeks to install, depending on a number of factors which include the weather, and size of the structure. There are many variants including a drilled and grouted pile, in which a large diameter hole is drilled into the ground. The pile is then placed into the hole and grouted into position. For the more difficult seabed sediments a combination of the two methods could be used, such as the procedure developed for the Goodwyn A platform.

Pile design procedures for clay and sand are pretty well developed and verified - most of these procedures have been extrapolated from design guidelines developed for onshore use. The load-bearing for the pile comes from friction on the outside of the shaft and bearing over the base of the pile. Usually, for very long piles, the resistance is derived primarily from the shaft friction. Piles are still the most commonly used foundation, due to expanse of knowledge that exists about their performance, under various loading regimes, in many different soils. They can be used for most applications, however, their use in deep water maybe restricted, unless there is an increase in the technological development of underwater pile-driving hammers, and associated paraphernalia.

1.2.2 Shallow Foundations

More recently shallow foundation options have become viable and preferable. A shallow foundation bears on the upper sediments, with resistance derived principally from the bearing of the base area on the seabed material. Shallow foundations are typically circular and may have diameters as small as 10m (for mobile drilling units or jack-ups) or over 100m in the case of gravity base structures. Calculations can be performed as to the maximum permissible vertical pressure that can be carried by these foundations. If a moment load and/or horizontal load is also applied to the foundation, along with the vertical load, the maximum bearing pressure is reduced. These extra loads are referred to as combined or deviatoric loads. It is usual practice, particularly for the spudcan footings of jack-ups, to preload the foundation to twice the working vertical load, so that the foundation may safely carry these combined loads. The gravity base concept is where the worst loadings are resisted by a large mass spread over a very large shallow foundation system. Complex calculation procedures have been developed to determine the safety factors of applied loads, however most of these use two-dimensional limit equilibrium approaches. Leading the development of these solutions has been the Norwegian Geotechnical Institute, who have, over the past thirty years, been involved with many shallow foundation design projects around the world. This thesis is concerned only with the response of shallow foundations, as this is an area of offshore foundations where a substantial contribution to the knowledge base can be made. Shallow foundations may be used on sand or clay soils, however, different response modes are evident, dependent on the rates of loading and size of foundation.

1.2.2.1 Shallow Foundations on Clay

The response of shallow foundations on clay during typical loading conditions is often described as undrained. This is because the time over which the load increment is applied is very small when compared to the typical fluid drainage times within the clay macro-structure. The clay sample under load cannot undergo any volumetric change (most typically contractant) because there is insufficient movement of water. The entire load increment is taken by the pore water fluid, though as drainage, hence volume change, occurs, the load is transferred from the pore water to the soil skeleton - this process is referred to as consolidation. As it is not possible to determine the amount of stress being carried by the soil skeleton (effective stress) during a storm it is usual to carry out a total stress analysis of the foundation-soil combination. Over the depth of interest it is typical to assume an undrained shear strength profile, usually determined via numerous site-specific

laboratory and field experiments, in which zero volume change occurs. By making these assumptions it is then possible to take advantage of analytical and numerical techniques such as limit equilibrium and finite element analyses to determine the foundation stability.

1.2.2.2 Shallow Foundations on Sand

The response of foundations on sand is slightly different to that of clay, because the size of pores in the soil matrix are much larger, so that a much greater fluid flow for the same rates of loading occurs. This affects the response of the soil. At very slow rates of loading the response of the soil is drained. The load increment is applied to the soil so that fluid flows freely within the soil matrix, allowing volumetric change to occur, as the load is applied. The volumetric movement (expansion or contraction) depends on the initial density of the sand, however in typical offshore circumstances the sand is usually in a dense state, so that dilation occurs. The drained response of the soil is reasonably easy to estimate and it is typical to undertake an effective stress analysis. The strength of the soil is related to the peak angle of friction of the soil, as well as the effective stress on the soil element in question. Methods of calculation for these parameters are well established.

At very fast rates of loading the response of the soil is undrained, such as occurs during the typical loading of clay. The undrained strength of sand is particularly difficult to estimate as relatively little investigation of this response mode has been undertaken (although see McManus and Davies, 1997). When the sand is in a dense state the particle mass tries to dilate upon the application of the very fast shearing load. This dilation leads to the creation of suction within the pore matrix as the sand grains try to move apart, but are restricted under the constant volume condition. Large effective stresses result, and may typically increase until either the load increment drops off, or the sand element in question reaches a critical state. For very dense sand this can occur at very large mean effective stresses and so huge undrained strengths result. In reality the undrained strength of sand is probably limited by cavitation of the pore fluid. This is shown in Figure 1.3 where undrained triaxial tests on sand (McManus and Davies, 1997) show very high dilative strengths, limited by cavitation. At any rates between drained and undrained the response of the soil (called partially drained) is very difficult to estimate. This partially drained performance has had little exposure from experimental investigations and is the subject of chapters 4 and 5.

1.2.3 Definitions of Foundation Loading

Since this thesis is concerned with the response of foundations to a variety of loading conditions it is appropriate to provide definitions of these different loading types. These

definitions apply to the response of the soil and not to the response of any structural component.

a) Monotonic Loading : A monotonic load is a force or displacement path applied in a constant direction. It may be applied over a sufficiently long time period that there are no dynamic or transient effects (usually referred to as a static load) or it may be applied so that there are time dependent effects (occasionally referred to as a transient load).

b) Transient Loading : A transient load is one where there is a time dependent response associated with the loading. Transient loading is relevant to the case where the soil is saturated with a pore fluid, as the soil response will depend on the timescale of the loading, compared to the rate of fluid flow within the soil matrix. Transient effects may also be evident for loading of dry soils, particularly in the case of foundations subjected to blast forces (rocket launch pads for example). Transient loading may also be referred to as dynamic loading.

c) Cyclic Loading : Cyclic loads are those which involve reversals of load about a mean level and are periodic in nature. The nature of the amplitudes are such that they correspond to a specified probability distribution, and hence amplitude power spectrum. Examples of cyclic loads would be a constant amplitude sine wave, or a random amplitude loading path with periods (in this case) corresponding to the relevant time-scale for loading of offshore structures. Cyclic loading may also include repeated loading where exactly the same load or displacement path is applied to the foundation in a repetitive fashion. Cyclic loads may or may not be transient depending on the period (short or long) and nature of the soil (saturated or dry).

1.2.4 Current Understanding of Shallow Foundation Response to General Loading

A shallow foundation on the soil surface undergoes two different modes of response when it is loaded. There is the initial plastic behaviour during installation and initial loading. In this case there can be significant vertical deformation as the soil is compressed into a state where the structure and soil matrix is in static equilibrium. If the foundation is then unloaded to a state less than that initially applied the response of the foundation-soil system is much stiffer and said to be elastic. These two different responses also apply for the combined load components. This behaviour is important when it comes to examining the serviceability performance of the foundation during typical working loads. A framework which encapsulates the material response during these two different modes is essential for accurate modelling of foundation performance.

1.2.4.1 Elasticity

The American Petroleum Institute (1993) recommends the elastic solutions of Poulos and Davis (1974) for determining the elastic footing behaviour for offshore structures. These solutions are for a rigid flat circular footing on the surface of a homogeneous material. Bell (1991) conducted a finite element investigation of the elastic behaviour of footings, finding that for typical Poisson ratio values there was significant cross coupling of the horizontal and moment terms. This means that on the application of a moment load, and zero horizontal load, there is a horizontal movement as well as the expected rotational displacement. This effect reduced as Poisson's ratio increased. This cross coupling was not accounted for in the analytical solutions. Ngo Tran (1996) also studied the elastic behaviour of footings, finding that the embedment depth had a significant effect on the vertical stiffness, and a more pronounced effect on horizontal and moment stiffness. He derived empirical expressions to determine these elastic coefficients.

1.2.4.2 Footing Failure and Empirical Bearing Capacity Factors

Initially researchers were interested in what maximum permissible load could be applied to the footing and be sustained by the soil - this problem is known as the bearing capacity problem. Not many exact solutions to the bearing capacity problem have been found since Prandtl (1921) published the solution for a strip footing on a weightless perfectly plastic material. Terzaghi (1943), whilst not publishing an exact solution, suggested the separation and superposition of the effects of soil weight (g), cohesion (c) and overburden (q) for determining bearing capacity. He defined the bearing capacity factors N_g, N_c, and N_q to represent the effect of the various components:

$$V_{peak} = \left(\frac{1}{2} BgN_g + cN_c + qN_q \right) A_{footing} \quad \text{..... 1.1}$$

These bearing capacity factors are dependant on the angle of friction and several workers have suggested alternative expressions for them (for example Meyerhof, 1953; Hansen, 1963). This expression, initially developed for the plane strain case, can easily be modified for other footing shapes by using various shape factors (Meyerhof, 1953; De Beer, 1970; Hansen, 1970; Vesic, 1973). Typical failure mechanisms for bearing failure are shown in Figure 1.4.

Foundations for offshore structures are subjected to large horizontal and moment loads in addition to vertical loads, particularly during extreme environmental conditions. It is recognised that the vertical bearing capacity is reduced as larger horizontal and/or moment

loads are applied. Initial advances in the understanding of combined loading on foundations probably date to Meyerhof (1953), whilst there have been contributions over the years by Hansen (1970) and Vesic (1975). The approach by Vesic has been adopted by the API (1993) for determination of the bearing capacity of shallow foundations. All deal with the application of horizontal load by introducing inclination factors, which reduce the vertical bearing capacity depending on the ratio of horizontal to vertical load. Each researcher proposes different formulations of this factor but broadly speaking each maps out an approximate parabolic surface in $\{V/V_{peak}:H/V_{peak}\}$ space (as shown in Figure 1.5 - for f = 35). Peak values for the three curves all occur at approximately V/V_{peak} ~ 0.41, though the maximum ordinates clearly differ. Interestingly, only in the theory of Meyerhof does the friction angle make any difference to the shape.

Moment loading is dealt with by examining a statically equivalent vertical load, acting at the centre of a reduced footing, where the reduced size is determined by the load eccentricity ($e = M/V$). This idea of effective area was introduced by Meyerhof (1953), taken up by Hansen (1970) and adapted by Vesic (1975) to allow for circular footings. Typical $\{V:M/B\}$ interaction diagrams are similar in shape to the $\{V:H\}$ diagrams, with maximum M/BV_{peak} ordinates occurring at similar values of V/V_{peak}. For a fully combined $\{V:M/B:H\}$ load both processes are used, that is an inclined load acting on a foundation of reduced area. Further factors are introduced to account for the effects of footing embedment. These relationships were developed initially as reduction factors on the allowable vertical load, rather than for the development of interaction diagrams.

1.2.4.3 The Yield Surface Approach and Work Hardening Plasticity Theory

More recently the approach to the bearing capacity problem has been to view the load state $\{V:M/B:H\}$ in terms of a three-dimensional yield surface (interaction diagram). By adopting this strategy it is possible to develop an incremental plasticity solution to the response and thus describe displacements as well as maximum permissible loads. The advantage of representing the foundation by a plasticity 'macro' model is that a realistic representation of the foundation can be included within structural analyses packages. Therefore, during the design process the structural engineers can use a much better representation of the foundation response than say linear springs, or, in some cases, pinned footings (as in the analysis of jack-up units). To develop a working incremental plasticity model it is necessary to determine the following features (as shown in Figure 1.6):

(i) The definition of a yield surface in $\{V:M/B:H\}$ space for a strip footing of width B, or, in $\{V:M/2R:H\}$ space, for a footing of radius R. If the load state of the foundation is

such that it touches or exists outside the yield surface then plastic displacements occur else the response of the foundation is elastic (the work-conjugate displacements denoted by $\{w:Bq:u\}$ or $\{w:2Rq:u\}$ respectively).

(ii) A hardening relationship, which determines the size of the yield surface. This typically is a relationship between the apex of the surface (referred to as V_o) and the vertical plastic displacement.

(iii) A plastic potential, which defines the direction of the incremental displacement vector upon plastic yielding. For most plasticity models this is assumed to be the same as the yield surface and is described as associated. In the development of footing plasticity models it is reasonably clear that associated flow is only relevant for the $\{M/2R:H\}$ plane.

(iv) A description of the elastic behaviour of the foundation for any load combinations within the yield surface. This has been studied extensively using finite element modelling at Oxford (Bell, 1992 and Ngo Tran, 1996).

Butterfield and Ticof (1979) were amongst the first to investigate footing behaviour in this manner, doing so for strip footings on dense sand. By conducting large numbers of load controlled 'probe' tests, they were able to map out a three-dimensional yield surface (Ticof, 1979). They suggested that a 'cigar shaped' yield surface would capture the data and sized it by dimensionless peak loads $M/BV_{peak} = 0.1$, and $H/V_{peak} = 0.12$, occurring at V/V_{peak} of 0.5 (shown in Figure 1.7). Other investigations, including that of Gottardi (1993), have validated the general shape of this surface in $\{H/V_{peak}:V/V_{peak}\}$ and $\{M/BV_{peak}:V/V_{peak}\}$ space, whilst showing that in $\{M/BV_{peak}:H/V_{peak}\}$ space the failure surface can be approximated by a rotated ellipse (Butterfield, 1981; Georgiadis and Butterfield, 1988; Georgiadis, 1993; Gottardi and Butterfield, 1993). Dean *et. al.* (1993) suggests that the extent of the rotation is a function of the load reference point.

Tan (1990), using the geotechnical centrifuge at Cambridge, mapped out the behaviour of spudcan footings in $\{V:H\}$ space on saturated sand. The majority of tests were horizontal sideswipe tests, in which the footing was loaded to a certain level, before being horizontally moved whilst keeping the vertical displacement locked. By considering the sand foundation to be elastically incompressible under vertical load, then by analogy with undrained triaxial test paths, the sideswipe paths could be regarded as close approximations to yield loci (Dean *et. al.*, 1993). Tan suggested that the $(H/V_o)_{max}$ occurred at a value of $V/V_o \sim 0.4$, where V_o was the maximum pure vertical load experienced by the foundation. For a surface footing the value of $(H/V_o)_{max}$ was 0.14 with it increasing at a rate of 0.13 per non-dimensional embedment depth, $w/2R$. Tan (1990) conducted investigations

into the effect of embedment, finding that the shape remained similar, with the maximum H/V_o ordinate increasing slightly with increase of depth. Influence of cone angle and roughness was also examined. Based on the empirical findings of the experiments a plasticity model was developed for {V:H} space.

Tan's (1990) investigation, however, was limited in several respects. In the experiments there was poor control of the vertical displacement, which suggests that the load paths measured during the swipe tests were probably not reflective of the true failure surface. There was no measurement of the moment load applied to the footing, which was unlikely to be zero, due to the nature of the loading apparatus. This suggests that, as the failure surface is elliptical in {M/2R:H} space, it is difficult to interpret where on the failure surface the experimental results lie. Finally, in the context of jack-up units (for which Tan's experiments were aimed), the critical reason for the development of such plasticity models is to understand the amount of moment fixity that the foundation provides to the structure. An increased understanding of the moment fixity may lead to a better understanding of the member stresses at the hull connection of the leg, which may lead to a more favourable assessment of sites for particular drilling units. By investigating only the {V:H} space this important problem is not addressed.

A more rigorous use of sideswipe testing was made by Martin (1994), at the University of Oxford, when mapping out the behaviour of spudcan footings on an increasing strength with depth clay. To undertake this investigation Martin (1994) developed a sophisticated loading apparatus capable of probing any part of the {V:M/2R:H} failure surface with the loads and displacements measured to a high degree of accuracy. Martin (1994) introduced the concept of conducting swipe tests at different ratios of {$2Rq$:u} so that the entire three dimensional surface could be mapped. It was found that the general shape of yield surface could be normalised with respect to the pure vertical load capacity at any depth, similar in shape to the surface suggested by Butterfield and Ticof (1979). Martin used a mathematical function to describe his yield surface (named 'Model B'), defined by the maximum ordinates of H/V_o (h_o = 0.127) and $M/2RV_o$ (m_o = 0.83), as well as the curvature at high (β_2 = 0.764) and low (β_1 = 0.882) stresses, and the eccentricity of the ellipse (a = 0.316).

Martin (1994) was then able to develop a three dimensional work hardening plasticity theory based on the experimental results. He used theoretical stiffness coefficients for elastic behaviour, and theoretical lower bound bearing capacity solutions to define the vertical bearing capacity with penetration. Martin incorporated his plasticity model in a structural analysis package for examining the static pushover behaviour of a jack-up. Such

a model correctly represents the amount of moment fixity of the footing so that the jack-up member stresses may be correctly interpreted. Thompson (1996) incorporated this footing 'macro' model within a full dynamic structural analyses package for jack-up units. This represented a significant step-forward from the typically used assumption of pinned footings, which gives no moment fixity, and thus overestimates the leg member stresses as well as other response variables of interest.

Recent experimental work at the Oxford (Gottardi and Houlsby, 1995), which made use of the rig developed by Martin (1994), followed a programme specifically tailored to develop a three dimensional plasticity model for circular footings on dense sand. A numerical model, named ‘Model C’, has since been created based on these results and shown to accurately provide simulations of the test results (Cassidy, 1999). This model assumes, similarly to Martin’s and Tan’s work, that the yield surface could be normalised with respect to V_o, the maximum pure vertical load experienced by the footing. An empirically derived hardening law was used. The surface, as expected, was again similar in shape to that found by the previous researchers (similar to that shown in Figure 1.7). The peak value for H/V_o was 0.116 and for $M/2RV_o$ was 0.9. This model has been incorporated within a complex dynamic analysis package used to investigate jack-up unit response to extreme wave events (Cassidy, 1999). Cassidy (1999) shows that for the reliability levels of interest the 'Model C' foundations provide a significantly lower response (for example deck displacements) than the typically used pinned footing assumption, illustrating the power of using the footing macro-model. A sensitivity analysis carried out indicated that the moment dimension of the footing yield surface was a very critical variable, ranked second out of the eleven selected key variables in the jack-up unit problem.

More recently Mangal (1999) has carried out experimental research on the partially drained response of flat footings on oil saturated sand. Mangal was interested in the plastic penetration response of the foundation during initial loading. In the experiments Mangal applied monotonic movements to the footing at different displacement rates. He conducted tests from two different levels of initial vertical load. He had difficulty in obtaining repeatable soil specimens, which complicated the analysis of the results. He concluded that for monotonic vertical loading there was a rate dependency during an initial viscous loading response, but rate independency for the steady state secondary response. He obtained qualitatively similar results for combined load increments though did not formulate any quantitative relationship between rate and response.

These models represent the current state-of-the-art for the understanding of shallow foundation response to general loading.

1.3 SUCTION CAISSONS

Recently, a novel shallow foundation type has been used in place of the piles (Tjelta, 1994). They are best described as upturned buckets, typically 15m in diameter and 5m long, and are usually called suction caissons. These foundations are installed by providing a slight suction to the inside of the caisson by pumping water out, once it has made a sufficient seal within the soil (see Figure 1.8). In the North Sea, where a large part of the seabed is covered by a layer of very dense sand, the suction assists penetration by temporarily reducing the resistance of the sand, as well as increasing the net downward force on the caisson. These novel foundation systems can be installed within 24 hours, and are preferred to piles because of the substantial savings that are afforded by the reduced materials and installation times. They are also more environmentally friendly than piles as they maybe removed as easily as installed, simply by reversing the direction of pumping. Suction caisson foundations have therefore become the focus of much current research. Some of this research is described in this thesis, where investigations have been carried out of caissons installed in sand, as this is a common offshore design condition.

Offshore foundations are generally exposed to higher horizontal and moment loading than are encountered onshore due to wave, current and wind forces. Additionally, during wave loading, particularly in the North Sea where waves can be as large as 25m, there can be sudden changes in the loads applied to the foundation. Whilst pile design procedures have evolved from onshore experience and theory, design guidelines for shallow foundation systems, such as suction caissons, have yet to be devised for the intense loading conditions found offshore. In the particular case of suction caissons there are no precedents in onshore experience available for exploitation, as well there is little offshore experience, though this is developing at an increasing rate (Bye *et. al.*, 1995). This means that there are no accepted procedures, like the API guidelines for piles, nor are there large amounts of published data, as firms seek to keep any acquired knowledge in-house so as to gain competitive advantage.

One of the critical aspects, which affect the design, is the ability of the caisson to resist tension, which may be applied under extreme environmental conditions. The important issue is the relative rate at which the caisson is loaded, compared to the rate of fluid flow within the soil matrix (degree of drainage), as the latter affects the soil response. The

typical loading on the foundation will consist of random variations about some mean value, which results in a complex flow regime within the soil matrix, that in turn dominates the response of the foundation.

Before outlining the exact focus of this thesis it is appropriate to detail the history of suction caisson use, in field trials, and in projects. By reviewing this literature it is possible to establish the areas of uncertainty which warrant attention. It is also possible to draw together all the appropriate calculations that can currently be made, as well as those which can not. A review is also made of the current research around the world being undertaken to redress these issues.

1.3.1 Field Trials

There are several published records of small scale field trials of suction caissons in typical soils. In most cases the field trial represents a scaled down model of an actual prototype structure subjected to field scale conditions. The main objective of the tests has been to develop insight of site specific conditions. Table 1.1 gives the various field trials, the earliest recorded being in 1980, whilst the latest was performed in 1999. Each series of field tests are innovative in their own right and each is the subject of many publications. However, it is important to point out several key tests.

1.3.1.1 Gullfaks C Large Scale Penetration Test

This test was carried out during 1985 in the North Sea during the detailed design of the Gullfaks C gravity base structure. It was necessary to determine the feasibility of installing a 22m skirted foundation into layered soil using self weight and suction. The test was successful and included the examination of the variation of penetration rate on resistance, the effect of soil set-up on installation, several cyclic loading tests as well as a novel water injection system to reduce tip resistance. The results of the test confirmed that large skirted structures could be feasibly installed resulting in the Gullfaks C gravity base structure being designed with 22m skirts.

1.3.1.2 Snorre Model Tests

These tests were carried out on an inland site in Norway chosen specifically because of the similarity of soil characteristics with the prototype field soil. These tests were significant because they allowed the Norwegian Geotechnical Institute to assess their in-house developed calculation procedures for shallow foundations in clay. The tests consisted of static and cyclic load tests. The tests were carried out to examine specific loading conditions relevant to the Snorre tension leg platform.

1.3.1.3 Statoil Field Trials

These trials were the first reported trials at an offshore location in which a suction caisson was used in very dense sand. They were conducted during the development of Statoil's Draupner E platform. They consisted of a large suite of tests looking at both installation and capacity aspects of the problem. The results of the tests are largely confidential.

1.3.1.4 Offshore Data Limited

Conducted off the Welsh coast during 1998 these tests are significant as they show that installation in sand primarily depends on the development of seepage gradients in the soil. In all cases the caisson was installed in very shallow water (less than 2m water depth) as well as being very easily removed. Several capacity tests were undertaken to look at typical loading conditions experienced by proposed monopod renewable energy structures.

1.3.2 Project Usage

The field tests described in Table 1.1 enabled the development of the suction caisson foundation concept for several projects in a variety of soils, as described in Table 1.2. Again there are many publications associated with each of these projects however it is prudent to point out key installations.

1.3.2.1 Gorm

The anchoring system used for the floating storage facility at Gorm in 1980 is perhaps the earliest recorded use of the suction anchor concept. The suction installed piles were preferable to the typically used drag anchors as it was possible to install the anchors with a precise location. The use of the caissons in this context is the most popular use of large aspect ratio suction caissons in the present day, most usually in clay.

1.3.2.2 Gullfaks C

The Gullfaks C platform was installed in 1989 and consisted of 16 cells each of 28m diameter and 22m depth. These skirts were installed successfully with a combination of self weight and suction. The skirted foundation design concept was used to transfer the loads on the foundation to the deeper and stronger sediments. A complex drainage system was developed within the skirted compartments to enhance drainage and thus accelerate consolidation of the upper softer sediments within the skirts. The main design of the structure, however, revolved around the gravity base concept.

1.3.2.3 Snorre TLP

The foundation for the Snorre tension leg platform (TLP) was a combination of suction caisson and gravity base. The basic concept of a TLP is a buoyant platform tethered tightly to the foundations such that a long term tension is applied to the foundation. This long term loading leads to the soil acting in a drained condition, and the frictional tensile capacity of suction installed caissons are typically small. To ensure that the skirts would not pull out of the soil, ballast was added to the top of the foundations, such that the net downward resistance was greater than the predicted long term tension. Short term fluctuations in the loading can easily be accounted for by the partially drained, or undrained, behaviour of the soil, in which the strengths are usually greater than the drained response.

1.3.2.4 Europipe 16/11E (renamed Draupner E) and Sleipner Vest (renamed Sleipner T)

These two Statoil structures were the first jackets to be designed and installed with caisson foundations, replacing the steel piles at each of the four corners. This was also the first instance of caisson foundations being designed for use in dense sand where there are significant concerns about what tensile capacity can be mobilised. The concerns for tensile capacity were more relevant for the Sleipner T structure where much harsher loading conditions are expected, including large tensile loads. In both cases the foundations were designed to be primarily tension-compression members by using a flexible attachment with the steel jacket structure. Installation proved to be straightforward and fast with a small amount of heave observed within each caisson. Grout was injected into each caisson to ensure full contact between each caisson top and the internal soil plug.

1.3.2.5 YME

In the case of the YME jack-up, skirts were added to the spud-cans to enhance the moment resistance and thus reduce member stresses near the hull. Although the foundations were installed without the use of suction, this concept will clearly be used more often as jack-up operators strive to use their units in harsher environmental conditions. This may also be the case where longer times are spent at individual sites, such as when the jack-up takes on the role of production. In this case harsher environmental criteria would be applicable when the site specific assessment is carried out.

1.3.2.6 Summary of Projects

All the examples of project use of caisson foundations are shown in Figure 1.9 in which two categories of use emerge. There is a rather large band in the anchor category, used for FPSOs, in which the mean diameter is about 5m, mean skirt depth is about 12m and the

typical use is in clay. Another category is immediately observable, that of the large diameter, short skirt depth, primarily used for fixed structure applications. It is highly likely that a new category will become prevalent in the future. This will consist of small scale suction caissons, similar in size to the field trial foundations, used for much smaller applications. These projects may include minimum facility structures or the emerging renewable energy structures.

1.3.3 Perceived Problematic Areas

During the review of the field and project cases several problematic areas became apparent. Although the technology is in its infancy, there has been a substantial interest in the development of the technology and several investigations are in the public domain. It is worthwhile to point out these problematic areas, which are associated with all shallow foundation design, but particularly to suction caissons. The remainder of the thesis attempts to focus on the more complex capacity issues in sand that are perceived to be problems.

1.3.3.1 Installation in Sand

Installation is a very complex issue, particularly in granular sandy material. As the suction is applied to the inside of the caisson, flow fields are induced within the soil matrix. This induced flow, importantly, reduces the bearing capacity at the skirt tip and the internal friction, whilst, increasing the external friction. The pressure differential also provides a net downward force on the caisson but this contributes only slightly to the installation. During this installation phase the soil at the skirt tip has close to zero effective stress (Erbrich and Tjelta, 1999). Due to this mechanism there can be significant problems with buckling of the caisson as the lateral stability of the soil-structure combination is quite low. This effect is more pronounced during the early stages of installation.

1.3.3.2 Stiff Fissured Clay

During installation in clay it is the net downward force caused by the pressure differential which causes the caisson to be forced into the soil. The caisson can be designed to withstand the large suction pressures which may be required for such an installation. Information for the design scenario where the soil consists of stiff fissured clay is relatively scarce. In most cases (for example Visund, Njord and Aquila) the soil conditions consisted of a layer of soft clay overlying much stiffer clay. In these cases it appears that the soft clay layer is deep enough so that a seal could be created. From the results found in the literature it is not clear whether installation in stiff fissured clay is possible or not.

1.3.3.3 Layered Material

When the installation occurs in a layered soil there are questions as to whether the caisson will penetrate through a sand layer after it has moved through a clay layer, as it will not be possible to develop the flow regime which degrades the skirt tip resistance to zero. There are several field case studies which provide evidence that this may still be possible. The most notable of these studies is the large scale deepwater penetration test (Tjelta *et. al.*, 1986) which was conducted during the investigations for the Gullfaks C platform. The soil conditions consisted of interspersed layers of dense sand and clay over the depth of interest. A maximum suction of 480 kPa (linearly increasing with depth) was required to install the caisson to its full depth. Removal was also achieved with a maximum overpressure of 250kPa.

1.3.4 Capacity

The capacity of a shallow foundation subjected to typical combined loading is an area of great interest which has received a great deal of attention over many years. It is one of the fundamental problems of geotechnical engineering with most attention being focussed on monotonic load combinations, with the soil in either a drained (typically dry sand) or undrained (typically clay) state. The current state-of-the-art for understanding and modelling was described in Section 1.2.3. This understanding is limited as no account is taken of loading rate (partial drainage) or reversals of loadings (cycles). These two phenomena are key components of offshore geotechnical problems.

1.3.4.1 Partially Drained Monotonic Capacity

Relatively little work has been performed on this aspect of capacity, which is likened to the capacity of the foundation during the passage of one large impact on the structure. Vesic *et. al.* (1965) examined the dynamic bearing capacity of soil observing that the bearing capacity increased with fast loading rates, though occurring at very large displacements (up to 40% of diameter). Mangal (1999) examined the partially drained response of flat footings on sand during the initial plastic penetration. He noted an initial viscous stiff response, which appeared to be rate dependent, followed by a steady state response, which appeared to rate independent.

1.3.4.2 Cyclic Capacity

Information about cyclic vertical loading in dense sand is scarce (Bye *et. al.*, 1995; Jostad *et. al.*, 1997; Tjelta, 1994; Tjelta *et. al.*, 1986), as most of it is proprietary and unpublished (for example results from model testing at NGI and Oxford University for Statoil's Sleipner

Vest platform). Most interest centres around the effects of cycling the foundation into tension, as this is believed to be a critical loading condition. Bye *et. al.* (1995) propose a method for evaluating cyclic capacity, they suggest that there are zones of cyclic amplitudes which can be sustained, but once these boundaries are breached there can be rapid degradation of performance.

Information about cyclic vertical loading on clay is slightly more abundant particularly from NGI (Andersen *et. al.*, 1992; Andersen *et. al.*, 1993; Clukey and Morrison, 1993; Dyvik *et. al.*, 1993; Tjelta *et. al.*, 1986, Jeanjean *et. al.*, 1998; Andersen and Jostad, 1999). Most of the research on this aspect of the problem has been specific to particular projects, especially the Snorre project. The primary purpose of these tests has been to evaluate the capabilities of the in-house NGI developed numerical programs, which have been well documented in the literature for problems of shallow foundation behaviour. These consist of limit equilibrium analyses using reduced shear strengths based on the cyclic loading history, and have been used in the design of a large number of offshore developments. A further method is proposed by Clukey *et. al.*, 1995 based on a Miner's law approach to assessing cyclic loading.

There is a paucity of published data on cyclic combined loading (either clay or sand), although there have been several proprietary laboratory investigations at Oxford University and the Norwegian Geotechnical Institute. Intuitively, combined cyclic loading is a much harsher loading on the foundation, so that the degradation of performance is likely to increase with the application of large deviatoric loads.

The review of the literature has indicated that the performance of shallow foundations (specifically suction caissons) on sand is the area of the greatest uncertainty. Figure 1.10 summarises the current state of the art for shallow foundations on sand. There are still large gaps in the knowledge required for design purposes. The results developed in this thesis redress this slightly and will allow focussed subsequent investigations on the more appropriate aspects of the problems.

1.3.5 Summary of Calculations For Performance in Sand.

It is clear that, whilst, there are several largely incalculable aspects of shallow foundation behaviour, there are parts which are readily calculable. It is appropriate to briefly outline these calculable quantities for caissons in sand as they are of use to designers.

1.3.5.1 Installation

Installation of caissons in sand deposits relies more on the hydraulic gradients generated in the sand than the downward force on the caisson caused by the applied suction. It is therefore imperative that a good seal is made between the caisson and the sandbed so that suction can be generated within the caisson chamber. Once this is achieved it is important not to increase the suction too quickly as a piping failure may occur at the edge of the skirt. Opening or closing an inlet from the ocean could control the amount of suction applied.

The initial self-weight penetration of the caisson is calculated as the sum of friction on both outside and inside (in this case equal) and the end bearing on the annulus. The end bearing would in turn be the sum of an N_q and N_g term:

$$V' = g'(\pi D)\left(h^2 (K \tan\delta) + htN_q + \frac{t^2}{2} N_g \right) \quad \text{..... 1.2}$$

Once the self-weight penetration has been achieved the suction pressure is applied quite slowly at first, and then at a constant rate with penetration. Figure 1.11 shows a typical pressure differential - penetration response from a small-scale field test. The response is reasonably linear, in line with experimental evidence (Aldwinckle, 1994). Whilst the resolution of the pressure transducer was not ideal the broad trend of the data is evident. The penetration of the caisson stopped at 1.22m, at which stage the pumps being used to apply suction were operating at their limit.

From a theoretical viewpoint if the net 'underpressure' in the caisson is -u_o with respect to the ambient seabed water pressure, it is assumed that the pressure at the tip of the caisson is -αu_o. The capacity is again calculated as the sum of the external and internal friction, as well as the bearing on the skirt tip. It is assumed that the internal vertical effective stress is reduced sufficiently so that the failure mechanism occurs entirely inwards, so that the capacity is:

$$V' = g'(\pi D)\left(h^2 (K \tan\delta) + htN_q + t^2 N_g\right) + u_o(\pi D)\left(\left(\alpha - \frac{1}{2}\right)h(K \tan\delta) + (\alpha - 1)tN_q\right) \text{.. 1.3}$$

This expression has been used with appropriate material parameters to determine a theoretical value for u_o as a function of the penetration depth. This relationship is superimposed onto Figure 1.11 and shows a very good fit, given the variation of α with depth, also shown on the figure. The value of α reduces from 0.5 for very shallow penetrations to 0.2 at a penetration of 1m, which is again in line with experimental

observations (Aldwinckle, 1994). It is worthwhile noting that the water depth, whilst not appearing to affect penetration, will control the maximum amount of suction that could be applied. This upper limit, which is determined by cavitation of the pore-fluid within the caisson chamber, determines the maximum skirt depth.

1.3.5.2 Vertical Compressive Capacity

The vertical drained (long term) compressive capacity is expected to be in most cases very large and can be calculated using standard bearing capacity theory:

$$V' = \gamma' L N_q^* \left(\frac{\pi D^2}{4} \right) + \gamma' \frac{D}{2} N_\gamma^* \left(\frac{\pi D^2}{4} \right) + \frac{\gamma' L^2}{2} \pi D K \tan\delta \quad \text{..... 1.4}$$

The bearing capacity factors (N_q^* and N_γ^*) are those defined for circular footings and may be found in the paper by Bolton and Lau (1993). For footings on saturated sand, where the loading rate becomes important, the bearing capacity becomes more difficult to calculate. On very dense sands it is expected that the undrained bearing capacity will be greater than the drained sand, whilst on loose sands it is possible that the bearing capacity is lower than for the drained case. As an example of the ultimate resistance on saturated sand Figure 1.12 shows a series of tests conducted by Vesic *et. al.* (1965) investigating the effect of loading rate of flat footings on both saturated and dry sands. In general the results from flat footings will give guidance as to the response for skirted footings. Clearly the final bearing capacity on dry sand was indifferent to the rate of loading, whilst on the saturated sand an effect was evident. At the higher rates of loading the bearing capacity factor (N_γ) increased by a factor of at least two. This increase in soil strength was, however, at the expense of much greater ultimate displacements. Vesic *et. al.* (1965) noted that on dry sand a general shear failure was observed. They also noted that on saturated sand at low displacement rates the same general shear failure was observed. They did, however, observe that at the faster displacement rates, the failure mode appeared to move from a general shear failure to a punching shear failure. Punching shear is generally observed for soils that are very loose, whilst general shear is observed for soils that are very dense. This change in failure mode can be explained by understanding the response of the pore fluid underneath the footing. At the very low displacement rates the pore fluid response to any applied load is minimal, as there is sufficient time for dissipation to occur. This suggests that the soil will behave as a dry sand. When the footing is moved at a faster rate it is likely that an undrained increment of load is applied to the fluid directly beneath the footing. This leads to a reduction in strength of the soil in that region. This leads to a downward movement

and volumetric change which leads to dilation of soil at regions further afield from the footing. This in turn leads to negative pressures and increases in the overall soil strength as indicated by the increases in bearing capacity factor. It is quite likely that a fast downward penetrating footing on very dense sand will have a capacity limited only by the cavitation of the pore fluid at the regions where dilation is occurring.

1.3.5.3 Vertical Tension Capacity

The drained tensile capacity of a skirted foundation is simply the sum of the external and internal frictional resistance of the skirt. In general this will be very small and equal to:

$$-V' = \frac{g' L^2}{2} pDK \tan d + \frac{g' L^2}{2} pDK \tan d \quad \text{..... 1.5}$$

provided that the internal frictional resistance is less than the weight of the soil plug:

$$\frac{g' L^2}{2} pDK \tan d \le g' L \left(\frac{pD^2}{4} \right) \text{..... 1.6}$$

The short term tensile capacity relies on the dilatant potential of the dense sand and the loading rate. In most cases this capacity is likely to be limited by the maximum amount of suction resistance that can be mobilised. In very dense sand, at very fast loading rates, very high suctions will lead to high effective stresses and thus high frictional strengths. The limit of the suctions will of course be the cavitation of the pore fluid:

$$-V' = \left(- f p_a + p_a + g_w d + gL\right) \frac{pD^2}{4} + \frac{g' L^2}{2} pDK \tan d \quad \text{..... 1.7}$$

This formula does not account for the increase in effective stress along the side of the caisson. This can be done by assuming a linear increase from zero at the surface to {(1-f) $p_a + g_w d + gL$} at the caisson base and adjusting the friction appropriately.

It is possible that the cavitation does not occur at the caisson base but occurs at the underside of the caisson top-plate. In this case the appropriate calculation is:

$$-V' = \left(- f p_a + p_a + g_w d\right) \frac{pD^2}{4} + g' L^2 pDK \tan d \quad \text{..... 1.8}$$

It is noted that the frictional terms do not take account of the changes in the effective stress distribution along the skirt. This distribution is difficult to estimate.

If the water is deep enough that cavitation does not govern the capacity it will be necessary to carry out either (i) an effective stress analysis in which the large suctions are taken account of, or (ii) a total stress analysis in which it is necessary to determine an undrained strength of the sand. It is highly likely that if cavitation is not an issue then the resulting capacity is probably far greater than any typical capacity requirement. These calculations do not give any indication of the required displacements necessary to mobilise these capacities.

Figure 1.13 details the different stress paths that are followed for drained frictional strength and for undrained frictional strength. Critical state soil mechanics suggests that for drained loading there is sufficient drainage that volume change can occur easily, whilst for undrained loading there is no volume change at all. However, most loading rates that occur in the field will be such that there will be partial drainage and therefore the volume change will be somewhere in between. It is still highly probable that in this situation the capacity is still limited by cavitation of the pore fluid.

1.3.5.4 Combined Loading

The area of combined loading has been discussed previously in this chapter. At present it is only possible to make a calculation for the horizontal capacity which is clearly the sum of the frictional sliding resistance and the resulting wedge resistance (passive less the active):

$$H = V' \tan f' + \frac{1}{2} g' L^2 D\left(K_p - K_a\right) \quad \text{..... 1.9}$$

It is not currently possible to carry out a calculation for the moment resistance. It is also not currently possible to carry out any theoretical calculation for the combinations of limiting load that may be sustainable at load combinations between the two. At present the best methods for footings in general are empirical formulations based on a large number of experimental observations.

1.3.6 Recent and Current Research Effort WorldWide

In line with the field testing and project usage described above there have been several laboratory testing programmes undertaken investigating a variety of problems, mostly associated with those mentioned above.

1.3.6.1 Norwegian Geotechnical Institute

The Norwegian Geotechnical Institute have been at the forefront of shallow foundation design for the past twenty years and have been intimately involved with a number of

shallow suction foundation designs. They have conducted field studies, laboratory investigations, and numerical modelling. Most of their experimental investigations have been used to validate their suite of in-house numerical models. Some of this research is in the public domain (Jostad *et. al.*, 1997), however, most of it remains as proprietary data, particularly the work on the foundations for the Sleipner T platform. During the investigations for this structure they conducted an extensive series of large scale model tests (600mm diameter) in the laboratory and were also involved in small scale field tests (Tjelta, 1995).

1.3.6.2 SINTEF/NTH

Confidential research was undertaken on the installation procedures for suction installed foundations, particularly during the design phase of the Draupner and Sleipner platforms. This involved carrying out some small scale laboratory tests, as well as being involved in with field scale testing. From these investigations a calculation procedure was developed to determine the penetration resistance of the foundation.

1.3.6.3 Offshore Technology Research Centre, The University of Texas

Work has been conducted primarily looking at the use of large aspect ratio suction caissons for deep water Gulf of Mexico applications. Laboratory testing investigated the tensile capacity, as well as the cyclic capacity under typical tension leg platform loading conditions (for example El-Gharbawy, 1998).

1.3.6.4 University of Delft

Using a centrifuge, work has been undertaken examining the installation performance of large aspect ratio caissons in layered soils. More recent work has detailed the horizontal capacity of large aspect ratio suction piles, using both numerical and experimental methods (Allersma *et. al.*, 1999 (a) and (b)).

1.3.6.5 Centre for Offshore Foundation Systems, Australia

Work has been undertaken on a wide range of problems associated with shallow foundations, specifically suction caissons, on carbonate sands. These are problematic soils which possess very contractant behaviour upon shearing, usually leading to a rapid reduction of frictional strengths, as highlighted in the case of the North Rankin A piles. Additional problems can be presented by the presence of very thin cemented layers within the soil strata, highlighted by the problems of the Goodwyn A foundations. Shallow foundations can present significant economic and installation advantages for this type of soil, in which the behaviour is treated primarily as undrained. The work is ongoing and

covers many different aspects of behaviour, primarily response under monotonic and cyclic loadings (for example Bransby and Randolph, 1999; Watson and Randolph, 1998), buckling response during installation, the installation and performance of large aspect ratio caissons (House *et. al*., 1999).

1.3.6.6 Suction Caisson Literature Database

The preceding sections have outlined key trials, projects, calculation procedures and research efforts concerning the suction caisson technology. This review of the literature represents a section of the available literature on the topic of the suction caisson technology. Papers which are not explicitly referred to in this thesis but are part of a database which has been collected during the course of the research can be found in Appendix A.

1.4 OUTLINE OF CURRENT WORK

The current work looks to outline the response of the suction caisson foundation, and more generally shallow foundations, to typical loading regimes.

1.4.1 History of Shallow Foundation Research at Oxford

Before discussing the work contained in this thesis it is appropriate to outline the history of research on shallow foundations at Oxford University as this provides a good setting for the presented material. Figure 1.14 shows in very brief form the progression of work on foundations on both sand and clay. The interesting feature of this recent history is the concurrency of the experimental and numerical work. The work has progressed with one key feature that the experimental investigations are approached in a manner which allows footing 'macro' models to be developed. These 'macro' models are then used to develop a greater understanding of certain offshore structures to a variety of wave loadings (Thomson, 1996; Cassidy, 1999). It is with this same goal that the work presented in this thesis was approached.

1.4.2 Description of Current Research and Thesis Outline

It is recognised that the loads placed on the foundation are typically not monotonic nor are they applied in isolation. Offshore environmental loads are usually random, cyclic, and applied in combinations. It is felt that to understand the behaviour under any representative cyclic loading, behaviour under monotonic loading must first be understood. The work undertaken in this research leads to a basic level of understanding of skirted foundations, firstly under monotonic loading situations, before progressing to representative cyclic

loading. Three different phases of work have been completed, each of which is summarised below.

i) The investigation of the behaviour of the foundation when subjected to monotonic load combinations. This was an experimental study during which the behaviour of the foundation was mapped out under drained and partially drained conditions. Drained conditions were modelled utilising dry sand, whilst partially drained conditions required a saturated sand sample. An oil-saturated sample was used to correctly model the timescale of the events in relation to the size of the foundation and rate of loading. Under both conditions tests were carried out to determine the effect of the embedment ratio (skirt depth to diameter). Tests were mainly carried out on a very dense silica sand with some supplementary tests carried out on a very loose carbonate sand.

ii) The examination of the behaviour of the foundation when subjected to cyclic loading regimes. One of the critical issues for foundations on sand is the effective stress response of the soil to the loading on the foundation. A novel method of pseudo-random cyclic loading is used to account for the effect of loading rate, and, the occurrence of an extreme event. This leads to a realistic representation of the loading time history. It is felt that previously used sinusoidal type loading regimes may give results which could be irrelevant to the understanding of the foundation performance at prototype level. The testing proceeded from vertical loading regimes to simple combinations of load. The effect of scale was investigated using data obtained through a fourth year undergraduate project (Johnson, 1999) which took advantage of equipment developed for the new Structural Dynamics Laboratory (Williams *et. al.*, 1998).

iii) The numerical representation of these problems has been best understood in a work hardening plasticity theory, in which the behaviour in a three-dimensional space $\{V{:}M/2R{:}H\}$ is defined. The tests in phase one provided sufficient information to define behaviour under drained loading within this plasticity model. Concurrently with this experimental research efforts have been directed at developing an appropriate theory capable of modelling cyclic loading (for example Houlsby and Puzrin, 2000). The tests from phase two have enabled this theory to be validated as well as provide guidance on developmental issues.

1.5 POTENTIAL APPLICATIONS

There are many exciting potential applications for the use of the suction caisson concept providing that there is sufficient understanding of the performance and limitations of such

foundations. Such applications include for marginal field development, for floating facilities, for shallow water installations, for subsea facilities (including riser bases, anchoring underwater pipelines), or for river bridges. The use of the suction caisson could lead to significant cost savings in each of these applications.

1.5.1 Renewable Energies Structures

One of the more exciting applications of suction caisson foundations which has come to the fore recently is as foundations for offshore wind energy applications. Early developments in this sector will most probably involve structures fixed to the seabed in shallow water (say 5m - 20m). The hub of a typical large turbine would be located about 60m above water level. The turbine and supporting structure, which would typically be a single column, might have a weight of about 2 - 3MN. The structure would be subjected to large horizontal forces, due to wind, waves and current. The maximum horizontal force might be of the order of 2MN, and would result in overturning moments at foundation level of say 50 - 80MNm. Furthermore these loads would be pseudo-random and repetitive in nature. Foundations must be designed to withstand these forces.

There is of course extensive knowledge and experience of foundation design for offshore structures within the offshore oil and gas industry. However, by comparison with typical oil and gas applications, the offshore wind turbine problem differs in several key aspects:

(i) the vertical loading is much smaller (by a factor of say 5 to 200),

(ii) as a proportion of the vertical loading the horizontal load and overturning moment are much larger,

(iii) water depth is typically much smaller,

(iv) multiple installations (say 10 to 100) of relatively economical designs are required, rather than “one-off” foundations for large high-cost structures. Since these may be spread over a large area, less detailed site investigation information may be available.

Whilst piled foundations and gravity bases are adaptations of well-proven technology, the suction caisson solutions are in their infancy. They are attractive for this application in that they offer the possibility of very economical installation as well as their eventual removal. Perhaps the simplest concept for a foundation for an offshore wind turbine or anemometer mast is as shown in Figure 1.15(a). This shows a “monopile” foundation, in which a single pile is driven into the seabed. The supporting structure would be attached to the top of the pile either through an appropriate connection at seabed level, or above the water line. The pile itself is relatively cheap, but the installation is expensive due to the need for heavy

pile-driving equipment. Removal of the pile at the end of the life of the structure is expensive, and currently the only realistic option appears to be to cut off the pile at seabed level.

There are two main possibilities for a caisson foundation for a wind turbine. Firstly a tripod foundation could be used (Figure 1.15(b)). The large overturning moment would in this case be resisted by combinations of tension and compression on the upwind and downwind legs. The design of suction caissons to resist transient tensile loads is therefore of particular interest (as in chapter 4). The second possible design would involve a single “monopod” foundation (Figure 1.15(c)), and in this case the primary loading which is of interest is the overturning moment. The tripod offers possible advantages in that the caissons can be smaller, and that separate control of the installation of the caissons would allow levelling of the structure. The monopod foundation has the great advantage of simplicity. As their use is in its infancy there is a relatively small amount of information available about the response under these various loading regimes and certainly there are no codified design methods. The understanding of performance under these loading histories can be most conveniently observed from experimental research, some of which is outlined in Chapter 5.

CHAPTER TWO

DESCRIPTION OF EXPERIMENTAL TECHNIQUES

2.1 BACKGROUND

Recent studies of footings subjected to combined loads have led to successful descriptions of the elasto-plastic deformation behaviour of the footing by the use of work hardening plasticity models (Tan, 1990; Martin, 1994; Gottardi *et. al.*, 1999). The postulate is that after a given footing penetration a yield surface is established within {*V*:*M*/2*R*:*H*} space. Any footing behaviour within this surface is assumed to be elastic, whilst elasto-plastic behaviour occurs once the load point reaches the yield surface (as shown in Figure 1.6). Roscoe and Schofield (1957) were the first to use a yield surface approach whilst Butterfield and Ticof (1979) were amongst the first to examine experimentally footing behaviour in this manner.

To investigate the combined load problem there are two methods which can be pursued; (a) numerical modelling, or, (b) laboratory testing, either at unit gravity or enhanced gravity. Ngo Tran (1996) used the finite element method to pursue an investigation of {*V*:*M*/2*R*:*H*} loading of a circular foundation on a material possessing different shear strength profiles. The numerically derived yield surfaces were compared with those experimentally obtained (Martin, 1994), finding favourable agreement. However, undertaking such an investigation for granular materials is at present not realistic. Problems centre around two areas; (i) the lack of detailed material models for granular soils, and (ii) the difficulty in obtaining convergence of solutions at high values of friction angles (above 35 degrees). At high friction angles there are large stress gradients across the elements located close to the edge of the footing. It is possible to overcome this problem slightly by using a very fine mesh at those places where the high stress gradients are perceived to be problematic. In view of these difficulties there have only been a limited number of attempts at determining the vertical bearing capacity factor, N_g (for one example see Frydman and Burd, 1997), and no attempts at examining the combined loading problem. It is probable that, in light of the current increases in computing power, these computational problems will be overcome within the next few years.

The second approach is to make observations from controlled laboratory experiments. These may be conducted in a geotechnical centrifuge where soil stresses are appropriately scaled, but the detail of the experiments may be limited as the apparatus must be designed to work in the enhanced gravity field. Problems may also be encountered when examining

transient behaviour as the consolidation processes for saturated material scale with the square of the gravity level (N^2). It becomes necessary to increase the viscosity of the fluid, and, the rate of foundation loading, so that the model and prototype behaviour are matched, which may not always be possible. The other alternative is to conduct experiments at one-gravity, which allows complex experimental apparatus to be used to complete detailed experiments at small costs. Investigations of a fundamental nature, such as this, which require numerous experiments to be completed are favoured by one-gravity investigations. Care needs to be taken when scaling numerical results to prototype situations as the stress-strain behaviour of soil does not scale linearly with stress. It is also necessary to ensure correct scaling of the transient behaviour however this is possible by using a combination of decreases in soil particle sizes and increases in the pore fluid viscosity and loading rate. The fundamental behaviour at model scale will, in general, be similar to that at prototype scale, even if the numerical values are not.

This chapter details the necessary equipment that was used and developed during the course of the research project. The testing proceeded in three phases on three different materials, a very loose uncemented dry carbonate sand, a very dense dry silica sand and a very dense saturated silica sand. The submerged sand was saturated with silicon oil to model drainage times relevant to the offshore situation. The main technical innovations include i) the development of a high quality bulk testing methodology, ii) a sophisticated transient three degree of freedom loading rig allowing individual load or displacement control on all three axes, and, iii) a high precision data acquisition system which allowed the acquisition of a large amount of high quality experimental data. The main innovation in the testing methods is the development of a pseudo-random approach to cyclic load testing.

2.2 MECHANICAL AND ELECTRONIC APPARATUS

To test the plasticity hypothesis it is essential to establish:

a) The shape of a yield surface.
b) The mechanism of hardening of the surface.
c) A flow rule or plastic potential.
d) The elastic behaviour within the surface.

Studies of this kind normally usually use eccentric inclined loads (Gottardi and Butterfield, 1993), or begin by examining the two-dimensional cases {V:H}, and {V:M/2R} (Nova and Montrasio, 1991).

2.2.1 Loading Rig

At the University of Oxford a loading rig has been developed, initially to explore the behaviour of spudcan footings on clay (Martin, 1994). It has undergone several stages of modification, and it is adaptable to any soil medium. The unique feature of this apparatus is that any combination of displacement path can be applied to the model footing using computer controlled stepper motors. The response of the footing is determined by measuring the resultant loads using a 'Cambridge' load cell, whilst accurate foundation displacements are measured using a system of LVDTs. The primary advantage of using this displacement controlled apparatus is the ability to explore work softening behaviour. Figure 2.1 shows the loading rig, further mechanical details of which can be gained from Martin (1994), Gottardi and Houlsby (1995) and Mangal (1999). The co-ordinate systems, sign conventions and notations for the loads and displacements are shown in Figure 2.2 following that set out by Butterfield *et. al.* (1997). The load reference point was located at the base of the footing (*i.e.* mudline), consistent with previous work conducted on flat footings at Oxford University.

2.2.2 Data Acquisition System

Since the original version developed by Martin (1994) extensive modification has been undertaken on the data acquisition and control side of the apparatus. Whilst the prime motivation for upgrading the electronic side of the equipment was the need for better control and acquisition during transient and cyclic testing on saturated samples, the increased performance allowed for rather sophisticated testing on dry samples of sand. Transducer excitation was provided by a separate RDP Modular 600 amplifier unit capable of supplying regulated DC and AC excitation voltages. Transducer signals could then be amplified as appropriate to produce a ±10 Volt DC output range. The data acquisition has become the responsibility of a 16-bit, 32 channel analogue-digital card located in a Pentium 200 computer. A MSVisualBasic program issues acquisition commands to this board, and downloads the subsequent digital values. To eliminate noise induced by radio-frequency interference emanating from the stepper motors, each channel is averaged over a 40 ms period. The program duly processes the raw data, writes to file both raw data and processed data, and provides a graphical display of the processed data. The processing of the data reduces the moment to units of force ($M/2R$) and rotation to units of displacement ($2R\delta\theta$). The data processing also accounts for the rotation of the footing on the vertical and horizontal components of load. The acquisition interval can be controlled directly from the

program, with a peak rate of 20 Hz available, when acquiring in this mode (not 25 Hz due to processing and graphics overheads which occur during the acquisition sub-routine).

2.2.3 The Transducer System and Typical Calibration

The loads on the footing are measured using a 'Cambridge' style load cell which is capable of detecting *V*, *M*, and *H* loads applied to the footing (Bransby, 1973). A schematic diagram of the load cell is shown in Figure 2.3. Two blocks are joined by a system of strain-gauged webs. There are two pairs of vertical webs located at each end of the load cell (*LV*1 and *LV*2), whilst there are four horizontal webs (*LH*). Each web is strain-gauged on both sides, with the gauges connected into Wheatstone bridge circuits. The vertical circuits (*LV*1 and *LV*2) are comprised of the four active gauges plus four dummy gauges (which are located on a solid part of the load cell), whilst the horizontal circuit is comprised of all eight active gauges. The load cell is wired so that each circuit is powered by the same regulated 10 Volt DC supply. The resulting signal from each circuit is amplified to appropriate levels using the RDP unit.

The active face incorporates the horizontal webs and is bolted to the footing whilst the passive face is bolted to the shaft of the loading rig. As the loading arm moves through the desired displacement path the soil resistance leads to loads being transferred through the different webs from the loading arm to the footing. Clearly the average strain of the vertical webs provides the vertical component of load, the difference of the strain in the opposing vertical webs the moment load, and the strain in the horizontal webs will provide the horizontal load. There is a small degree of cross-coupling depending on where the load reference point is taken. Each of the webs has been designed so that the maximum strain does not exceed 1000 με which is the maximum permissible working strain of the strain gauges. In general the absolute maximum working loads of the load cell are calculated to be 2400N (vertical), 500N (horizontal) and 50Nm (moment at low vertical loads). The amount of allowable moment load is restricted by the amount of vertical load also being applied, and at high vertical loads the allowable moment load is reduced considerably.

The load cell needs to be calibrated for the load reference point that is appropriate for the tests. In all testing that took place the load reference point was taken to be at the mudline, which was 33mm below the active face of the load cell. A special calibration unit had been previously devised for calibration of these particular load cells. The passive face of the load cell is bolted to the calibration unit, whilst a spacer and load application block are bolted to the active face. A typical set-up is shown in Figure 2.4. Calibration involves changing one of the components of load (*i.e. V*) whilst keeping the others constant (*i.e. H*

and *M*). Electronic readings of each of the strain gauge circuits are taken. In this way it is possible to evaluate the cross-coupling due to the applied loads. A typical calibration chart looks like Figure 2.5 for vertical loading. Clearly as the vertical load is increased there are changes in the electronic output for both of the vertical web strain gauge circuits. The increase in vertical load has a small, but not negligible, effect on the measurements for the horizontal circuit. It is possible to develop a matrix relating loads to output measurements from each strain gauge circuit by taking the slopes of these curves. The inversion of such a matrix leads to the relationship between loads and the output digital signals. This can then be used within the acquisition program so that loads can be determined quickly during the testing:

$$\begin{Bmatrix} V \\ H \\ M \end{Bmatrix} = \begin{bmatrix} 161.3008 & 157.5077 & 0.6270 \\ -0.5801 & 1.7611 & 67.8285 \\ -4.1301 & 4.0946 & 2.4342 \end{bmatrix} \begin{Bmatrix} LV1 \\ LV2 \\ LH \end{Bmatrix} \quad \text{.....} \quad 2.1$$

The appropriate units for V and H are Newtons, M is in Nm, and $LV1$, $LV2$ and LH are specified in volts.

Throughout the testing the load cell was calibrated three times and there was no significant difference in the resulting calibration matrix. A further check on the accuracy of the calibration is to apply known combinations of load and compare to the electronically determined combinations. Table 2.1 shows such a test where for the load combinations applied the maximum error was less than two percent, and was for load combinations which consisted of large combinations of all three load components. It might be that the cross-coupling between the different circuits is slightly non-linear, though in deriving the calibration matrix it has been assumed to be linear.

A system of three long range LVDTs have been used to provide coarse measurement of the footing displacement. These LVDTs are clearly shown in Figure 2.1, where it can be seen that they measure the displacement of the two sliding plates and the rotating arm of the loading rig. From these measurements it is possible to determine what the corresponding footing displacement is. It is clear that as loads are applied to the footing it becomes necessary to adjust for the finite stiffness of the loading rig system. For loading tests on clay or on a loose carbonate material this adjustment represents a small proportion of the measured displacements. However, on dense sand the adjustment becomes a large percentage of the total measurement, and it becomes necessary to determine another means of measuring footing displacement. The coarse displacement system was used in the carbonate sand tests, due to the large displacements encountered, and was also used in the

dense sand tests primarily for a global reference system as well as allowing some cross-checking on displacements. The LVDTs were obtained from RDP Electronics and are powered by a 5 Volt RMS AC power supply. The resulting output signal is amplified so that suitable resolution on the measurement can be obtained. All relevant details of the coarse LVDTs are shown in Table 2.2, which also lists appropriate calibration constants. Calibration involves moving the LVDT through a known distance and observing the change in digital output. In all cases the output was observed to be linear, as expected.

On the dense sand the long range displacement measuring system is clearly inappropriate, as the uncertainty gained by adjusting for the rig stiffness is of the same order as the actual measurements. It is necessary to use an alternative system of small LVDTs to measure explicitly the movements of the footing. The LVDTs are attached to the footing from a small frame which is attached to the sample tank - this means that the LVDT measurement is free from any load related stiffness complications. Each LVDT has a range of 10mm and they are arranged so that it is possible to determine trigonometrically the components of movement $\{\delta w : 2R\delta\theta : \delta u\}$. This transformation can be easily coded within the control and data acquisition program. The measure of rotation is converted to units of displacement by accounting for the footing diameter. Similarly it is necessary to adjust the measure of moment to units of force by dividing by the diameter. This standardises the measurements according to the guidelines set out by Butterfield *et. al.* (1997) which are work conjugate and dimensionally consistent. The small displacement transducers are also powered by 5 Volt RMS AC voltages, and the resulting output signals are amplified by the RDP unit so that acceptable resolution is obtained.

The calibration was carried out using a micrometer measurement device converted for LVDT calibration. The accuracy of the small transducer system could be determined by comparing the measurements from the large displacement LVDT system for large movements under zero load. The large movements guarantee that resolution errors become smaller, whilst zero load guarantees that rig stiffness becomes negligible. The measured displacements could also be compared to dial gauge measurements, and specified movements of the stepper motors. Accuracy was within the noise levels of the signals. Appropriate information about the transducers can be obtained also in Table 2.2 whilst information about the trigonometric transformation can be obtained be obtained from Appendix B.

For footings on the saturated sand a system of pore fluid transducers were used to determine the fluid response. These transducers consist of a strain-gauged diaphragm, one

side of which is vented to the atmosphere, whilst the other side is exposed to the fluid of unknown pressure. They are typically powered by a 10 Volt DC regulated supply, and require the resulting output signal to be amplified substantially to gain significant resolution. In all tests on saturated sand a single transducer located in the centre of the footing was used, and in some of the tests three pressure transducers were used. Where three were used the other two were placed along the plane of the loading at the perimeter of the footing. This was to enable an estimation of the distribution of pore fluid load underneath footing in response to the applied loading. All transducers were calibrated with air over their full range of operation with details shown in Table 2.2. The use of air in calibration has a negligible effect on the response of the transducer when compared to the response under the effect of silicon oil. The transducers are screwed into the footing but are isolated from the soil by the use of a saturated vyon filter. They are usually fixed to the footing at the last possible moment.

Figure 2.6 shows the typical noise levels for the transducers sampled at 2Hz over a period of 60 minutes. A measure of the level of noise is shown as the standard deviation of the acquired signals for each transducer. It is clear that very good resolution on measurements is possible under the present set-up coupled with an ability to sample at a much faster rate than could be previously attainable.

2.2.4 Control of Rig

The program allows the control of each of the three stepper motors independently. Typical control commands are issued from the program, via a RS232 link, to an independent stepper motor control unit. This unit accepts ASCII commands, which specify displacements, velocities, and accelerations in terms of steps and seconds where appropriate. Where the movement of the axis is entirely displacement controlled the unit will instruct the stepper motor to travel a certain displacement at the specified velocity and acceleration. Where much better control is required on the axis movement a digital PID (Clarke, 1984) control loop is used in which the velocity and direction of the stepper motor is used as the control signal. Typically the new control signal depends on the error and can be determined by:

$$u = k\left(e + T_d \frac{de}{dt} + \frac{1}{T_i}\int e dt \right) \quad \text{2.2}$$

where e is the error, k is the gain, T_d is the derivative time and T_i is the integral time. The error used in the algorithm is the current value (as taken from the analogue-digital

conversion) less a set-point that must be specified. The derivative and the integral are evaluated numerically within the program. To control the contribution of the derivative part of the algorithm it has been necessary to adopt an exponential smoothing process on the error. To determine the values of the gain, derivative time and integral time a series of preliminary experiments were undertaken in which a step change in load (or displacement) was attempted to be followed. These parameters depend heavily on the mean vertical load being applied to the footing, the range in loads being applied, as well as the stiffness of the soil sample.

As the testing progressed it was thought to be most useful to allow for manual control of the gain (via buttons on the main program panel) particularly during the cyclic testing. Using this implementation it was possible to provide independent control on all three axes using either force or displacement set-points, or a combination of both. A more sophisticated control implementation could make use of an adaptive generalised predictive control (Clarke *et. al.*, 1987) algorithm, though this was seen to be beyond the needs of the present set-up. An adaptive algorithm is self-tuning, and as such is very difficult to implement in a stable and effective manner. Clearly, the best results are obtained if the PID loop is being run as fast as signals can be sent to the stepper motor controller (~20Hz). However for certain long tests (cyclic tests up to 20 minutes) there will be an excess of data collected if it is also sampled at that rate (12 channels at 20 Hz at double precision numbers). In this case the data logging subroutine is altered so that data are collected at a slower rate.

The program has been structured such that the user can implement sequences of moves as and when required, often utilising prior test results to decide future test sequences (on the same test site). The most important moves are stored using a sequence control dialog box - these include constant velocity move routines, displacement routines (incorporating either vertical displacement hold, vertical load hold or no hold routines) and hold routines. More complicated moves are imported by reading line-by-line a file stored on disc which contains the set-points, for that time step, for the three axes.

The various routines that are used typically incorporate some component of control implicitly within the program. For example the vertical moves downward and upward are written such that the components of horizontal and moment load are kept to less than one percent of the vertical load. Therefore the model footing may rotate or move horizontally slightly during the vertical movement phases of the testing. This was seen to be important as it makes the interpretation of the test results much simpler. This is particularly useful for

the swipe tests, in which it is important to start from the vertical load apex of any yield surface that may exist. Control on vertical penetration was also incorporated within the swipe sub-routines, such that the effect of the rig-stiffness on vertical displacement could be accounted for within the experiment. Load control was also available within the swipe procedures.

2.2.5 Sample Containment, Loading Rig Attachment and Plumbing

During the testing program three different types of samples were used. The first was a loose carbonate sand, which was placed into 450mm diameter tubs, of height 450 mm, similar to those used by Martin (1994) and Mangal (1999). The loading rig was bolted firmly to the top flange of the tanks, as was the small LVDT system.

The dense sand was contained within large sample tanks of internal diameter 1100mm, and depth 250mm, the purpose of which was to provide a single sample large enough to perform multiple tests upon. Figure 2.7 shows a schematic diagram of the typical layout of the test sites, where loading of a footing was performed on the perimeter sites, and a vertical bearing capacity test was performed in the centre (for sample characterisation). Figure 2.8 shows the general layout of the test apparatus. Two I-beams span the tank, upon which the loading rig is firmly bolted. The small LVDT system is located on a small rectangular hollow section which also spans across the tank, bolted firmly to the flange, so that measurements of foundation movements relative to the tank are taken.

For the saturated dense sand testing the sample was saturated with a silicon oil of viscosity 100 centistoke to model drainage times appropriate to offshore structures. To prepare the sample into a dense state it was necessary to have suitable drainage at the base of the sample container. A sheet of vyon was stretched and fixed to the base plate to prevent any soil being washed through the plumbing fixtures. The set-up for the loading rig and LVDT system was similar as for the dry sand.

2.3 THE FOUNDATIONS

For the carbonate sand testing the compressible nature of the material dictated that a footing of diameter 150mm was used. The footing was flat. However, at the typical testing load of 1600N (vertical load) the footing had penetrated 60mm into the soil.

Four footings were used during the dry sand testing to explore the various effects of skirt penetration - the footing diameter used during this testing was 100mm. It is useful to define

the non-dimensional embedment ratio (y), as the skirt length (L) divided by the diameter (D);

$$y = L/D \quad \text{.....2.3}$$

to compare different suction caissons. The two platforms that have used the suction caisson technology on dense sand strata both used caissons with an embedment ratio of 0.33 - the previous testing at Oxford and NGI aimed at resolving site specific problems associated with the second of these platforms (Sleipner Vest) and therefore also was at this ratio (unfortunately these results are proprietary). It was therefore appropriate to carry out some of the testing at this ratio. It is necessary to be able to compare the results with a variety of different skirt depths so ratios of 0, 0.166 and 0.66 were also used. The results from an embedment ratio of 0 can be compared to a large database available in the literature, particularly the series of tests, also conducted at Oxford, by Gottardi and Houlsby (1995). It should be noted from Figure 1.9 that there is a wide range of embedment ratios used, though caissons on sand tend to have a ratio of unity or less, whilst caissons in clay can have ratios of up to five.

During the saturated sand testing it was necessary to use a footing of diameter 150mm so that partially drained behaviour could be obtained. Again an embedment ratio of 0.33 was used, as well as a flat footing. Several of the 100mm footings were also used to investigate the effects of scale. It was necessary to measure pore fluid pressures, and in most cases this was done at the centre of the footing. In some cases it was also possible to measure the pore fluid pressures at the perimeter of the footings along the plane of loading. However, this was restricted to the 150mm diameter footings. The choice of footing size was dictated by the relative pore fluid movement within the soil - this depends on a number of factors including the footing size, the soil grain size distribution and the viscosity of the fluid.

2.4 THE SAND SPECIMENS

2.4.1 Carbonate Sand

The material used for the carbonate sand testing was obtained from a grab sample at the Goodwyn site off the North West Shelf of Western Australia. Carbonate sands can have in-situ void ratios of up to two, and are problematic soils in that upon shearing there can be large volume contraction. For this testing program the decision was taken to test the material at its loosest state, primarily to maximise the diversity with other data. The material, which had been stored in a saturated state, was firstly dried, then broken up

before being sieved to remove the larger shell particles. The sieving process involved two phases, firstly through a 2.36mm sieve to remove any large shell particles, before being passed through a 1mm sieve. The resulting grading curve for the material is shown on Figure 2.9. Each individual sample was prepared by carefully allowing the material to fall slightly from a scoop into the test container. This method had been used before in the preparation of loose samples and produces reasonably uniform loose samples (particularly given that large footing displacements were expected). A repeatable density of 9.32 kN/m^3 was obtained, with the sample being levelled using a vacuum technique, prior to the test sequence.

A program of five different test types was developed (described in detail later) to explore the yield surface and its evolution. It was expected that large displacements would occur during the testing, thus the large transducer system was used (except for the elasticity tests, where the smaller more accurate measurement system was used). This large transducer system necessitates the need to account for the stiffness of the rig between the measured locations and the footing via a 3x3 rig stiffness matrix, [RSM].

$$\begin{Bmatrix} dw \\ du \\ 2R\,dq \end{Bmatrix}_{Footing} = \begin{Bmatrix} dw \\ du \\ 2R\,dq \end{Bmatrix}_{Measured} + [RSM] \begin{Bmatrix} V \\ H \\ M/2R \end{Bmatrix} \quad \text{.....2.4a}$$

where [RSM] is defined as:

$$\begin{bmatrix} -5.09E-4 & -1.60E-4 & 8.31E-4 \\ -1.07E-4 & -2.06E-3 & 3.83E-3 \\ 8.92E-6 & 2.61E-4 & -1.81E-3 \end{bmatrix} \text{ for } H < 0 \text{.....2.4b}$$

$$\begin{bmatrix} -5.09E-4 & 1.70E-6 & 8.31E-4 \\ -1.07E-4 & -2.06E-3 & 3.83E-3 \\ 8.92E-6 & 2.49E-4 & -1.81E-3 \end{bmatrix} \text{ for } H > 0 \text{.....2.4c}$$

where displacements are in mm and forces are in N. The use of the large LVDTs was justified, as the ratio of vertical elastic stiffness to vertical plastic stiffness (k_e/k_p), were typically greater than 50, which suggests that the load path tracked during the tests would in fact closely approximate the yield surface. The increase in vertical displacement due to the finite rig stiffness could also be assumed to be minimal, when comparing the tracked load path to the actual yield surface.

2.4.2 Dry Dense Sand

The sand used throughout the main testing was Baskarp Cyclone sand produced using a cyclone separation system. The choice of sand was dictated by fact that it had been used previously in laboratory testing of the transient behaviour of shallow foundations (Houlsby, 1995 and Mangal, 1999). It was, in both instances, saturated by silicone oil, to model drainage times appropriate to the loading of offshore foundations. Figure 2.9 shows the grading curve of the sand in relation to various other materials that have been used for 1g scale modelling of footings. Also shown on the Figure are the grading curve boundaries of the two sands found at the site of the Draupner E and Sleipner T platforms. Table 2.3 gives the standard geotechnical characteristics of the sand.

The samples were prepared by loosely placing the soil within the sample container. A smooth wooden lid was placed upon the very loose sand, along with a very small amount of lead weights (to apply a slight confining pressure), and the sample was vibrated until no further downward movement of the wooden lid was observed. This method, also used by Lau (1986), led to the production of very dense samples with typical characteristics shown in Table 2.4.

At the start of a test the footing was lowered down to the sample surface until a slight vertical load (~5N) was registered by the load cell. If the footing was flat the short LVDT frame and transducers were fixed to both the sample tank and the footing, after which they were zeroed. If the footing had a skirt it was lowered into the soil until the underbase of the footing made contact with the soil. This proceeded at a rate of 0.05 mm/s and for an embedment ratio of 0.33 the vertical load required to reach full touchdown was up to 130N. The vertical load was then reduced to zero, after which the short LVDT system was attached and zeroed. The test then proceeded, incorporating as many events as were possible, to maximise the use of each test-site. The use of multiple testing on each site could be justified in that, unless there was significant disturbance to the site, by further plastic vertical penetration of the footing, an essentially undisturbed state could be reached. Once all events had been undertaken the footing was unloaded to $V = 0$ N, at which stage the short LVDT system was removed. The footing was then extracted from the soil sample, and the rig moved to a new location.

2.4.3 Saturated Dense Sand

The saturated sand samples were prepared using a slightly different procedure, to that of dry sand, as it was not possible to permeate the oil upwards, through an already densely formed bed of soil - the oil was too viscous for such a procedure. The sample was initially

saturated by allowing the silicon oil to filter up from the base of the tank through very loosely placed sand. A vacuum was applied above the liquefied soil/oil mixture to ensure that the sample was fully saturated. The sample was then allowed to sediment under the self weight of the particles. Once the soil had undergone a sufficient amount of sedimentation it was then possible to start the densification procedure. This consisted of applying alternate combinations of vibration, via a large vibrating motor attached to the base of the sample, and downward hydraulic gradient. The downward hydraulic gradient is created by developing a positive pressure in the chamber above the fluid surface. The containment tank had been specifically designed to withstand a positive pressure of up to 100 kPa. The theory being that the vibration reduces the effective stresses acting on the particles, whilst the downward hydraulic gradient increases the effective stresses pushing the particles into a denser configuration. By alternating this combination over many hours it is possible to produce very dense sand samples. A large stirring device has also been developed so that the soil sample could be reconstituted, thus allowing a large number of samples to be prepared. This preparation procedure has allowed a cost-effective approach which can enable a large throughput of testing to be performed. The testing on saturated sand described in this thesis has been restricted to one sample of sand.

The preparation for a test on the saturated sand follows a procedure similar to that on the dry sand. Prior to attaching the footing to the loading shaft the central pressure transducer is added to the footing, the external transducers are not added until the footing is totally embedded. This assists with keeping them de-aired. The footing is lowered slowly into the oil and onto the sand until the skirt makes contact. It is necessary to have a small bleed hole for these footings so that air can escape from within the bucket cavity without causing a piping failure around the base of the skirt due to an overpressure. It is also important to maintain a slow embedment speed - a value of 0.05mm/s was chosen during these tests. Touchdown of the base of the caisson can be observed by the escape of small amount of soil from the bleedhole, as well as the noticeable increase in total vertical load. In most tests the vertical load was taken to 75N before the bleedhole was closed. The footing load was then reduced to zero so that the external pressure transducers, and the small LVDT system, could be attached. The pressure transducers and the LVDT system were then zeroed. The test usually commenced by loading the footing to 75N and holding for several minutes so that consolidation could occur. The main test sequence could then begin.

2.4.3.1 Element Testing of the Baskarp Cyclone Sand

The main material used during the testing was Baskarp Cyclone sand (see Table 2.3 for geotechnical properties). This material was chosen so that when used with the 100 centistoke oil, a specific degree of drainage occurred for a given loading situation. The silicon oil (also see Table 2.3 for properties) modifies the stress strain behaviour of the material slightly when compared water. This modification of the stress strain behaviour is evident in Figure 2.10 which illustrates results (NGI, 1994) from drained triaxial compression tests on two samples (one saturated in oil, the other in water), both conducted from an initial axial stress of 10kPa. Further results of drained triaxial compression tests on samples of the same relative density (80%) are shown in Figure 2.11. Three tests using water saturated samples and the one test using an oil saturated sample are illustrated. It is observed that the oil saturated sample possesses a peak friction angle reduced by about three degrees compared to water, with the dilation rate also modified (the peak rate is about half that of the water saturated sample). Interestingly the dilational behaviour of the oil-saturated sample is comparable to the water-saturated sample with an initial vertical stress of 50kPa. Figure 2.12 shows three undrained triaxial tests (NGI, 1994) highlighting that the oil tends to soften the stiffness response of the soil element, which is in line with the observation of the reduced peak friction angle.

2.4.3.2 Drained Testing

Characterisation of the prepared samples was essential so that a comparison across different sample tanks could be made. The initial characterisation was made in terms of relative density, in a similar way to Gottardi and Houlsby (1995). A mean relative density of 97.8% and a standard deviation of 1.81% was obtained throughout the testing. A more important characterisation was made by determining a bearing capacity factor (and hence friction angle) of the sample by conducting a vertical loading test. This test, typically conducted in the centre of the sample, used a 50mm diameter footing which was loaded through failure to a displacement of about 10mm. On several samples multiple bearing capacity tests were conducted to examine the consistency of the samples. Figure 2.13 shows all the bearing capacity tests (these are also tabulated in Table 2.4) conducted during the study - on each curve the maximum value is indicated by a closed circle. If the peak vertical bearing capacity of a flat footing is defined as;

$$V_{peak} = \frac{1}{2} D N_g^* g' \left(\frac{\pi D^2}{4} \right) \quad \text{.....2.5}$$

then it is possible to determine a value for the bearing capacity factor, N_g^*. By following the procedures of Bolton (1986) it is possible to deduce a value for the angle of friction (either triaxial or plane strain) based on the relative density of the sand. In this case the triaxial angle of friction has been plotted against N_g^* in Figure 2.14, and compared to a theoretical curve determined by Bolton and Lau (1993) using the method of characteristics. There is a reasonable correlation between the experimental and theoretical results. The level of scatter within the experimental results is because the bearing capacity factor varies significantly for small changes in the relative density, at the high friction angles being explored. A further measure of consistency across the sample was undertaken with the use of a 7.94mm diameter cone penetrometer. These tests were carried out on three individual samples and indicated that the samples were reasonably uniform in both depth and breadth. To give an example of the degree of variation on one sample Figure 2.15 shows the five cone penetration tests carried out on tank DM7, with positive load indicating penetration, negative load being the extraction of the cone. The sample appears to be reasonably consistent.

2.4.3.3 Transient Testing

The sand sample, on which the majority of the transient testing was conducted, was estimated to have a dry relative density of approximately 83%. To determine the geotechnical properties of the sample it was necessary to conduct more extensive site investigation tests. Cone penetration tests were performed throughout the sample to confirm uniformity between test sites and over the depth of the sample. Typical cone penetration tests are shown in Figure 2.16. This cone penetrometer had been used in previous model testing (Mangal, 1999) during which empirical correlations were developed between cone penetration test results and soil parameters. Mangal (1999) could only perform one test per sample, and as such had to develop a rigorous method for comparing sample properties. From a large number of test results the following relationship had been defined between q_c (in kPa) at 75mm depth and relative density (%):

$$q_c = 0.044 \exp(0.11 R_D) \quad \text{.....2.6}$$

From this empirical correlation it is possible to estimate the local relative density at the reference depth of 75 mm. This leads to an estimation of relative density of approximately 79% and a peak friction angle of 41 degrees. It is clear from the cone penetration tests that the strength of the soil increases slightly with depth - it is possible that the relative density

increases towards the base. These cone tests were conducted on sites after the footing tests had been completed, so the surface soil has been slightly disturbed and is thus weaker.

After five test sites had been used the sample underwent further preparation so that the final three sites were in a denser state. This was so the more interesting experimental results could be investigated further. This denser state was estimated to have a relative density of 94%. Cone penetration tests conducted before and after the footing tests indicated a relative density of 92% (a friction angle of 43 degrees). It was possible to conduct a large number of transient tests (up to 150) on each site, which was believed to lead to a better understanding of critical behaviour, than to conduct numerous tests on many undisturbed sites. The initial testing was very exploratory in nature, but as the key mechanisms and behaviour became more apparent, the testing became more focussed. The key results presented in the thesis are extracted from four highly focussed tests.

2.4.3.4 Consolidation Tests

During the saturated sand testing it was possible to carry out consolidation tests to give an indication of the rate of fluid movement within the soil matrix. A consolidation test involves applying a step change in load to the footing and measuring both the resulting displacement path and the pore fluid response. Initially the increment is undrained so the entire load is transferred to the fluid, as the time passes there is sufficient migration of fluid away from beneath the footing base that the fluid pressure drops off. The migration of fluid allows volume change (consolidation) of the soil matrix as the sand grains in various positions beneath the footing are allowed to move (dilate or contract as appropriate).

Figure 2.17(a) shows the response of a consolidation loading test undertaken during the initial loading of the foundation. It is clearly shown that upon application of the 25N load most of the load (20N) is transferred to the pore fluid. After a significant amount of time the load transfers to the soil skeleton as volume change occurs. This suggests that in the initial stages of loading of the foundation it is critical that drainage is provided so that the soil skeleton can consolidate quickly. Failure to provide for drainage may result in instability of the caisson foundation during the first onset of large loading. It was clear that as the testing proceeded on each footing the soil within the caisson skirt became heavily consolidated, such that the fluid pressure response dissipated more quickly. It was unclear how the soil beneath the skirt tip behaves, and at what stage this became consolidated, as it was not possible to measure pore fluid responses at that location. A typical consolidation test conducted at a later stage during the testing is shown in Figure 2.17(b) where the t_{50} time (~80s) is considerably less than indicated in Figure 2.17(a) (t_{50} ~ 300s). The cyclic

loading tests were carried out at rates such that transient pore pressures would be significant, as indicated by these t_{50} times.

Figure 2.18 shows the evolution of consolidation times throughout the testing sequence SM1-6. The evolution can be followed by realising that as the testing program progressed the initial vertical loads for the consolidation tests are increased - the subsequent step change is equal to the initial vertical load. Clearly it can be seen that as the vertical loads are increased the coefficient of consolidation also increases. There is also a secondary effect that there is a net increase in c_v due to previous consolidation tests and loading histories, as indicated in Figure 2.17. Figure 2.19 shows the ratio of pore fluid pressure developed underneath the base of the footing with the initial vertical load. As the vertical load is increased, due to the increase in the consolidation coefficient, the pore pressure ratio drops off, appearing to level out at 60%. At the very low levels of loads the pore pressure ratio is close to unity, implying that all load is transferred to pore fluid load.

Finnie (1993) defined a non-dimensional footing velocity (for spudcan footings) to determine the mode of footing response that was being investigated:

$$v_n = \frac{vD}{c_v} \quad \text{.....} \quad 2.7$$

It is suggested that for $v_n > 10$ then the footing response is undrained, however for $v_n < 0.01$ the footing response is essentially drained. Finnie based these limits on investigations into footing response on carbonate sand and silt in a medium to loose state. Figure 2.20 shows the relationship, noting that for loose sands the undrained response is lower than for the drained case. Kolk *et. al.* (1997) suggest that these limits may also apply to dense sands where the reverse response is true. In this investigation the range of non-dimensional velocities that could be achieved was on the lower end of the scale with a maximum of about 3 and a minimum well below 0.01. The typical c_v values encountered in this investigation were estimated to be between 50 mm^2/s and 500 mm^2/s depending on the loading history as described previously. The higher end of the scale was investigated in a fourth year project (Johnson, 1999) in which much faster velocities could be obtained using hydraulic actuators in Oxford University's Structural Dynamics Laboratory. However, if one considers a design c_v of 0.5 m^2/s such as that suggested for the Draupner platform in the paper by Bye *et. al.* (1995), and a bucket diameter of 12m then the drained response would occur at a velocity of 0.42 mm/s whilst an undrained response would occur at a velocity of 0.42 m/s. Clearly the loading on the structure, where typical wave loading occurs at periods of 16 seconds, is going to result in responses at the lower end of the scale.

This is also going to be very much the case for minimum facility designs, where the diameter of the foundation are likely to be around 5 m through to 10 m. The responses investigated in this thesis are at the partially drained loading rate likely to be experienced by real offshore foundations.

2.5 TYPICAL DRY SAND TESTING PROCEDURES

Before examining the results of the investigation, it is worthwhile detailing the various types of tests that were used to map out the drained response of the footing - these are shown schematically in Figure 2.21. Initial testing and interpretation of footings on dense sand led to a further hypothesis that the behaviour of the footing has a dependence on the ratio of the maximum vertical load previously experienced by the footing to the peak bearing capacity sustainable by the soil (that is V_o/V_{peak}). The testing program was thus designed to explore this hypothesis as well as the usual hypotheses associated with plasticity theory, as described in section 2.2. Different tests carried out included:

a) Swipe Tests: The majority of the testing comprised of swipe testing. A swipe test involves loading the footing to a given load ratio (V_o/V_{peak}) and then rotating or displacing horizontally (or any combination) the footing whilst keeping the vertical displacement constant. Using analogies with undrained triaxial testing Tan (1990) and Martin (1994) suggest that the load path traced under these imposed displacements paths is a direct indication of the shape of the yield surface. An initial assumption is that the hardening of the yield surface is a function of the vertical plastic stiffness. If the ratio of vertical elastic stiffness to vertical plastic stiffness is large then as the swipe test is being performed there should be relatively little hardening of the yield surface. This allows a reasonable estimate of the yield surface to be inferred. A correction can be made for the slight expansion of the yield surface, based on a predetermined hardening law, if this stiffness ratio is small. Similarly, the stiffness of the rig is finite, and, a correction needs to be made for the expansion of the yield surface, as a result of the increased penetration of the footing. This penetration is associated with the relaxation of the rig as the vertical load level drops off. During these tests this correction was performed by using the vertical displacement for feedback within the control program. By conducting swipe tests at different ratios of overconsolidation the behaviour with in the yield surface could also be examined. Swipe tests at very high overconsolidation ratios give an indication of the yield surface at low vertical load levels.

b) Constant Load Tests: The expansion of the yield surface (that is the hardening behaviour) can be examined by conducting swipe tests at constant vertical load rather than constant vertical displacement.

c) Vertical Loading Tests: These tests comprise of loading the footing vertically, usually to 2400N (the limit of the rig), and include unload/reload loops at 1000N and 2000N. At the very simplest level the hardening of the yield surface is linked solely to the vertical plastic displacement, thus these tests give an explicit indication of a possible hardening relationship - though no indication of the effects of sideways movement on the hardening is given.

d) Elasticity Tests: Whilst the main objective of the testing was to obtain information about the plastic response of the footing several tests were undertaken to evaluate the elastic behaviour within the yield surface. The results from these tests can be compared to finite element results (Bell, 1991), though care should be taken in the interpretation due to the possible effects of the close boundaries imposed by the sample tank. In these tests the footing was typically cycled between increasing values of load (keeping other loads constant) so that the boundary between elastic and plastic behaviour could be evaluated.

e) Loop Events: These events consist of completing a circle in $\{2R\,dq : du\}$ space through the use of control on three axes. The vertical load level is kept constant, whilst individual values for horizontal and rotational displacement are used as set-points for the appropriate axes. By completing the test at constant vertical load the displacement path imposed should produce an indication of the shape of the yield surface in $H:M/2R$ load space.

f) Radial Loading Tests: These tests involve applying a distinct path in load space to the footing, and examining the resultant path in displacement space. Typically the level of horizontal and/or moment load is specified as a fraction of the vertical load level, using the various control routines as described above. These tests can also give an indication of the possible hardening relationship for the yield surface.

For the drained dense sand testing a total of ten sample tanks were prepared, which enabled 80 test sites, and 250 individual test events to be completed. Table 2.5 briefly describes the purpose of each of the 10 different test tanks. For the loose carbonate sand a total of 18 tests were completed, these are tabulated in Table 2.6. A complete factual compilation of all dry sand test results can be found in Byrne and Houlsby (2000).

2.6 TYPICAL SATURATED SAND TESTING PROCEDURES

As with the dry sand testing, there were also a variety of tests used for investigating the partially drained response of the soil. One such test is a monotonic move test in which the footing is moved through a particular displacement path at a prescribed velocity. These tests were mainly performed to investigate tensile behaviour but were also performed to investigate deviatoric movements. The main bulk of the testing, however, involved cyclic loading. To establish a framework for cyclic loading it is necessary to examine the processes that lead to the loading on the foundations.

2.6.1 From Wave Mechanics to Soil Mechanics

An understanding of the state of the ocean environment is an essential step to describing the typical loading regimes prevalent on an offshore structure. Ocean waves can be thought of as composed of a large number of wavelets of different heights, periods and directions superimposed on one another, thus leading to the confused appearance of the water state (Figure 2.22). Over an interval of say three hours the statistics of the sea surface do not change dramatically, so that a power spectrum of the surface elevations will represent the sea state for that particular three-hour period. The surface elevation spectrum (power spectrum) takes the form where the spectral ordinate is amplitude density^2/2 plotted against frequency (Figure 2.23). For complex wave descriptions (to include directional spreading) these would be described in a three dimensional space giving a complete characterisation of the ocean environment. However as the sea approaches extreme states it is assumed to adopt a single direction (Tromans *et. al.,* 1991).

Several spectra have been developed based on information gathered at certain sites (for example Bretschneider, 1959, Pierson *et. al.*, 1964 and Hasslemann *et. al.*, 1980). These spectra are essentially of the same form described by two variables - H_s (significant wave height) and T_z (zero mean crossing period):

$$S_{hh}(f) = \frac{AH_s^2}{T_z^4 f^4} \exp\left(\frac{-B}{T_z^4 f^4}\right) \quad \text{.....2.8}$$

where A and B depend on the general locality of the data obtained and f is frequency. Typically North Sea structures are designed using the JONSWAP spectrum (Hasslemann *et. al.,* 1973). The significant wave height, H_s, is in fact the average height that observers would report. However, it is also statistically the average height of the highest one third of the waves in the sea state. The zero mean crossing period, T_z, is obtained from the mean time between up crossings of the mean water level. Cartwright and Longuet-Higgins

(1956) have described in great detail the statistics of heights of waves in seastates and suggest many useful relationships, based on the assumption of a Rayleigh distribution of wave heights. One of the more useful relationships is that the height of the most probable highest wave in 1000 waves (H_{max}) would be $1.86H_s$. The relationship between T_z and H_s is usually site dependent and would entail the production of a sea state scatter diagram. However, as the significant wave height approaches an extreme value (50 or 100 year return value) an association with the zero crossing period is assumed (Barltrop and Adams, 1991), dependant on the wave steepness:

$$2.46\sqrt{H_{\max}} < T_z < 3.70\sqrt{H_{\max}} \quad \text{.....} \quad 2.9$$

where H_{max} is in metres. Typically a storm may last for twenty-four hours or more, with the values of H_s and T_z initially increasing to a peak, before subsiding.

2.6.2 State of the Art Modelling of Extreme Events

The theory of large ocean waves has been the focus of much research over the past ten years, principally at Shell's research laboratory in Rijswijk, The Netherlands (Tromans *et. al.*, 1991, Tromans *et. al.*, 1992, Taylor, 1992, Elzinga and Tromans, 1992, Jonathan *et. al.*, 1994, Taylor *et. al.*, 1995, Tromans *et. al.*, 1995). The impetus for this research is a renewed understanding of extreme environmental conditions as data from instrumented platforms becomes available, and is consequently analysed. The outcome of the research is that the extreme events from lengthy time domain simulations of random waves in a storm can be generated within short time sequences using a deterministic method. The use of this wave model means that a probabilistic representation of the extreme response of a structure can be generated within manageable computing times. This approach, appropriately named 'NewWave' (Tromans *et. al.*, 1991), assumes that if wave elevations are modelled as a Gaussian random process, a probabilistic analysis can be used to calculate the most probable ocean surface elevation around a crest (based on the work of Lindgren, 1970). This most probable surface elevation is distinguished from other deterministic methods (such as Stokes V) by its probabilistic basis and its broad banded, non-periodic nature. The typical 'NewWave' shape is shown in Figure 2.24, and is derived by taking the autocorrelation function of the surface elevations, which are described by the wave spectrum. As the distance from the crest increases then the average elevations tend to a flat sea.

The 'NewWave' surface elevation provides a straightforward model for the wave kinematics, and hence loading. Tromans *et. al.* (1991) shows that the results predicted

match the lengthy time domain simulations and are much better than the deterministic periodic models. Several researchers have provided further research on the kinematics to account for non-linearities inherent in the severe storm waves (for example Taylor, 1992). This newer model compares well to both time domain simulations as well as measured extreme loading (Elzinga *et. al.*, 1992), when predicting the extreme loading on quasi-static structures. It is recognised that when determining the response of a structure, which behaves dynamically, the extreme response may not occur at the extreme surface elevation. Taylor *et. al.* (1995) suggests a method in which the extreme event can be embedded in a randomly generated sea state, so that the response of a jack-up may be studied. This method allows the 'NewWave' to be constrained at a certain point in time such that, in statistical terms, it is indistinguishable from a purely random occurrence of a crest of that height. A typical constrained crest is shown in Figure 2.25.

2.6.3 Novel Geotechnical Storm Loading

A new experimental method for cyclic loading of caisson foundations has been used for this work, which has led to a better understanding of the foundation performance. Wave mechanics theorists have, as described above, made rapid progress over the past twenty years in developing new and improved models for representing the randomness of the sea surface, the most probable shape of extreme events, the kinematics of the waves and the subsequent loading on the structure (for example Tromans *et. al.*, 1992). A distinct lag is evident between this understanding and the types of loading regimes typically employed for cyclic loading in geotechnical model testing. A typical geotechnical storm sequence may consist of packets of sinusoidal cycles, of increasing amplitude (but same period), with the design wave amplitude at the finish (Schjetne *et. al.*, 1979). An example of a 3 hour duration storm is shown in Figure 2.26 (Hansteen, 1981). This duration can be varied to suit the circumstances being modelled, by using different storm compositions. Two assumptions are made, that random loading on the foundation can be represented by deterministic periodic waveforms, and that the total deformation of the foundation can be taken as the sum of deformations under these components (Miner, 1945). This approach is similar to that taken during fatigue analysis of an offshore structure (Wirsching *et. al.*, 1980), and is probably sufficient for foundation analysis where drainage times are sufficiently long, when compared to the length of the storm, that the response of the soil is essentially undrained.

It is debatable whether this approach is sufficient when dealing with the caisson foundation response on sand, in which drainage conditions and capacity are dependent on rates of

loading. Previous confidential research at Oxford (Houlsby, 1995) and NGI (Jostad *et. al.*, 1997) had indicated that the cyclic performance of the foundation was dependant on the amplitude and period of cycling. The tests at Oxford, which consisted of applying sinusoidal displacement paths, indicated that under some circumstances cycling could continue without foundation degradation, but under other circumstances the foundation suffered massive degradation. Figure 2.27 shows some typical test results, the axes labels have been removed but the reader will appreciate that on different occasions there appears to be stable or unstable behaviour. Tests at NGI (Jostad *et. al.*, 1997) show that the application of a small number of large amplitude cycles can cause rapid foundation degradation, even after the amplitude had been reduced. A typical example of this response is shown in Figure 2.28, in which three packages of cycles are applied to the foundation (as in Figure 2.29). The foundation under the first packet of cycles suffers relatively modest foundation settlement probably tending to a limiting value due to 'shakedown' effects. The middle package, consisting of three larger amplitude cycles appears to precipitate foundation failure. The three cycles of larger load cause some massive displacements, these displacements continue for the smaller cycles that follow. This would indicate that the existence of an extreme event within some cyclic parcels, and the associated mechanism of effective stress change dominate the foundation behaviour.

A typical result from a time domain analysis for the worst loaded leg for a jack-up unit is shown in Figure 2.30. This illustrates the problems of using the deterministic periodic waveform when the case of interest is the extreme event, and the ambient pore pressures are caused by some prior smaller level of cycling. The NGI represented similar occurrences for their model testing in the manner illustrated in Figure 2.29. They nested three larger amplitude sine waves within a long history of small amplitude sine waves of the same period. This is an attempt at developing an appropriate loading history but falls short of the physical reality (as shown in Figure 2.30). A new framework for developing the loading regimes to mimic expected regimes in the field is suggested. This framework, which requires some simplifying assumptions, is general enough so that boundaries to the overall performance can be found, rather than boundaries specific to any site or structure.

The number of cycles of various load magnitudes in a design storm are usually obtained from a Rayleigh distribution of wave loads, assuming that wave loads are proportional to wave heights (for example Lee and Focht, 1975; Schjetne *et. al.*, 1979; Høeg *et. al.*, 1977; Hansteen 1981). This assumes that the wave loading on the structure, and the associated structural response to that loading are linear processes. Both processes are actually non-

linear, and can lead to such effects as frequency multiplying of certain incident waves, as well as affecting the statistics of the random process (Barltrop and Adams, 1991). Much research is being pursued to determine the appropriate statistical response of loading on the structure (Tromans *et. al.*, 1992), but this response depends on the very complex non-linear transformation functions that are unique to each structure. Other research has determined methods in which the non-linear drag term of the Morison relationship (Morison *et. al.*, 1950) for wave loading can be appropriately linearised (for example Borgman, 1967, Borgman 1969, Rodenbusch *et. al.*, 1985, Teng *et. al.*, 1991). The approach followed in this thesis is to assume, similarly to previous methods, that the response spectra of the structure are linearly related to the wave height spectra. An alternative approach is to assume that the loading on the foundations follows the Gaussian distribution. Any deviation from this assumption being no different to the deviation from the Gaussian assumption, that is made for the waves themselves, and, which forms the basis for many wave mechanics theories.

Two further assumptions are required about the nature of the structure and the foundation. It is usual for fixed offshore structures, such as those likely to use suction caissons as foundations, for the structure to be designed so that its natural frequency is sufficiently different from the dominant frequency of the waves. It may be designed so that it is very stiff (fixed structure) or very flexible (compliant tower). The final assumption is that the natural frequency of the foundation is sufficiently different from the dominant frequencies of the load spectrum acting on each individual foundation. Rowe *et. al.* (1977) suggest that natural frequencies of the range 0.5 to 5 Hz might be typical for large offshore foundations. If these design approaches are adopted the effects of structural dynamics, and thus high dynamic amplification factors, are reduced. The use of these assumptions in this study is entirely appropriate, as they are typically used during the initial design of many offshore structures.

By making these assumptions the constrained 'NewWave' theory can be used to generate the necessary extreme events using a power spectrum of the same form as the wave spectrum. Typical extreme events are illustrated in Figure 2.31. Thus for vertical loading a significant load, V_s, and zero crossing period, T_{zv}, would encapsulate the vertical loading spectrum for one part of the foundation. The zero crossing period for the load magnitudes would be related to the zero crossing period for the wave heights. Horizontal and moment load would also be represented in a similar fashion. Foundation response can then be found for a variety of extreme events that change as V_s and T_{zv} are varied. As more research is

conducted into the areas of wave mechanics, wave loading, structural response and geotechnics, improvements on the 'NewWave' model for geotechnical cycling could be made. This would lead to a much greater understanding of the response of the soil to the foundation loading.

The testing regime suggested should allow the broad behaviour of the caisson in dense sand when subjected to some representative loading to be mapped out. The procedure outlined reduces the amount of variables to be examined thus leading to a manageable testing program. This program should lead to an identification of where the boundaries to behaviour lie and an understanding as to what mechanisms are important. This technique is viewed as better than using deterministic periodic cycling for this particular situation but it is only a ***first step*** to a solution of the problem of representative cyclic loading. Accurate modelling of the foundation behaviour would require a real-time simulation of random foundation loads including the non-linear effects of waves and wave loading on structures as well as the non linear-structural responses. Due to the dependence of these non-linear effects on the structure this very advanced type of modelling would be restricted to determination of foundation behaviour for specific cases, and would be difficult to use to map out general behaviour. Much more research is required before this idea could be implemented, though the development of a new laboratory in structural dynamics (Williams *et. al.*, 1998), coupled with recent research in wave mechanics (Suastika, 1997) could be used to meet this end.

A typical wave loading input sequence is shown in Figure 2.32, along with the actual loading sequence, which shows a very close correlation - an indication that the PID control loops were indeed working well. The power spectrum of both loading histories compare quite favourably. During the testing sequence it was necessary also to control the other components of load. These were usually kept constant at zero for horizontal and moment load, or at the initial load for vertical load. In total six major cyclic loading tests were conducted on different test sites and the full data set can be found in Byrne and Houlsby (2000). They are denoted by the prefix SM1. Table 2.7 shows the test sequence for test SM1-5. In this table the cyclic loading data indicate the size of the planned random loading sequence, and not the actual loading sequence, which may differ depending the performance of the load control routines. It was possible to conduct multiple sub-tests as long as account was taken of the loading history (in some cases up to 150 tests were performed). For example it was typical to load up to a small mean vertical load, carry out a suite of different loading, load up to a larger mean vertical load, carry out another suite of

loading and so on. It was important to ensure that each consecutive mean vertical load was greater than any vertical loads reached during the cyclic loading (*i.e.* ensuring normal consolidation). Once this was exhausted it was then important to examine overconsolidated behaviour. This was felt to be a more important approach to the testing then to complete a large number of tests on individual clean sites. The justification for this comes from the fact that foundations on offshore structures are usually exposed to initial bedding-in loading before being exposed to the larger storm loadings. It was possible to investigate the initial loading behaviour at the beginning of each test, and then continue to explore other behaviour as the test progressed. This maximised the value of each test site.

CHAPTER THREE
FOOTING BEHAVIOUR ON DRY SANDS

3.1 SUMMARY

This chapter explores the experimental drained response of a variety of circular foundations on very dense sand within the context of work-hardening plasticity theory. The foundations, representative of suction caissons, are differentiated by a variety of skirt depths, whilst dry sand is used to ensure drained behaviour. The results concentrate on four embedment ratios (0, 0.16, 0.33 and 0.66) on a dry sand of 95% relative density. The research indicates a change in shape of the yield surface with increase in embedment ratio. Whilst concentrating primarily on the plastic deformations consideration is given to the boundary between elastic and plastic behaviour within the yield surface. A conceptual model, based on work-hardening plasticity, is presented.

The chapter concludes by presenting some further data obtained from tests conducted on a carbonate material in a very loose state. This provides valuable evidence of the wide applicability of such a plasticity approach once fully formulated.

3.2 FOUNDATION BEHAVIOUR ON VERY DENSE SAND

A detailed description and interpretation of the results gathered during the investigation will be presented, including also a re-interpretation of previously published data specifically relating to flat footings.

3.2.1 Vertical Loading Behaviour and Interpretation of Hardening Law

An explicit indication of the hardening of the yield surface can be observed in the vertical loading sequences, in which the horizontal and moment loads are kept to a minimum whilst the vertical load is increased. For the tests analysed in this chapter a relatively simple representation of the hardening law can be used. The tests in question probed very low values of the ratio V/V_{peak}, at which stage the vertical loading relationship is essentially linear, as depicted in Figure 3.1. It is necessary, however, to define the vertical displacement, dw, as the sum of elastic and plastic displacements;

$$dw = dw_e + dw_p \quad \text{.....} \quad 3.1$$

where dw_e is the elastic vertical displacement and dw_p is the plastic vertical displacement. Any vertical loading behaviour inside the yield surface can be represented by;

$$V = k_e w_e \quad \text{.....3.2}$$

where k_e is the elastic stiffness of the foundation on the sand. An initial hypothesis is to link the hardening of the surface to the plastic vertical displacements such that the apex of the yield surface, V_o, is defined as;

$$V_o = k_p w_p \quad \text{.....3.3}$$

where k_p is the plastic stiffness of the foundation on the sand. Adopting this idealisation proves to be most convenient when interpreting the swipe tests. During the swipe test the vertical penetration remains constant while the vertical load reduces. The elastic vertical displacement is negative, and is balanced by an equal positive plastic vertical displacement. This implies an increase in V_o, which must be taken into account in subsequent analysis, as it is advantageous to normalise the forces by dividing by V_o. The modified value V_{oN} can be calculated as:

$$V_{oN} = \frac{V_{oI} k_e - V k_p}{k_e - k_p} \quad \text{.....3.3}$$

where V_{oN} is the new value for V_o, V_{oI} is the value for V_o at the start of the swipe and V is the instantaneous value of vertical load. Figure 3.2 shows an accumulation of vertical loading tests, for various footings, taken up to a vertical load of 2400N, the limit of the loading rig. During these tests two unload-reload loops were undertaken to determine the vertical elastic stiffness. Throughout the later stages of the tests further unload-reload loops were undertaken to determine a value for the elastic stiffness. An accumulation of these results is given in Figure 3.3, showing good repeatability between the different sample tanks, and little effect of footing skirt depth. In general there is also to distinguish between the vertical loading tests for the different skirt depths. It is probable that the overburden effect on the foundation response is not great at these low values of V/V_{peak}. It is also likely that the slight disturbance to the sample immediately around the skirt, caused during the penetration, may mean that the skirt itself contributes little to vertical capacity at small penetrations. From the elastic unloading/loading results it is clear, whilst there is some hysteresis evident, that 4000N/mm would be an appropriate representative elastic stiffness. A value of 600N/mm is representative of the plastic stiffness, in the range of loads from 500N to 2000N.

Throughout the following analysis V_{peak} refers to the peak vertical bearing capacity of a flat surface footing (unless otherwise specified by the subscript *peak(skirted)*). In places the

skirted footings are referenced to a bearing capacity of a skirted footing, so as to account for overburden effects. This value could be estimated by;

$$V_{peak(skirted)} = \gamma' L N_q^* \left(\frac{\pi D^2}{4} \right) + \gamma' \frac{D}{2} N_\gamma^* \left(\frac{\pi D^2}{4} \right) + \frac{\gamma' L^2}{2} (K \tan\delta)(\pi D) \quad \text{.....3.4}$$

using values for the bearing capacity factors taken from Bolton and Lau (1993). The frictional component is typically small for the short skirt depths being studied, but the overburden effect can add significantly to the bearing capacity. The value for N_q^* can be obtained by interpolating between values from Bolton and Lau (1993), based on N_γ^* determined from the bearing capacity tests. A typical value for $K\tan\delta$ is 0.25, and it is recognised that $V_{peak(skirted)}$ is insensitive to slight changes in this value. From above it is clear that:

$$\frac{V_{peak(skirted)}}{V_{peak(flat)}} = 1 + \frac{L}{D} \frac{2}{N_\gamma^*} \left(N_q^* + \frac{L}{D} 2K \tan\delta \right) \quad \text{.....3.5}$$

Equation 3.5 can be approximated for the values of L/D being explored in this study, combined with the appropriate bearing capacity factors, by the following linear relationship:

$$\frac{V_{peak(skirted)}}{V_{peak(flat)}} = 1 + 0.89 \frac{L}{D} \quad \text{.....3.6}$$

If the peak bearing capacity for the flat footing is scaled directly from the results of the 50mm diameter footing bearing capacity test used for characterisation, then it is straightforward to estimate the value for the skirted footing bearing capacity. Unfortunately, in this study, no skirted footing was taken to bearing capacity so the values for $K\tan\delta$ and N_q^* could not be verified. However, it is clear that the capacity increases significantly with skirt depth.

3.2.2 Swipe Testing of Flat Footings

Before examining the behaviour of skirted footings it is necessary to explore fully the response of a flat footing, as that provides the baseline for examining the skirted footing performance. The results from study by Gottardi and Houlsby (1995), interpreted by Gottardi *et. al.* (1999), provide a convenient starting point.

3.2.2.1 A Conceptual Understanding of Swipe Test Results

Gottardi *et. al.* (1999) assumed that the yield surface remained constant in shape, while expanding according to the work-hardening rule. The yield surface was based on the results of the main group of swipe tests conducted from V_o = 1600N, at a ratio of V_o/V_{peak} of 0.78. Several additional swipe tests (in tests GG09, GG24, GG13 and GG27) started from different vertical load levels. Examining firstly the behaviour of the footing in the $\{V{:}H\}$ plane, Figure 3.4(a) shows a series of tests with forces normalised by V_{peak}, indicating that the tests are conducted at varying levels of vertical loads. Figure 3.4(b) shows the same tests all starting from $V/V_o \approx 1$, with forces normalised by the V_o value. It is clear that the shape of the yield surface changes in a consistent way with the ratio V_o/V_{peak}.

Tan (1990) defined a 'parallel point', analogous to a critical state, where for continuing horizontal movements at a constant vertical displacement there was no change in the load state on the footing. This point is a transition between heave that occurs at low vertical loads and penetration that occurs at high vertical loads. It would appear the 'parallel point' for horizontal loading is close to the origin, as the load on the foundation does not tend to a finite limiting value, as would be expected if the parallel point existed at some distance from the origin. This observation is confirmed by Gottardi and Houlsby's horizontal swipe test on a sample starting at low V/V_o. This is further illustrated in Figure 3.5, which shows the entire horizontal swipe load deformation curves, which do not tend to a limiting load level, even at large displacements.

The observation of the location of the parallel point conflicts slightly with those recorded by Tan (1990), who noted that the parallel point for horizontal movement occurred at V/V_o of 0.152. It is quite probable that his swipe tests contained a slight moment loading, which was not measured during the testing. It may well be that the parallel point moves significantly away from the origin, towards the location for pure moment loading (as detailed below), for quite small amounts of moment loading (as may have been applied in Tan's tests). By looking at the problem statically, it is clear that the limiting ratio of H/V must be equal to m (the sliding criterion), where $m = \tan\delta$ and δ is the interface friction angle. Figure 3.6 shows the results plotted in this manner indicating that the resulting interface friction angle is approximately 25°.

Examining the behaviour in the $\{V{:}M/2R\}$ plane, a slightly different behaviour appears. Again a dependence of the shape of the yield surface on the ratio of V_o/V_{peak} is indicated, as shown in Figure 3.7(a) and 3.7(b). The parallel point appears in this case to be located at

some distance from the origin. It can be defined more consistently in the plot normalised with respect to V_{peak}, and occurs at about V/V_{peak} of 0.26 and $M/2RV_{peak}$ of 0.061. The convergence of the dimensionless rotational load deformation curves at large rotations, shown in Figure 3.8, are quite conclusive. Using these limiting values it is clear that the value for $M/2RV$ tends to about 0.25 for large rotations. By simple rearrangement this leads to a load eccentricity, e, of $R/2$ given that $M=Ve$.

Whilst a model with a fixed shape of the yield surface captures approximately the behaviour of the foundation, a subtler modelling is necessary to capture the features mentioned above. This is particularly important given that the typical ratios of V_o/V_{peak} applicable to the design of offshore structures would often be below about 0.25. Figure 3.9 shows a new understanding of the yield surface, in which the shape depends on the V_o/V_{peak} ratio. In the rest of the chapter the surface through V_{peak} will be referred to as the 'outer' surface, and those through lower V_o values the 'inner' surfaces (of variable shape). The 'inner' surfaces each appear to intersect the 'outer' surface, so that at low V/V_o all yield points fall on the 'outer' surface. The research presented in this chapter is aimed at the very low values of V_o/V_{peak} as this is a probable situation for offshore foundations. The ‘parallel point’ concept discussed throughout the text is related only to the ‘outer’ yield surface and not to the ‘inner’ surfaces. The definition of the ‘parallel point’ is that at large deviatoric displacements a steady state situation will occur. The ‘outer’ surface is only concerned with the response at large displacements and so is directly related to the ‘parallel point’.

3.2.2.2 Behaviour of Flat Footings in the {V:H} Plane and the {V:M/2R} Plane (DM2 and DM3)

The first two series of tests on very dense sand were used to further the understanding of the flat footing phenomena illustrated in the Gottardi and Houlsby tests. Under horizontal loading, five swipe tests were carried out from $V/V_o = 1$, but at different ratios of V_o/V_{peak}, including values much lower than those examined by Gottardi and Houlsby (1995). Figure 3.10 shows the results normalised with respect to V_{peak} as well as with respect to V_o. For the tests at very low stresses there is a significant change in the shape of the yield surface. After an initial reduction of V, the vertical load increases again as the footing slides at approximately constant H/V. This is indicative of dilatant behaviour for the tests at lower stress levels. At large displacements sliding failure continues with a reduction of V again occurring. The tests confirm that the 'parallel point' for horizontal loading is either at or very close to the origin. Two further tests (shown as thin lines on Figure 3.10) are for swipe tests starting at $V/V_o < 1$. The filled square points indicate approximately the

transition from 'elastic' to 'plastic' behaviour for these tests. The test starting from V/V_o = 0.5, shows significant elastic behaviour until the load point encounters the yield surface, as shown for the test from $V/V_{peak} = V_o/V_{peak}$ = 0.22 (the corresponding test at V/V_o = 1). The other test, at a significantly lower V/V_o, suggests that a transition is reached slightly within the 'outer' yield surface (sliding line). Both tests reach the sliding line and move towards the 'parallel point' at or close to the origin.

A further example of the location of the boundary between elastic and plastic behaviour can be seen in Figure 3.11. This shows the load and displacement paths for three different tests. The first (A) test is a swipe test from V/V_o = 1 and V_o/V_{peak} = 0.16. It shows slightly dilatant behaviour as the sliding failure line is reached, after which the load point moves towards the origin. The point at which the sliding line is intersected is represented by a solid square point on both plots. As expected there is significant plastic horizontal displacement during the swipe test. The second test (B) is a constant vertical load test, from V/V_{peak} = 0.1, with again a value V_o/V_{peak} = 0.16. Test (A) would be expected to give an indication of the position of the yield surface that existed prior to the constant V test. The open square on the graphs indicates the location of the boundary between 'elastic' and 'plastic' behaviour, whilst the solid square indicates when the sliding line is reached. It is clear that there is minimal displacement until after the yield surface is intersected, after which stage there are large combined displacements, which continue after the sliding line is reached. There is substantial vertical penetration during the plastic displacement, which is consistent with the loss of vertical load during the horizontal swipe. The third test (C) shown on the Figure is a radial loading test, which again was preloaded to V_o/V_{peak} of 0.16. A similar range of 'elastic' behaviour, in load space, compared to the constant load swipe test can be observed.

Under rotational loading it is clear that a 'parallel' point may exist, as observed in the Gottardi *et. al.* (1999) results. However the location of this point was beyond the limits of the loading rig. Seven swipe tests from V/V_o = 1 were performed as shown in Figure 3.12, showing clearly that the load paths follow a yield surface before moving upward to a parallel point. Figure 3.12 shows that the shape of the yield surface remains approximately constant, except for the tests performed at very low values of V_o/V_{peak}. Also shown on Figure 3.12 are five tests (shown as thin lines) from $V/V_o < 1$. One test (D) shows some 'elastic' behaviour before following the appropriate yield surface to the rotational boundary. Upon reaching the rotational boundary the load path moves towards the 'parallel

point'. The other swipe tests all move towards the 'parallel point' directly, but show only small horizontal displacements until close to the sliding line.

Three tests similar to those shown in Figure 3.11 were performed to assess the elastic boundary for moment loading, and are presented in Figure 3.13 in the same format as Figure 3.11. The closed square symbol shows where the swipe test encountered the rotational boundary, and a change of load path follows. The second test (B) is the constant load test, which was preloaded similarly to the swipe test (preloaded to V_o/V_{peak} = 0.16). The open square symbol on both plots shows the transition from 'elastic' to 'plastic' behaviour, which occurs at some distance from the yield surface anticipated from the swipe test. Upon reaching the rotational boundary significant heave is apparent as the soil beneath the foundation dilates strongly. This is consistent with the movement towards the 'parallel point' in the swipe test. The third test (C) is a radial loading test, again on a foundation which has been preloaded to V_o/V_{peak} = 0.16. The elastic/plastic transition point is marked by an open square symbol, and the position is consistent with the constant V test. These tests indicate that the 'pseudo elastic' region within the yield surface is reasonably significant.

For both radial loading tests there were significant vertical elastic movements, compared to the rotational and horizontal movements respectively. This was principally due to the fact that after the preload was applied, the vertical load was reduced to zero, before the radial load path was imposed on the footing. The hysteresis behaviour of the unload/reload loop is highly non-linear, particularly when the footing load is reduced to zero. An example of such a response is shown in Figure 3.14 where minimal displacements are required to reduce the footing load from 2400N to 200N, but proportionately larger changes in displacement are seen as the load on the footing is reduced to zero.

The two radial loading tests are also compared to the load deflection curve from a purely vertical loading test. The slope of the plastic section of the load-deflection curves appears to be similar though the magnitudes of the vertical loads for similar displacements are reduced. This is to be expected though as an estimation of the apex (V_o) of the yield surface would take into account the added horizontal and rotational loads, as well as the vertical load. Figure 3.15 shows an estimation of V_o plotted with respect to w_p, the vertical plastic penetration. Whilst the vertical displacement curves provide a reasonable estimate of the hardening behaviour it is clear that other mechanisms also contribute to the determination of V_o. A rational approach would be to include horizontal and rotational movements as well as vertical movements in the expression of a hardening law;

$$V_o = f\left(\dot{w}_p + C_1\left|\dot{u}_p\right| + C_2\left|2R\dot{q}_p\right|\right) \quad \text{3.7}$$

where C and C_2 are non-dimensional weighting factors. This approach to hardening behaviour is also indicated by the carbonate sand tests and is dealt with in more detail in the analysis of those tests.

3.2.2.3 Current Results and Conventional Bearing Capacity Theory

Conventional theories of bearing capacity, such as that proposed by Meyerhof (1953) and Hansen (1961) are usually regarded as conservative when compared to experimental evidence (see for example Ingra and Baecker, 1983). These theories use reduction factors on the vertical bearing capacity to account for shape, load inclination and load eccentricity amongst other effects. These factors are largely derived from empirical observations, together with some theoretical input. By manipulations of the reduction factor expressions it is quite simple to derive an interaction envelope for say {V:H} or {M:H} or even {V:M:H} space. For example the maximum vertical bearing capacity of a surface strip footing is:

$$V_{Peak} = A_{footing}\left(0.5\gamma' BN_\gamma\right) \quad \text{3.8}$$

If an inclined load is applied then the sustainable vertical load is reduced by a factor i_γ such that;

$$V = A\left(0.5\gamma' BN_\gamma i_\gamma\right) \quad \text{3.9}$$

where Meyerhof (1953) suggests:

$$i_\gamma = \left(1 - \frac{\Omega}{f}\right)^2 \text{ and } \Omega = \arctan\left(\frac{H_{Peak}}{V}\right) \quad \text{3.10-3.11}$$

By simple rearrangement it is possible to obtain;

$$\frac{H}{V_{Peak}} = \frac{V}{V_{Peak}}\tan\left[\left(1 - \left(\frac{V}{V_{Peak}}\right)^{0.5}\right)f\right] \quad \text{3.12}$$

which is an expression of interaction between H and V. An alternative expression for i_γ as suggested by Hansen (1961) is;

$$i_\gamma = \left(1 - \frac{H}{V}\right)^4 \quad \text{3.13}$$

which leads to an interaction solution of:

$$\frac{H}{V_{Peak}} = \frac{V}{V_{Peak}}\left[1-\left(\frac{V}{V_{Peak}}\right)^{0.25}\right] \quad \text{.....3.14}$$

Surprisingly the Hansen solution makes no mention of the angle of internal friction of the soil, which intuitively needs to be included if horizontal sliding of the foundation is incorporated at the low ratios of V/V_{peak}. These relationships can be compared to the 'outer' yield surface suggested in Figure 3.9.

A similar relationship can be obtained for the interaction between moment load and vertical load. Meyerhof (1953) suggested that a footing under moment loading be considered as the statically equivalent vertical load acting at an eccentricity *e* from the centre of the footing. The footing then has reduced width, called an effective width, of *(B-*2*e)*, and the appropriate interaction relationship can be derived:

$$\frac{M}{BV_{Peak}} = \frac{1}{2}\frac{V}{V_{Peak}}\left[1-\left(\frac{V}{V_{Peak}}\right)^{0.5}\right] \quad \text{.....3.15}$$

Hansen (1961) also adopts this approach. A similar approach can be found in the procedures recommended by the American Petroleum Institute (1993) for the drained design of shallow foundations. Care should be taken when using these expressions to evaluate the results of experimental investigations. Typically it is suggested that the expressions provide a conservative estimate to the capacity interaction, but they also provide quite a close approximation to the experimentally observed 'outer' yield surface. This can be seen in Figures 3.16 and 3.17 which show the appropriate curves with the experimental data reported here as well as that obtained by Gottardi and Houlsby (1995). Clearly the conventional theories would provide a conservative estimate if they were to be used in terms of V_o instead of V_{peak} and then applied to results from tests conducted at ratios of $V_o/V_{peak} < 1$. Figure 3.18 shows the comparison of loci between the conventional theories and the footing plasticity model adopted by Cassidy (1999), referred to as 'Model C', based on the experiments reported by Gottardi *et. al.* (1999). As the 'Model C' formulation was derived primarily from swipe tests conducted from a V_o/V_{peak} ratio of 0.78 it is not surprising its loci are non-conservative at V_{peak}.

3.2.2.4 Pre-Peak Three Dimensional Flat Footing Behaviour (DM9)

Further testing was carried out to determine the shape of the yield surface at different ratios of V_o/V_{peak} and $2RH/M$ for a flat footing. During the testing, in tank DM9, the footing was

moved not more than 0.75mm, such that the 'outer' yield surface was not intercepted. By conducting the testing in this manner it was possible to carry out multiple tests on individual sites, to build a complete three-dimensional picture of the shape of the yield surface. One series of tests conducted from a V_o/V_{peak} ratio of 0.28 is shown in Figure 3.19. Swipe tests were conducted at several ratios of $2RH/M$, to provide sufficient data for a simple surface fitting exercise to be carried out. By assuming that the 'inner' yield surfaces can be mapped onto a three dimensional geometric shape, it is possible to determine parameters with which to assess the development of the yield surfaces with the increase of V_o/V_{peak}. A simple mathematical form of such a shape (a rotated parabolic ellipsoid), first suggested in this context by Butterfield and Gottardi (1994) and elaborated on by Martin (1994), is;

$$\left(\frac{H}{h_o V_o}\right)^2 + \left(\frac{M}{m_o 2RV_o}\right)^2 - \frac{2aHM}{h_o m_o 2RV_o^2} - 16\left(\frac{V}{V_o}\right)^2\left(1-\frac{V}{V_o}\right)^2 = 0 \quad \text{.....} 3.16$$

where the values of m_o, h_o and a can be determined from a least squares analysis of the given data. A simpler assessment of the data can be obtained by normalising individual data points $\{M/2R{:}H\}$ using the expression (Butterfield and Gottardi, 1994);

$$q = \sqrt{\left(\frac{H}{h_o V_o}\right)^2 + \left(\frac{M}{m_o 2RV_o}\right)^2 - \frac{2aHM}{h_o m_o 2RV_o^2}} \quad \text{.....} 3.17$$

which collapses the data onto a single plane in $\{V/V_o{:}q\}$ space. In this space the yield surface becomes the parabola $q - 4v(1 - v) = 0$, where $v = V/V_o$. Figure 3.20 shows such a normalisation for the data given in Figure 3.19, showing swipes conducted from $V = 1800N$. Greater accuracy in the fit of the data can be obtained by modifying the shape of the parabola using non-dimensional weighting parameters β_1 and β_2 (as suggested by Nova and Montrasio, 1994) such that q becomes:

$$q = \left(\frac{(\beta_1+\beta_2)^{(\beta_1+\beta_2)}}{\beta_1^{\beta_1}\beta_2^{\beta_2}}\right)\left(\frac{V}{V_o}\right)^{\beta_1}\left(1-\frac{V}{V_o}\right)^{\beta_2} \quad \text{.....} 3.18$$

The choice of β_1 and β_2 affect the initial and final curvature of the parabola, as well as the location of the peak. Setting both β_1 and β_2 to 1 gives the original parabola $4v(1 - v)$. Using these parameters is not appropriate in this instance, as the slight improvement of fit does not alter significantly the general trend of the data.

An alternative view of the results is in the {M/2R:H} plane in which individual planes of V/V_o (slices through the yield surface) are shown in Figure 3.21. The results are normalised for the curvature of the parabola by dividing through by $4v(1 - v)$, that is:

$$m_n = \frac{M}{8RV\left(1-\frac{V}{V_o}\right)} \text{ and } h_n = \frac{H}{4V\left(1-\frac{V}{V_o}\right)} \quad \text{.....3.19, 3.20}$$

The swipe tests conducted from V = 1800N fall neatly within the data of the swipe tests from V = 900N. This observation supports the hypothesis that the shape of the yield surface changes with the ratio V_o/V_{peak}.

3.2.2.5 Accumulation of Test Results for Flat Footings

The accumulation of test results reported here and those by Gottardi and Houlsby are shown in Figure 3.22. In both instances the footing diameter was 100mm, bearing on dense to very dense sand. The h_o and m_o values are mainly derived by modelling individual swipe tests with a simple parabola (assuming the weighting functions β_1 and β_2 are equal to one). There is a strong correlation in the data with trend lines given by;

$$h_o = h_{opeak}\left(1-0.36\ln\left(\frac{V_o}{V_{peak}}\right)\right) \quad \text{.....3.21}$$

$$m_o = m_{opeak}\left(1-0.36\ln\left(\frac{V_o}{V_{peak}}\right)\right) \quad \text{.....3.22}$$

where h_{opeak} = 0.11 and m_{opeak} = 0.08, corresponding to the yield surface at the peak bearing capacity. These expressions have been validated for $0.025 < V_o/V_{peak} < 1$. The peak values compare well with the interaction loci that Meyerhof (1953) suggests for ϕ = 43°, where h_{opeak} = 0.113 and m_{opeak} = 0.074 (occuring at V/V_{peak} = 0.44).

3.2.3 Swipe Testing of Skirted Footings

A large proportion of the testing was to study the effect of a skirt on the drained behaviour of the foundation. Broadly speaking the behaviour of a flat footing will give indications of the general behaviour of the skirted foundation. The effects of different ratios of $V_o/V_{peak(skirted)}$ was not therefore examined in detail for the skirted footings. The testing at individual test sites was restricted to not more than two swipes before the site became sufficiently disturbed to affect the results.

3.2.3.1 Behaviour of Footings in the {V:H} Plane and the {V:M/2R} Plane for Different Ratios of y (DM4 and DM5)

Several tests were conducted in which the only parameter varied during the tests was the embedment ratio, $y = L/D$. Swipe tests were performed at similar ratios of V_o/V_{peak} for different footings to ascertain the effect of the skirt depth. For each set of tests the value for $2RH/M$ was fixed. The feedback routines in the control program determined the appropriate displacement path for the footing to maintain this load path. In tank DM4 the value for H was set to 0, whilst in DM5 the value for $M/2R$ was set to 0. Figure 3.23 shows the results from tank DM5, the horizontal swipe tests at $V/V_o = 1$ were conducted from starting values of V_o/V_{peak} of 0.08 and 0.21. The flat footing tests show behaviour typical of swipe tests, in which the load path traces around a yield surface, before tracking down the sliding line, towards the origin. At the low stress level the strongly dilatant sand causes a slight increase in capacity as it expands in volume, before allowing the footing to follow the sliding line as the soil beneath the footing begins to contract. Looking at displacement paths, it is clear that, if associated flow is assumed in the $\{M/2R:H\}$ plane, the yield surface for the flat footing is almost perpendicular to the H axis. A very slightly different displacement path is followed once the sliding line is reached.

Three skirted footings were used during these tests, with y ratios of 0.16, 0.33 and 0.66. There are minimal differences in the load paths tracked by these three footings, though it is clear that there is a significant difference between the shallowest of the skirted footings and the flat footing. In all three cases strongly dilatant behaviour is observed as the load paths track slightly up the sliding line. If the tests had been taken to further displacements it is clear that contractant behaviour would have been observed, as for the flat footing. There are, however, significant differences in the behaviour in displacement space, but for deeper embedment depths these differences become progressively smaller. For the embedment ratio of 0.16 the yield surface crosses the horizontal axis at an angle of approximately 67° to the horizontal (assuming associated flow). However at the embedment ratio of 0.33 and 0.66 it crosses at approximately 47° and 43° respectively. Clearly, for the skirted footings, the displacement path is such that both horizontal load and moment load are developed as the footing is displaced horizontally. To reduce the negative moment load developed the footing would have to rotate positively. The larger the skirt depth the larger are the positive rotations required to keep the moment to zero.

Similar observations can be made about the results of tank DM4, in which rotational swipes at $V/V_o = 1$ were carried out with horizontal loading set to zero (shown in Figure

3.24). There is no significant difference in the load paths traversed by the footing, but in displacement space there is a significant difference. This is to be expected because as the footing rotates positively to create positive moments, a negative horizontal load is induced on the footing. To reduce this horizontal load to 0 the footing must experience positive horizontal displacements, the magnitude of which depends on the skirt depth of the footing. There is a well-defined relationship between the skirt depth and the ratios of rotational to horizontal footing movement in this case. Again assuming normality of flow in this plane it is clear that the yield surface crosses the moment axis at approximately 9° (y = 0), 14° (y = 0.16), 22° (y = 0.33) and 34° (y = 0.66).

The surprising aspect of these tests is that the drained capacity for pure moment loading is not significantly enhanced by the skirt. It is clear though that as the skirt depth increases that the size of the yield surface in the horizontal loading direction becomes larger. This ties in with the variation of h_o with V_o/V_{peak} (evident in flat footing tests), given that V_o was constant for all tests, but $V_{peak(skirted)}$ increases for the skirted footings.

3.2.3.2 Swipe Testing at Different Ratios of H2R/M for L/D = 0.33 (DM6 and DM7)

To evaluate the changes of shape of the internal yield surface, two sets of testing were carried out at different ratios of $V_o/V_{peak(skirted)}$, and consisted of swipe tests from V/V_o = 1 at different ratios of $2RH/M$. Test series DM6, accumulated on Figure 3.25, consisted of 16 swipes at $V_o/V_{peak(skirted)}$ = 0.16, whilst DM7 consisted of seven swipe tests at $V_o/V_{peak(skirted)}$ = 0.1 (accumulated on Figure 3.26). Both sets of tests used a footing of diameter 100mm and embedment ratio of 0.33.

Examining only test series DM6 (as DM7 shows similar trends). Figure 3.27 shows the load paths in the $\{M/2R:H\}$ plane. The solid squares on the graph indicate the estimated transition points from the 'inner' yield surfaces to the 'outer' envelope. They serve as an indication of the shape of the 'outer' yield surface. The open symbols on the graph are points at selected values of V/V_o, and indicate possible shapes of the 'inner' yield surface. It appears that both 'inner' and 'outer' surfaces can be approximated by ellipses. Also included on Figure 3.27 is an indication of the yield surface shape, determined during a loop event at a constant load of 800N and V/V_o of 0.33.

An assumption made previously was that normality applied in the deviator plane (that is $\{H:M/2R\}$) of load space, this has been indicated by other studies (for example Gottardi *et. al.*, 1999; Martin, 1994; Cassidy, 1999). It is possible to check whether this is also true for these tests by plotting the force ratios against the plastic displacement ratios as in Figure

3.28. If normality holds true then standard plasticity theory gives the plastic strain rate ratio as:

$$\frac{du_p}{2R dq_p} = \frac{H 2R \frac{m_o}{h_o} - aM}{M \frac{h_o}{m_o} - aH 2R} \quad \text{.....3.23}$$

This relationship has been plotted on Figure 3.28 using least squares derived parameters from the experimentally determined yield surface shape. The experimental data supports an associated flow rule throughout most of the range, although there is some scatter in the data, particularly in the negative quadrant in which the curvature of the yield surface is greatest.

It is clear from Figures 3.25 and 3.26 that there is a difference in the occurrence of the transition point from 'inner' to 'outer' yield surfaces in terms of V/V_o. Quite evidently for moment loading the transition point occurs at $V/V_o \sim 0.7$ (V=860N), whilst for horizontal loading the transition point occurs at $V/V_o \sim 0.4$ (V = 480N). This is shown more clearly in Figure 3.29 where the location of the transition point as a function of the force ratio is given. One possible way of incorporating this behaviour into the model would be to adjust the weighting parameters β_1 and β_2 appropriately. These parameters not only control the slopes at high and low values of V/V_o, but in combination control the location of the peak of the parabola along the V/V_o axis. In the case of series DM6, for the transition points indicated on Figure 3.27, an appropriate relationship could be defined as;

$$\frac{\beta_1}{\beta_1 + \beta_2} = \frac{5}{9} + \frac{1}{7}\sin\left(\frac{6\pi}{10} - 2\left(\tan^{-1}\left(\frac{2RH}{M}\right)\right)\right) \quad \text{.....3.24}$$

where β_1 and β_2 can not be greater than 1 or less than 0.

Incorporating this sort of feature into the model still requires a significant amount of work - it would be necessary to examine whether the behaviour is prevalent for a large range of values of $V_o/V_{peak(skirted)}$ and whether it becomes more evident for larger skirt depths. At this stage of model development it would be more appropriate to assume a constant for the transition location, based on the average value.

3.2.4 Behavioural Changes due To Skirt Depth

It is clear from section 3.1.3 that there is a significant change in the yield surface shape with increasing skirt depth. The most noticeable changes occur in the {-H:+M} and the

{+*H*:-*M*} quadrants, which are not typically encountered in normal loading regimes. The yield surface shape in the positive quadrant becomes flatter with increasing embedment.

3.2.4.1 Determination of Shape of Outer Yield Surface (DM8)

To determine the shape of both sets of yield surfaces, 'inner' and 'outer', would require a significant amount of normally consolidated swipe tests to be carried out. It is possible to determine the shape of the 'outer' yield surface by performing loop events at constant load. These are performed by imposing a circular displacement path on the footing in deviator displacement space whilst keeping the vertical load constant. If the footing is undergoing plastic deformations the load path traced should be an indication of a yield surface. If the footing is at low V/V_o and V/V_{peak} then small deformations will be required to push the footing through the elastic region to the 'outer' yield surface, as shown in Figure 3.30. If on the other hand the footing is at a high V/V_o then the load path traced will consist of expanding yield surfaces, once the elastic 'inner' yield surface region has been overcome (interpretation of these would be difficult).

By using constant load loop events it is possible to map out the probable yield surface shape for different embedment depths on the same sample of sand. This is important, as it simplifies interpretation by minimising the possible effects of material differences. Each site on the sample was subjected to several loop events at different levels of vertical load. An accumulation of these results, normalised as defined by equations 3.25 and 3.26, are shown in Figure 3.31. The normalisation is comprised of:

$$\frac{H}{V_{peak(skirted)} h_o C v^{b_1} (1-v)^{b_2}} \text{ and } \frac{M}{2RV_{peak(skirted)} m_o C v^{b_1} (1-v)^{b_2}} \quad \text{.....3.25, 3.26}$$

where $v = V/V_{peak(skirted)}$ and C is defined as:

$$C = \frac{(b_1 + b_2)^{(b_1+b_2)}}{b_1^{b_1} b_2^{b_2}} \quad \text{.....3.27}$$

The constants used in the normalisation are separately defined by least squares fitting of the yield surface for each skirt depth. It is clear that as the skirt depth increases the shape of the ellipse also does, as indicated in normalised deviator load space by the pronounced elongation of the surface.

3.2.5 Elastic Behaviour

The main thrust of the research program was the investigation of the plastic response of the circular footings under different loading combinations. It is clear from section 3.2.2 that

there is considerable elastic behaviour as the 'pseudo-elastic/plastic' boundary is marginally inside the yield surface determined by the swipe test. The elastic behaviour is hysteretic and highly non-linear as shown in Figure 3.14. However, it is typically assumed to be linear. Several tests were undertaken investigating the response of the foundation (typically a flat footing) to loading within the yield surface, primarily to determine elastic stiffness coefficients:

$$\begin{Bmatrix} V \\ M/2R \\ H \end{Bmatrix} = 2GR \begin{bmatrix} k_v & 0 & 0 \\ 0 & k_m & k_c \\ 0 & k_c & k_h \end{bmatrix} \begin{Bmatrix} dw_e \\ 2R dq_e \\ du_e \end{Bmatrix} \quad \text{.....3.28}$$

These coefficient have been determined by Bell (1991) and Ngo Tran (1996) using finite element analyses. In order to determine these coefficients for the present set of tests, some small elastic excursions were performed on a flat footing. The footing was preloaded to 2400N before being unloaded to 800N so that the footing was located in a significant elastic region. The footing was then subjected to ±100N vertical loop, ±100N horizontal loop and ±150N moment loop. The results of these tests are shown in Figure 3.32. Plotted with these results are theoretical lines, obtained using the elastic stiffness matrix, with a suitable value for G (12 MPa). It was found that k_h (2.3), k_c (-0.14) and k_m (0.46) were the same as those obtained by Bell (1991) for shallow footings using a Poisson's ratio of 0.2. The vertical elastic stiffness coefficient, k_v (5.3), was found to be approximately double that determined by Bell.

3.2.5.1 Increasing Cycles of Horizontal Load

Examining the changes in elastic behaviour, as the load state moved towards the yield surface, was an essential part to determining the boundaries to elastic performance. This was initially explored by cycling between increasing values of horizontal load whilst keeping the vertical load constant and moment to zero. Figure 3.33 shows the results of a footing test with a V/V_o of 0.33. Clearly as the load on the footing increases there is increasing plastic behaviour, with a relatively small 'elastic' region concentrated below 100N. A stiffer response is revisited on small amplitude unload-reload cycles. The effect of the ratio V/V_o was also investigated. The results of such tests are shown in Figure 3.34, which shows that the 'elastic' behaviour becomes stiffer as the ratio V/V_o increases. This sort of behaviour is not included in any standard analysis of elastic performance. This behaviour, which is relevant to offshore foundations, is explored in greater detail in Chapter 5.

3.3 FOUNDATION BEHAVIOUR ON LOOSE UNCEMENTED CARBONATE SAND

The work reported above shows that plasticity models in terms of force resultants are appropriate for modelling of skirted foundations on very dense sand. Previous work has shown that such a model is equally useful for foundations on clay (Martin, 1994) and medium to dense silica sand (Tan, 1990; Gottardi *et. al.*, 1999). Another series of tests were carried out to examine foundation behaviour on a material of a very different type - uncemented loose carbonate sand. Typically this material is problematic as there can be large volume contraction upon shearing. The properties and response of the soil, where void ratios may be as high as 2, is quite different to that of very dense silica sand described previously in the chapter. A testing programme was therefore undertaken to determine yield surface shape and the mechanisms associated with yield surface expansion or hardening. A long capacity displacement transducer system was used, compromising slightly the resolution of the displacement measurements, although necessary due to the quite large displacements that occurred. A footing of diameter 150mm, and side-wall of 70mm, was used which, when loaded to V = 1600N, displaced to a vertical penetration of about 60mm - an indication of the compressibility of the soil. A total of 18 tests were completed, and the full data set can be found in Byrne and Houlsby (1998, 2000). Illustrative results are presented here.

3.3.1 Vertical loading

Compressive loading on this loose material produced a response rather like a consolidation test in which the void ratio of the material directly beneath the footing decreased with increase in load. Figure 3.35 compares the vertical loading responses from all available data, with bedding effects removed by matching all curves at a vertical load of 1000N. In all of these tests, after reaching 1000N the footing was unloaded to 200N before being reloaded to 1000N to obtain an estimate for the vertical elastic stiffness of 4.5 kN/mm. The tests display remarkable consistency. No test was carried out which reached a peak load as it was envisaged that this load, if it indeed existed, would not be within the capabilities of the loading rig. Also shown on Figure 3.35 is the vertical loading responses from Gottardi *et. al.* (1999) illustrating a typical response of a dense silica sand.

3.3.2 Swipe testing

Swipe tests were performed to determine the three dimensional yield surface shape which can be mathematically represented as (Martin, 1994);

$$\left(\frac{H}{h_o V_o}\right)^2+\left(\frac{M}{m_o 2RV_o}\right)^2-\frac{2aHM}{h_o m_o 2RV_o^2}-\left(\frac{(\beta_1+\beta_2)^{(\beta_1+\beta_2)}}{\beta_1^{\beta_1}\beta_2^{\beta_2}}\right)\left(\frac{V}{V_o}\right)^{\beta_1}\left(1-\frac{V}{V_o}\right)^{\beta_2}=0 \quad ....3.29$$

where V_o is the apex of the yield surface and is determined by the hardening rule. By defining the quantity q as;

$$q=\sqrt{\left(\frac{M/2R}{V_o m_o}\right)^2+\left(\frac{H}{V_o h_o}\right)^2-2a\frac{M/2R}{V_o m_o}\frac{H}{V_o h_o}} \quad .....3.17bis$$

it is possible to reduce all the data to fit a weighted parabola in $\{V/V_o{:}q\}$ space such as shown in Figure 3.36 where four swipe tests from high loads (V = 1600N) are shown. These tests were performed along different paths in $\{2Rq{:}u\}$ space at constant w to map out the general shape of the yield surface. Two further tests were carried out from low loads (V = 50N after a load of 1600N had been applied), analogous to overconsolidated triaxial tests. It is clear that a fair match is obtained for most values of V/V_o, with the match only slightly less good at the lower V values. All the swipe tests were carried out to the maximum displacements within the capabilities of the loading rig to investigate both peak and residual loads.

An alternative way of viewing these results is in the $\{M/2RV_o{:}H/V_o\}$ plane, where the extent of the ellipse is quite evident. Shown in Figure 3.37 are the four swipe tests from high loads (and their reflections) with slices of the ellipse passing through V/V_o = 0.95, 0.9, 0.75 and 0.5. The appropriate values for the parameters have been defined by a least squares fitting of the data where m_o = 0.094, h_o = 0.154, a = -0.25, and, β_1 = β_2 = 0.82. These values can be compared to those for dense silica sand (Gottardi *et. al.*, 1999) where m_o = 0.09, h_o = 0.1216, a = -0.2225, and β_1 = β_2 = 1. Clearly there is an expansion of the surface in the horizontal dimension, due to the increased embedment of the footing, but there is minimal increase in the size of the surface in the moment dimension.

It has generally been assumed that the shape of the footing yield surface remains constant, increasing in size with increases in vertical plastic penetration (Cassidy, 1999; Gottardi *et. al.*, 1999; Martin, 1994). The work presented earlier in this chapter suggests that for dense frictional materials a slightly different pattern occurs. An 'outer' yield surface exists outside of which no loads can be sustained and with a size related to the peak bearing capacity (V_{peak}). Within this 'outer' surface exists a family of 'inner' surfaces, whose shape depends on the ratio of the maximum vertical load experienced by the footing to the peak bearing

capacity. Based on the results of a number of experiments the following expression has been proposed for the variation of the yield surface in the horizontal plane:

$$h_o = h_{opeak}\left(1 - 0.36\ln\left(\frac{V_o}{V_{peak}}\right)\right) \quad \text{3.21bis}$$

This expression was validated for $0.025 < V_o/V_{peak} < 1$ where $h_{opeak} = 0.11$ is the horizontal dimension for the yield surface at peak bearing capacity. This suggests that at low values of V_o/V_{peak} the value for h_o is about twice that at high values of V_o/V_{peak}, providing that a peak bearing capacity exists.

This relationship is not appropriate for the contractant carbonate sand tests, as there is no observed peak bearing capacity. In this case the horizontal response of the footing is largely dependent on the passive pressures that develop against the footing sidewall. During the carbonate testing programme six horizontal swipe tests were conducted, at varying levels of embedment, to examine this effect. The moment load was kept close to zero and the maximum horizontal load during the swipe was recorded as H_{peak}. These tests are summarised in Figure 3.38, where the value of H_{peak}/V_o is plotted against the non-dimensional embedment depth, $w/2R$, where the best fit trendline is given by:

$$\frac{H_{peak}}{V_o} = 0.138 + 0.093\frac{w}{2R} \quad \text{3.29}$$

It is clear that as the footing penetrates into the carbonate material the maximum ordinate of the horizontal yield surface increases. Results from a centrifuge study of footing behaviour on medium silica sand by Tan (1990) are also shown on Figure 3.38 and where:

$$\frac{H_{peak}}{V_o} = 0.155 + 0.135\frac{w}{2R} \quad \text{3.30}$$

It should be noted that in Tan's tests the moment applied to the footing was not measured, and was probably not zero. Assuming normality of flow, and a horizontal displacement path, Tan's H_{peak} values relate to the maximum ordinate of the ellipse in the horizontal direction and thus slightly overestimate the true zero moment H_{peak} value.

3.3.3 Hardening and Flow

The relationship that determines the way in which the yield surface expands or contracts is defined as the hardening law. Gottardi *et. al.* (1999) suggest that the relationship observed

for vertical penetration be used as a first estimate for the hardening rule. Tan (1990) and Martin (1994) also used this approach in which the apex of the yield surface, defined by V_o, is a function of the vertical plastic penetration, w_p. In order to examine whether this is an appropriate hypothesis for the hardening law it is possible to interpret radial displacement and constant load tests determining the V_o value for each load increment. Figure 3.39 shows these calculated values for radial displacement tests, determined using the yield surface parameters defined from the swipe tests, and plotted against the vertical plastic penetration. It can be seen clearly that for the different ratios of deviatoric displacement, there appears to be differing degrees of hardening. A closer approximation to the hardening behaviour can be obtained if the hardening is defined as a function of all three components of plastic movement. An appropriate expression would be;

$$V_o = f\left(\dot{w}_p + C_1\left|\dot{u}_p\right| + C_2\left|2R\dot{\theta}_p\right|\right) \quad \text{.....3.7bis}$$

where C_1 and C_2 are constants. This new assumption has important implications for the use of swipe tests. Under the initial hypothesis in which hardening, controlled by V_o, was a function of w_p the swipe tests were the only test required to define the yield surface shape. However, under this new hypothesis, where during the swipe test the amount of u_p and θ_p are large, the value of V_o changes significantly during the actual test (i.e. hardening behaviour occurs). In order to establish the true shape of the yield surface it is necessary to use other tests in conjunction with the swipe tests. These tests include the radial displacement tests and the constant vertical load tests which give information of the expansion of the yield surface. It is therefore necessary to iterate several times using information from both swipe tests and yield surface expansion tests to infer the actual shape of the yield surface. After several iterations it is possible to come up with new best fit parameters. The resulting hardening relationships for the radial displacement tests are shown to group more closely in Figure 3.40. The parameters for the fit shown are m_o = 0.089, h_o = 0.1505, a = -0.3, $\beta_1 = \beta_2$ = 0.75, C_1 = 0.5, and, C_2 = 0.2.

Once the yield surface shape and hardening rules become consistent it is then necessary to determine a relevant plastic potential to define the magnitudes of plastic displacements. It has become generally observed that associated flow is prevalent for displacements in the $\{2Rd\theta_p : dh_p\}$ plane. This assumption is confirmed in Figure 3.41 by plotting plastic strain ratios against load ratios and comparing them to the theoretical associated flow line, which is defined as:

$$\frac{du_p}{2Rdq_p} = \frac{H\,2R\frac{m_o}{h_o} - aM}{M\frac{h_o}{m_o} - aH\,2R} \quad \text{.....3.23bis}$$

This result is in line with the results of many other studies (for example Martin, 1994; Cassidy, 1999)

3.4 THE CURRENT STATE OF THE PLASTICITY MODEL

At this stage it is appropriate to re-state the plasticity model taking into account what has been observed from the research. For footings on dense sand, where there is a peak bearing capacity, the research has suggested that there are 'inner' and 'outer' yield surfaces, which characterise behaviour until V_{peak} is exceeded. The 'outer' surface provides a boundary outside of which no load combination can exist unless substantial displacements occur. The size and shape of the 'outer' surface may be determined from conventional methods (e.g. Meyerhof (1953), Hansen (1970) or Vesic (1975)) or by experimental studies (e.g. Butterfield and Gottardi, 1994, Gottardi et. al., 1999). Table 3.1 lists a compilation of the values for parameters which are referred to in this discussion, and which control the size and shape of these yield surfaces. A rotated parabolic ellipsoid maybe used to define this 'outer' surface in {V:M/2R:H} space:

$$\left(\frac{H}{h_oV_o}\right)^2 + \left(\frac{M}{2Rm_oV_o}\right)^2 - \frac{2aHM}{h_om_o2RV_o^2} - 16\left(\frac{V}{V_o}\right)^2\left(1-\frac{V}{V_o}\right)^2 = 0 \quad \text{.....3.16bis}$$

For flat footings, on a medium to dense sand, a large accumulation of test results indicates that h_o at V_{peak} may be approximated by 0.11 and m_o by 0.08. This 'outer' yield surface is sized by V_o which is given by the peak bearing capacity:

$$V_o = V_{peak} = g'\frac{D}{2}N_g^*\left(\frac{pD^2}{4}\right) \quad \text{.....1.1bis}$$

N_g^* may be determined from Bolton and Lau (1993). It is also necessary to define the value for a which determines the eccentricity of the ellipse. Gottardi *et. al.* (1999) suggest a value for a of -0.2225 for medium dense sand. Analysis of the loop events for the flat footing (section 3.2.4.1) led to broadly similar results for m_{opeak} and h_{opeak} as above but gave a as 0.06. The value for a determined in this study was from tests conducted at low values of V_o/V_{peak}, whilst in the Gottardi *et. al.* (1999) study it was determined from tests at large values of V_o/V_{peak}. It is likely that the eccentricity is a function of V_o/V_{peak} however

such a modelling feature has not been developed yet. The variation of eccentricity with V/V_o was also observed in tests on overconsolidated clay (Martin, 1994). This 'outer' surface remains fixed until V_{peak} is surpassed. Within the 'outer' surface exist a family of expanding yield surfaces, also defined by equation 3.16, but sized by V_o, and where the shape varies with V_o/V_{peak}:

$$h_o = h_{opeak}\left(1 - 0.36\ln\left(\frac{V_o}{V_{peak}}\right)\right) \quad \text{3.21bis}$$

$$m_o = m_{opeak}\left(1 - 0.36\ln\left(\frac{V_o}{V_{peak}}\right)\right) \quad \text{3.22bis}$$

h_{opeak} = 0.11 and m_{opeak} = 0.08 correspond to the yield surface at the V_{peak}. These expressions are valid for $0.025 < V_o/V_{peak} < 1$. The eccentricity of these 'inner' surfaces, for simplicity, is given by the same coefficient as for the 'outer' yield surface. The expansion of the 'inner' yield surface is given by the hardening law where the apex (V_o) of the yield surface is linked to the footing movements:

$$V_0 = f\left(\dot{w}_p + C_1\left|\dot{u}_p\right| + C_2\left|2R\dot{q}_p\right|\right) \quad \text{3.7bis}$$

C_1 and C_2 may be taken as 0.5 and 0.2 respectively in the first instance. At low values of V_o/V_{peak} the unknown function may take the form of a linear relationship, defined by a stiffness, k_p, as indicated in equation 3.3. It is less clear how this function may vary at high values of V_o/V_{peak}. As the 'inner' surfaces track back from high V_o they will intersect with the 'outer' surface. The intersection of the two surfaces will define a region of elastic behaviour. For surfaces tracking from low values of V_o/V_{peak} abrupt changes in slope occur at the intersection point. This is similar to the behaviour observed for experimental horizontal loading and shown in Figure 3.10. As V_o approaches V_{peak} the intersection of the two surfaces becomes more gradual.

When V_{peak} is reached, or if V_{peak} does not exist, as in the carbonate sand tests, slightly different behaviour occurs. The rotated parabolic ellipsoid (Equation 3.16) is still used to describe the three-dimensional yield surface. The hardening of the yield surface is defined by Equation 3.7 where the function will take the form of either an exponential or linear expression. For post-peak behaviour in dense sand there may be substantial softening (as dilation occurs) before any overburden effects begin to dominate. The values for m_o and h_o are taken either to be m_{opeak} and h_{opeak} for the dense sand, or equal to 0.089 (m_o) and 0.138

(h_o) for a loose sand (e.g. carbonate). The results of the carbonate sand tests suggest that for depths of embedment of interest the m_o value does not change significantly whilst h_o increases at a rate of 0.1 with non-dimensional embedment ($w/2R$). Tan's (1990) results suggest a rate of increase for h_o of 0.13, but does not address the m_o value. The eccentricity of the ellipse suggested by the loose carbonate sand is -0.3. However, there is no information about what this value might be for post peak behaviour in dense sand.

For the skirted footings in dense sand similar behaviour will occur as described for the flat footings. A series of 'inner' and 'outer' yield surfaces will exist sized by the peak skirted bearing capacity given by:

$$\frac{V_{peak(skirted)}}{V_{peak(flat)}} = 1 + 0.89\frac{L}{D} \qquad \text{3.6bis}$$

The values of the three parameters necessary to describe the 'outer' surfaces have been estimated from the loop events described in section 3.2.4.1. This is a difficult task as typically the load level at which the event was conducted is very small compared to the peak bearing capacity. For an embedment ratio of 0.33 it was estimated that $h_{opeak} \sim 0.17$, $m_{opeak} \sim 0.074$ and $a \sim -0.75$. The size of the moment dimension was similar for an embedment ratio of 0.16 but increased to 0.09 for an embedment ratio of 0.66. The horizontal dimension was estimated to be 0.15 for an L/D of 0.16 and to decrease to 0.13 for an L/D of 0.66. This decrease for the large embedment ratio ties in with the results shown in Figure 3.23. In this Figure the swipe test from the deepest footing falls inside the swipe tests from the two shallower skirted footings. The eccentricity of the ellipse increases with skirt depth with values of 0.06 (L/D=0), -0.25 (L/D = 0.16), -0.75 (L/D = 0.33) and -0.93 (L/D = 0.66). It is likely that the highly frictional response of the dense sand dramatically affects the value for these parameters and it would be interesting to compare results to tests at a lower density. For instance in the carbonate sand tests the footing was embedded to an L/D ratio of 0.4. The eccentricity parameter, a, was -0.3 compared to approximately -0.8 for the dense sand. Finally the 'inner' yield surfaces will conform to Equations 3.21 and 3.22 with the values for m_{opeak} and h_{opeak} as mentioned.

A plastic potential is also necessary so that a full description of behaviour can be accomplished. The analysis of the tests suggested that this potential would be associated in the deviatoric plane, but non-associative in the vertical plane, as has been suggested by other studies (Martin, 1994; Gottardi *et. al.*, 1999; Cassidy, 1999). The main observation from the presented research is that the location of the parallel point is different for moment

and horizontal loading. For horizontal loading the parallel point appears to be close to the origin whilst for moment loading it appears to be located at V/V_{peak} of 0.26 and $M/2RV_{peak}$ of 0.061. For combinations of load between the two a linear variation may be sufficient. No formal definitions of plastic potentials are presented here, however Cassidy (1999) covers the issue of flow rules for footing behaviour quite thoroughly.

3.5 IMPLICATIONS FOR OFFSHORE DESIGN

The results presented in this chapter have provided information that enables an improved understanding of the behaviour of footings under combined loading, on very dense sand, as well as, loose carbonate sand. The results on dense sand are particularly relevant to the design of small shallow foundations for offshore structures, in which the drained behaviour will be the limiting design case. The drained behaviour also provides a lower bound to the partially drained performance of foundations, and as such the results must also be considered in the design of much larger foundations. The results from the carbonate sand tests suggest that the plasticity approach is extremely versatile.

3.5.1 Effects of Scale

The objective of this research was to establish the general behaviour of a foundation subjected to combined loading. The effects of scale are not significant, as the generic behaviour of the foundation at model scale is not expected to differ significantly from one at prototype scale. However, it worthwhile making some comments on scaling of results, as the numerical values of parameters may change with scale. It is assumed that the model and prototype sands are the same, and deposited with the same density. The vertical capacity is a function of the loaded area and the soil strength. If N is a geometric scaling factor then:

$$Area_{prototype} = N^2 Area_{model} \quad \text{.....3.31}$$

Soil strength is a function of stress levels in the soil, and these stress levels will factor by N. Soil strength does not scale linearly, because at the low stress levels (in the model) the peak friction angle and dilation rate of the sand are higher than at the high stress levels at the prototype level. Thus soil strength will scale only with approximate order of magnitude N. Combining the two leads to all forces (that is $\{V{:}M/2R{:}H\}$) scaling with approximate order N^3. Bolton (1986) gives an indication of the dependence of strength of a granular material on the stress level, acknowledging the non-linearities involved. To examine further how these parameters may differ with scaling to prototype situations it would be

necessary to perform key one gravity tests at either field scale or in a geotechnical centrifuge.

3.5.2 Positive Quadrant Negligibly Affected by Change in Skirt Depth

One surprising aspect of the results, as discussed above, is that the quadrant of positive loading is relatively unaffected by the depth of the skirt. The loading that would typically be applied to an offshore foundation under normal service conditions falls in this quadrant. Whilst the overall shape of the positive quadrant remains similar, it is clear that for the same diameter footings, a skirted footing will have a larger compressive vertical capacity. Given that the non-dimensional sizes of the yield surface are similar, the maximum horizontal and rotational capacities will factor with the increase in $V_{peak(skirted)}$ due to the increased embedment. By adopting a deeper skirt it might be possible to reduce the diameter of the foundation and still achieve suitable performance. The depth of the skirt is limited to that which can be installed by suction and dead weight.

3.5.3 The Concept of Safety Factors

The research has indicated that two possible approaches can be made for defining safety factors for a footing on sand. It is possible to define a safety factor against significant or plastic movements, as would be required for serviceability requirements. Load combinations crossing the internal yield surfaces can be sustained by the sand, but at the expense of some limited plastic footing displacements. If load combinations are such that the 'outer' yield surface is reached then substantial footing displacements, and foundation 'failure', will be observed. These 'outer' yield surfaces, such as those defined by Meyerhof (1953) and Hansen (1961) in their early studies, indicate the maximum combinations of load that can be sustained by the sand, regardless of displacements. Safety factors could be defined in terms of these 'outer' surfaces. For maximum performance of the foundation it would be preferable to preload to a large percentage of the bearing capacity, before reducing to a working load of $V/V_{peak} \approx 0.5$ (which should lead to the largest safety factors against failure for typical loading patterns). In most situations it may not be possible to apply preload to the foundations, however, it may still be preferable to design the footing for operation at $V/V_{peak} \approx 0.5$.

3.5.4 Development of Numerical Models for Use within Structural Analyses Packages

Numerical models based on work-hardening plasticity theory can be used to model skirted foundations on dense sand as 'macro' elements within structural analyses packages. The behaviour of the soil-foundation combination is highly complex, as illustrated in this

chapter, and needs to be appropriately represented within such analyses so that realistic results can be obtained (such as by Cassidy, 1999). This is gradually being undertaken, though primarily at a research level, rather than as part of a typical analysis of an offshore structure. This is in part due to the lack of data available for the derivation of parameters to define the numerical model, although this is being addressed (Martin and Houlsby, 1994; Gottardi and Houlsby, 1995; Byrne and Houlsby, 1998). The model development has so far been focussed on the drained behaviour of granular soil, in response to loading on the foundation. It is clear from this chapter that the understanding of the drained response has improved significantly over the past few years. The next step forward, so that a closer approximation of the physical reality is obtained, is to consider the partially drained behaviour of the foundations on granular materials. The response of the soil then depends on the effective stress, which was defined by Terzaghi (1943) as the total stress less the pore fluid pressure:

$$\sigma'_{ij} = \sigma_{ij} - u_w \delta_{ij} \quad \text{.....3.32}$$

where δ_{ij} is the kronecker delta. This clearly adds a further dimension to an already complicated response. The pore fluid pressure is a function of the history of loading, the nature of the loading, the design of the foundation, as well as, the nature of the granular material. This is the subject of chapters 4 and 5. The effects of a single wave travelling over the structure, which would impart a load change over a short period of time, may be modelled by incorporating rate effects into the plasticity model. It is less clear how the modelling of load reversal could be undertaken. However, the first approach being undertaken is to use realistic loading regimes on the foundation to study the boundaries to behaviour and the mechanisms of response.

3.6 CONCLUDING REMARKS

This chapter has presented the results of a series of loading tests undertaken on footings on very dense dry sand. Over 250 individual tests were used to determine the behaviour of footings with different skirt depths under a variety of conditions. These footings are representative of a novel offshore foundation, called a 'suction caisson', which has become a viable alternative in the development of marginal offshore resource fields. The results represent the long-term (drained) response to general loading regimes, and are seen to be the limiting design criteria, particularly for these marginal field applications.

Previous studies have indicated that plasticity theory may be able to provide an extremely powerful solution to this complex non-linear geotechnical problem. This chapter has shown that the response of a skirted footing can be successfully described within a plasticity context. The yield surfaces in $\{V{:}M/2R{:}H\}$ space are shown to be well described by parabolic ellipsoids, as indicated by several previous studies (Gottardi and Butterfield, 1993; Martin, 1994; Gottardi *et. al.*, 1999). The study indicated that the shape of these yield surfaces, during pre-peak bearing capacity behaviour, was a function of the ratio V_o/V_{peak}. The study also indicated the change in shape of the yield surface with increasing embedment ratio. In all cases the use of an associated flow rule in the deviatoric $\{M/2R{:}H\}$ plane was supported by the tests.

The results will provide the basis for the development of simple numerical solutions to various aspects of the combined loading problem. They provide evidence of trends and relationships, which were previously not quantified. The development of numerical solutions is important as they make the design process simpler for the engineer, particularly during the conceptual stages of a project. The results have also provided the basis for the development of much more complicated models, which would only be used during the detailed design stage of a project.

The research has highlighted several areas which warrant further investigations. These include the understanding of footing behaviour inside the yield surface, under elastic loading. It was apparent that the deviatoric elastic stiffness was dependent on the overconsolidation ratio of the load on the footing. The research indicated, in agreement with previous studies, that the hardening law is more complex then being just a function of vertical plastic penetration. It was apparent that significantly more hardening occurred during radial loading tests, then could be determined from the $\{V_o{:}w_p\}$ relationship.

The research on the dense sand was complemented by an auxiliary series of tests on very loose carbonate sand. The evidence presented suggested that the plasticity approach works equally well for such a material. Differences were observed in the variation of yield surface shape and the hardening law with embedment. These differences were attributed to the fact that a peak bearing capacity was not observed and that the footing response was affected by embedment. It is clear that the hardening law needs to take into account deviatoric movements as well as vertical movements, as also indicated by the dense sand tests.

CHAPTER FOUR
CYCLIC AND MONOTONIC VERTICAL LOADING

4.1 INTRODUCTION

Suction caisson foundations are clearly subjected to combined loading that is moment and horizontal loading as well as vertical loading. The horizontal loading can be estimated from the calculated shear load on the structure with the loading on each caisson estimated by using a structural analysis program or by assuming an equal distribution between caissons. The moment loading is harder to estimate since it depends on the complex interaction between the stiffness of the structure and the foundation. The moment loading can be kept deliberately low by designing a flexible connection between the structure and the foundation, as was the case for Statoil's Sleipner T structure. If this connection is assumed to be pinned, then accurate estimates of horizontal and vertical loads can be made with zero assumed moment loading. The design of caisson foundations subjected to combined loading is an area of great uncertainty, however, some progress has been made in Chapter 3 and 5 of this thesis. If, however, the pinned connection is adopted then the vertical loading components (especially the tensions) are likely to be most important.

Research on the cyclic vertical loading problem for sand is particularly scarce, and most has been in commercial confidence. For suction caissons in clay, where the response is typically undrained, there have been a number of research programs investigating cyclic behaviour (more recently El-Gharbawy, 1998). This is due in part to the more extensive use of suction caissons in clay dating back to Gorm in 1980 (Senpere *et. al.*, 1982). However, suction caisson use in sand has been very limited, partly due to scepticism about what tensile capacity can be expected - it has been typically thought to be limited to the drained tensile capacity. However, if the dilative capacity of dense sand is taken into account, combined with typical wave loading rates, it is possible that significant strengths (tensile and compressive) can be realised. These are likely to be only limited by the cavitation of the pore fluid (for example see Figure 1.3), which for water depths associated to most offshore structures occurs at very high pressures.

In recent years the Norwegian state oil company 'Statoil' has made use of the suction caisson concept successfully for two jackets installed on dense sand (Sleipner T and Draupner E). To prove the concept they undertook laboratory investigations at the Norwegian Geotechnical Institute and Oxford University as well as field scale investigations. Most of the results from these investigations remain proprietary, though

there are several papers in the public domain which detail small parts of the investigation (for example Tjelta, 1994; Bye *et. al.*, 1995; Baerheim *et. al.*, 1995). Bye *et. al.* (1995) detail the design approach which was developed during the course of the Draupner E foundation design, and subsequently improved upon during the Sleipner T detailed design. The design of the second jacket was such that significant tensions were expected during the most extreme storms anticipated during the life-time of the structure. A significant amount of model testing was therefore undertaken to determine the response of the foundation to various cyclic loading regimes, which included tensile loadings. In parallel with this, a significant effort was directed towards developing finite element methods, combined with cyclic triaxial test results, which were capable of predicting response. The overall framework that was developed during the course of the above investigations consisted of zones of cyclic amplitudes that could be sustained, but once these boundaries were breached there was rapid degradation of performance, as indicated in Figure 4.1. Clearly shown on the Figure are zones of acceptable cyclic loads, which increase proportionally with the static capacity.

4.2 EXPERIMENTAL RESULTS

The results discussed in this chapter have been selected from a large accumulation of tests to show the behaviour of suction caissons under vertical cyclic loading. Other loading paths, consisting of moment and horizontal cyclic loading, have also been applied and are the subject of chapter 5. All test results discussed in this chapter will refer to a 150mm suction caisson foundation with a 50mm skirt unless otherwise specified. Table 4.1 lists the key tests used to illustrate cyclic vertical loading behaviour in this chapter, with the key parameters. Tables 4.2, 4.3 and 4.4 breaks the tests into groups which were used to establish an understanding of frequency, loading history, and, cyclic load ratio. Table 4.5 presents the tests which were used to establish the vertical tensile loading behaviour. Where the data are presented in figures the Figure number is listed. In most tests it was typical to load the footing to a desired initial load, carry out a series of loadings, then load to the next desired load and so on. Only at the very start of a sequence of tests is the foundation load state on the virgin penetration curve. In most of the testing the foundation is in the 'elastic' region, only experiencing significant plasticity when the load state retouches the virgin penetration line, or yield surface for the case of combined loading. This is representative of the physical situation, particularly for vertical loading. Offshore structures are usually installed in the months of the year where there is calm weather and relatively long weather windows. This is beneficial for the structure's foundations as they

may experience relatively minor loadings after installation leading to consolidation and hence strengthening of the soil. It is probably appropriate to provide sufficient drainage initially so that this consolidation can occur quickly and in a controlled fashion. For sand the timescale for consolidation is particularly quick, and it is likely to occur within the period of most storms. After a very short period of time and small number of loadings the foundations would be operating within the elastic region of the yield surface. Each subsequent storm is only likely to cause a small incremental amount of plasticity to occur - even during the harshest of storms. Most tests were carried out in a fashion which mimicked this situation - progressively harsher conditions were applied to the foundation to observe behaviour. To observe virgin penetration behaviour, the foundation was usually moved to a load state which it had not previously experienced. It was observed that if any consolidation occurred, it usually occurred in the first few cycles of the loading.

Figure 4.2(a) shows the load-penetration results for a typical test where there are about 50 cyclic subtests as well as monotonic pull tests. After a large monotonic pull tests it is thought that the load penetration response will be similar to the virgin penetration. One such test was conducted at the end of this test sequence and is superimposed at the start for comparative purposes. It is clear that there is a substantial amount of accumulation of displacement due to the cyclic tests, much more than would be predicted in a conventional work hardening plasticity footing model. Figure 4.2(b) shows a magnified view of the initial cyclic tests where it is observed that there are substantial displacements on excursions into tension.

4.2.1 Introduction to Typical Cyclic Loading Results

In the initial development of the program of research it was apparent that there were certain events that would cause or precipitate failure as indicated by the framework set out by Bye *et. al.* (1995). It was felt necessary to develop a technique which could be used to produce a load train that incorporated an extreme event such as would occur when large waves pass an offshore structure. The first approach to developing such a technique is to use current state-of-the-art wave loading methods. This technique, which is called 'Constrained NewWave' (Taylor *et. al.*, 1995), enables an extreme event to be placed within a sequence of random loading such that statistically it is indistinguishable from a random occurrence of that event. It is a very powerful technique which has been used to decrease the amount of computation required to develop extreme value response statistics (as in Cassidy 1999). One of the main features is that the shape of the extreme event is proportional to the autocorrelation function of the power spectrum of the seastate. This

method was used for developing load paths, such as that shown in Figure 4.3(a), to study the effects of extreme loading events. This appears to be a more satisfactory representation of the physical reality than the typical application of many sinusoid cycles. The usual methods would create an unrealistic amount of degradation of the foundation and perhaps leading to very conservative methods for design. All cyclic tests were composed in a manner similar to that shown in Figure 4.3(a), comprising of approximately 100 cycles within which four extreme events are embedded. This is felt to be a long enough sequence to capture any behaviour that may be associated with an extreme loading. The displacement response associated with the above load path is shown in Figure 4.3(b) and the load displacement response is shown in Figure 4.3(c). Interestingly the load displacement response changes gradually to an asymmetric response as the load on the footing moves closer to tension.

This load sequence is one of approximately 200 cyclic sequences (spread over eight separate test sites) which were used to examine the different effects of load repetition, loading rate and loading history. Figure 4.4 shows a typical test in which the variation of loading rate has been examined. The series consists of three cyclic tests in which the mean crossing period differs by a factor of two in each subsequent test (in this case periods of 3s, 6s and 12s). Shown on Figure 4.4(b) is the pore fluid response, in which the pore fluid appears to take most of the load that is applied to the footing. A better indication of this is to plot the effective footing load, defined as the vertical load minus the pore fluid load, against time (also plotted on Figure 4.4(b)). The effective load appears to be cycling with small amplitudes about the mean total load. It is clear that the loading rate is such that there is a significant pore fluid response (almost an undrained response). However, there appears to be no accumulation of pore fluid pressure. In most tests, where it was possible, two pressure transducers were used at the perimeter of the footing. The response from these transducers is plotted on Figure 4.4(c) along with the response of the central transducer and the total load. The response is similar in magnitude to that recorded at the centre of the footing.

4.2.2 A framework for analysing results

The experimental application of cyclic loading results in a large amount of data to analyse. It was necessary to develop some method of data reduction, so that different test results could be compared, and which captured the main features of the loading and displacement paths. Such a method is shown in Figure 4.5. In most cases cycling is load controlled about a mean load. If the data is examined between the consecutive mean load crossings, a

permanent offset can be observed according to the applied load in the half-cycle. If, during the half cycle, the maximum displacement is obtained, it is then also possible to estimate the temporary displacement (elastic displacement) during that half cycle. This process is simple enough to automate within a MSExcel spreadsheet using a VisualBasic macro and leads to very easy data reduction. A set of results is shown in Figures 4.6(a) - (c). The first shows the recoverable response of the footing, which clearly becomes asymmetric once the load reduces below the mean load, towards tension. Similar results are evident when the permanent deformation is plotted against the applied load. The most interesting graph, in terms of displacements, is the third where the permanent displacement is plotted against the recoverable displacement. There is a distinct change in slope at or near the origin.

Figure 4.7(a) shows results reduced in this way for cyclic tests conducted at four different mean loads. The temporary displacement is plotted against the difference between the peak load and mean load. Whilst there is a clear relationship for each individual test there is no correlation between different mean loads. It is necessary to develop a system of normalisation so that results can be compared. An initial set of normalisations might be to divide the difference between peak load and mean load by the mean load (V_{norm}) and normalise the displacement by the footing diameter. This has been done for both temporary displacements (Figure 4.7(b)) and permanent displacements (Figure 4.7(c)). Also shown in Figure 4.7(d) are the displacement quantities plotted against each other - there is again little correlation between the quantities for different tests.

Dimensional analysis (Buckingham, 1914) can be used to determine a suitable method of normalising variables so that it is possible to determine relationships between the key variables. Typically

$$\Pi_1 = f\left(\Pi_2, \Pi_3, ..., \Pi_{n-k}\right) \quad \text{.....} \quad 4.1$$

where n is the number of dimensional parameters and k is the number of fundamental dimensions. The form of f is not provided by dimensional analysis but is usually approximated by an empirical dimensionless equation fitted to either model or prototype data. In the cyclic loading problem the following are the relevant variables, listed with their dimension:

Variable	Description	Dimension
d	Footing displacement	L^*
V_m	Mean cyclic load	F
V_p	Peak cyclic load (trough and crest) (defined as V_{peak} - V_{mean})	F
D	Diameter of footing	L
G	Shear stiffness of the soil (which has been expressed as stress divided by strain)	$\frac{F/L^2}{L^*/L}$
g'	Effective unit weight of soil	F/L^3

It should be noted that L^* is a special length dimension associated with the definition of strain and corresponds to the small footing displacements. The footing displacement is the variable of interest such that:

$$d = f(V_m, V_p, D, G, g') \quad \text{4.2}$$

It follows that there are three dimensionless groups to be formed, given that $n = 6$ and $k = 3$:

$$\frac{dGD}{V_m} = f\left(\frac{V_p}{V_m}, \frac{V_m}{g'D^3}\right) \quad \text{4.3}$$

The three formulated groups suggest that the foundation displacements are dependent on the peak cyclic load and the mean stress level. It is also generally suggested for granular material that the shear stiffness is proportional to the square root of the effective mean stress level (Wroth and Houlsby, 1985) such that:

$$\frac{G}{p_a} \propto \sqrt{\frac{V_m}{D^2 p_a}} \quad \text{4.4}$$

If the mean load is assumed to be very small compared to the peak bearing capacity, it can be assumed that the second of the two independent dimensionless groups will not have a significant influence, then the following can be postulated:

$$d\sqrt{\frac{p_a}{V_m}} = f\left(\frac{V_p}{V_m}\right) \quad \text{4.5}$$

This provides a powerful normalisation which in this chapter appears to show consistent trends for a variety of different experimental conditions. Figure 4.8 shows how the normalisation works for the different mean loads from Figure 4.7, where the footing

diameter remains constant. In the figures V_p/V_m will be referred to as V_{norm} whilst $d\sqrt{\frac{p_a}{V_m}}$ as d_{norm}. Although there is some scatter, it appears that, for the range of mean stress levels shown, the second of the two independent dimensionless groups does indeed have little effect on the response of the foundation. The normalisation is particularly successful for the temporary displacements.

In all of the testing it was evident that there was limited degradation of footing response. In general the response of the foundation was such that there was a gradual transition from a stiff symmetric response at low load levels to an asymmetric response at larger cycles (dipping into tension). As the amplitudes of the cycles increased the levels of the permanent and cyclic displacements increased gradually, such as indicated in the summary figures plotted in this chapter. There was no threshold of load at which there was rapid degradation of performance as suggested by Bye *et. al.* (1995), even when the caisson was cycled into tension, for the cyclic loading applied. This lack of sudden transition to degradation by cyclic loading is examined further later in the chapter.

4.2.3 The Effect of Loading History

The methods developed in the previous section allowed the rapid evaluation of a large amount of raw cyclic data, which provides the opportunity for a succinct analysis. Each cyclic test completed used a loading history of 100 cycles of pseudo random loads so that the effect of extreme events could be evaluated. The emphasis of these tests was to determine the critical mechanism of caisson performance. It was usual to perform tests in which there were several packets of cycles with each successive test having a larger significant load than the previous test (*i.e.* 100 ± 25 N, 100 ± 50 N, ... ,100 ± 250 N). It became clear that the most relevant tests were those in which the significant load was the greatest. The normalised results from these tests incorporated all of the features of the tests with the lower significant loads. In considering the displacement response of the caisson foundation several further key points required investigation:

a) Was a 100 cycle packet long enough?

It could be argued that the testing used cyclic tests with too few cycles to establish any destabilising behaviour, even given the four extreme events. This was tested by running a sequence in which over 2000 cycles were used, with an extreme event every 25 cycles. The response is shown in Figure 4.9 where there is no significant difference between the first

100 cycles and the last 100 cycles, thus it is concluded that a 100 cycle packet is long enough.

b) Did the loading history make any difference?

Given that there appears to be no destabilising behaviour, even associated with the extreme events, is it necessary to use the 'constrained NewWave' approach as opposed to any other pseudo-random sequence? To test this three different load-time histories of essentially the same period were used. These are shown in Figure 4.10 and consist of a i) 'constrained NewWave', ii) a modulated sinewave, and, iii) a stepped sinewave. The responses are shown in Figure 4.11 and in this case it appears to be irrelevant what loading history was used, as they all appear to develop the same response. However, the use of the 'constrained NewWave' approach is still justified because it mimics the actual physical loading conditions on the foundation. It is appropriate to discuss extreme responses further at this point. The 'NewWave' is derived from Gaussian statistical theory and represents the most probable distribution of points around a local maximum or minimum. If the extreme process that is being modelled is assumed to behave in a Gaussian manner then the 'NewWave' approach can be used. However, it is necessary to scale the shape to the desired maximum level for different cases. For maxima having a Rayleigh distribution (i.e. a Gaussian system) the largest maximum in 1000 (the typical three hour stationary period for sea-states) is approximately a factor of 1.86 greater than the significant wave height. If the offshore structure were a linear system, such as an inertia dominated structure, as might be expected for a structure in shallow water, then this extreme level would be appropriate. As the structure becomes more drag-dominated, and thus non-linear, the one in one-thousand maxima can increase substantially. The current state-of-the-art is that it is not possible to develop generic force-time histories, though progress is being made (see for example Suastika, 1997 or Tromans *et. al.*, 1995). It is clear, that in the completed tests, large displacements occurred during the tensile extreme events - these would be even larger if the maxima were increased to represent the physical situation more closely.

c) Was there any effect of loading rate at the rates studied?

During the tests the loading rate was varied from periods of 1s through to 30s. In all cases there was no noticeable change in the response of the foundation. One specific test aimed at examining the effect of loading rate is shown in Figure 4.12. Two time histories where the periods differed by a factor of 10 (3s to 30s) were used. Interestingly, even in the very slow test there is a strong pore fluid response even though the t_{50} time estimated just prior to this test was of the order of 24s. The much longer period in the second test meant that

the tensile responses (in terms of displacements) were greater. It was possible in this test, because of the increased amount of time and thus feedback, to maintain a much better control on the desired load path. Therefore the tensile displacements are greater. The poorer control on the quicker test, and the maximum speed of the loading rig, meant that the same displacements were not mobilised. This is shown in both the displacement time history as well as the load displacement figure. In excess of 1mm is required to mobilise 200 N of tensile capacity. This displacement can not be mobilised in the shorter test. An interesting observation lies in the plot of pore fluid load against the total vertical load. The data all appear to lie in a straight line with the pore fluid load corresponding to approximately 80% of the total vertical load. This is the same for both tests regardless of period of cycling. On reduction of the data in the standard manner, shown in Figure 4.13, there appears to be no difference between the two tests. Further evidence of this can be obtained by examining the displacement responses, also shown on Figure 4.13, of the test shown previously in Figure 4.4. On reduction again there appears to be no significant difference between loading rates even though the three tests span periods of 3s to 12s.

4.2.4 Scaling and further remarks on loading rate

Many of the results shown so far have been from tests conducted on footings of 150mm diameter. One aim of the research was to examine the effects of scale on the results. This was possible within the present set-up by using a 100mm footing. Other testing has also been undertaken in the Structural Dynamics Laboratory at Oxford University as part of a fourth year project (Johnson, 1999). This testing was performed on a footing of diameter 300mm, and involved various cyclic loading routines, at loading rates between 0.1Hz and 10Hz thus spanning the full range of transient response conditions. The nature of the loading apparatus was such that the mean load applied to the footing was 50kN, which is a substantial increase over the mean loads studied during the main bulk of the research (100N - 800N). Typical test results are shown in Figure 4.14 for the 'NewWave' loading. These results are reduced and shown in Figures 4.15 (a)-(c) using the appropriate normalisation. Included on the charts are results from footings of diameter 150mm, and 100mm. It is clear that there is good agreement between the various test results, indicating that the behaviour does indeed scale, at least at laboratory scales. The slight discrepancies are probably due to the influence of the ratio $V_m/(g'D^3)$ on the response which has been assumed to have negligible effect. In reality this factor is significantly larger for the 0.3m diameter footing than for the 0.15m diameter footing.

Of interest in this research has been the effect of loading rate. Previous coverage of this topic in the literature is relatively scarce (Vesic *et. al.*, 1965; Mangal, 1999). The testing covered during the period of the above research tends to indicate (somewhat surprisingly) that loading rate has little effect on the transient response. Cyclic tests were carried out at periods of 1s, 3s, 6s, 12s and 30s with no significant difference observed between tests. The results of the experiments conducted by Johnson (1999) also indicated very little effect of loading rate on behaviour. Further analysis of the results from experiments undertaken by Mangal (1999) tend to support this conclusion. In those tests the footing was penetrated along the virgin penetration line until a specified load level (500N or 1000N) was reached. The footing was then penetrated at a specified rate for a specified distance (nominally 0.5mm). Two distinct phases of behaviour were observed, a stiff initial response, followed by a softer final response. This stiff initial response is shown in Figure 4.16(a) where the stiffness of the response is plotted against the loading rate. The results shown are expressed in terms of stiffness due to the fact that the displacement was not equal in all cases. The loading rates span three orders of magnitude, whilst the stiffness only marginally increases towards the faster loading rates. Mangal (1999) characterised his soil samples by a drained plastic penetration stiffness, K_{eq}, as the uniformity between different soil samples varied greatly. If the initial stiff response plotted in Figure 4.16(b) is normalised to this K_{eq} parameter the effect of loading rate on the response is inconclusive - it is clear that the initial transient stiffness is a factor of 15 greater than the drained stiffness. The softer secondary response is shown in Figure 4.16(c), again normalised to K_{eq}. The secondary response appears to be of the same magnitude as the drained virgin stiffness with no real correlation to loading rate.

4.2.5 An Empirical Framework for Prediction of Response

A simple method for providing a prediction for the displacement response of these caisson foundations subjected to various loadings would consist of an empirical curve-fit to the data. Such a curve-fit would require dividing the data into positive and negative sectors. The temporary compression segment can easily be fitted by a linear trendline:

$$d = V_{norm}/k \quad \text{.....} \quad 4.6$$

whilst all other sectors can be fitted by an equation of the hyperbolic form:

$$d = \frac{V_{norm}\left(c_{ult} - (2-s)V_{norm}\right)}{k_{init}\left(c_{ult} - V_{norm}\right)} \quad \text{.....} \quad 4.7$$

Figure 4.17 shows data from vertical loading tests conducted at V_{mean} = 100N and V_{mean} = 200N on the medium dense sand (relative density 79%). The appropriate fits to the data, as shown on the Figure, are obtained using the following:

Compression temporary displacements	$\{k\} = \{900\}_{\text{comptemp}}$
Tension temporary displacements	$\{c_{ult}, s, k_{init}\} = \{\text{-}1.35, 2, 900\}_{\text{tenstemp}}$
Compression permanent displacements	$\{c_{ult}, s, k_{init}\} = \{2.25, 2.5, 2000\}_{\text{compperm}}$
Tension permanent displacements	$\{c_{ult}, s, k_{init}\} = \{\text{-}1.25, 1.5, 2000\}_{\text{tensperm}}$

Note that there is continuity of the slopes where they cross at the origin. These curve-fits may be used easily within a spreadsheet program to evaluate displacement responses to various loading paths. An example loading time history is shown in Figure 4.18, the corresponding predicted and actual displacement path is shown in Figure 4.19. Clearly the general trend of the prediction is accurate, but after the caisson experiences a load close to tension (normalised load less than -0.95) the next vertical permanent displacement is underpredicted. This is shown on the load displacement plot in Figure 4.20(a) where after every low load excursion the caisson experiences a much larger penetrative displacement. By highlighting all permanent displacements after tensile loadings on Figure 4.20(b) it can be seen that a much softer curve-fit is needed to represent these points. Such a curve-fit is overlain on the data using $\{2.5, 2.5, 2000\}_{\text{compperm}}$ for most data. However, if the previous load point goes close to tension then $\{2, 2.5, 2000\}_{\text{compperm}}$ is used. Figure 4.20(c) shows the resulting time history of displacements which provides a much closer match than previously. This approach has also been used for the back-analysis of the data in Figure 4.21, which shows a vertical loading test at three different rates on denser sand (relative density 92%). The appropriate curve fit parameters are:

Compression temporary displacements	$\{k\} = \{1200\}_{\text{comptemp}}$
Tension temporary displacements	$\{c_{ult}, s, k_{init}\} = \{\text{-}1.35, 2, 1200\}_{\text{tenstemp}}$
Compression permanent displacements (1)	$\{c_{ult}, s, k_{init}\} = \{3.5, 2, 2500\}_{\text{compperm (normal)}}$
Compression permanent displacements (2)	$\{c_{ult}, s, k_{init}\} = \{3.5, 2.5, 1500\}_{\text{compperm (after large tension)}}$
Tension permanent displacements	$\{c_{ult}, s, k_{init}\} = \{\text{-}1.5, 1.5, 2500\}_{\text{tensperm}}$

As in most curve-fitting exercises, the values of the parameters are fairly arbitrary in that they cannot be derived theoretically or from standard site-investigation tests. It is fairly likely that the tensile parameters would not vary in magnitude from the values stated as the small displacement tensile capacity is likely to be low and the response soft. Clearly the stiffness parameters, particularly the temporary stiffness, could be related to the soil density with some empirical correlation, though this has not been done at present. The parameters of the highest uncertainty are those for the compression, including the change in strength parameters immediately following a large tension. These hyperbolic curve fits are valid only for small displacements, particularly the tensile curve fits.

4.2.6 Partially Drained Loading Rates - Monotonic Pull Tests

It was felt important to determine the effect of rate on the tensile response of the caissons. Preliminary analysis of the cyclic loading data revealed little evidence of the anticipated rate dependant dilation induced strengths. One method used to examine this tensile response was to perform monotonic pull tests at different rates. This can be seen in Figure 4.22(a) which shows five pull tests conducted at velocities differing by three orders of magnitude. In each case the test was taken to 1mm in extension, which should have been sufficient to mobilise a dilative tensile response. The estimated drained tensile capacity is of the order of 15N, which is lower than the response observed, indicating that indeed a partially drained response was being invoked. This is confirmed by examining the pore fluid load response measured by the pressure transducers, shown in Figure 4.22(b). Clearly most of the applied tension load appears in the pore fluid load. There is little difference in the amount of load taken by the pore fluid with respect to the rate of load application.

Pull tests were performed at a number of different stages of the testing program revealing some interesting trends. Figure 4.23 shows three such pull tests performed on the same caisson foundation at different stages of its loading history. All three pull tests were performed at the same rate, and it is clear that there is an effect of disturbance on the subsequent performance of the foundation. An initial pull test performed after some preliminary horizontal and moment cycling establishes a vertical load of about -75N within the 1mm extension. Several more pull tests were performed immediately after this test with each subsequent test showing a marked reduction in capacity. The final test of this batch is also plotted on Figure 4.23 (shown as the test after significant loosening) which shows a softened response and a maximum load of -40N. It is clear that the dilative response of the soil at the skirt tip has been dramatically reduced. Following these tests a program of testing to redensify the soil around and beneath the caisson was performed. This included a large amount of horizontal and moment cycling as well as vertical push tests. The pull test immediately after this "recuperative" work shows significantly better strength properties than any of the previous two tests, both in stiffness and maximum load (-100N). It is clear that the increase in local relative density has improved the performance.

Several tests were taken to very large displacements, in fact in two tests the caisson was pulled completely out of the soil. These two tests are shown in Figure 4.24, in terms of stress as they were conducted on caissons of differing diameters. The end points of the test paths shown in Figure 4.24 are at the instant when the load drops to zero and the caisson pulls freely from the soil. It is not quite clear what precipitates the failure at this stage.

However, it is probably piping or localised failure around the skirt. In both cases the load paths follow very similar trajectories, both reaching about -63kPa, at which stage the failure occurs. By inspection after the test it is clear that the whole plug of soil remains within the caisson skirt. The pore fluid pressure measured beneath the caisson top reaches about -50kPa in both cases, but at extremely large displacements. It was not possible in these two tests to reach a cavitation limit. The trend of the fluid pressure curve shows that there is a lag between the application of a negative load at the caisson skirt tip, and the corresponding decrease in the fluid pressure measured directly beneath the caisson top. In both cases there is about 10 mm of vertical movement between the initial partially drained negative fluid response (the dilation response), and the subsequent fluid pressure decrease associated with the development of suctions within the soil beneath the caisson. This suggests that the limiting design criterion is not whether tension can be mobilised, but whether serviceability requirements will be breached during the course of the tensile response.

It was necessary to investigate further the softened response associated with the pull tests by conducting similar tests on a denser sample of sand. The sand sample was vibrated, and a combination of vacuum and downward hydraulic gradients were applied to the sample to produce a much denser sample. Cone penetration tests conducted before and after the footing tests indicated a relative density of 92% (a friction angle of 43 degrees). The initial response was then investigated, as shown in Figure 4.25, by conducting successive pull tests at different rates (three orders of magnitude difference) for small displacements (less than 1mm). It is clear that as long as the displacements are kept relatively small there is little degradation of response. However once the footing was pulled to greater displacements there was a gradual degradation of the response until only the drained capacity was mobilised (the fully plugged caisson response). This final capacity was confirmed to be the same as the final weight of the soil plug by examining the weight of the caisson when the caisson was eventually pulled from the soil (with the soil plug intact).

To complete the testing a monotonic pull to failure is shown in Figure 4.26 where the 150mm diameter caisson is pulled completely out of this denser soil at 2 mm/s. Both the total load and pore fluid response are shown. It is clear that there is an initial soft response followed by a much stiffer response associated with massive dilationary effects. The capacity is clearly bounded by the advent of cavitation - the difference between the pressure curve and the load curve being the increased external friction (~400N) due to the large downward hydraulic gradient induced within the soil. The response of this secondary

dilational effect is clearly much stiffer than in the lower density sand, though there is little difference between the initial soft responses. An interesting observation is that of the pore fluid load, where on the initial application of the negative load the pressure response is almost immediately negative, suggesting an undrained increment at the caisson base plate. On continuation of the application of the negative displacement rate the pressure response dissipates until shearing occurs at the caisson skirt-tip level and the pressure response picks up. This suggests a transfer of load application from the caisson base plate to the caisson skirt tip, upon which soil loosening occurs at the skirt-tip level. The stiffness of the final section of the load response is therefore dependent clearly on the relative rate at which the fluid can travel through the soil to equilibrate the pressure difference created in this loosened soil mass.

Evidence of the effect of the caisson skirt has also been gathered. Figure 4.27(a) shows several load displacements paths for a flat footing of 100mm diameter. This test consisted of applying about 2000N of load to the footing and then performing a monotonic pull test at 2mm/s. After each successive pull test the footing is reloaded and penetrates further into the soil so that after seven pull tests the footing has penetrated 15 mm. The negative tensile response of the footing appears to be limited to a value of -380N. Interestingly the load displacement path for all tensile responses appears to follow the same trajectory regardless of the footing penetration, with the maximum load occurring at a footing position which is above the soil surface (~1.5mm) - the soil appears to be loosening substantially. Evidence of the pore fluid response is presented in Figure 4.27(b). On the application of an upward movement to the footing there appear to be two different fluid responses. Immediately there is a negative response, presumably an undrained or partially drained response to the reduction in load. This response dissipates quickly before a second effect occurs at a footing displacement corresponding to the mudline. Figure 4.28 shows the response of several flat footing tests and a skirted caisson test (e/D = 0.16, D = 100mm). The test was conducted such that the flat footing was loaded to 100N on a fresh bed of soil. Several pull tests were conducted spaced by monotonic loading to 100N. The flat footing was removed and replaced by the small skirted footing which was then loaded to 100N and moved in tension at 2mm/s. It is clear that due to the increased drainage paths the tensile capacity has been increased substantially and in this test is limited by cavitation of the pore fluid. The flat footing failure is initiated by the very short drainage paths at the edges of the footings. These two tests provide substantial evidence that footings on sand may benefit substantially from a small skirt - this may have particular relevance for mobile drilling

units (jack-up rigs) where a hybrid spud-can caisson foundation could be used to good effect.

There is corroborative evidence of these responses in the very small amount of published data in the Bye *et. al.* paper (1995) shown in their Figures 2.6 and 2.7 which are replicated in Figure 4.29. The model tests shown are monotonic pull tests as described in this section. However, they were conducted on a larger diameter footing embedded in water saturated sand. Figure 4.29(a) shows the typical asymmetric response for tension and compression that has been shown more conclusively in this chapter. Figure 4.29(b) shows the initial soft response and the subsequent effect of load rate on the stiffness of the load curves that is expected (*i.e.* stiffness proportional to the relative rate of fluid flow through the soil). The limitations of the testing apparatus prevented any of these tests being taken to the cavitation limit. Of critical importance is that the axes labels on both graphs (importantly the displacement) have been omitted. It would appear that the rate dependent behaviour is crucial to the design. The current work suggests that in actual fact the displacements required to mobilise the rate dependent behaviour may possibly breach serviceability requirements. Furthermore, if this rate dependent behaviour is triggered, the response of the foundation to subsequent loading degrades substantially. Therefore the tension cyclic capacity boundary shown in Figure 4.1 may relate to the boundary between the initial soft response and the rate dependent response during tensile loading. It is not clear why there should be a boundary on the compression side as there has been no evidence of any degradation in this regime. It is most likely that Bye *et. al.* (1995) have taken this boundary to relate to the compression half cycle following the tension half cycle which invoked the rate dependent response and thus subsequent degradation. It is unlikely that single compressive loads exceeding this boundary will to trigger a degradation.

From the above discussion it is clearly appropriate to design the tensile capacity on the softened initial response which at present is difficult to quantify. In their paper Bye *et. al.* (1995) imply a lower bound to this may be taken as the non-dilational undrained capacity. However, this is clearly difficult to estimate due to the continual re-arrangement of the soil beneath the caisson on each large tensile excursion as postulated in this chapter. The presented experimental data tend to suggest that this capacity degrades eventually to the weight of the soil plug, but more research is required on this aspect of behaviour. It is perhaps instructive to observe the response in a pile load test in which there is significant skin friction. It is typical that the end bearing is only mobilised after a displacement of ten percent of the diameter whilst the skin friction is usually mobilised within one percent.

Analogies may exist between this result and the tensile loading tests of a short skirted footing. It is highly likely that the skirt friction is mobilised very quickly upon any displacement but that the end bearing is only mobilised after a substantial displacement. If the test were fully drained then the end bearing component would be extremely small (if not zero). As the test becomes progressively partially drained the end bearing resistance (through a reverse bearing capacity mechanism) is mobilised within smaller and smaller displacements though it is unlikely that the end bearing is mobilised faster than the skirt friction. It is also unlikely that there is a discontinuity at zero load as may be suggested from the evidence presented in this thesis. Due to the extremely low skin friction because of the low stresses involved with one gravity testing it may be suggested that the tension-compression transition is the trigger for the degradation. However, from evidence of pile load tests, it may be the case that there is a smooth transition between tension and compression and the trigger is the mobilisation of the drained friction.

It is very important to identify the important mechanisms that control this initial limit as the very act of suction installation will cause loosening of the soil at the caisson base which could have a crucial impact on the tensile response. Clearly the finite element analysis shown in Figures 4.29(a) and 4.29(b) do not model the critical part of the response well.

4.2.7 Comparison of Pull tests and Cyclic Loading Results

The pull tests have indicated some interesting phenomena which have implications for the cyclic loading tests. It is obvious that a pull test represents the tensile quarter-cycle of a large cycle in a cyclic loading test. It follows that there should be a close correlation between the pull tests and the cyclic loading tests. Figure 4.30 shows the results from a cyclic loading test conducted about a mean load of 200N, the displacements are such that the cumulative displacement has been removed. Also plotted on this chart is a corresponding pull test conducted immediately after the cyclic loading test. There is an impressive match between the two. This match is further confirmed in Figure 4.31 which shows cyclic loading tests and their corresponding pull tests which were conducted before and after densifying. In each case the pull tests were conducted immediately after the cyclic loading test. This trend may allow a significant reduction in future testing programs, as it may prove worthwhile to study only the tensile monotonic response and infer from that the cyclic response.

Figure 4.32 shows the accumulation of the pore fluid response readings for several monotonic pull tests. Also shown on the plot are pore fluid response readings from a cyclic

loading test. Interestingly there is a strong correlation between the vertical load and the pore fluid load from the two different types of test (~80% total vertical load).

4.2.8 Comparison with results from El-Gharbawy (1998)

El-Gharbawy (1998) conducted a series of tensile monotonic and cyclic tests on suction caissons in clay of increasing strength with depth. He states "in general the LTC (long term capacity) of the caissons also represented the maximum peak cyclic load that could be withstood before excessive displacements occurred". He examined caissons from embedment ratios of 2 up to 12, which are the typical aspect ratios encountered for caisson anchors used in clay. The testing sequence consisted of drained and undrained tensile tests to establish ultimate capacities. He also undertook tensile cyclic loading tests, including combined horizontal and tensile loading, of the sort encountered in the typical floating facility anchoring application. He found that cyclic frequency and load inclination had a minor effect on the displacement response, as long as the peak cyclic load was lower than the drained response. However, once the peak cyclic load exceeded the drained response, the performance deteriorated rapidly on the application of either inclined loads or faster cyclic periods. This evidence is in line with the observations presented for sand that as long as the cyclic loading is kept within the drained tensile capacity then problems should be avoided. This results in a rather cautious approach to design, and may be alleviated by allowing for ballast to be placed upon the caissons.

4.3 CONCLUDING COMMENTS

This chapter has presented selected results from a variety of vertical loading routines on novel offshore foundations called suction caissons. The results indicate some interesting trends which provide powerful insights into the behaviour of the foundations under both monotonic and cyclic loading routines.

A novel method of applying cyclic loading was used and a new data reduction method for analysing the resulting data was developed. Dimensionless groups were then suggested for normalising the cyclic loading summary data. When these techniques were applied the behaviour between the various tests could be compared. There was little evidence of cyclic degradation of response as detailed by Bye *et. al.* (1995) at the displacements and loads that would typically be encountered in cyclic loading. There was also little evidence of rate dependent behaviour. The footing behaviour scaled between footing diameters at the laboratory scale.

The cyclic loading results tend to indicate that serviceability requirements will dictate the design of the foundation. Monotonic loading tests, conducted at different rates, where undertaken to investigate the tensile response further. It became clear that large tensile capacities were possible though these were bounded by the cavitation of the pore fluid. In these tests the large tensile capacities occurred at large displacements relative to the footing diameter. A dilative response was evident at small displacements, which was substantially larger than the drained tensile capacity. At these small serviceable displacements there was little degradation of the foundation as was found for the cyclic loading. Surprisingly the rate of loading appeared to have little effect on this initial transient response. At larger displacements it is clear that the behaviour becomes rate dependent. However, the initial soft response degraded upon application of successive tensile loads, with a limiting value equal to the drained tensile capacity.

There was a close correlation between the cyclic loading results and the monotonic pull tests. This indicates that future testing programs may be reduced to performing monotonic tests and inferring cyclic behaviour from them. It would then only be necessary to perform a small number of cyclic tests to confirm inferred behaviour.

CHAPTER FIVE

CYCLIC AND MONOTONIC COMBINED LOADING

5.1 INTRODUCTION

The response of caisson foundations to vertical transient loading has been discussed at length in Chapter 4. It is clear that design for vertical loads will centre around serviceability requirements rather than capacity. By increasing the fixity of the connection between the structure and the foundation it is possible to take advantage of the moment resisting capacity of the caissons. Alternatively by adopting the monopod design, as suggested for renewable energy applications, it becomes very important to be able to determine the moment response to the applied loads. This chapter focuses on the response of the foundation to these combined load combinations, under monotonic and the more relevant cyclic transient loading conditions.

5.1.1 Drained Monotonic Moment Behaviour at Low Vertical Loads

One of the important aspects of the wind energy application is the drained combined load response of the suction caisson under very low vertical loads. The drained capacity is the response under long term load conditions such as a predominant wind or current, and will give a lower bound to the overall response. Figure 5.1(a) shows a simplified diagram of applied forces and reactions from the soil for the case of no vertical load. Figure 5.1(b) shows how the yield surface at low vertical loads would vary in the horizontal plane. As the embedment ratio increases the intercept at zero vertical load increases. The slope of the curve would increase with increases in the friction angle.

In Figure 5.1(a) the contribution of the moment resistance on the base is ignored, as it is difficult to quantify. If it is assumed that there is a pivot point at some depth, l, of the caisson then a non-dimensional transition depth $x = l/L$ can be defined. By equating horizontal forces (assuming that K is the earth pressure coefficient equal to K_p - K_a, effective unit weight of γ', and peak friction angle ϕ):

$$H = \frac{K\gamma' D}{2}\left(2l^2 - L^2\right) - \left(\tan\phi\right)\gamma' L\left(\frac{\pi D^2}{4}\right) \quad \text{.....5.1}$$

To obtain moment equilibrium (ignoring the moment resistance on the base):

$$M = \frac{K\gamma' D}{3}\left(L^3 - 2l^3\right) + \left(\tan\phi\right)\gamma' L^2\left(\frac{\pi D^2}{4}\right) \quad \text{.....5.2}$$

To obtain meaningful expressions it is necessary to non-dimensionalise the loads, accomplished by dividing through by $g'D(\pi D^2/4)$ (the moment is divided by $2R$ to reduce it to units of force).

$$h = \frac{4H}{g'\pi D^3} \text{ and } m = \frac{4M}{g'\pi D^4} \quad \text{.....5.3,5.4}$$

By utilising this normalisation the initial expressions of equilibrium become (assuming $y = L/D$):

$$h = \frac{2Ky^2}{\pi}\left(2x^2 - 1\right) - y\tan\phi \quad \text{.....5.5}$$

$$m = \frac{4Ky^3}{3\pi}\left(1 - 2x^3\right) + y\tan\phi \quad \text{.....5.6}$$

These expressions provide simple estimates of the boundaries to response and are plotted on Figure 5.2(a). This enables preliminary dimensions of the foundation to be determined. Several tests were aimed specifically at determining the limiting drained load capacity at these low load levels (such as those detailed in chapter 3). The laboratory tests performed, called loop events, consist of following a circular path in $\{2R\delta\theta : \delta u\}$ space on a highly overconsolidated footing. The resulting load path gives the cross-sectional shape of the yield surface in the deviatoric load space $\{M/2R : H\}$. One such test is shown in Figure 5.2(a) for caisson of embedment to diameter ratio of 0.66 and vertical load constant at zero. The theoretical response is lower than this experimental result, which maybe improved slightly on the inclusion of the base moment resistance.

The offshore wind energy application consists of large overturning moments applied for little vertical load. It is clearly important to understand how the limiting moment capacity increases with small increases in vertical load above zero. This is shown in Figure 5.2(b) where the non-dimensional moment is plotted against the non-dimensional vertical load for a caisson of embedment to diameter ratio of 0.66. Shown on the Figure are points from individual loop event tests conducted at different values of constant vertical load. A line of best fit (yield surface) is shown as an outerbound to these tests. These points will fall within the limiting capacity yield surface as the tests were conducted at some intermediate strain level, above the elastic level, but below the truly plastic level. Also plotted on the Figure is a swipe test conducted from a low level of vertical load. This shows that indeed the loop tests were mobilising a significant amount of the moment capacity. Of course on the tension side there will be a limiting drained capacity equal to the internal and external

skin friction. The results shown in Figure 5.2(b) are for purely moment loading with zero horizontal loading. Clearly, though, in the wind energy application the moment applied to the foundation will be due to horizontal loads acting at some distance from the base (up to 30m). Therefore the available moment capacity may be reduced depending on the horizontal load as depicted in Figure 5.2(a) and described in chapter 3.

5.1.2 Field Scale Testing

In combination with the experimental and theoretical research the author has been able to observe two full scale field trials. These were conducted in order to observe the effect of scale on the moment response. In these trials, horizontal loads, and hence moments, were applied to the caisson. Figure 5.3(a) shows the set-up for one of these tests. The test was conducted in a river mouth where a very high tidal flow was prevalent. The caisson was installed during high tide, whilst the test could be performed at any stage, as the assessment of the drained capacity was important. Figure 5.3(b) shows the response for one of the trials. It is clear from the figure that there is a range of loads for which there is a stiff response, followed by more flexible behaviour as plastic deformations occur, this pattern also occurs in the laboratory experiments. These two trials allow the curves shown in Figure 5.2 to be evaluated for larger footing diameters, however more extensive work is required in this area, most probably using a geotechnical centrifuge to scale soil stresses appropriately.

5.2 CYCLIC EXPERIMENTAL RESULTS

If caissons are used for the renewable energy application, or other more traditional applications, they will certainly be subjected to cyclic combined loading. This chapter will present selected results to illustrate the significant behaviour of suction caissons under cyclic combined loading. The key tests used to illustrate moment loading behaviour are listed in Table 5.1 and Table 5.2. Where the data appear in specific figures the Figure number is listed. Table 5.3 and 5.4 list the key horizontal loading tests. The typical tests, which will be described further below, were monotonic tests and combined cyclic loading tests (moment, horizontal and both) under constant vertical load. A test sequence is shown in Figure 5.4 where both vertical and moment loads are plotted against the vertical displacement. It is clear that significant vertical displacements occur when the moment loading is applied to the caisson under a constant vertical load, particularly at the beginning of the test. The magnitudes of the vertical displacements due to moment loading

depend on the position of the load state with respect to the yield surfaces and the slope of the plastic potentials at these points.

5.2.1 Cyclic Loading

In the initial development of the program of research it was felt that extreme events were of prime importance. This was indicated in a framework of response set out by Bye *et. al.* (1995), which detailed selected results from an intensive program of confidential research undertaken during the development of Statoil's Sleipner T jacket and foundation system. They suggested that there were zones of cyclic amplitudes that could be sustained, but once those boundaries had been breached there was rapid degradation of performance (shown in Figure 4.1). Although this framework was developed for vertical loading there did not appear to be any logical reason why it should not also apply to horizontal and moment loading.

The 'NewWave' method, described previously, was used for developing load paths, such as that shown for moment loading in Figure 5.5(a), in order to study the effects of extreme loading events. This appears to be a more satisfactory representation of the physical reality than the typical application of many sinusoid cycles. The typical rotational displacement response to such a load path is shown in Figure 5.5(b) and the load displacement response is shown in Figure 5.5(c). Many other load paths were also used to examine the different effects of load repetition, loading rate and loading history. Other tests were also performed to aid in the development of a new theoretical model for cyclic loading. During the application of the combined cyclic loading it was necessary to keep the vertical load constant which would typically be the case for a monopod structure (vertical load equal to the weight of the structure).

5.2.2 A Manageable Representation of the Data

The large amount of data that is accumulated during a cyclic testing program is unwieldy in its raw form. The method used for vertical cyclic loading, depicted in Figure 5.6, was also used for combined cyclic loading. A set of these reduced results is shown in Figures 5.7(a) - (c). These results show data reduced from three different cyclic moment loading tests under the same constant vertical load. The first, SM1-3, are results after the foundation has experienced a large amount of combined load cycling and hence the response of the foundation is essentially within the yield surface. SM1-4 show results from a cyclic test on a normally consolidated foundation, prior to any form of deviatoric loading. Clearly on the displacement load graphs there is a substantially softer response, as more plasticity occurs and the yield surface expands. The SM1-4 after cycling results show a

cyclic load test completed after the yield surface had been expanded significantly by repeated cycling. The foundation load state is then acting within the yield surface, and consequently the foundation experiences a much stiffer response. This test result is equivalent to the test result denoted SM1-3, which was a corresponding sub-test in a previous footing test. The initial stiffness of all three tests is approximately similar. The larger strain stiffness is much lower for the normally consolidated test than for the over-consolidated test. This also applies for the temporary displacement where there is considerably less scatter and a much stiffer response.

5.2.3 Response to Initial Cyclic Loading

The first loading of the structure is a critical period in the life of the foundation, where it appears there is a greater propensity for plasticity to occur than at any other time in the foundations lifetime. Typically the foundation would be normally consolidated, particularly in the case of a suction caisson installed in sand, as no preload from the suction is possible. Figure 5.8(b) shows the shape of the yield surface before, during and after the initial storm loading where there is significant moment loading. Initially the load state is at the vertical load apex of the yield surface, as moment load is applied the yield surface expands, and vertical displacements occur depending on the shape of the plastic potential. It is probable that the plastic potential at the initial stages of yield will be very steep compared to the yield surface (as in Figure 1.6(a)) so that the ratio of vertical to rotational displacements will be high. To allow the yield surface to expand a significant amount of volumetric change must occur, due to the vertical displacements (shown in Figure 5.8(a)). This will lead to a reduction of effective stress, as the vertical load is transferred to the pore fluid, due to the limited drainage that can occur within the timescale of the loading event. It is possible that a significant reduction of effective stress in the soil beneath the caisson base may occur, perhaps even liquefaction, particularly during the occurrence of a large load where there is a large amount of plastic behaviour. This is shown in Figure 5.9(a)-(f) where the foundation is subjected to moment cycling after being normally consolidated to a vertical load of 200N. It is clear that there are large increases in the pore fluid pressure on the application of the large moment loads, and that there is a limited amount of drainage occurring during the passage of the loads. During the initial extreme event there is a large amount of vertical displacement (~0.1mm). Subsequent applications of similar loads will not lead to the same amount of displacement, or reduction in effective vertical stress, due to the load point being within the now expanded yield surface. However, if the foundation experiences loads larger than any previously applied, then yield surface expansion, and

hence volumetric change, will occur. Clearly, during the early life of the foundation, either preload must be applied, or drainage provided, so that yield surface expansion can occur with minimal effective stress consequences. The most opportune time to carry out this operation in a controlled manner would be during installation. Once the foundation is working within the yield surface small yield surface expansions will occur due to the loadings applied, but the displacement and effective stress consequences will be minimal.

5.2.4 Cyclic Loading at Different Constant Vertical Loads

Cyclic load tests were performed after a wide variety of loading histories. It was usual to perform tests on normally consolidated foundations to investigate the initial behaviour such as described above. It was also usual to perform tests on footings at varying degrees of overconsolidation so that the behaviour described in section 3.2.5 could be examined further. Typically the working state of an offshore foundation is such that the behaviour is mostly within the yield surface, and thus this stiffer 'elastic' response is appropriate. It is only during extreme events that yield surface expansion, and hence significant plasticity, occurs. The results from the combined loading on overconsolidated foundations suggest that the elastic foundation stiffness is dependant on the magnitude of vertical load applied to the foundation. Figure 5.10 shows results of tests conducted on the same foundation at different values of constant vertical load (and hence overconsolidation ratio). In each case the footing was vertically preloaded to 1400N before being unloaded to the vertical load mentioned for each test. It is clear that as the overconsolidation ratio decreases then the stiffness of the response is increased. These large changes in the elastic stiffness are not reflected within any design guidelines or within any modelling framework, such as conventional plasticity theory. This dependency is important for the tripod structural configuration (or jack-up platforms) as the vertical loads on each foundation are going to be different depending on the direction of the loading.

5.2.5 Comparison of Monotonic tests and Cyclic Loading Results (Masing Behaviour)

During the course of the research cyclic loading was applied at many different rates, including periods of 6s, 10s, and 12s to investigate the effects of partial drainage and transient response. The periods were chosen in parallel with the consolidation tests that were performed to determine consolidation t_{50} times. It became fairly evident that on the soil samples tested that there were no significant differences between the tests conducted at different rates. This was also the case for vertical cyclic loading tests. This observation, for horizontal cycling within the yield surface, was also made by Tan (1990) during a

centrifuge investigation of the response of spudcan footings on medium saturated silica sand. A further confirmation of the effect of rate is to determine if there is a relationship between monotonic tests (slow tests) and cyclic loading tests (transient tests). The simplest form of relationship is for kinematic hardening, which has been observed to be applicable to soil response in cyclic element testing (Prevost, 1977; Pyke, 1979; Vucetic and Dobry, 1988; Vucetic, 1990). Masing (1926) has suggested that a kinematic hardening material would behave according to the following rules:

i) The shear modulus on each loading reversal assumes a value equal to the initial tangent modulus for the initial loading curve.

ii) The shape of the unloading or reloading curves is the same as that of the initial loading curve, except that the scale is enlarged by a factor of two.

These rules suggest that the initial loading curve, called the backbone curve, maybe used to define all consequent load reversals. To prove that pure kinematic hardening governs behaviour it is only necessary to show that the second rule applies, as the first is consequential. It is also clear that these rules apply to a non-degrading material only. Clays (for example see Vucetic, 1990) clearly degrade on the application of cyclic loading, so it is necessary to degrade the backbone curve, by a factor, dependent on the history of loading.

To examine how the response of the soil could be categorised, slow monotonic tests were carried out, along with faster transient cyclic loading tests. These are shown in Figure 5.11(a) and (b) for moment and horizontal loading respectively. In both cases the cyclic test comprises of cycles of increasing stress magnitude. Clearly, there is a reduction in secant stiffness as the strain level increases. As well, on surpassing the previous maximum stress level, the unloading or reloading curve follows along an initial loading curve. This is confirmed by the monotonic test data that are overlain on each figure. In each case the monotonic tests pass through the extreme points of each cycle. Whilst this behaviour implies kinematic hardening under the Masing definitions, Pyke (1979), formally stated two additional rules (entitled the extended Masing rules) encapsulating these characteristics:

iii) the unloading and reloading curves should follow the initial loading curve (backbone curve) if the previous maximum shear strain is exceeded.

iv) if the current loading or unloading curve intersects the curve described by a previous loading or unloading curve, the stress-strain relationship follows that curve.

It is clear that the results in Figure 5.11, for both moment and horizontal loading, conform to these extended Masing rules, where the monotonic test clearly provides the backbone curve for the cyclic loading test. The second confirmation of Masing behaviour is to check whether shape of the reverse loading loop is a factor of two greater than the backbone curve (*i.e.* Rule ii) above). This confirmation is shown for different moment and horizontal load tests in Figure 5.12 and Figure 5.13. In these Figures the reverse loading data (unload path) has been extracted and scaled down by a factor of two and replotted from the origin. For the cases shown the scaled unload path gives a close approximation to the original loading path.

Finally evidence has been presented that the cyclic loading behaviour (in Chapter 4 and Figure 5.10) is dependent on the mean vertical load, and Figure 5.14(a) shows monotonic tests carried out at several different vertical loads, indicating similar behaviour. If Masing behaviour were applicable the peak data from each cycle of the tests shown in Figure 5.10 would plot close to the relevant monotonic curve shown in Figure 5.14(a). Indeed Figure 5.15 shows that there is an excellent correlation between monotonic and cyclic behaviour in accordance with Rule iii). This also implies that the response of the foundation is essentially rate-independent, as the monotonic tests were performed at a much slower rate than the cyclic tests.

Figure 5.14(b) shows the vertical displacement response during the moment monotonic tests where for low vertical loads there is a large amount of heave. As the vertical load level increases the amount of heave reduces, and eventually a level of overconsolidation is reached where there is settlement of the foundation. This gives important information about the nature of the plastic potential (or flow rule), which is an essential component of any plasticity theory that may be developed. This will be expanded upon in a later section.

5.2.6 Normalisation of Experimental Data

The results presented so far have indicated that the combined load response (i) conforms to Masing behaviour, (ii) appears to be rate independent, and, (iii) is dependent on the level of the vertical load. The experimental observation of points (i) and (ii) simplifies the task of developing a theoretical model for cyclic loading as rate independent Masing behaviour has been observed in other experimental studies of material response. The observation of point (iii) requires careful consideration so that the effect is described within any developed theoretical framework. The dimensional analysis adopted in chapter 4 worked successfully for the vertical load therefore it appeared logical that a similar approach could be used for deviatoric loading. The logical dimensionless group for the load is to divide by

the ultimate combined load capacity (i.e. M/M_{ult} or H/H_{ult}). It was then considered that the displacement response would again be proportional in some manner to the mean stress level of the soil. The logical approach was to use the same normalisation on displacement as used previously for the vertical case. For example the appropriate dimensionless relationship for moment loading (and for horizontal loading) would be:

$$\frac{M}{M_{ult}} = f\left(2R\delta q\sqrt{\frac{p_a}{V_m}}\right) \quad \text{.....5.7a}$$

$$\frac{H}{H_{ult}} = f\left(\delta u\sqrt{\frac{p_a}{V_m}}\right) \quad \text{.....5.7b}$$

Also it is useful to remember that $M_{ult}/2R$ or H_{ult} can be expressed as a factor (m_o or h_o) multiplied by the mean vertical load (*i.e.* $M_{ult} = 2Rm_oV_m$). The application of these normalisations provides some startling results, though not entirely unexpected given the results for the vertical loading. Figure 5.16 shows the normalisation applied to several of the monotonic tests shown in Figure 5.14. There is an impressive unique relationship between the curves. A hyperbolic curve of the form described in chapter 4 has been used to fit a backbone curve to the experimental initial loading data. Figure 5.17 shows these normalisations applied to the cyclic loading tests presented in Figure 5.10. As in the cyclic vertical loading the normalisation works very well and may well provide a significant step forward for the development of a general theoretical model for footing response. This understanding also provides a clearer step forward for the next stage of experimental study as it removes the effect of mean stress level on response. The scaling also applies equally well to the horizontal loading case as shown in Figure 5.18, where similarly a hyperbolic curve can be used to fit the data. Of interest is the magnitude of the parameters m_o and h_o. M_{ult} and H_{ult} for the cases described above are plotted against V_m in Figure 5.19. It is clear that m_o and h_o can be approximated by unity as M_{ult} and H_{ult} are approximated by V_m. The reason for this is that the outer yield surface which bounds the ultimate loads at these low vertical loads (compared to the peak bearing capacity) would have a slope close to 1.

5.2.7 Theoretical Framework for Modelling of Cyclic Loading

It is important that these experiments are interpreted within an appropriate theoretical framework, and not merely treated as an empirical collection of data from which observations are made. An appropriate framework for the understanding of the behaviour of foundations has been found to be plasticity theory as described in chapter 3. The reasons

for this choice are (a) theories can be constructed which reproduce the behaviour of the foundations well, and (b) the resulting models can readily be included in a numerical analysis of a complete offshore structure.

Plasticity theories for slow monotonic loading of foundations had been established prior to this research (see for example Tan, 1990; Martin, 1994; Cassidy, 1999), and previous monotonic data (chapter 3) were simply fitted within an existing framework. The results of typical cyclic tests have been shown in Figure 5.9(c) and 5.11(b). A remarkable feature about this result (which is typical of any cyclic horizontal or moment load test on a foundation) is that continuous smooth curves are obtained as the load is cycled. A conventional plasticity model could not model this type of behaviour, but instead would result in well-defined yield points at which a sudden change of stiffness would occur. The magnitude of plastic deformation predicted on reverse loading would also be at least an order of magnitude smaller than that observed.

Figure 5.20 shows the behaviour that would be obtained from a typical plasticity model for moment loading and load reversals. The footing has started from a normally consolidated position (at the apex of a yield surface), upon which the footing is slowly loaded to a rotational load of 40N, which causes yield surface expansion and plastic behaviour (as shown for example in Figure 5.3). The load is then reversed to -40N, following a path within the yield surface so elastic behaviour results. On application of positive loading the response is again elastic until 40N is reached where yield is observed and plastic behaviour re-occurs. This response is followed during further load reversals. If the footing is in an overconsolidated state, where the load state is located within the yield surface, then elastic behaviour will result. This behaviour will be the same regardless of the vertical load level, with plastic behaviour only occurring when the load state reaches the established yield surface.

One extension of these single yield surface plasticity theories is to include multiple yield surfaces so that a gradual transition of stiffness can be approximated. Each surface must also be accompanied by a plastic potential to describe the direction of plastic flow. This type of theory, called 'nested' yield surfaces, has been developed for constitutive modelling of soils (for example Houlsby, 1999). The main drawback is that a number of parameters must be specified for each discrete yield surface, which for accurate modelling of soil behaviour, leads eventually to an unwieldy theory. More recently advances have been made, using some of the experimental data described in this thesis, in a theory termed 'continuous hyperplasticity'. A complete exposition of this theory is inappropriate here as it

involves a considerable amount of mathematical development, however interested readers are directed to papers by Collins and Houlsby (1997), Houlsby and Puzrin (2000) and Puzrin and Houlsby (1999). This approach to plasticity theory has been formulated in such a way that any developed theory is guaranteed to obey thermodynamic principles. The following section (5.2.8) sets out the basic theory as developed by Puzrin and Houlsby (1999). Towards the end of the section the formulation is numerically coded and compared to some of the experimental data from this investigation. Section 5.2.9 suggests an extension of the basic hyperplastic formulation to the {*V*:*M*/2*R*:*H*} loading cases relevant to this thesis.

5.2.8 Basic 'Continuous Hyperplasticity' following Puzrin and Houlsby (1999)

In essence the theory replaces the "plastic strain" in conventional plasticity theory with a continuous field of an infinite number of plastic strain components, each associated with a separate yield surface. This is achieved within a manageable mathematical framework by deriving the plasticity theory for a dissipative material entirely from two potentials. The first function is the Gibbs free energy or the Helmholtz free energy. The second potential is the dissipation function. For the case of the infinite field of plastic strains these potentials are functionals ("functions of functions") of the plastic strain. Conventional plasticity theory is a special case of the new approach. The result is that theories can be constructed in which responses of the character shown in Figure 5.9(c) can be modelled accurately and computationally efficiently. The basic theory will be developed for a single yield surface system such as the St. Venant model with linear hardening shown in Figure 5.21. The St. Venant model consists of a spring in series with a parallel system of a spring (for hardening) and slider. The slider only moves when the applied load reaches a certain level. Therefore on the application of load the first spring compresses in an elastic fashion such as shown in Figure 5.21. When the resistance of the slider is overcome the overall system displacement consists of the first spring plus a contribution from the second spring. The contribution from the second spring is a permanent contribution to the total displacement as on unloading the slider locks and only the first spring decompresses. Eventually the load reaches a sufficient negative level that the second spring extends and contributes to the displacement response. Using the hyperplastic formulation, as set out and developed by Puzrin and Houlsby (1999), the Gibbs free energy potential for this St Venant case is defined as:

$$g = -\frac{P^2}{2k} + \frac{k_1 \alpha^2}{2} - P\alpha \qquad \text{.....5.8}$$

where α is the internal variable and in this case corresponds to the plastic displacement. The displacement response can be determined from the partial derivative of the Gibbs potential with respect to the load such that:

$$\delta = -\frac{\partial g}{\partial P} = \frac{P}{k} + \alpha \quad \text{5.9}$$

It is noted (for later reference) that the elastic component of displacement (P/k) is related only to the first part of the Gibbs free energy (denoted as g_1). A generalised load can be obtained as:

$$\bar{\sigma} = -\frac{\partial g}{\partial \alpha} = -k_1\alpha + P \quad \text{5.10}$$

which clearly in the case of a single slider (yield surface) is always equal to the current value of load, P, during elastic loading. However, once the load mobilises the second spring the generalised load is given by the strength of the slider, c.

The second function required is the dissipation function:

$$d = c\left|\dot{\alpha}\right| \geq 0 \quad \text{5.11}$$

where $c > 0$. Clearly the dissipation function is equal to zero until the slider is mobilised, upon which plastic displacements occur. A generalised dissipative load can be obtained as:

$$\sigma = \frac{\partial d}{\partial \dot{\alpha}} = c\,\mathrm{sgn}(\dot{\alpha}) \quad \text{5.12}$$

This generalised dissipative load is undetermined when the first spring is being compressed (elastic behaviour) or $\pm c$ when the slider resistance is overcome (dependent on loading direction). Therefore an appropriate yield function would be:

$$y = \sigma^2 - c^2 = 0 \quad \text{5.13}$$

The derivative of the yield function with respect to the load gives the flow rule:

$$\dot{\alpha} = \lambda \frac{\partial y}{\partial \sigma} = 2\lambda\sigma = 2\lambda c\,\mathrm{sgn}(\dot{\alpha}) \quad \text{5.14}$$

where λ is a non-negative multiplier which determines the magnitudes of the plastic displacement. Clearly when the generalised dissipative load is zero (elastic behaviour) then λ is equal to zero. However when the load state is on the yield surface then plastic

displacements occur with λ obtained by invoking the consistency condition of the yield surface which in this case is:

$$\dot{y} = \frac{\partial y}{\partial c}\dot{c} = 2c\dot{c} = 0 \quad \text{.....5.15}$$

Using the incremental generalised load and taking advantage of Ziegler's (1977) orthogonality assumption, which is equivalent to the assumption that $c = \bar{c}$, then $\dot{c} = \dot{P} - k_1\dot{\alpha} = \dot{P} - k_1 2\lambda c\,\mathrm{sgn}(\dot{\alpha})$ leads to a solution for λ:

$$\lambda = \frac{\mathrm{sgn}(\dot{\alpha})\dot{P}}{k_1 2c} \quad \text{.....5.16}$$

This solution allows the total incremental response to be defined. From this simple starting point of one yield surface it is possible to generalise to an infinite number of yield surfaces as described by Puzrin and Houlsby (1999). Figure 5.22 shows the St. Venant model generalised to a large number of parallel spring-slider combinations in series (called the Iwan model (Iwan, 1967)). As the number of these spring-sliders combinations increase the load-displacement response moves from that in Figure 5.23(a) where there are defined yield points to that in Figure 5.23(b) where there is a smooth change in stiffness. This is the response that is characteristic of soil under general loading. To generalise the above model to *N* spring-slider combinations it is necessary to keep account of the plastic displacement contributions to the total displacement response. For example the Gibbs free energy potential becomes:

$$g = -\frac{P^2}{2k} + \frac{1}{2}\sum_{n=1}^{N} k_n \alpha_n^2 - P\sum_{n=1}^{N}\alpha_n \quad \text{.....5.17}$$

and the dissipative function becomes:

$$d = \sum_{n=1}^{N} c_n \left|\dot{\alpha}_n\right| \quad \text{.....5.18}$$

The mathematics follows the same format as laid out above except that the formulation must be carried out for each individual yield surface. So for example the dissipative generalised stress and yield function are given by:

$$c_n = \frac{\partial d}{\partial \dot{\alpha}_n} = c_n\,\mathrm{sgn}(\dot{\alpha}_n) \text{ and } y_n = c_n^2 - c_n^2 = 0 \text{ for } n = 1....N \quad \text{.....5.19}$$

Houlsby and Puzrin (1999) take this one step further and take the limit as N tends to infinity where the Gibbs free energy is a function of the load and the plastic displacement such that:

$$g = -\frac{P^2}{2k} + \frac{k_1}{2}\int_0^1 \hat{\alpha}^2 \hat{\Gamma} d\eta - P\int_0^1 \hat{\alpha}\hat{\Gamma} d\eta \quad \text{.....5.20}$$

where $\hat{\Gamma} = \Gamma(\eta)$ is a distribution function such that $\hat{\Gamma} d\eta$ is the fraction of the total number of yield surfaces having a dimensionless size parameter between η and $d\eta$. In this case the hardening stiffness k_1 is assumed constant but the strengths of the sliding units are assumed to be proportional to η (*i.e.* $c\eta$). The dissipative stress is then given by:

$$d = \int_0^1 c\eta \left|\dot{\hat{\alpha}}\right| \hat{\Gamma} d\eta \quad \text{.....5.21}$$

The dissipative generalised stress function, $\hat{c}$, and the field of yield functions are given by:

$$\hat{c} = \frac{\partial \hat{d}}{\partial \hat{\alpha}} = c\eta \,\mathrm{sgn}\left(\dot{\hat{\alpha}}\right) \; and \; \hat{y} = \hat{c}^2 - c^2\eta^2 = 0 \quad \text{.....5.22}$$

Puzrin and Houlsby (1999) work through the mathematics to show that for monotonic loading:

$$\dot{d} = \left[\frac{1}{k} + \frac{1}{k_1}\int_0^{\eta^*} \hat{\Gamma} d\eta\right]\dot{P} \quad \text{.....5.23}$$

where η^* is the largest η such that $\hat{c}^2 - c^2\eta^2 = 0$. This model simulates the one-dimensional elastic non-linear plastic load displacement behaviour observed in the Iwan model as *N* tends to infinity, and consequently models well the experimental work. The first term contributes an elastic displacement whilst the second term contributes a plastic term depending on how many slider elements have been mobilised (η). Puzrin and Houlsby (1999) show that the distribution function, $\hat{\Gamma}$, is related uniquely to the second derivative of the initial backbone curve, such as those which are shown in Figure 5.16 and Figure 5.18. The relationship is:

$$\frac{d^2 d}{dP^2} = \frac{1}{ck_1}\Gamma\left(\frac{P}{c}\right) \quad \text{.....5.24}$$

The hyperbolic function that has been used to fit the backbone curves is:

$$\delta = \frac{P\left(c - \left(2 - k/k_{50}\right)P\right)}{k\left(c - P\right)} \quad \text{5.25}$$

which leads to a distribution function of:

$$\hat{\Gamma} = \frac{k\left(1-\eta\right)^3}{2\left(k/k_{50} - 1\right)} \quad \text{5.26}$$

Where k is the initial stiffness, k_{50} is the stiffness at 50% stress and c is clearly the peak strength. The formulation above has been defined in terms of $\{P, \delta\}$ which can easily take the form of $\{H, \delta u\}$ and $\{M/2R, 2R\delta\theta\}$. This formulation has been implemented within a numerical program to model some of the experimental work that has been carried out. Figure 5.24(a) shows the result of a moment test in which cycles of increasing amplitude have been applied. Figure 5.24(b) shows the fitted response using the continuous hyperplastic model. Whilst the fitting is not exact, the model captures the main features of the cyclic test.

Figure 5.25 shows the data reduced to the temporary and permanent components for both the experimental and theoretical model results. The elastic component is slightly underpredicted by the theory whilst the permanent component is slightly overpredicted. A visual comparison of the two results shows clearly that the theoreti4cal results have slightly wider loops than for the corresponding experimental results. This fact is reinforced in the plot of the damping ratio which is a measure of openness of the loop during the cycle. The experimental results show a damping ratio constant at approximately 0.2 for all peak moment loads. The theoretical results on the other hand show the damping ratio increasing almost linearly with the peak moment loads. However despite these small differences the results indicate a very impressive quantitative agreement, which far surpasses any known methods, and thus illustrates the power of this theoretical approach.

Figure 5.26 illustrates the experimental data shown in Figure 5.16 modelled using parameters which defined the hyperbolic curve also shown on Figure 5.16. The theoretical model is fitted to the dimensionless unique curves and then the results are scaled up to be compared to the original data as in Figure 5.27. Horizontal loading also displays similar agreements. The data in Figure 5.18 has been modelled and the theoretical results scaled to represent the original curves in Figure 5.28(a) (compare to the original curves in Figure 5.28(b)). Some further comparisons are made in Figure 5.29(a) and Figure 5.29(b). Even the small load reversals in Figure 5.29(a) are modelled very closely by the theoretical

model. Finally Figure 5.30 shows the 'NewWave' loading displayed in Figure 5.9 modelled using the appropriate parameterisation. The broad behaviour of the response is captured closely.

Clearly there have been some large steps taken in the development of an appropriate method for modelling cyclic behaviour - both theoretically and experimentally. From the experimental point of view the possibility of a large amount of complicating factors has been reduced by several key observations. There is still however a large amount of experimental work to be completed but this can now be done on a much more focussed basis. Of prime importance is determining how the shape of the hyperbolic form of the load displacement response varies with loading history. For example Figure 5.31 shows the normalised response of two moment rotation tests, on dry sand, under constant vertical load. The softer curve was a test conducted from a normally consolidated initial footing load state. The nature of the response is that the footing is continually at 'plastic' yield throughout its entire trajectory consequently expanding the yield surface. The second stiffer curve represents a test conducted from within the footing yield surface and as such possesses an 'elastic' response before plasticity occurs as the loads are increased.

5.2.9 An Extended 'Hyperplasticity' Model for Footings on Sand

The further development of theoretical methods is often driven from experimental observations. Figures 5.32(a) and 5.33(a) show the displacement response for four monotonic moment load tests, conducted at different mean vertical loads. Figures 5.32(b) and 5.33(b) show that the dimensional analysis applies equally well to the other components of displacement. These results (as well as those from Chapter 4) indicate that the footing stiffness scales with the square of the mean vertical load. This knowledge can be used to develop part of the Gibbs free energy function g_1 (the elastic component). According to Bell (1991) and Ngo Tran (1996) the elastic stiffness matrix can be represented as:

$$\begin{Bmatrix} dV \\ dM/2R \\ dH \end{Bmatrix} = 2GR \begin{bmatrix} k_v & 0 & 0 \\ 0 & k_m & k_c \\ 0 & k_c & k_h \end{bmatrix} \begin{Bmatrix} dw_e \\ 2Rd\boldsymbol{q}_e \\ du_e \end{Bmatrix} \quad \text{.....5.27}$$

where there is significant coupling between the deviatoric movements. Typical factors for the elastic coefficients have been developed by Bell (1991). For a Poisson's ratio of 0.2 they are:

$$k_v = 2.65;\ k_m = 0.46;\ k_h = 2.30;\ k_c = -0.14 \quad \text{.....5.28}$$

Continuous hyperplasticity is well formulated when the displacements are in terms of the loads so the compliance matrix is required rather than the stiffness matrix.

$$\begin{bmatrix} dw_e \\ 2Rd\boldsymbol{q}_e \\ du_e \end{bmatrix} = \frac{1}{2GR}\begin{bmatrix} 1/k_v & 0 & 0 \\ 0 & k_h/d & -k_c/d \\ 0 & -k_c/d & k_m/d \end{bmatrix}\begin{bmatrix} dV \\ dM/2R \\ dH \end{bmatrix} \quad \text{.....5.29}$$

where $d = k_m k_h - k_c^2$. As has been shown in the formulation of the basic hyperplasticity model the elastic increments of each displacement are related to the first part of the Gibbs free energy function by the partial derivative with respect to that load:

$$dw_e = -\frac{\partial g_1}{\partial V};\ 2Rd\boldsymbol{q}_e = -\frac{\partial g_1}{\partial M/2R};\ du_e = -\frac{\partial g_1}{\partial H} \quad \text{.....5.30}$$

As such it is possible to determine the form of g_1 from which the stiffness matrix derives:

$$g_1 = -\frac{1}{2GR}\frac{1}{2}\left(\frac{V^2}{k_v} + \frac{k_h(M/2R)^2}{d} - \frac{2k_c(M/2R)H}{d} + \frac{k_m H^2}{d}\right) \quad \text{.....5.31}$$

The results of the experiments presented for vertical, horizontal and moment loading indicated a strong dependence of stiffness on V_{mean} (= V) such that:

$$\frac{G}{p_a} = g\sqrt{\frac{V}{\boldsymbol{p}R^2 p_a}} \quad \text{.....5.32}$$

Which can be re-arranged and substituted for $2GR$ in the above formulation for g_1:

$$g_1 = -\frac{\sqrt{\boldsymbol{p}}}{2g\sqrt{p_a}}\frac{1}{2}\left(\frac{V^{3/2}}{k_v} + \frac{k_h(M/2R)^2}{d\sqrt{V}} - \frac{2k_c(M/2R)H}{d\sqrt{V}} + \frac{k_m H^2}{d\sqrt{V}}\right) \quad \text{.....5.33}$$

so that the full form of the free energy for a hyperbolic model of load response becomes:

$$g = g_1 - \int_0^1 V\hat{a}_v + \frac{M}{2R}\hat{a}_m + H\hat{a}_h d\boldsymbol{h} + \int_0^1 \frac{(1-h)^3}{2s}\frac{2g}{\sqrt{\boldsymbol{p}}}\sqrt{Vp_a}\,\frac{1}{2}\left(k_v\hat{a}_v^2 + k_m\hat{a}_m^2 + 2k_c\hat{a}_m\hat{a}_h + k_h\hat{a}_h^2\right)d\boldsymbol{h} \quad \text{.....5.34}$$

where s is a shaping factor for the hyperbola and represents E_0/E_{50} - 1. This would be used in conjunction with a dissipation function of the form:

$$d = \int_0^1 V\boldsymbol{h}\sqrt{m_o^2\dot{\hat{a}}_m^2 + h_o^2\dot{\hat{a}}_h^2}\,d\boldsymbol{h} \quad \text{.....5.35}$$

From this formulation it is possible to determine the vertical deformation which is due just to the dependence of the stiffness on the stress level. Houlsby (2000) has considered the special case where:

a) there are no coupling terms (i.e. $k_c = 0$)

b) $H = 0$

c) there is no vertical plastic strain term ($\hat{a}_v = 0$)

This simplifies the resulting integration greatly and leads to analytical solutions for the displacement responses $\{dw:2Rdq\}$ for both loading and unloading. These are shown on Figure 5.34 (compared to curves from Figure 5.32(b) and 5.33(b)) using the appropriate numerical values for the variables, so that a fit can be obtained for the response in the $\{2Rdq:M/2R\}$ space. The extremely promising aspect of the theoretical solution is that it predicts broadly similar responses, which suggests that the broad framework for the theoretical model is correct. The theoretical model underpredicts the displacement however it should be noted that the model only includes the dependence of stiffness on stress level, there may well be other contributory factors to the vertical displacement which have not been included as yet.

5.3 CONCLUDING COMMENTS

This chapter has presented selected results from a high quality laboratory testing program aimed at investigating the response of suction caisson foundations to combined loading. It is quite likely that new applications of this technology, particularly in the renewable energy sector, will seek structural forms where large combined loads are applied to the foundations. It is therefore necessary to be able to determine the appropriate response of the foundations under these loads so that design calculations can be carried out.

One area of particular importance is the capacity and performance during low levels of vertical loads. Several experiments were conducted investigating this behaviour and simple design curves were suggested. It is an area which requires much more research, particularly on the effects of translating laboratory scale tests to full scale behaviour.

A novel method of developing load time histories was employed during the research in order to study the transient foundation response under the action of extreme events. It was found that the critical stage of the foundation's life is during the first loading, unless preload has been applied, and, the foundation is working within the elastic region of its yield surface. During this loading, as the yield surface expanded, there was potential for

effective stress decreases, as volumetric change occurred, and the foundation experienced consolidation behaviour. It is clear that during this period drainage should be allowed so that settlement can occur without risk of liquefaction.

A large amount of testing was focussed on the response of the foundation at varying levels of overconsolidation ratio, as this is the typical working condition of a foundation. It was found, in contrast to current methods, that the response was dependent on the applied vertical load. Dimensional analysis revealed a simple scaling relationship which could lead to much reduced testing procedures in the future. It will be necessary to observe whether this scaling law translates across a larger range of vertical stresses than was encountered within this investigation.

Finally the chapter described a theoretical framework, that has been developed that captures the main features of the experimental cyclic tests - that of change in stiffness with strain level and the hysteresis observed on unloading. This model, termed 'continuous hyperplasticity', represents a significant improvement on conventional plasticity theory which could not capture this behaviour. The model was used to reproduce experimental results and compared favourably quantitatively. The combination of the observed scaling relationship and this state-of-the-art theoretical model may lead to a fully generalised footing model. Once fully extended to the three dimensional load case this framework will enable a much closer representation of the physical reality when used within typical structural analyses programs.

CHAPTER SIX
CONCLUDING REMARKS

6.1 INTRODUCTION

An investigation has been undertaken of a novel suction caisson foundation that might be used for an offshore structure. High quality experiments have been completed consisting of applying typical loading regimes to a model scale foundation on sand using a sophisticated three degree of freedom loading rig. The following sections outline the technological developments necessary for the research, the major contributions that have been made, as well as discussing several avenues for further research.

6.2 TECHNOLOGICAL DEVELOPMENTS

During the course of the research it was necessary to develop the following technologies:

1. Previous testing on saturated samples at Oxford University (Mangal, 1999) showed that it was very difficult to prepare similar samples of very dense saturated sand. The complications exist due to the necessity of saturating the samples with silicon oil to model drainage times appropriate to the offshore situation. This dissimilarity between soil samples leads to difficulties in interpreting results. It was therefore necessary to develop a method of bulk testing on the same sample of sand. A system involving large tanks in which it was possible to perform eight tests on virgin sites was developed. Further it was possible to perform multiple tests on the same site as long as the disturbance at the site was not too great. This methodology enabled a large number of tests to be performed on sands in very similar states. The tests were performed on both dry sand and saturated sand.

2. For equipment development it was necessary to upgrade the electronics on the existing three degree of freedom loading rig (Martin, 1994). This included developing a fast data acquisition system capable of logging transducer readings up to 20Hz over the period of the longest test (40 minutes). The increased speed of data acquisition enabled the development of a suitable independent feedback control system on each loading axis. This system allowed either displacement or load control on each of the three loading axes leading to very sophisticated tests on dry sand and saturated sand. The control system enabled high quality testing procedures to be carried out leading to simplification of interpretation of data. The data acquisition system used was of 16 bit resolution and so there were greater accuracy on the data than previously. The control system and data

acquisition were incorporated within a programme written in VisualBasic running on a Pentium 200 computer.

3. Previous confidential tests on suction caisson foundations indicated that there were certain loading regimes which resulted in stable behaviour, whilst others resulted in unstable behaviour. It was believed that the presence of an extreme event within the background loading precipitated a degradation of behaviour. With this in mind it was felt appropriate to develop a load time history capable of incorporating extreme events within a pseudo random background. The methodology adopted was taken from the current state-of-the-art in wave mechanics known as 'Constrained NewWave'. In this methodology only two variables are required to describe an entire pseudo-random loading sequence containing the appropriate frequency content relevant to offshore wave loading. This greatly reduces the amount of testing to a level that can be achieved within a suitable timeframe. The improved feedback control system on the loading rig enabled the implementation of such a loading sequence. The use of load controlled cyclic tests was viewed as being very important due to the ease of interpretation.

4. The electronic and feedback control development of the loading apparatus allowed a large number of high quality tests to be performed. The testing covered the broad spectrum of foundation behaviour including (i) monotonic tests on a loose carbonate sand (40), (ii) monotonic tests on a dense dry silica sand (~250), and, (iii) cyclic and monotonic tests on a dense saturated silica sand (~300). The data gathered throughout the tests consisted of the work conjugate components of load and displacement $\{V:M/2R:H\}$ and $\{dw:du:2Rdq\}$. In addition during the tests on saturated sand the pore fluid response was obtained in the centre of the footing underneath the top-plate. The resolution of the data was ~2N for loads and ~3 micron for displacements.

5. The main loading on offshore caisson foundations is cyclic and psuedo-random in nature therefore a large number of tests were carried out utilising the method outlined in point 3. A large amount of quality data was accumulated due to the long periods of cycling and fast data acquisition rates. A method of reducing the data was devised in which the displacements are assessed between each mean load crossing. The displacements are broken into 'elastic' and 'permanent' components. A method of comparing the reduced data from different tests was developed based on dimensional analysis.

6.3 ORIGINAL CONTRIBUTIONS

This thesis has made the following contributions:

1. The first stage of testing involved a comprehensive set of monotonic tests of caisson foundations under combined loading. The purpose of these tests was to establish in detail the response of the caisson foundations to slow monotonic loading. A number of different types of tests were used; each specifically designed to explore a particular aspect of the behaviour of the foundation under combined loads. The theoretical framework used for the understanding of these tests was work-hardening plasticity theory, and the tests were designed to give information that could be used directly to derive plasticity models. The monotonic tests examined three different depth/diameter ratios of caissons, as well as flat surface footings. The results of the monotonic tests broadly confirmed that the patterns of behaviour observed for flat foundations (*i.e.* without the skirt which is present on the caisson foundation) also applied to the suction caisson. The main difference was that the caisson tests concentrated on the region (highly relevant to the field case) where the ratio of the vertical load to the ultimate static bearing capacity is small (say less than 0.1). Under these conditions the earlier assumption that the "yield surface" for the foundation expands with vertical load but does not change shape is inadequate. At low ratios of V_o/V_{peak} the yield surface was almost double the size at high ratios of V_o/V_{peak}. A new framework was proposed for understanding the change of shape in which an inner yield surface expands within a fixed outer yield surface.

2. The testing on the loose carbonate sand followed a similar approach to that on dense sand as it was designed to provide evidence of the versatility of the plasticity approach to theoretical modelling. In contrast to the results from the dense silica sand the shape of the yield surface was found to expand in shape as well as size with the increase in embedment. The very loose nature of the carbonate sand meant that the footing typically penetrated 60mm under a load of 1600N whilst on dense silica sand the footing would only penetrate 2mm. Thus on the carbonate sand it is highly likely that the resistance of the soil on the sidewalls of the footing is likely to cause an increase in the shape of the horizontal yield surface. The moment yield surface was found to be unaffected by the increased embedment. Similar results were found by Tan (1990) who investigated the horizontal response of flat footings on loose sand. Differences were observed in the variation of yield surface shape and the hardening law with embedment to that of dense silica sand. These differences were attributed to the fact that a peak bearing capacity was not observed and that the footing response was affected by embedment. It is clear that the hardening law

needs to take into account deviatoric movements as well as vertical movements.

3. The scaling technique provided a powerful normalisation, which appeared to scale across three different diameters (100mm, 150mm and 300mm) and two orders of magnitude of load (200N through to 50000N). The comparison of many test results showed that the rate of loading had little or no effect on the response. This surprising result may possibly be due to the very small displacements that are typically encountered during the cyclic loading. This result was also evident in an auxiliary series of tests carried out by Johnson (1999) in which very fast undrained loading rates could be attained on a 300mm diameter footing. Contrary to previous beliefs there was no degradation of footing behaviour under the cyclic loading even under many cycles. There was gradual transition from a stiff response at small displacements through to a softer response at greater displacements.

4. During the initial bedding in phase of installation there was a significant pore pressure response measured beneath the caisson top. The initial loading on the foundation also exhibited large displacements and the associated pore pressure response. This behaviour could be explained by the fact that initially the footing load state is at the apex of a yield surface and any loading leads to an expansion and plasticity. The plasticity in turn leads to volume change and thus pore pressure response until the footing load state is sufficiently within the yield surface that little plasticity occurs. It is crucial that drainage be provided during the bedding in phase and initial loading so that the foundation can move to an optimal position within the yield surface prior to any serious storm loading.

5. It was noted during the analysis of the cyclic test results that the backbone curves could be well represented by the slow monotonic test results (*i.e.* Masing behaviour). This is due to the fact that there is little effect of loading rate on response of the foundation. Further Masing behaviour was evident from the unload loops which were approximately twice the stiffness of the initial load path. This is an important result as it means that the amount of time dedicated to doing cyclic load testing in future research projects can be reduced substantially. Significant behavioural patterns can be observed from easily performed monotonic loading tests. By using this approach it was possible to observe that the horizontal and moment loading response within the yield surface was dependent on the value of V/V_o (the overloading ratio). This contrasts with generally accepted methods. The normalisation technique used for the vertical loading was also applicable for the deviatoric loading. The results indicated that the backbone curves found for one stress level scaled to other stress levels with the inverse of the square root of the mean vertical load.

6. One area of significant interest in the vertical cyclic loading tests was the effect of cycling into tension. The cyclic loading tests showed no signs of the degradation that was previously thought to exist however they did indicate that the tensile response was significantly softer then the compressive response. This tensile response was investigated further using monotonic tensile loading tests. The tests indicated that as long as the displacements were kept to low levels there was no sign of degradation. However once displacements exceeded a certain level the tensile capacity degraded to the drained tension response at serviceability levels of displacement. The absolute maximum tensile capacity was confirmed to be at the cavitation limit, with the soil plug remaining intact within the caisson skirt. This occurred at significant displacement levels. It was suggested that as soon as displacements reached the level at which the dilatant response of the soil was mobilised this ultimately led to the degradation of the soil response. These displacements were large compared to that typically encountered in the cyclic loading tests tending to confirm point 3 above. Design for tension will almost certainly be governed by serviceability requirements and not capacity.

7. The current work hardening plasticity models are not appropriate for the modelling of cyclic loading as they do not model the change in stiffness with strain level for reverse loading cycles. A new method has recently been developed which is thermodynamically admissible and based on only two potential functions. Several tests were carried out as part of this research project to specifically aid and validate this new model development. It is clear that the new 'continuous hyperplasticity' theory successfully models the experimental data and undoubtedly is a major breakthrough in the search for a suitable theoretical model for cyclic loading. The results of point 5 led to the reformulation of the potential function for $\{V{:}M/2R{:}H\}$ loading accounting for the dependence of stiffness on vertical load. The vertical displacement results for the special case when H or $M/2R = 0$ matched those obtained experimentally validating further the proposed framework.

6.4 FUTURE DIRECTIONS

Fundamental investigations such as this provide a suitable starting point for much more research. The following points outline areas in which valuable research could be carried out.

6.4.1 Further research on circular footings on granular materials

It is clear that whilst the research has provided some preliminary guidelines that much more research needs to be carried out on both the combined loading aspect as well as the

cyclic loading aspect. Of particular interest will be tests carried out to examine the initial soft tensile response. It has been suggested that this occurs after the skirt friction has been exceeded. In the current set of tests the drained skirt capacity is of the order of 10N, which is not much larger, then the resolution of the measuring system. Therefore it is clear that tests will need to be carried out where foundation has a substantial drained tensile capacity. Such tests could be carried out (i) in a geotechnical centrifuge, (ii) at one gravity by using a larger footing, or (iii) in a sample which is hydraulically surcharged so that the soil stresses are increased.

All the testing carried out thus far has been on the lab floor in the atmosphere. It would be prudent to carry out tests in which the effect of the water depth is also modelled - this could be done by doing tests within a pressurised vessel. This will have the effect of increasing the cavitation limit for the fluid. It is thought that the effect of increasing the equivalent water depth will cause the maximum capacity to change (with the increase in cavitation limit), but will leave the softened tensile response as is.

One of the more important areas that needs attention will be how these one gravity experiments scale to prototype levels. Key one-gravity tests need to be targetted and repeated at different gravity levels to explore the well-documented pressure dependence of granular materials. This is particularly important for the results of moment tests carried out at close to zero vertical load which could be used to design shallow-water renewable energy structures. Results from these tests will also allow the verification of the normalisations that have been proposed in chapters 4 and 5.

6.4.2 Theoretical Modelling of Cyclic Loading

The 'continuous hyperplasticity' approach appears to offer a simple theoretical framework for cyclic loading. Further research will be required to combine this approach with the work hardening plasticity method that is typically used for monotonic loading. The experimental results presented in chapters 3 to 5 will focus the appropriate theoretical developments in a way as described towards the end of chapter 5. This would lead to the formulation of a general model for the response of the foundation under typical loading conditions.

6.4.3 Physical and Numerical Modelling of Offshore Structures

An offshore structure is a highly non-linear system. In this thesis assumptions have been made so that a start can be made in developing appropriate loading histories to be applied to the foundation. For progress to be made it will be necessary to develop a more

integrated approach to dealing with the design of the structure. The loading on the foundation is dependent on how the wave loads are transferred through the structure. In order to develop foundation loading time-histories which represent more closely that experienced by actual offshore foundations it will be necessary to take advantage of the latest structural response methods such as the 'Designer Wave' approach developed at Shell in The Netherlands (Suastika, 1997). For specific offshore structures (such as a spaceframe structure or a gravity base) it is possible to derive the base shear and moment associated with the extreme wave in a computationally efficient manner.

In order for the derived foundation models to be improved it will be necessary to conduct simultaneous numerical and physical modelling of the offshore structure. This will involve modelling some aspect of the structure, in this case the foundation, physically on the lab floor, whilst modelling the rest of the structure within a computer. Once fully implemented this should incorporate all aspects of non-linear behaviour of the waves, the structure as well as the foundation response, and should provide an accurate indication of how well suited the developed foundation models will be for predicting response. The tests will then provide a basis for formulating improvements to the models.

6.5 CONCLUSION

This thesis has been concerned with the development of a novel foundation concept for offshore structures - a suction installed caisson. The design guidelines for these shallow foundations are presently in their infancy as it has not been possible to draw from any existing onshore guidelines. The work covered in this thesis consists of the presentation and analysis of high quality experimental data investigating a variety of critical aspects of shallow foundation performance on dense sand.

REFERENCES

Aldwinckle, G. (1994). *The installation of offshore plated foundations for oil rigs*. Engineering Science Part II Project Report, Department of Engineering Science, Oxford University.

Allersma, H.G.B., Kirstein, A.A., Brinkgreve, R.B.J. and Ferres, B. (1999). Centrifuge and numerical modelling of methods to optimise the horizontal bearing capacity of suction piles. *Proc. of 18th International Conference on Offshore Mechanics and Arctic Engineering*, St. Johns, Canada.

Allersma, H.G.B., Kirstein, A.A., Brinkgreve, R.B.J. and Simon, T. (1999). Centrifuge and numerical modelling of horizontally loaded suction piles. *Proc. of 9th International Symposium on Offshore and Polar Engineering*, Brest, France.

American Petroleum Institute. (1993). *Recommended practice for planning, designing and constructing fixed offshore platforms - load and resistance factor design*. RP 2A-LRFD, 1st Ed., Washington DC.

Andersen, K.H., Dyvik, R. and Schroder, K. (1992). Pull-out capacity analyses of suction anchors for tension leg platforms. *Proceedings of the International Conference on the Behaviour of Offshore Structures*, BOSS 92. London, United Kingdom.

Andersen, K.H., Dyvik, R., Schroder, K., Hansteen, O.E. and Bysveen, S. (1993). Field tests of anchors in clay. II : Predictions and interpretation. *ASCE Journal of Geotechnical Engineering* **119** (10), 1532-1549.

Anderson, K.H. and Jostad, H.P. (1999). Foundation design of skirted foundations and anchors in clay. *Offshore Technology Conference*, Houston, Texas. Paper 10824.

Baerheim, M., Hoberg, L., and Tjelta, T.I. (1995). Development and structural design of the bucket foundations for the Europipe jacket. *Offshore Technology Conference*, Houston, Texas. Paper 7792.

Barltrop, N.D.P and Adams, A.J. (1991). Dynamics of fixed marine structures. Butterworth Heineman, 3rd Edition, Oxford.

Bell, R.W. (1991). *The analysis of offshore foundations subjected to combined loading*. M.Sc. Thesis, University of Oxford.

Bolton, M.D. (1986). The strength and dilatancy of sands. *Geotechnique* **36**, N° 1, pp. 65-78.

Bolton, M.D. and Lau, C.K. (1993). Vertical bearing capacity factors for circular and strip footings on mohr-coulomb soil. *Canadian Geotechnical Journal* **30**, pp. 1024 - 1033.

Borgman, L.E. (1967). Spectral analysis of ocean wave forces on piling. *Journal of Waterways and Harbours Division*, American Society of Civil Engineers **93**, pp. 128-156.

Borgman, L.E. (1969). Ocean wave simulation for engineering design. *Journal of Waterways and Harbours Division*, American Society of Civil Engineers **95**.

Bransby, M.F. and Randolph, M.F. (1998). Combined loading of skirted foundations, *Géotechnique* **48**, N° 5, pp. 637-655.

Bransby, P.L. (1973). *Cambridge contact stress transducers*. Report No. CUED/C-SOILS/LN2, Cambridge University Engineering Department.

Bretschneider, C.L. (1959). Wave variability and wave spectra for wind generated gravity waves. US Army Corps of Engineers. Beach Erosion Board, US Army Memo N° 18.

Buckingham, E. (1914). On physically similar systems: illustrating the use of dimensional analysis. *Phys Rev* **4**, pp. 345-376.

Butterfield, R. (1981). Another look at gravity platform foundations. *CISM Course*, Soil Mech Fndn Engng in Offshore Technology, Udine.

Butterfield, R. and Ticof, J. (1979). Design parameters for granular soils (discussion contribution). *Proc 7th Int Conf Soil Mech Fndn Engng*, Brighton, **4**, pp. 259-261.

Butterfield, R. and Gottardi, G. (1994). A complete three-dimensional failure envelope for shallow footings on sand. *Géotechnique* **44**, N° 1, pp. 181-184.

Butterfield, R., Houlsby, G.T. and Gottardi, G. (1997). Standardised sign conventions and notation for generally loaded foundations. *Geotechnique* **47**, N° 4, UK.

Bye, A., Erbrich, C., Rognlien, B., and Tjelta, T.I. (1995). Geotechnical design of bucket foundations. *Proc. of Offshore Technology Conference*, OTC 7793.

Byrne, B.W. and Houlsby, G.T. (1998). *Model testing of circular flat footings on uncemented loose carbonate sand: experimental data*. Report N° OUEL 2192/98. Department of Engineering Science, University of Oxford

Byrne, B.W. and Houlsby, G.T. (2000). *Investigations of suction caissons in dense sand: experimental data*. Report N° OUEL 2227/00. Department of Engineering Science, University of Oxford

Cartwight, D.E. and Longuet-Higgins, M.S. (1956). The statistical distribution of the maxima of a random function. *Proc. Royal Society* **237 A**, pp. 212-232.

Cassidy, M.J. (1999). *The nonlinear dynamic analysis of jackup platforms under random ocean waves*. DPhil Thesis. Oxford University.

Clarke, D.W., Mohtadi, C., and Tuffs, P.S. (1987). Generalised predictive control - 1 - the basic algorithm. Automatica **23**, N° 2, pp.137-148.

Clarke, D.W. (1984). PID algorithms and their computer implementation. *Trans Inst M C* **6**, N° 6, pp. 305 - 316.

Clukey, E.C. and Morrison, M.J. (1993). Centrifuge and analytical study to evaluate suction caissons for TLP applications in the Gulf of Mexico. *Design and Performance of Deep Foundations: Piles and Piers in Soil and Soft Rock*. pp 141-156.

Clukey, E.C., Morrison, M.J., Garnier, J. and Corte, J.F. (1995). The response of suction caissons in normally consolidated clays to cyclic TLP loading conditions. *Offshore Technology Conference*, Houston, Texas. Paper 7796.

Collins, I.F. and Houlsby G.T. (1997). Application of thermomechanical principles to the modelling of geotechnical materials. *Proc. Royal Society* **453 A**, pp. 1975-2001.

De Beer, E.E. (1970). Experimental determination of shape factors and the bearing capacity factors of sand. *Geotechnique* **20**, N° 4, pp. 387-411.

Dean, E.T.R., James, R.G., Schofield, A.N., Tan, F.S.C, and Tsukamoto, Y. (1992). The bearing capacity of conical footings on sand in relation to the behaviour of spudcan footings of jack-ups. *Proc Wroth Memorial Symposium, Predictive Soil Mechanics*, Oxford, pp. 230-253. Thomas Telford, London.

Dyvik, R., Andersen, K.H., Hansen, S.B., and Christophersen, H.P. (1993). Field tests of anchors in clay. I : description. *ASCE Journal of Geotechnical Engineering* **119**, N° 10, pp. 1515-1531.

El-Gharbawy, S.L. (1998). *The pullout capacity of suction caisson foundations for tension leg platforms*. PhD dissertation. The University of Texas at Austin.

Elzinga, T., and Tromans, P.S. (1992). Validation of NewWave theory and RDWF predictions against measured global loading on a North Sea jacket. *Proc of Conference of Behaviour of Offshore Structures*, London, United Kingdom, pp. 495-505.

Erbrich, C. and Tjelta, T.I. (1999). Installation of bucket foundations and suction caissons in sand: geotechnical performance. *Offshore Technology Conference*, Houston, Texas. Paper 10990.

Finnie, I.M.S. (1993). *Performance of shallow foundations in calcareous soils*. PhD Thesis, University of Western Australia, Perth.

Frydman, S. and Burd, H.J. (1997). Numerical studies of the bearing capacity factor Ngamma. *ASCE Journal of Geotechnical Engineering* **123**, N° 1, pp. 20-29

Georgiadis, M and Butterfield, R. (1988). Displacements of footings on sand under eccentric and inclined loads. *Canadian Geotechnical Journal* **25**, pp. 199-212.

Georgiadis, M. (1993). Settlement and rotation of footings embedded in sand. *Soils and Foundations* **33**, N° 1, pp. 169-175.

Gottardi, G. (1992). *Modellazione del comportamento di foundazioni superficiali su sabbia suggette a diversi condizioni di carico*. PhD Thesis, Universita di Padova.

Gottardi, G and Houlsby, G.T. (1995). *Model tests of circular footings on sand subjected to combined loads.* Report N° OUEL 2071/95, Oxford University Engineering Laboratory.

Gottardi, G. and Butterfield, R. (1993). On the bearing capacity of surface footings on sand under general planar loads. *Soils and Foundations* **33**, N° 3, pp. 68-79.

Gottardi, G., Houlsby, G.T. and Butterfield, R. (1997). The plastic response of circular footings on sand under general planar loading. *Géotechnique* **49**, N° 4, pp. 453-470.

Hansen, J.B. (1961). A general formula for bearing capacity. *Bulletin N^o 11*, Danish Geotechnical Institute, Copenhagen.

Hansen, J.B. (1970). A revised and extended formula for bearing capacity. *Bulletin N^o 28*, Danish Geotechnical Institute, Copenhagen, pp. 5-11.

Hansteen, O.E. and Hoeg, K. (1994). Soil-structure interaction analysis of embedded caisson anchor under tension load. *Proceedings of the International Conference on the Behaviour of Offshore Structures*, BOSS 94. Massuchusetts Institute of Technology, Cambridge, USA.

Hasselmann, D.W., Dunckel, M., and Ewing, J.A. (1980). Directional wave spectra observed during JONSWAP in 1973. *Journal of Phys Oceanography* **10**.

Høeg, K. and Tang, W.H. (1977). Probabilistic considerations in the foundation engineering for offshore structures. *Proceedings of 2nd International Conference on Structural Safety and Reliability*, Munich, pp. 267-296.

Houlsby, G.T. (1995). Geotechnical model testing at Oxford University. Report to Kvaerner Earl and Wright No C034-A-N-RE-011. Oxford University Engineering Laboratory.

Houlsby, G.T. (1999). A model for the variable stiffness of undrained clay. *Proc. Int. Symp. On Pre-Failure Deformation Characteristics of Geomaterials*, IS Torino 99, Vol. **1**, pp. 443 - 450.

Houlsby, G.T. (2000). Private Communication.

Houlsby, G.T. and Puzrin, A.M. (2000). A thermomechanical framework for constitutive models for rate-independent dissipative materials. *International Journal of Plasticity*, in press.

House, A.R., Randolph, M.F. and Borbas, M.E. (1999). Limiting aspect ratio for suction caisson installation in clay. *ISOPE '99 9th International Offshore and Polar Engineering Conference and Exhibition*, Brest, France.

Ingra, T.S. and Baecker, G.B. (1983). Uncertainty in bearing capacity of sands. *ASCE Journal of Geotechnical Engineering* **109**, N^o 7, pp. 899 - 914.

Iwan, W.D. (1967). On a class of models for the yielding behaviour of continuous and composite systems. *Journal of Applied Mechanics* **34**, pp. 612-617.

Jeanjean, P., Andersen, K.H. and Kalsnes, B. (1998). Soil parameters for design of suction caissons for Gulf of Mexico deepwater clays. *Offshore Technology Conference*, Houston, Texas. Paper 8830

Johnson, K. (1999). *Partially drained loading of shallow foundations*. Fourth Year Project. Department of Engineering Science, The University of Oxford.

Jonathan, P., Taylor, P.H., and Tromans, P.S. (1994). Storm waves in the northern North Sea. *Proc of the Conference of the Behaviour of Offshore Structures*, pp. 481-494.

Jostad, H.P., Andersen, K.H., and Tjelta, T.I. (1997). Analyses of skirted foundations and anchors in sand subjected to cyclic loading. *Proc of Conference on the Behaviour of Offshore Structures*, Delft, The Netherlands. Vol **1**, pp. 149-162.

Kolk, H.J. and Campbell, K.J. (1997). Significant developments in offshore geosciences. *Proc. 8th International Conference on the Behaviour of Offshore Structures*, Delft, The Netherlands, **2**, pp. 259-272, Elsevier Science, Amsterdam.

Lau, C.K. (1988). *Scale Effects in tests on footings*. PhD Thesis, University of Cambridge.

Lee, K.L., and Focht, J.A. (1975). Liquefaction potential at Ekoisk tank in the North Sea. *ASCE Journal of Soil Mechanics and Foundations* **101**, GT1, pp. 1-18.

Lindgren, G. (1970). Some properties of a normal process near a local maximum. *Annals of Mathematical Statistics* **41**, pp. 1870.

Mangal, J. (1999). *Partially drained loading of shallow foundations on sand*. DPhil Thesis, Oxford University.

Martin, C.M. (1994). *Physical and numerical modelling of offshore foundations under combined loads*. DPhil Thesis, University of Oxford.

Martin, C.M. and Houlsby, G.T. (1994). *Combined loading tests of scale model spudcan footings on soft clay: experimental data*. Report N^o OUEL 2029/94. Oxford University Engineering Laboratory.

Masing, G. (1926). Eiganspannungen und Verfestigung beim Messing. Proceedings of the Second *International Congress of Applied Mechanics*, pp. 332-335.

McManus, K.J. and Davis, R.O. (1997). Dilation induced pore fluid cavitation in sands. *Geotechnique* **47**, N^o 1, pp. 173-177.

Meyerhof, G.G. (1953). The bearing capacity of foundations under eccentric and inclined loads. *Proc 3rd Int Conf Soil Mech Fndn Engng* **1**, pp. 440-445.

Miner, M.A. (1945). Cumulative damage in fatigue. *Trans. ASME* **67 A**, pp. 159-164.

Morison, J.R., O'Brien, M.P., Johnson, J.W., and Schaaf, S.A. (1950). The force exerted by surface waves on piles. *Trans. Am. Inst. Min. Metall. Engrs*, Petroleum Branch **189**, pp. 149-154.

NGI (1994). *Sleipner T - Special laboratory testing.* Report N^o 932514-1. Norwegian Geotechnical Institute, Oslo.

Ngo Tran, C.L. (1996). The analysis of offshore foundations subjected to combined loading. DPhil Thesis. University of Oxford.

Nova, R and Montrasio, L. (1991). Settlements of shallow foundations on sand. *Geotechnique* **41**, N^o 2, pp. 243 - 256.

Pierson, W.J. and Moskowitz, L. (1964). A proposed spectral form of fully developed wind seas based on the similarity theory of SA Kitaigorodskii. *Journal of Geophysical Research* **69**.

Poulos, H.G. and Davis, E.H. (1974). *Elastic solutions for soil and rock mechanics*. John Wiley and Sons, New York.

Prandtl, L. (1921). Uber die eindringungfestigkeit plastisher baustoffe und die festigkeit von scneifen. *Zeitschrift fur Angewandte Mathematik und Mechanik* **1**, N^o 1, Basel, Switzerland.

Prevost, J.H. (1977). Mathematical modelling of monotonic and cyclic undrained clay behaviour. *International Journal for Numerical and Analytical Methods in Geomechanics* **1**, pp. 195-216.

Puzrin, A.M. and Houlsby, G.T. (2000). A thermomechanical framework for rate-independent dissipative materials with internal functions. *International Journal of Plasticity*, in press.

Puzrin, A.M. and Houlsby, G.T. (1999). *Fundamentals of kinematice hardening hyperplasticity.* Report N^o OUEL 2218/99. The University of Oxford.

Pyke, R. (1979). Non linear soil models for irregular cyclic loadings. *ASCE Journal of the Geotechnical Engineering Division* **105**, GT6, pp. 715-726.

Rodenbusch, G., Garrett, D.L. and Anderson, S.L. (1986). Statistical linearization of velocity squared drag forces. *Proc of 1st Conference on Offshore Mechanics and Arctic Engineering* **1**, pp. 123-129.

Roscoe, K.H. and Schofield, A.N. (1957). The stability of short pier foundations on sand, discussion. *British Welding Journal*, January, pp. 12-18.

Rowe, P.W., Craig, W.H. and Procter, D.C. (1977). Dynamically loaded centrifugal model foundations. *Proc of 9th International Conference on Soil Mechanics and Foundation Engineering* **2**, pp359-364.

Schjetne, K., Andersen, K.H., Lauritzen, R., and Hansteen, O.E. (1979). Foundation engineering for offshore gravity structures. *Marine Geotechnology* **3**, N^o 4, pp. 1- 15.

Senpere, D. and Auvergne, G.A. (1982). Suction Anchor Piles - A proven alternative to driving or drilling. *Offshore Technology Conference*, Houston, Texas. Paper 4206.

Suastika, I.K. (1997) *Ringing of gravity base structures*. MSc Thesis. Delft University of Technology, The Netherlands.

Tan, F.S.C. (1990). *Centrifuge and numerical modelling of conical footings on sand*. PhD Thesis, University of Cambridge.

Taylor, P.H. (1992). On the kinematics of large ocean waves. *Proc of the Conference of the Behaviour of Offshore Structures*, London, United Kingdom, pp. 134-145,

Taylor, P.H., Jonathan, P., and Harland, L.A. (1995). Time domain simulation of jack-up dynamics with the extremes of a gaussian process. *Proc of Conference on Offshore Mechanics and Arctic Engineering* **1A**, pp. 313-319.

Teng, B., and Li, Y.C. (1991). The wave-current force spectrum on inclined cylinders. *Ocean Engineering* **18**, N^o 6, pp. 535-553.

Terzaghi, K. (1943). *Theoretical soil mechanics*. John Wiley and Sons, New York.

Thompson, R.S.G. (1996). *Development of non-linear numerical models appropiate for the analysis of jack-up units*. DPhil Thesis. University of Oxford.

Ticof, J. (1978). *Surface footings on sand under general planar loads*. PhD Thesis, Southampton University.

Tjelta, T.I. (1994). Geotechnical aspects of bucket foundations replacing piles for the Europipe 16/11E jacket. *Offshore Technology Conference*, Houston, Texas. Paper 7397.

Tjelta, T.I. (1995). Geotechnical experience from the installation of the Europipe jacket with bucket foundations. *Offshore Technology Conference*, Houston, Texas. Paper 7795.

Tjelta, T.I., Guttormsen, T.R. and Hermstad, J. (1986). Large-scale penetration test at a deepwater site. *Offshore Technology Conference*, Houston, Texas. Paper 5103.

Tromans, P.S., Anaturk, A. and Hagemeijer, P. (1991). A new model for the kinematics of large ocean waves - application as a design wave. *Proc of 1st International Symposium on Offshore and Polar Engineering*, Edinburgh, Vol **3**, pp. 64-71.

Tromans, P.S., Efthymiou, M., van de Graaf, J.W., Vanderschuren, L., and Taylor, P.H. (1992). Extreme storm loading on fixed offshore platforms. *Proc of Conference of Behaviour of Offshore Structures*, London, United Kingdom, pp. 325-336

Tromans, P.S., Hagemeijer, P.M. and Wassink, H.R. (1992). The statistics of the extreme response of offshore structures. *Ocean Engineering* **19**, N^o 2, pp. 161-181.

Tromans, P.S. and Vanderschuren, L. (1995). Response based design conditions in the North Sea: application of a new method. *Offshore Technology Conference*, Houston, Texas. Paper 7683.

Vesic, A.S. (1973). Analysis of ultimate loads of shallow foundations. *Journal of the Soil Mechanics and Foundations Division*, American Society of Civil Engineers **99**, N^o 1, pp. 45-73.

Vesic, A.S. (1975). Bearing capacity of shallow foundations. In *Foundation Engineering* Handbook (ed H.F. Winterkorn and H.Y. Fang), pp. 121-147. Van Nostrand, New York.

Vesic, A.S., Banks, D.C., and Woodard, J.M. (1965). An experimental study of dynamic bearing capacity of footings on sand. *Proc. 6th International Conference on Soil Mechanics and Foundation Engineering*, Montreal **2**, pp. 209-213.

Vucetic, M. and Dobry, R. (1988). Degradation of marine clays under cyclic loading. *ASCE Journal of Geotechnical Engineering* **114**, N^o 2, pp. 133-149.

Vucetic, M. (1990). Normalised behaviour of clay under irregular cyclic loading. *Canadian Geotechnical Journal* **27**, pp. 29-46.

Watson, P.G. and Randolph, M.F. (1998). Skirted foundations in calcareous soil, *Geotechnical Engineering* **131**, N^o 3, pp. 171-179.

Williams, M.S., Blakeborough, A., Houlsby, G.T., and Williams, D.M. (1998). Development of a real time hybrid dynamic testing system. *Proc 6th SECED Conference on Seismic Design Practice into the Next Century*, Oxford, 26-27 March, Balkema, ISBN 90-5410-9343, pp. 373-379

Wirsching, P.H., and Light, M.C. (1980). Fatigue under wide band random stresses. *ASCE Journal of the Structural Divison* **106**, ST7, pp. 1593-1607.

Wroth, C.P. and Houlsby, G.T. (1985). Soil mechanics - property characterisation and analysis procedures. *Proceedings 11th International Conference on Soil Mechanics and Foundation Engineering*. San Francisco, N^o 1, pp. 1-50.

Ziegler, H. (1977). *An introduction to thermomechanics.* North Holland, Amsterdam.

Name/Reference	Date	Location	Tests undertaken	Diameter	Depth	H/D	Soil Type
Shell Offshore Research trials (Hogervost, 1981)	1980	The Netherlands	Installation procedure, lateral loading and vertical loading at three different test sites.	3.8	5 8	1.31 2.1	(a) Sand (b) Sand over clay (c) Clay
Gullfaks C Large scale penetration test (Tjelta *et. al.*, 1986)	1985	North Sea	Two tests were carried to examine variation in penetration rate, check for set-up effects, cyclic tests, and water injection	6.5 (two cylinders)	22	3.38	Layers of sand and clay
GBS Model Test (Andreasson *et. al.*, 1988)	1986	Baeckebol, Gothenburg	Penetration resistance during installation, static and cyclic capacity, load distribution between skirts and base, foundation stiffness, and moment load capacity	0.6 (seven cells)	0.5	0.28	Clay
Snorre model tests (Dyvik *et. al.*, 1993)	1989	Lysaker, Oslo	Model tests to check calculation procedures developed at the NGI. The tests consisted of one static and three cyclic load tests.	0.9 (4 cells)	0.9	1	Clay
NGI Horizontal loading (Keaveny *et. al.*, 1994)	1990	Lysaker, Oslo	Study the effect of attachment of tether and anchor on pullout resistance and mechanism, study the effect of the use of a plastic liner, and study the impact of load cycling.	0.7 (2 cells)	1.5	2.14	Clay
Statoil Field trials (Tjelta, 1994)	1991	North Sea	Penetration by weight and suction, rapid loading tests, long term loading tests, cyclic loading tests and permeability tests	1.5	1.7	1.13	Dense Sand
Saga Field Trial (Olberg *et. al.*, 1997)	1996	North Sea	Full scale field trial of taut leg moorings using suction anchors in 200m water depth	5	8	1.6	Soft n.c. clay over sand
Offshore Data Limited	1998	Offshore Wales	Tests to determine installation feasibility, tensile capacity and moment capacity	2 4	2 2.5	1 0.625	Medium dense river sands

Table 1.1 - Historical sequence of recorded scale field testing of suction foundations.

Name	Date	Location	Application	Number	Diameter	Depth	H/D	Soil Type
Gorm (Senpere *et. al*., 1982)	1980	North Sea	Anchors	12	3.5	8.5	2.4	Sand over clay
Gullfaks C (Tjelta *et. al.*, 1986; 1988; 1992)	1989	North Sea	Concrete Gravity Base	16 multiple cells	28 (125x170)	22	~0.17	Layers of sand and clay
Snorre TLP (Andersen *et. al.* 1992; 1993; Christopherson *et. al*. 1992; Jonsrud *et. al.* 1992; Stove *et. al.* 1992)	1991	North Sea	Tension Leg Platform	4 (triple caisson)	17	12	0.71	Soft clay
Europipe 16/11E (Baerheim *et. al*. 1995; Barbour *et. al*. 1995; Bye *et. al*. 1995; Rusaas *et. al.* 1995; Svano *et. al.* 1997; Tjelta 1994; Tjelta 1995)	1994	North Sea	Steel Jacket	4	12	6	0.5	Dense sand
Heidrun TLP (Mitcha *et. al*., 1996)	1994	Norwegian Sea	Tension Leg Platform	4 (19 cylindrical cells)	48.3 long x 43.3 wide	4.6	0.1	
Nkossa Process Barge (Colliat *et. al*., 1995; 1996; 1997)	1995	Gulf of Guinea	Anchors	8 4	4 4.5	11.8 12.5	3 2.8	Soft clay
YME (Eide *et. al*., 1996)	1995	North Sea	Jack-Up (No suction used)	3 (multiple cell)	18	4.8	3.8	Dense sand
YME	1995	North Sea	Anchors	8		12.5		Dense sand
Harding	1995	North Sea	Anchors	8		10		Dense sand
Sleipner Vest SLT (Barbour *et. al.*, 1995; Bye *et. al.*, 1995)	1996	North Sea	Steel jacket	4	14	5	0.36	Dense sand
Aquila (Chimisso *et. al.*, 1998; Alhayari, 1998)	1997	Adriatic	Anchors	8	4.5 (lower) 5 (upper)	16.2	3.6 3.24	Soft to stiff clay
Schiehallion (Hagen *et. al*., 1998)	1997	North Sea	Anchors	14	6.5	12.8	1.97	Soft - firm clay
Curlew (Alhayari, 1998)	1997	North Sea	Anchors	9	5 7	12.6 9.5	2.52 1.35	Dense silty sand
Visund (Solhjell, 1998)	1997	North Sea	Anchors	16	5	11	2.2	Soft clay
Njord (Solhjell, 1998)	1997	North Sea	Anchors	20	5	10	2	Soft clay
Laminaria	1998	North West Shelf	Anchors	9	5	12	2.4	Carbonate sand
Transocean Marianas (Delmar Inc)	1998	Gulf of Mexico	Anchors		4	20	5	Soft clay
Asgard C	1999	North Sea	Anchors	9		15.7		

Table 1.2 - History of recorded use of suction foundations in large project developments.

Applied Loadings (N)			Readings (N)			Absolute Error (N)			Relative Error (%)		
V	H	M	V	H	M	V	H	M	V	H	M
597.9	0.0	0.0	598.0	0.1	0.2	0.12	0.14	0.20	0.02	#N/A	#N/A
597.9	-174.6	0.0	594.7	-175.0	0.1	-3.22	-0.48	0.08	0.54	0.28	#N/A
597.9	-174.6	12.0	594.4	-174.0	12.1	-3.55	0.59	0.14	0.59	0.34	1.20
597.9	-174.6	-17.9	596.1	-175.5	-17.8	-1.86	-0.96	0.15	0.31	0.55	0.84
597.9	-323.6	-17.9	593.5	-324.6	-17.9	-4.39	-1.00	0.04	0.73	0.31	0.20
597.9	0.0	-17.9	599.5	-0.1	-17.7	1.57	-0.12	0.26	0.26	#N/A	1.43
597.9	0.0	0.0	598.1	0.1	0.2	0.16	0.08	0.20	0.03	#N/A	#N/A
339.2	0.0	0.0	341.6	-0.2	0.1	2.45	-0.16	0.11	0.72	#N/A	#N/A
339.2	-93.7	-5.1	341.9	-94.4	-5.1	2.70	-0.75	-0.02	0.80	0.80	0.39
339.2	-263.3	0.0	339.5	-264.3	0.0	0.33	-0.94	0.03	0.10	0.36	#N/A
339.2	0.0	11.9	344.5	0.4	12.0	5.36	0.45	0.18	1.58	#N/A	1.48
509.1	0.0	0.0	509.1	0.4	-0.1	-0.05	0.36	-0.06	0.01	#N/A	#N/A
509.1	93.7	0.0	509.7	94.4	0.0	0.52	0.68	-0.02	0.10	0.72	#N/A
509.1	174.6	-7.6	509.5	174.9	-7.6	0.41	0.29	0.02	0.08	0.17	0.23
509.1	323.6	12.7	516.9	326.3	12.8	7.77	2.77	0.03	1.53	0.86	0.23
509.1	0.0	15.3	512.4	3.9	15.5	3.29	3.88	0.23	0.65	#N/A	1.48

Table 2.1 - A series of load check tests for the load cell showing the applied loads, measured loads from the load cell, difference in loads and relative difference.

Transducer	Range	Type	Calibration
Long Range Vertical LVDT	±150 mm	ACT600C (RDP)	16.18 ± 0.38%
Long Range Horizontal LVDT	±25 mm	D5/1000A (RDP)	-2.97 ± 0.056%
Long Range Rotational LVDT	±50 mm	ACT2000C (RDP)	5.82 ± 0.056%
Short Range LVDT (1)	±5 mm	D5/200AG (RDP)	-0.65 ± 0.012%
Short Range LVDT (2)	±5 mm	D5/200AG (RDP)	-0.67 ± 0.009%
Short Range LVDT (3)	±5 mm	D5/200AG (RDP)	-0.64 ± 0.015%
Pressure Transducer (Centre)	±100 kPa	Custom (Gaeltec Ltd)	24.45 ± 0.18%
Pressure Transducer (Trailing)	±70 kPa	PDCR910 (Druck)	8.04 ± 0.05%
Pressure Transducer (Front)	±70 kPa	PDCR910 (Druck)	8.09 ± 0.05%

Table 2.2 - Information about the various transducers used on the loading rig (NB: calibration is in units/V for a range of ± 10V.

Coefficient of Uniformity, C_u	3.64
Specific Gravity, G_s	2.69
Minimum density, γ_{min}	12.72 kN/m^3
Maximum density, γ_{max}	16.85 kN/m^3
Critical state friction angle, ϕ_{cs}	32.5°
Permeability (80% Rd with water), k	7 x 10^{-6} m/s
Oil - Kinematic viscosity, μ	100 mm^2/s (at 25° C) (compared to 0.897 mm^2/s for water)
Oil - Specific gravity, G_s	0.96 (at 25° C)
Oil - Bulk Modulus, K	800 MPa for ε < 1% (compared to 2200 MPa for water at 25° C)

Table 2.3 - Properties of the Baskarp Cyclone Sand and Silicon Oil.

Sample	Test	γ kN/m^3	R_D	$V_{max(50)}$ kN	q_{fail} kPa	N_γ^*	f deduced from R_D (Bolton, 1986)	f deduced from N_γ^* (Bolton and Lau, 1993)
Trial	**Trial1_2**	16.77	98.60	900	458.37	1093.07	44.29	46.12
Trial	**Trial2_1**	16.77	98.60	902.93	459.86	1096.62	44.29	46.13
Trial	**Trial4_2 1**	16.77	98.60	918.99	468.04	1116.13	44.29	46.19
Trial	**Trial7_1**	16.77	98.60	940.53	479.01	1142.30	44.29	46.27
Trial	**Trial8_1**	16.77	98.60	895.37	456.01	1087.44	44.29	46.11
DM1	**DM1-BC**	16.56	94.63	1019.88	519.42	1254.53	43.70	46.61
DM1	**DM1-6**	16.56	94.63	1098.38	559.40	1351.09	43.70	46.90
DM2	**DM2-BC**	16.69	97.14	928.09	472.67	1132.49	44.07	46.24
DM3	**DM3-BC**	16.71	97.34	846.26	431.00	1031.96	44.10	45.92
DM4	**DM4-1**	16.75	98.25	937.78	477.61	1140.23	44.24	46.27
DM4	**DM4-2**	16.75	98.25	924.51	470.85	1124.09	44.24	46.22
DM5	**DM5-BC**	16.79	98.96	808.14	411.58	980.37	44.34	45.71
DM6	**DM6-BC**	16.74	97.93	703.68	358.38	856.48	44.19	45.21
DM7	**DM7-BC**	16.81	99.26	1107.23	563.91	1341.89	44.39	46.87
DM8	**DM8-BC**	16.56	94.60	884.16	450.30	1087.71	43.69	46.11
DM9	**DM9-BC**	16.67	96.74	785.06	399.83	959.20	44.01	45.63
DM10	**DM10-BC**	16.54	94.26	622.00	316.78	766.02	43.64	44.34
Standard Deviation		0.10	1.81	136.17	69.35	166.16	0.27	0.67
Average		16.69	97.08	892.93	454.77	1089.70	44.06	46.03

Table 2.4 - Summary of Bearing Capacity Tests carried out during testing series

Test Tank	Tank Notes
DM1	Test series DM1 was really used as a trial set of tests to enable the equipment to be commissioned, after which several corrections to the control and acquisition program were identified and carried out. It was found that during the vertical loading sections of the testing minor deviations in the sample surface resulted in the development of moment and horizontal load on the footing. A routine was developed in which the footing was slightly rotated or displaced horizontally to reduce these loads to acceptable levels. Swipes were conducted under both constant vertical load and constant vertical displacement.
DM2	The prime objective in this tank was to assess the performance of the flat footing under horizontal loading. In particular it was important to assess the variation in the swipes starting with different ratios of V_o/V_{peak} (and an OCR of 1).
DM3	The primary purpose of this tank was to examine the moment behaviour of a flat footing. Two tests were conducted in which the footing had an embedment ratio of 0.33.
DM4	The majority of the tests in this set consisted of moment swipes at various load levels to assess the difference in behaviour associated with the different skirt depths. The initial bearing capacity test was aborted due to computer malfunction, thus two bearing capacity tests were conducted on opposite sides of the sample which show a reassuring agreement.
DM5	The majority of the tests in this set consisted of horizontal swipes at various load levels to assess the difference in behaviour associated with the different skirt depths.
DM6	This tank comprised of 17 swipe tests, of a footing with an embedment ratio of 0.33, to evaluate the yield surface for a range of *H2R/M* ratios. The swipe tests were carried to reasonable displacements so that a transition between inner and outer yield surface could be observed. The sample was reformulated after the first eight swipes so that further tests could be undertaken - this was done principally by slightly loosening the soil and re-vibrating it to its previous state.
DM7	This tank comprised of tests similar to tank DM6 but at a higher V_o/V_{peak} ratio. Cone penetration testing was carried out to evaluate the consistency across the sample.
DM8	This tank comprises primarily of *du:2Rdq* loops to capture the shape of the *H:M/2R* cross-section for various vertical load levels, and different skirt depths. After completing the loop testing, two swipe tests were performed so that correlations between the loops and the yield surface associated with the swipes could be made. More information about the vertical bearing capacity could also be gained from several of these tests.
DM9	The behaviour of the flat footing was examined in this series of tests. Swipe tests were conducted at four levels of vertical load (450N, 900N, 1350N, 1800N) as well as at four different levels of overconsolidation ratios (4, 2, 1.33 and 10) for six different ratios of *2RH/M*. The horizontal and rotational movements were kept to less than 1mm so that minimal disturbance occurred to the test site, thus allowing further tests to be carried out at the same site. The tests were designed to capture the shape of the internal yield surface, movements stopping so that the transition to the outer yield surface was not made. A bearing capacity test was carried out so that an indication of the hardening law was captured. Cone penetration testing was also carried out to evaluate the consistency of the sample.
DM10	The tests conducted in this series were aimed primarily at the vertical loading behaviour. Secondary emphasis was placed on determining the behaviour under low vertical loads, particularly examining the shape of the yield surface at zero vertical load for the footings with an embedment ratio of 0.66. Some elasticity tests were conducted to examine whether an internal boundary of elastic and plastic behaviour could be defined.

Table 2.5 - Summary of the tests undertaken during dense sand study.

Test Group	Test Notes	Test Names	Notes
Vertical Loading	As far as possible with unload-reload cycles	FUF01, FUF02	
	Up to V = 1600N, with unload-reload cycles at V = 1000N	FUF05, FUF06, FUF08, FUF09, FUF10, FUF11, FUF13, FUF14, FUF15, FUF16, FUF23	
Swipe	From V = 1600N	FUF05 (H, 0)	atan(2Rdq/du) = 0.03
		FUF06 (0, M)	atan(2Rdq/du) = 89.6
		FUF08 (H, M)	atan(2Rdq/du) = 69.1
		FUF09 (H, -M)	atan(2Rdq/du) = -69.4
	From V = 50N after V = 1600N	FUF10 (H, 0)	atan(2Rdq/du) = -0.4
		FUF11 (0, M)	atan(2Rdq/du) = 89.7
	Multiple values of V	FUF21 (H, 0) from V = 400N, 800N, 1200N, 1600N and 1800N	atan(2Rdq/du) = 2.2 atan(2Rdq/du) = 2.5 atan(2Rdq/du) = 0.8 atan(2Rdq/du) = 2.9 atan(2Rdq/du) = 0.9
Constant V	At V = 1600N	FUF13 (H, 0)	atan(2Rdq/du) = 1.2
		FUF14 (0, M)	atan(2Rdq/du) = 87.9
		FUF15 (H, M)	atan(2Rdq/du) = 68.7
		FUF16 (H, -M)	atan(2Rdq/du) = -72.9
Monotonic Radial Displacement	Each test taken as far as possible	FUF17	du/dw = 0.997
		FUF18	du/dw = 1.509
		FUF19	2Rdq/dw = 0.491
		FUF20	2Rdq/dw = 2.356
Elastic Cycles	At V = 800N after V = 1600N	FUF23	V ± 100N excursion H ± 100N excursion M/$2R$ ± 50N excursion

Table 2.6 - Summary of the tests undertaken during carbonate sand study.

Embedment Ratio = 0.66, Diameter = 0.1m

	Vertical Movements	Consolidation Test	Vertical	Moment	Horizontal	Comments
1	=>75	=>100				
2			100	0±40	0	Cyclic (10 secs)
3			100	0	0±40	Cyclic (10 secs)
4			100±150	0	0	Cyclic (6 secs)
5	=>0					
6			100	0±40	0	Cyclic (10 secs)
7			100	0	0±40	Cyclic (10 secs)
8			100±150	0	0	Cyclic (10 secs)
9	=>200		200	0±40	0	Cyclic (10 secs)
			100	0±40	0	Cyclic (10 secs)
10			200	0	0±40	Cyclic (10 secs)
			100	0	0±40	Cyclic (10 secs)
11			200±350	0	0	Cyclic (10 secs)
12			100±150	0	0	Cyclic (10 secs)
13			100	0±30	0	Cyclic (10 secs)
14		=>100=>200=>100=>200				
15	=>600		600	0±80	0	Cyclic (10 secs)
16			600	0±80	0	Cyclic (10 secs)
17			200	0±40	0	Cyclic (10 secs)
18			100	0±40	0	Cyclic (10 secs)
19			600	0	0±80	Cyclic (10 secs)
20			200	0	0±40	Cyclic (10 secs)
21			100	0	0±40	Cyclic (10 secs)
22			100	0.25, -0.5, 0.25	0.25, -0.5, 0.25	Monotonic Moves
23			600±750	0	0	Cyclic (10 secs)
24		=>100=>200=>100=>200				
25		=>300=>400=>300=>400				
26			600±750	0	0	Cyclic (10 secs)
27			200±350	0	0	Cyclic (10 secs)
28			100±250	0	0	Cyclic (10 secs)
29	=>1000=>200=>2000=>200=>2300=>0					
30			0	0.25,-0.5,0.25	0.25,-0.5,0.25	Monotonic Moves
31			0	2.5	0	Montonic Move
32			100	0.25,-0.5,0.25	0.25,-0.5,0.25	Monotonic Moves
33	=>1000=>200=>2000=>200=>2300=>200					Monotonic Moves
34	-3mm@2mm/s					Pull Test
35	=>2300=>200					Monotonic
36	-75mm @ 2mm/s					Pull Test

Table 2.7 - Listing for cyclic loading test SM1-5.

Key for notation: '100±150' denotes a cyclic test with a mean load of 100N with the "NewWave" scaled to give a minimum load of -50N. '=>1000=>200' denotes a monotonic movement up to 1000N and then back down to 200N. Consolidation tests simply represent fast step changes between the loads specified. '-3mm@2mm/s' denotes a pull test for 3mm at a velocity of 2mm/s.

Notes	h_o	m_o	a	Reference
Silica sand, for V_{peak}, surface footings ('outer' yield surface).	0.11	0.08	-0.2225	Gottardi *et. al.* (1999)
	0.1216	0.086	-0.25	Cassidy (1999)
	0.13	0.074	0.06	This study
	0.113	0.074	NA	Meyerhof (1953) (for $f = 43^o$)
	0.0819	0.074	NA	Hansen (1960)
	0.1232	0.074	NA	Vesic (1975)
	0.12	0.1	NA	Butterfield and Ticof (1979)
	0.14	NA	NA	Tan (1990)
Silica sand, for V_{peak}, skirted footings ('outer' yield surface)	0.15	0.074	-0.25	L/D = 0.16 This study
	0.17	0.074	-0.75	L/D = 0.33 This study
	0.13	0.09	-0.93	L/D = 0.66 This study
Silica sand, pre - peak ('inner' yield surfaces).	$h_{opeak}\left(1-0.36\ln\left(\frac{V_o}{V_{peak}}\right)\right)$	$m_{opeak}\left(1-0.36\ln\left(\frac{V_o}{V_{peak}}\right)\right)$	as for outer surface	This study
Silica sand, post peak.	$h_{opeak}+0.13\frac{w}{2R}$	NA	NA	Tan (1990)
Carbonate sand (surface)	NA	NA	NA	
Carbonate sand (embedded)	$0.138+0.1\frac{w}{2R}$	0.089	-0.3	This study

Table 3.1 - Compilation of parameter values for three dimensional yield surface shape.

V (N) Mean ± Cyclic	Period (s)	Cyclic Form	Test Name	Relative Density (%)	Figure Number
200±250	10	NewWave	sm1-2_1 15	79	4.15
100±150	6	NewWave	sm1-5_1 5	79	4.17-4.20
100±150	10	NewWave	sm1-5_2 2	79	4.17-4.20
100±125	6	NewWave	sm1-3_1 41	79	4.7, 4.8
200±150	1.5	NewWave	sm1-4_3 17	79	
200±150	3	NewWave	sm1-4_3 12	79	
200±150	6	NewWave	sm1-4_3 7	79	
200±150	12	NewWave	sm1-4_3 21	79	
200±250	1.5	NewWave	sm1-4_3 18	79	
200±250	3	NewWave	sm1-4_3 13	79	
200±250	6	NewWave	sm1-4_3 8	79	
200±250	6	NewWave	sm1-3_1 8	79	4.7, 4.8, 4.15
200±250	12	NewWave	sm1-4_3 22	79	
200±350	3	Stepped Sine	sm1-4_3 30	79	
200±350	3	Modulated Sine	sm1-4_3 36	79	
200±350	3	NewWave	sm1-4_3 14	79	
200±350	4	Stepped Sine	sm1-4_3 33	79	
200±350	4	Modulated Sine	sm1-4_3 34	79	
200±350	4	NewWave	sm1-4_3 32	79	4.3, 4.6
200±350	4	NewWave	sm1-4_3 26	79	4.9
200±350	10	Stepped Sine	sm1-4_3 50	79	4.31
200±350	10	Stepped Sine	sm1-4_3 61	79	4.31
200±350	10	Stepped Sine	sm1-4_3 38	79	4.10, 4.11
200±350	10	Modulated Sine	sm1-4_3 35	79	4.10, 4.11
200±350	10	NewWave	sm1-3_1 9	79	4.10, 4.11, 4.30
200±350	12	NewWave	sm1-4_3 23	79	
200±50	1.5	NewWave	sm1-4_3 16	79	
200±50	3	NewWave	sm1-4_3 11	79	
200±50	6	NewWave	sm1-4_3 6	79	
200±50	12	NewWave	sm1-4_3 20	79	
500±650	10	Stepped Sine	sm1-4_3 66	79	
600±750	6	NewWave	sm1-3_1 26	79	4.7, 4.8
600±750	10	NewWave	sm1-3_1 25	79	
800±1000	6	NewWave	sm1-3_1 37	79	4.7, 4.8
100±250	3	NewWave	sm1-6_2 9_1	92	4.4, 4.13
100±250	6	NewWave	sm1-6_2 9_2	92	4.4, 4.13
100±250	12	NewWave	sm1-6_2 9_3	92	4.4, 4.13
200±300	3	NewWave	sm1-6_2 15_1	92	4.21
200±300	6	NewWave	sm1-6_2 15_2	92	4.21
200±300	12	NewWave	sm1-6_2 15_3	92	4.21
200±500	3	NewWave	sm1-6_2 27_1	92	4.12, 4.13, 4.32
200±500	30	NewWave	sm1-6_2 27_2	92	4.12, 4.13, 4.32
400±600	3	NewWave	sm1-6_2 32_1	92	
400±600	6	NewWave	sm1-6_2 32_2	92	
400±600	12	NewWave	sm1-6_2 32_3	92	

All tests were for caisson of diameter 150mm, skirt depth 50mm except for SM1-5 where the diameter was 100mm and skirt depth 66mm.

Table 4.1 - Key cyclic vertical loading tests.

Load	1.5 s	3 s	6 s	10 s	12 s	30 s	RD	Figure Number
200±50	sm1-4_3 16	sm1-4_3 11	sm1-4_3 6		sm1-4_3 20		79	
200±150	sm1-4_3 17	sm1-4_3 12	sm1-4_3 7		sm1-4_3 21		79	
200±250	sm1-4_3 18	sm1-4_3 13	sm1-4_3 8		sm1-4_3 22		79	
200±350		sm1-4_3 14	sm1-4_3 9	sm1-4_7 11	sm1-4_3 23		79	
600±150			sm1-3_1 21_1	sm1-3_1 21_2			79	
600±450			sm1-3_1 24	sm1-3_1 23			79	
600±750			sm1-3_1 26	sm1-3_1 25			79	
100±150			sm1-5_1 5		sm1-5_1 9		79	
100±50	sm1-6_2 7	sm1-6_2 3	sm1-6_2 4		sm1-6_2 5		92	
100±150		sm1-6_2 8_1	sm1-6_2 8_2		sm1-6_2 8_3		92	
100±250		sm1-6_2 9_1	sm1-6_2 9_2		sm1-6_2 9_3		92	4.4, 4.13
200±150		sm1-6_2 13_1	sm1-6_2 13_2		sm1-6_2 13_3		92	
200±300		sm1-6_2 14_1	sm1-6_2 14_2		sm1-6_2 14_3		92	4.21
200±500		sm1-6_2 15_1	sm1-6_2 15_2		sm1-6_2 15_3	sm1-6_2 27	92	4.12, 4.13
400±350		sm1-6_2 31_1	sm1-6_2 31_2		sm1-6_2 31_3		92	
400±600		sm1-6_2 32_1	sm1-6_2 32_2		sm1-6_2 32_3		92	
400±1000			sm1-6_2 33_1		sm1-6_2 33_2		92	

All tests were for caisson of diameter 150mm, skirt depth 50mm except for prefix SM1-5 where the diameter was 100mm and skirt depth 66mm. The loading was 'NewWave'.

Table 4.2 - Key cyclic vertical loading frequency comparison tests.

	NewWave	Stepped Sine	Modulated Sine	Figure Number
200±350 (3 s)	sm1-4_3 25	sm1-4_3 30	sm1-4_3 36	
200±350 (4 s)	sm1-4_3 32	sm1-4_3 33	sm1-4_3 34	
200±350 (10 s)	sm1-3_1 9	sm1-4_3 37	sm1-4_3 35	4.10, 4.11

Table 4.3 - Key loading history comparison tests.

V_{peak}/V_{mean}	0.25	0.75	1.25	Figure Number
Mean = 100N (6s)	sm1-3_1 39	sm1-3_1 40	sm1-3_1 41	4.7, 4.8
Mean = 200N (6s)	sm1-3_1 3	sm1-3_1 6_2	sm1-3_1 8	4.7, 4.8
Mean = 600N (6s)	sm1-3_1 21_2	sm1-3_1 24	sm1-3_1 26	4.7, 4.8
Mean = 800N (6s)	sm1-3_1 35	sm1-3_1 36	sm1-3_1 37	4.7, 4.8

Table 4.4 - Key cyclic load ratio tests.

Vertical Starting Load (N)	Displacement (mm)	Vertical Velocity (mm/s)	Test Name	Relative Density (%)	Figure Number
200	3	2	sm1-5_5 11	79	
200	pull out	2	sm1-5_5 13	79	4.24
200	1	0.001	sm1-4_3 40	79	4.22
200	1	0.01	sm1-4_3 41	79	4.22
200	1	0.02	sm1-4_3 42	79	4.22
200	1	0.1	sm1-4_3 43	79	4.22
200	1	0.1	sm1-4_3 43	79	4.23
200	1	0.1	sm1-4_3 49	79	4.23, 4.31
200	1	1	sm1-4_3 44	79	4.22
200	1.6	0.1	sm1-4_3 62	79	4.23, 4.31
200	2.5	0.001	sm1-4_3 46	79	
200	2.5	0.5	sm1-4_3 47	79	
200	4	0.5	sm1-3_1 44_1	79	
200	4	1	sm1-3_1 44_2	79	
200	4	1.5	sm1-3_1 44_3	79	
200	4	2	sm1-3_1 44_4	79	
1000	4	2	sm1-3_3 5_3	79	
500	20	0.01	sm1-4_8 7	79	
500	pull out	0.1	sm1-4_8 8	79	
250	pull out	2	sm1-3_4 2_1	79	4.24, 4.30
200	1	0.0001	sm1-6_3 4	92	
200	1	0.001	sm1-6_3 3	92	
200	1	0.005	sm1-6_2 18_4	92	4.25
200	1	0.005	sm1-6_2 25_2	92	
200	1	0.005	sm1-6_2 26_1	92	
200	1	0.005	sm1-6_2 26_3	92	
200	1	0.01	sm1-6_3 5_1	92	
200	1	0.05	sm1-6_2 18_3	92	4.25
200	1	0.1	sm1-6_3 5_2	92	
200	1	0.5	sm1-6_2 18_1	92	4.25
200	1	0.5	sm1-6_2 23	92	
200	1	0.5	sm1-6_2 25_1	92	
200	1	0.5	sm1-6_2 25_3	92	
200	1	0.5	sm1-6_2 26_2	92	
200	1	0.5	sm1-6_2 26_4	92	
200	1	1	sm1-6_3 5_3	92	
200	1	2	sm1-6_2 18_2	92	4.25
100	1.5	0.5	sm1-6_2 34_1	92	
200	1.5	0.5	sm1-6_2 34_2	92	
400	1.5	0.5	sm1-6_2 35_1	92	
600	1.5	0.5	sm1-6_2 35_2	92	
200	5	0.05	sm1-6_2 36_4	92	4.25
200	5	0.1	sm1-6_2 36_3	92	4.25
200	5	0.5	sm1-6_2 36_1	92	4.25
200	5	0.5	sm1-6_2 36_5	92	4.25
200	5	2	sm1-6_2 36_2	92	4.25
200	10	0.2	sm1-6_3 6_1	92	4.32
200	pull out	2	sm1-6_3 6_2	92	4.26, 4.32

All tests were for caisson of diameter 150mm, skirt depth 50mm except for SM1-5 where the diameter was 100mm and skirt depth 66mm.

Table 4.5 - Key monotonic vertical tensile loading tests.

Vertical Load, V (N)	$M/2R$ Mean±Cyclic (N)	Period (s)	Cyclic Form	Test Name	V_{max} (N)	Figure Number
100	0±incsine	10	Increasing Sine	sm1-4_3 69	1400	5.10, 5.15, 5.17
100	0±modsine	10	Modulated Sine	sm1-4_4 5	1400	
150	0±incsine	10	Increasing Sine	sm1-4_3 70	1400	5.10, 5.17
200	0±100	6	NewWave	sm1-3_1 20	600	5.7
200	0±20	6	NewWave	sm1-4_1 4	200	
200	0±40	6	NewWave	sm1-4_1 5	200	5.5, 5.7 5.8, 5.9, 5.30
200	0±60	6	NewWave	sm1-3_1 15	400	
200	0±60	10	NewWave	sm1-3_1 16	400	
200	0±incsine	10	Increasing Sine	sm1-4_3 53	600	5.7
200	0±incsine	10	Increasing Sine	sm1-4_3 68	1400	5.10, 5.17
200	0±modsine	10	Modulated Sine	sm1-4_5 2	1400	
200	0±stepsine	10	Stepped Sine	sm1-4_5 3	1400	
200	20±20	6	NewWave	sm1-4_3 1	200	
200	20±40	6	NewWave	sm1-4_3 2	200	
200	20±60	6	NewWave	sm1-4_3 3	200	
200	0±incsine	200	Increasing Sine	sm1-4_5 8	1400	5.11, 5.24,
300	0±incsine	10	Increasing Sine	sm1-4_3 71	1400	5.10, 5.15, 5.17
300	0±modsine	10	Modulated Sine	sm1-4_4 6	1400	
500	0±incsine	10	Increasing Sine	sm1-4_3 67	1400	5.10, 5.15, 5.17
500	0±modsine	10	Modulated Sine	sm1-4_4 7	1400	
100	0±40	10	NewWave	sm1-5_1 3	100	5.4
200	0±40	10	NewWave	sm1-5_1 10	400	5.4
600	0±80	10	NewWave	sm1-5_3 3	600	5.4

Vertical Load, V (N)	Movements (mm)	Test Name	V_{max} (N)	Figure Number
200	1, -2, 1	sm1-4_5 7	1400	5.14, 5.15
50	1, -2, 1	sm1-4_6 1_1	1400	5.14, 5.15
100	1, -2, 1	sm1-4_6 1_2	1400	5.14, 5.15, 5.16, 5.27
300	1, -2, 1	sm1-4_6 2_1	1400	5.14, 5.15, 5.16
500	1, -2, 1	sm1-4_6 2_2	1400	5.14, 5.15, 5.16
700	1, -2, 1	sm1-4_6 3_1	1400	5.14, 5.15
1000	1, -2, 1	sm1-4_6 3_2	1400	5.14, 5.15, 5.16, 5.27
100	1, -2, 1	sm1-4_7 5_1	2500	5.12, 5.32, 5.33, 5.34
300	1, -2, 1	sm1-4_7 5_2	2500	5.32, 5.33
500	1, -2, 1	sm1-4_7 5_3	2500	5.32, 5.33
1000	1, -2, 1	sm1-4_7 5_4	2500	5.12, 5.32, 5.32
100	0.25, -0.5, 0.25	sm1-5_3 9	600	
0	0.25, -0.5, 0.25	sm1-5_5 7	2300	
100	0.25, -0.5, 0.25	sm1-5_5 9	2300	

All tests were for caisson of diameter 150mm, skirt depth 50mm except for SM1-5 where the diameter was 100mm and skirt depth 66mm. The relative density was 79%.

Table 5.1 - Key moment loading tests.

Vertical Load, V (N)	*H* Mean±Cyclic	M/2*R* Mean±Cyclic	Period (s)	Test Name	V_{max} (N)	Figure Number
200	0±20	0	6	sm1-4_2 2	200	
200	0±20	0±20	6	sm1-4_2 9	200	
200	0±40	0	6	sm1-4_2 3	200	
200	0±40	0±40	6	sm1-4_2 10	200	
200	0±50	0	10	sm1-4_7 10	2500	
200	0±60	0	6	sm1-4_2 4	200	
200	0±60	0±60	6	sm1-4_2 11	200	
200	0±80	0	6	sm1-4_2 5	200	
200	0±100	0	6	sm1-4_2 6	200	
200	Increasing Cycles	0	200	sm1-4_6 7_2	1400	5.11, 5.13
100	0±40	0	10	sm1-5_1 4	100	
200	0±40	0	10	sm1-5_1 12	200	
200	0±40	0	10	sm1-5_3 7	600	
100	0±40	0	10	sm1-5_3 8	600	
600	0±80	0	10	sm1-5_3 6	600	

Vertical Load (N)	Movements (mm)	Test Name	V_{max} (N)	Figure Number
50	1, -2, 1	sm1-4_6 4_1	1400	5.13, 5.18, 5.28
100	1, -2, 1	sm1-4_6 4_2	1400	5.13, 5.18, 5.28
200	0.6, -1.2, 0.6	sm1-4_6 7_1	1400	5.11, 5.13, 5.18, 5.28
200	1, -2, 1	sm1-4_6 8	1400	5.29
300	1, -2, 1	sm1-4_6 5	1400	5.13, 5.18, 5.28
500	1, -2, 1	sm1-4_6 6_1	1400	5.13, 5.18, 5.28
700	1, -2, 1	sm1-4_6 6_2	1400	5.13, 5.18, 5.28
1000	1, -2, 1	sm1-4_6 6_3	1400	5.13, 5.18, 5.28
100	1, -2, 1	sm1-4_7 6_1	2500	
300	1, -2, 1	sm1-4_7 6_2	2500	
500	1, -2, 1	sm1-4_7 6_3	2500	
1000	1, -2, 1	sm1-4_7 6_4	2500	
100	0.25, -0.5, 0.25	sm1-5_3 9	600	
0	0.25,-0.5,0.25	sm1-5_5 7	2300	
100	0.25, -0.5, 0.25	sm1-5_5 9	2300	

All tests were for caisson of diameter 150mm, skirt depth 50mm except for SM1-5 where the diameter was 100mm and skirt depth 66mm. All cyclic tests used the 'NewWave' form and the relative density was 79%.

Table 5.2 - Key horizontal loading tests.

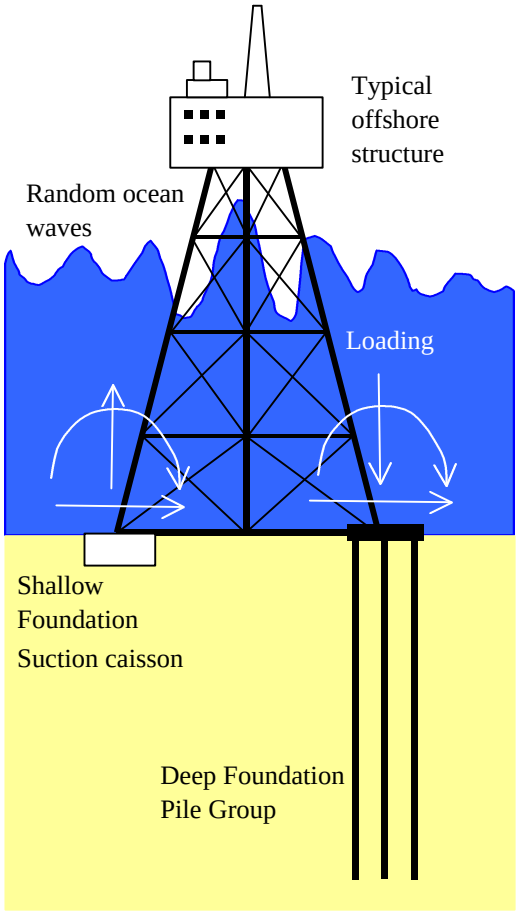

Figure 1.1 - Typical fixed oil and gas facility.

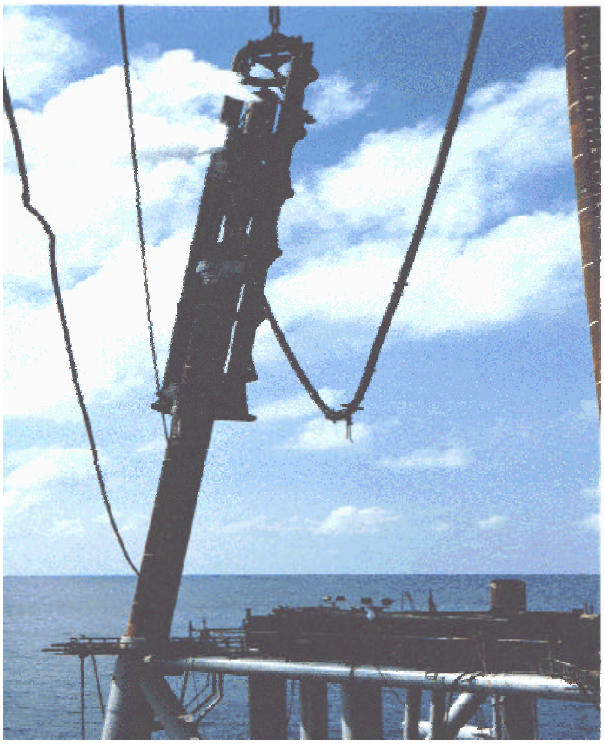

Figure 1.2 - Pile being driven into the ground using a steam operated pile driving hammer.

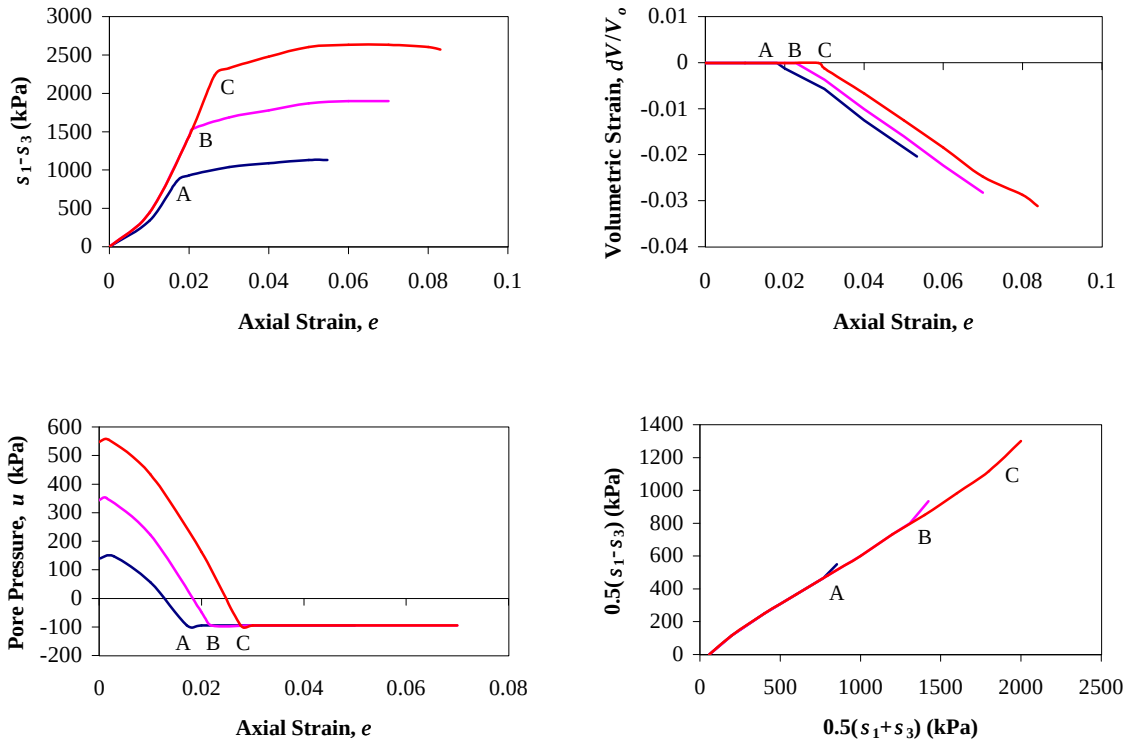

Figure 1.3 - Undrained triaxial tests on dense sand (McManus and Davies, 1997) showing increased strengths due to negative pore pressures, though capped by cavitation of the pore fluid - A, B and C represent the onset of cavitation.

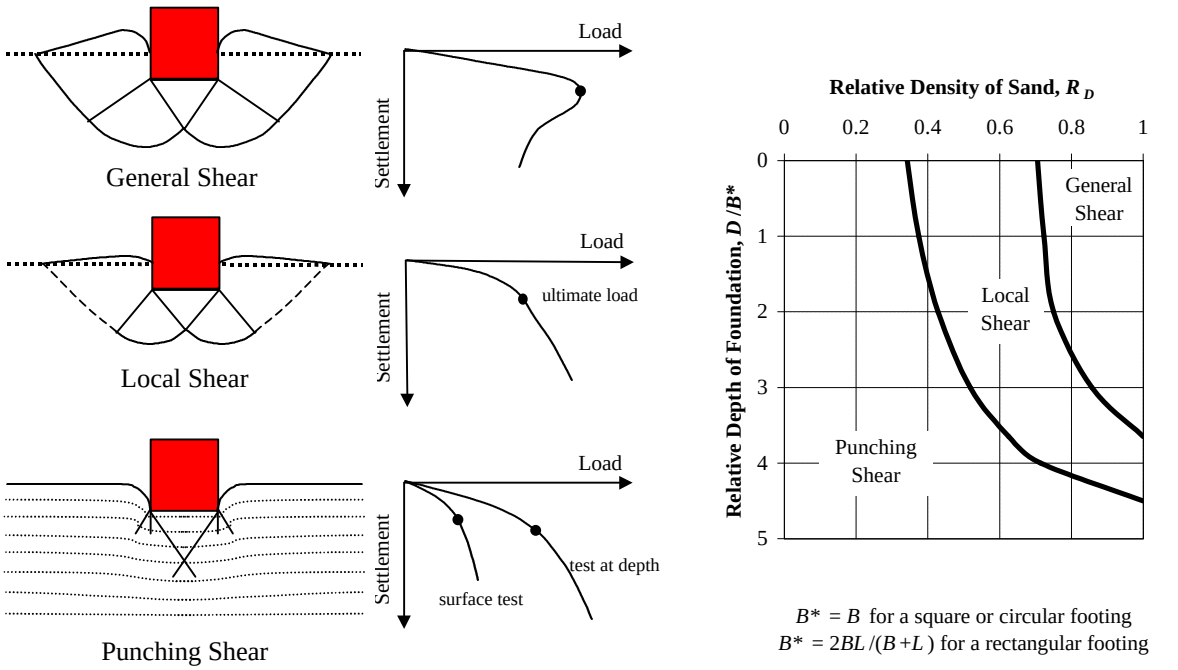

Figure 1.4 - Typical failure mechanisms for a shallow foundation (after Vesic, 1973).

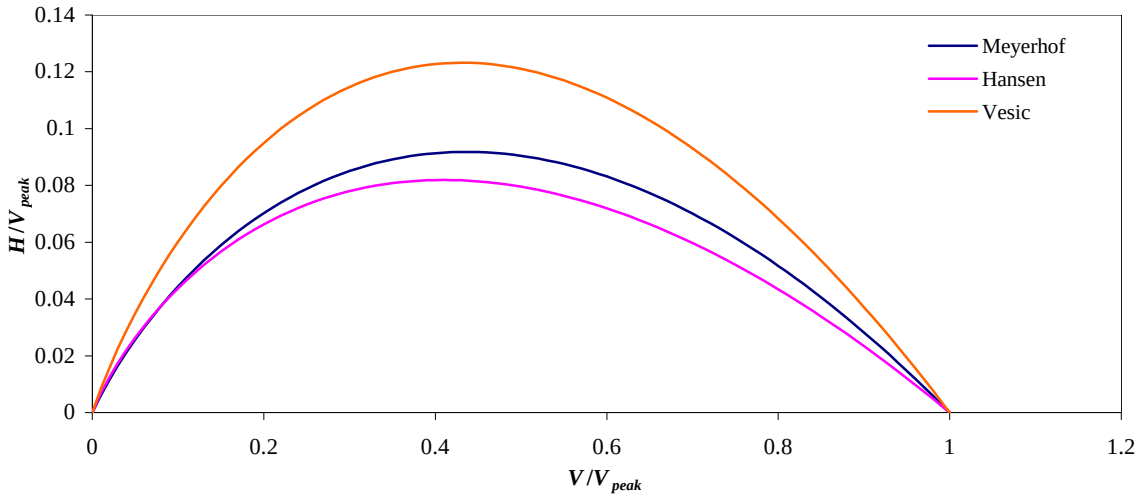

Figure 1.5 - Classic bearing capacity interaction factors interpreted as yield surfaces.

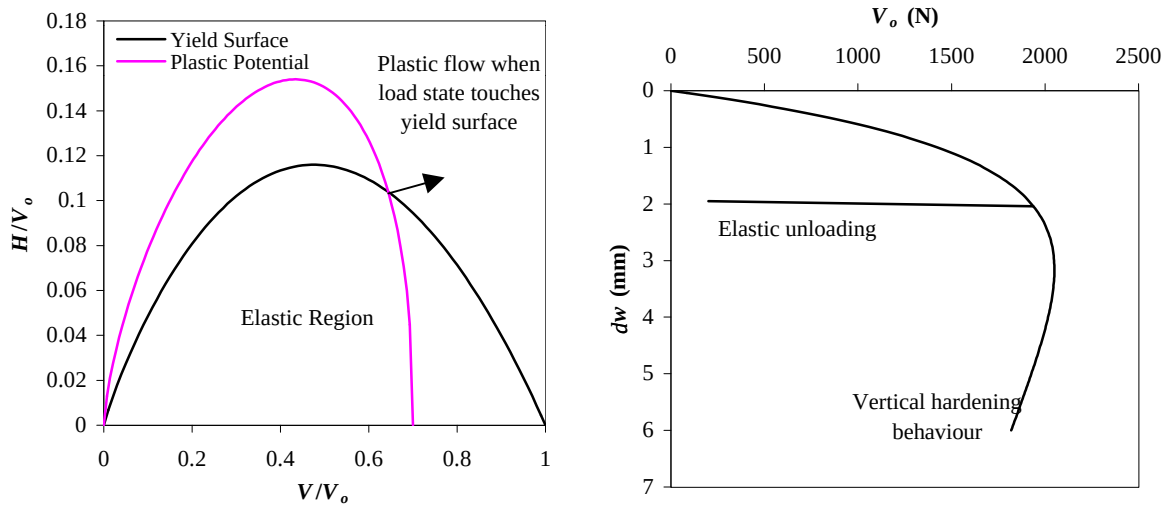

Figure 1.6 - Components of a work-hardening plasticity theory, (a) yield surface and plastic potential, (b) work hardening relationship and elastic behaviour.

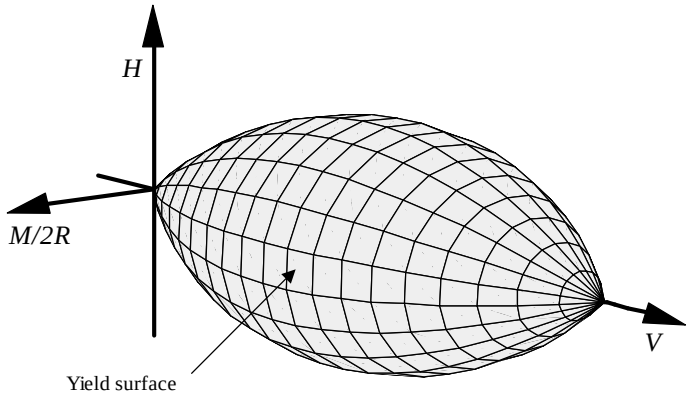

Figure 1.7 - Combined load yield surface postulated by many researchers.

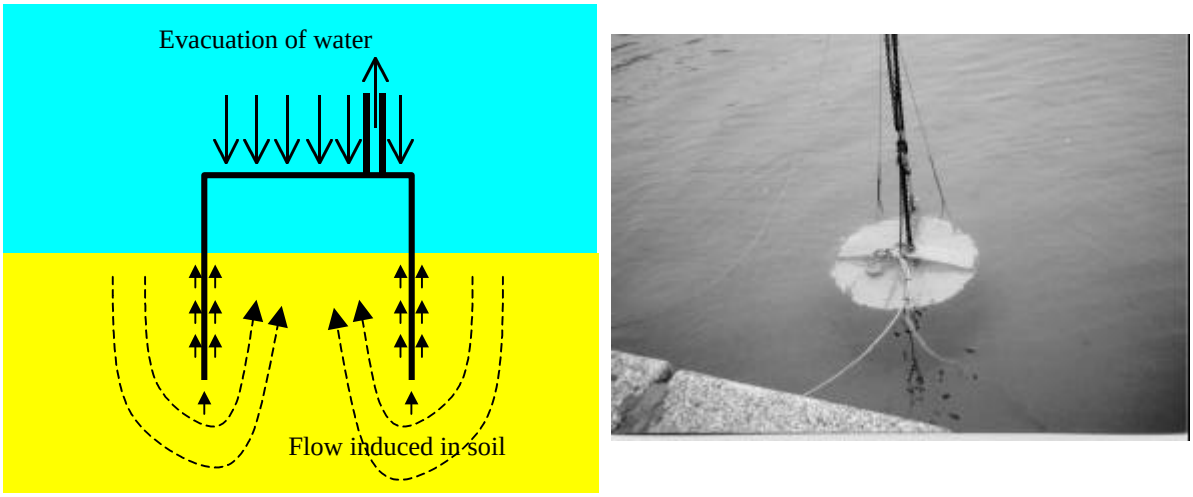

Figure 1.8 - Novel suction caisson foundation.

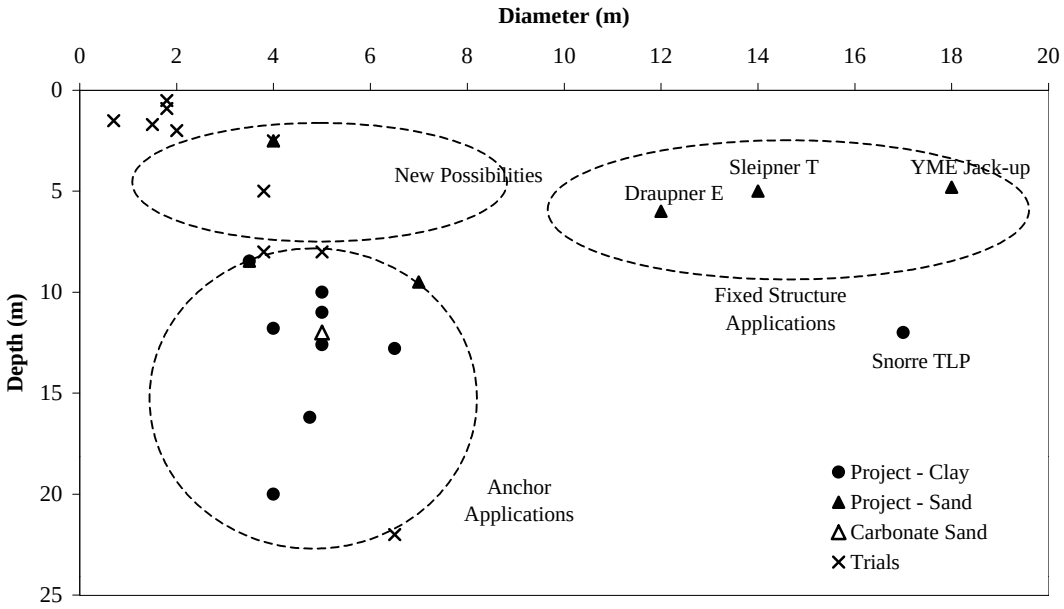

Figure 1.9 - Summary plot of various uses of caisson foundations.

Installation / Removal	
Gravity Penetration	Calculation
Suction	Calculation
Removal	Calculation

	Performance		
	Drained	Undrained	Cyclic
Compression	Calculation	Estimate (large)	Few data
Tension	Calculation	Estimate (large)	Few data
V, H, M	Model tests	Model tests	Very few data

Figure 1.10 - Summary of design problems for suction caissons and shallow foundations in general.

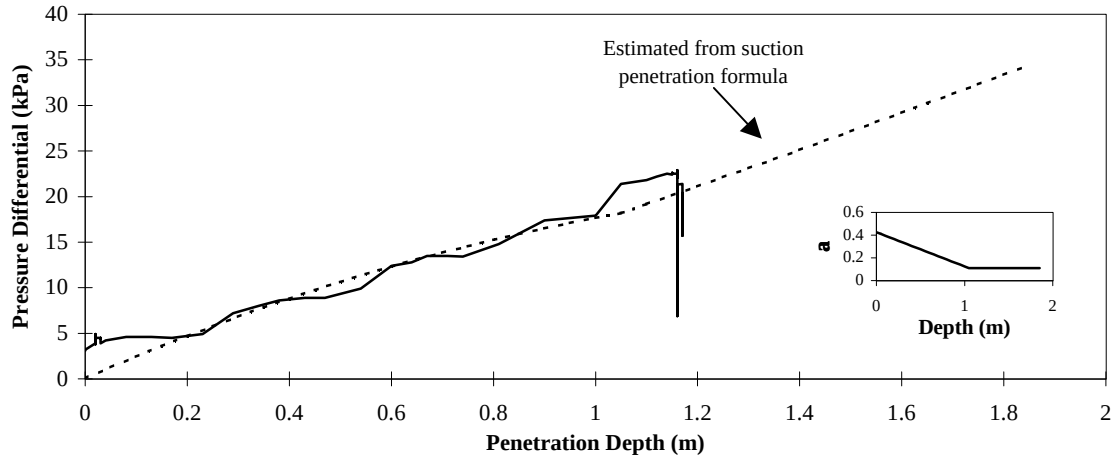

Figure 1.11 - Pressure differential with penetration depth for field scale suction caisson installation test.

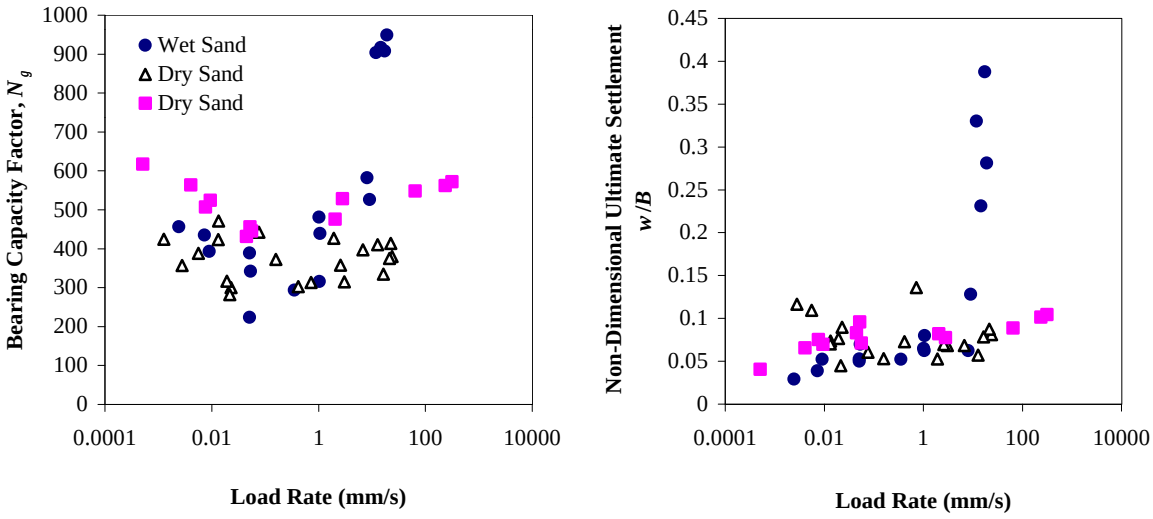

Figure 1.12 - Series of tests from Vesic *et. al.* (1965) illustrating results of footing tests on dry and submerged sand at different loading rates.

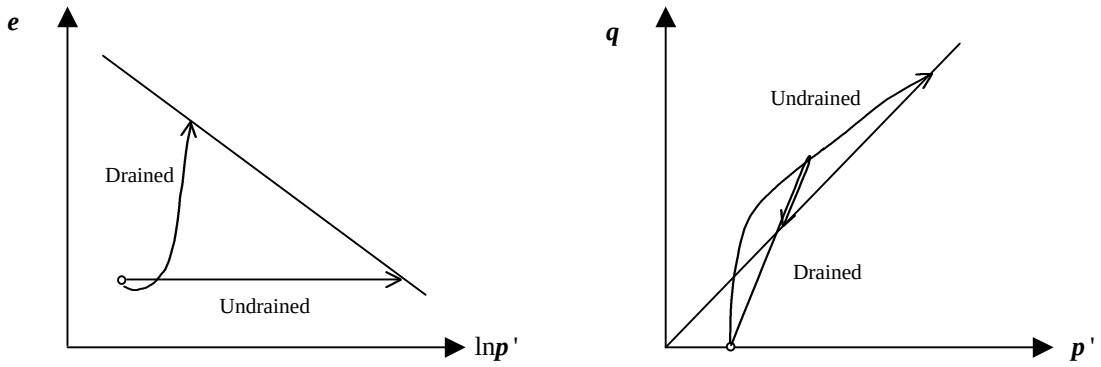

Figure 1.13 - Stress paths appropriate to drained and undrained behaviour.

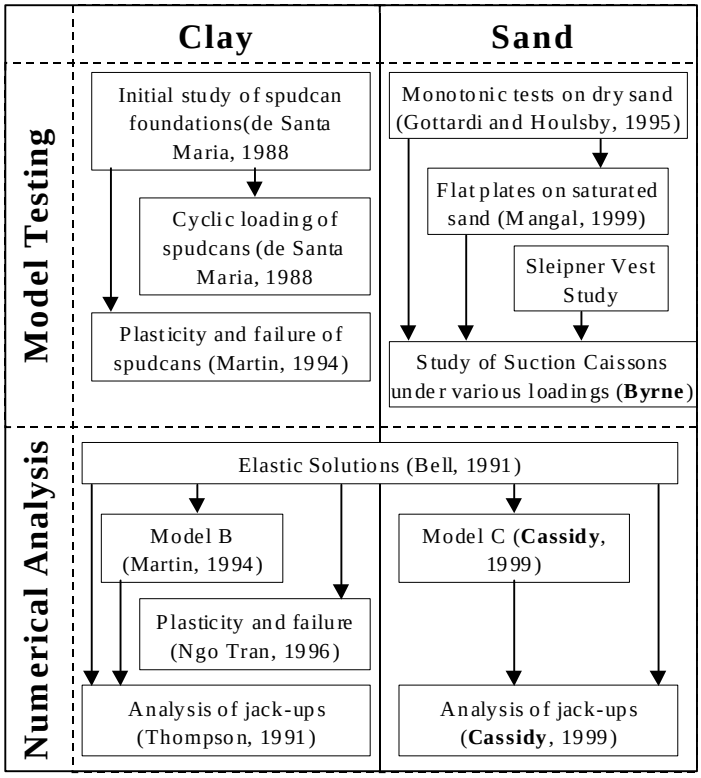

Figure 1.14 - History of research effort at Oxford University on shallow foundations.

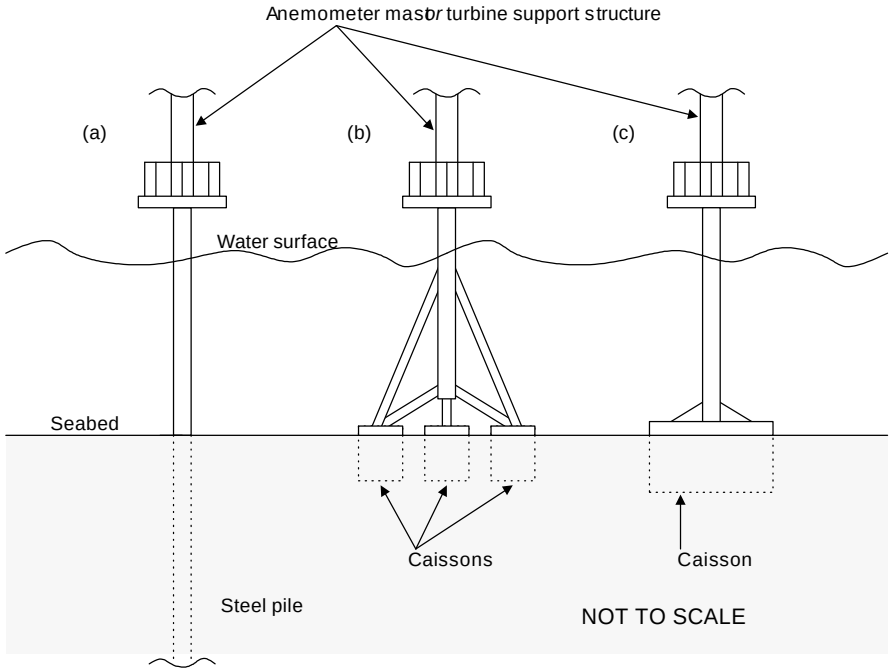

Figure 1.15 - Potential foundation and structural options for offshore wind energy facilities, (a) typical pile installation, (b) tripod structure on caissons, and (c) monopod caisson structure.

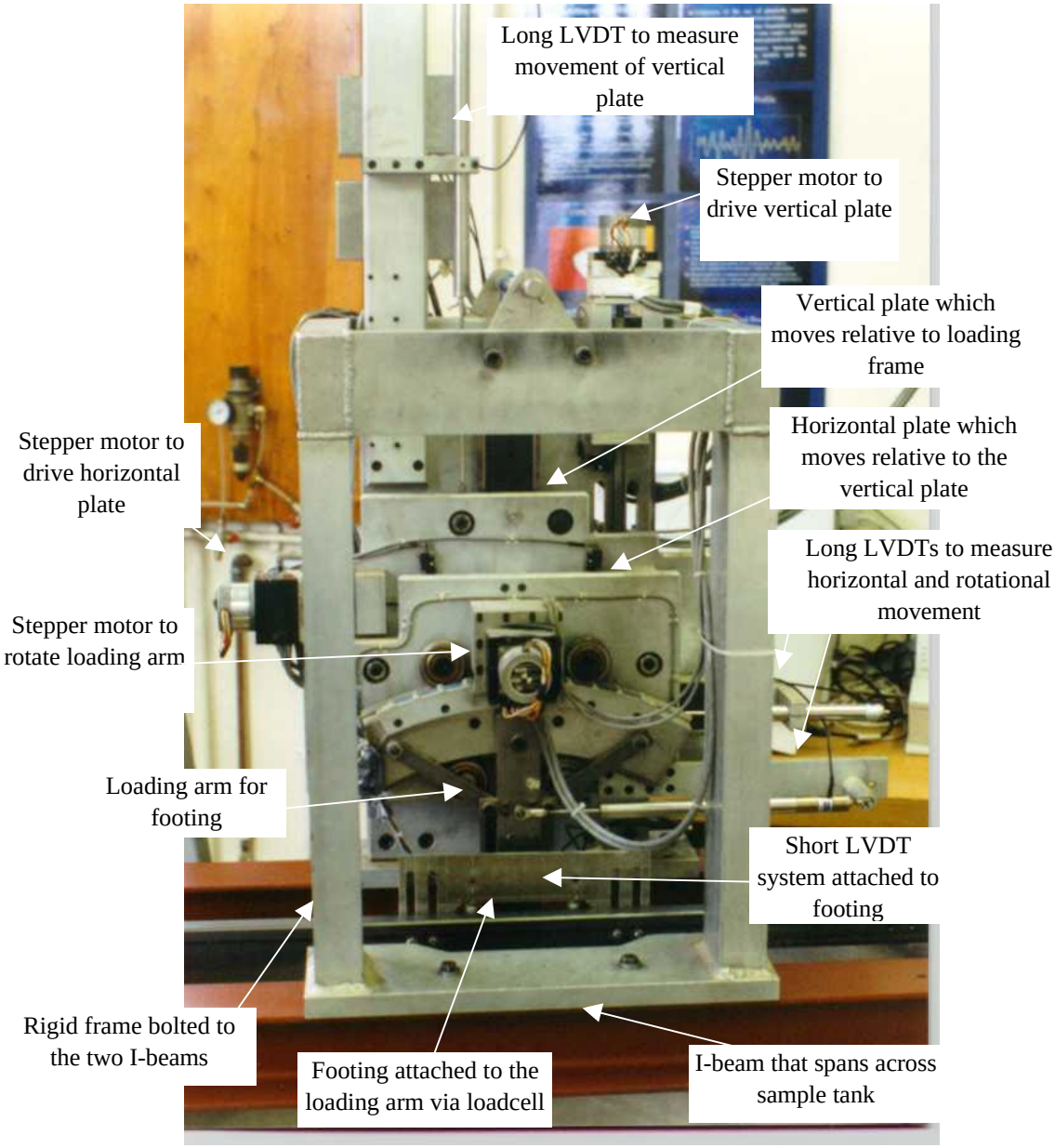

Figure 2.1 - The three degree of freedom loading rig at the University of Oxford

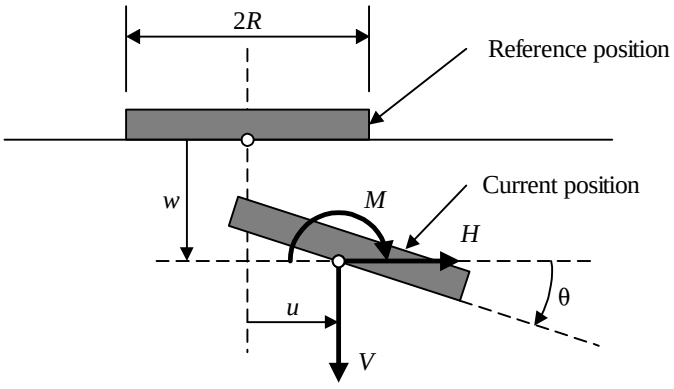

Figure 2.2 - Sign convention and notation used throughout study as set out by Butterfield *et. al.* , 1997.

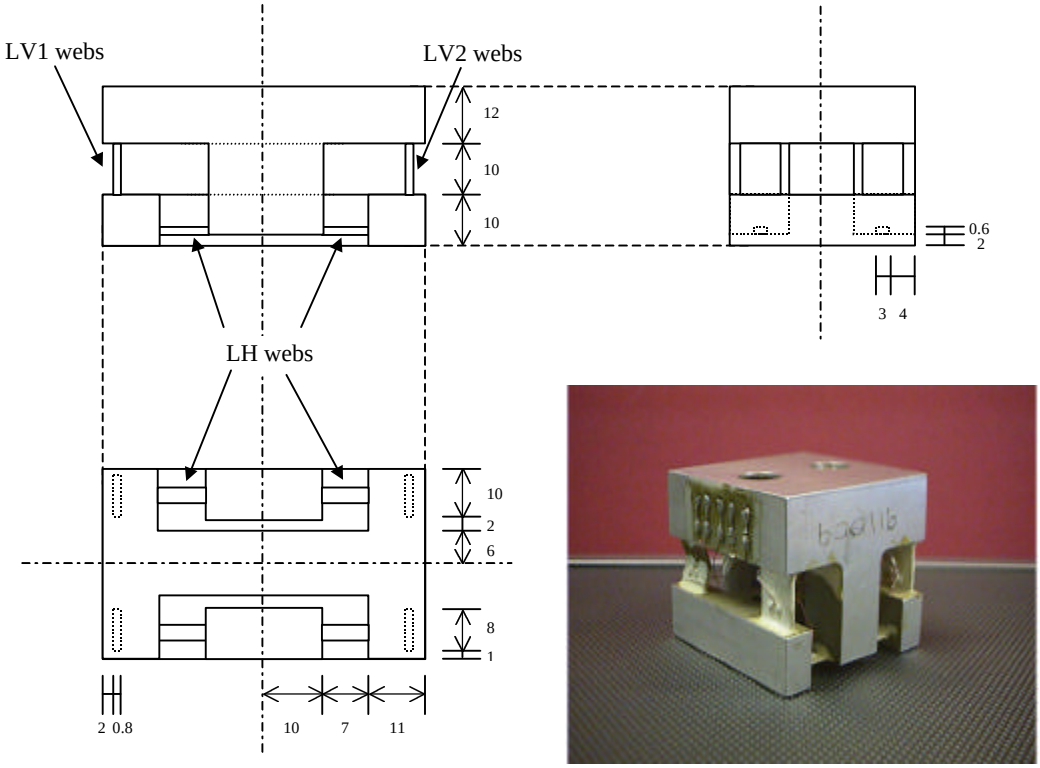

Figure 2.3 - Design of 'VMH' load cell used in the testing (from Mangal, 1999 with attachment holes omitted for clarity), and photo of a previously used load cell.

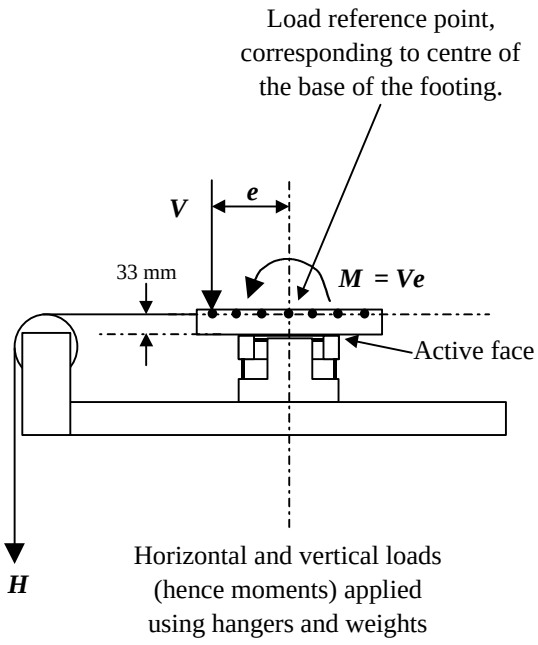

Figure 2.4 - Calibration set-up for 'VMH' load cell (from Mangal, 1999).

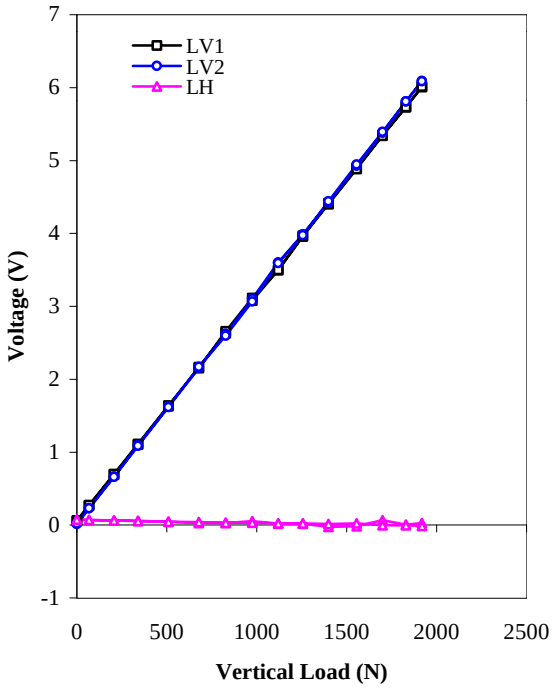

Figure 2.5 - Typical results from a calibration test for vertical load.

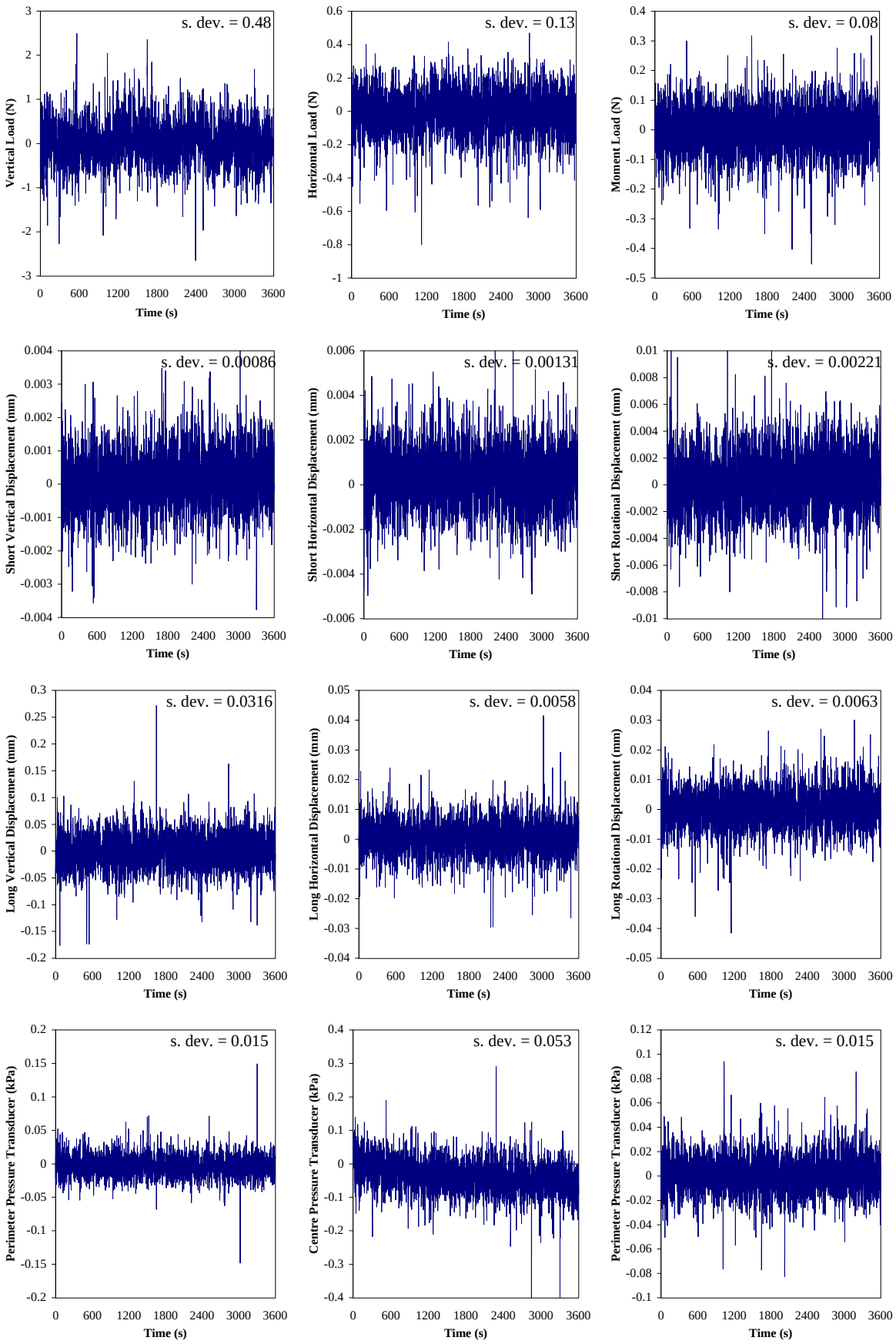

Figure 2.6 - Samples of all transducers over a period of one hour at 1 Hz.

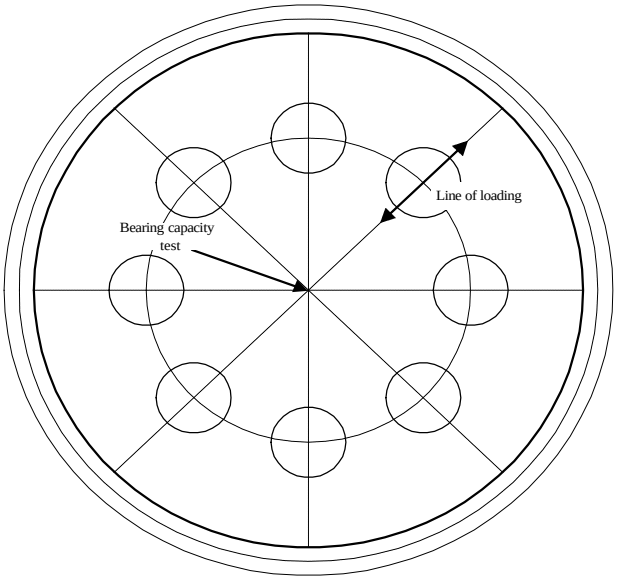

Figure 2.7 - Layout of testing sites within a single test-tank. The loading direction is radial.

Figure 2.8 - The general layout of the testing apparatus.

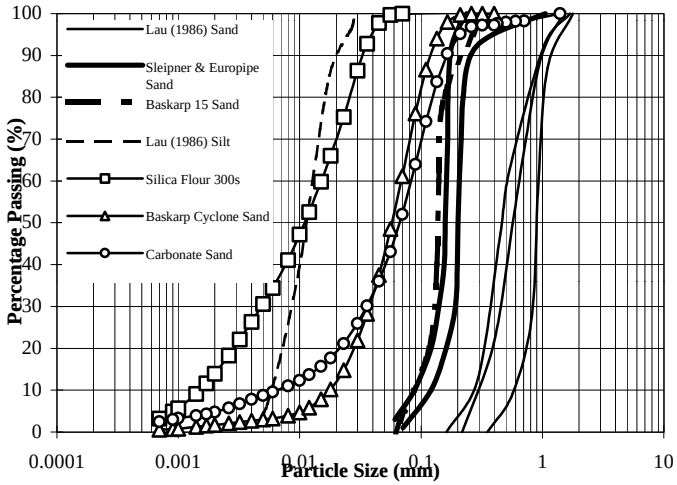

Figure 2.9 - The grading curves of sands used for 1-g tests of footing behaviour.

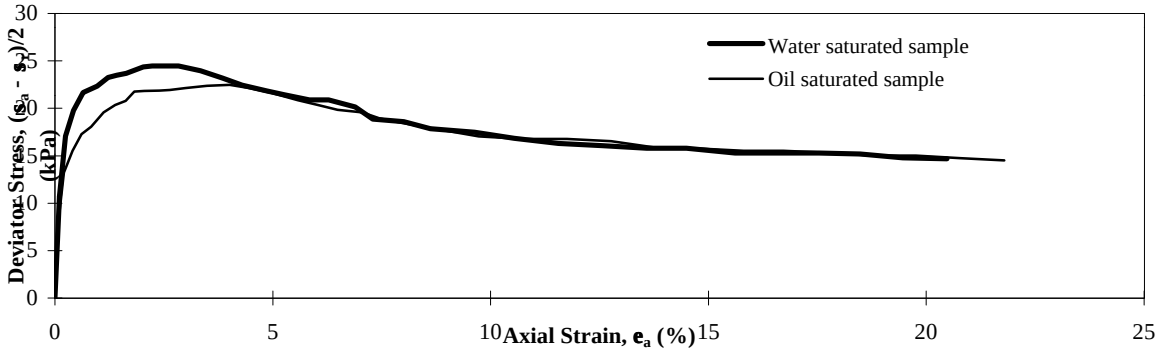

Figure 2.10 - Stress strain behaviour of samples in CID triaxial compression under an initial vertical stress of 10kPa

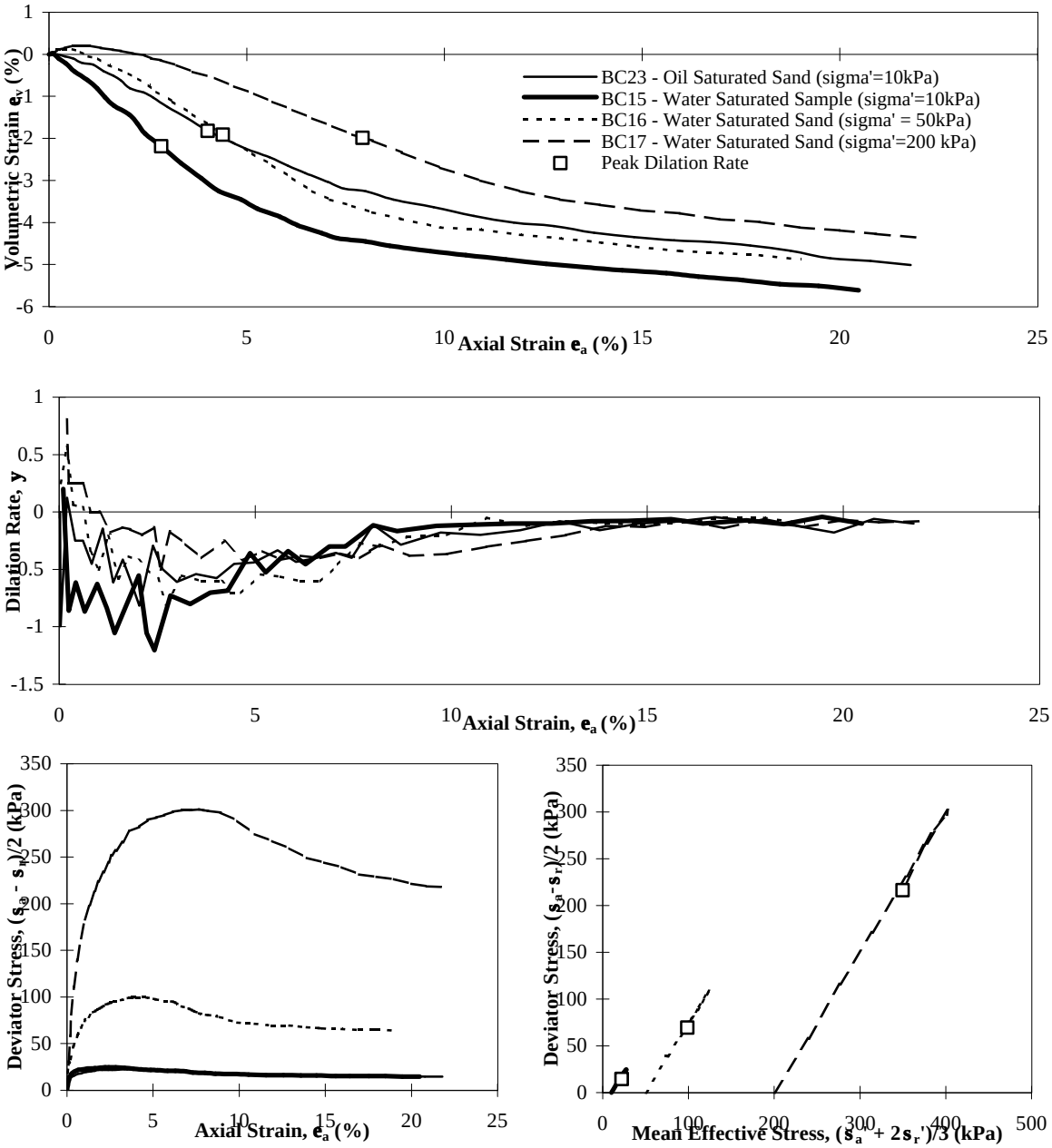

Figure 2.11 - Comparison of CID triaxial compression tests for Baskarp Cyclone sand prepared at a relative density of 80 % (utilising oil and water as the pore fluid).

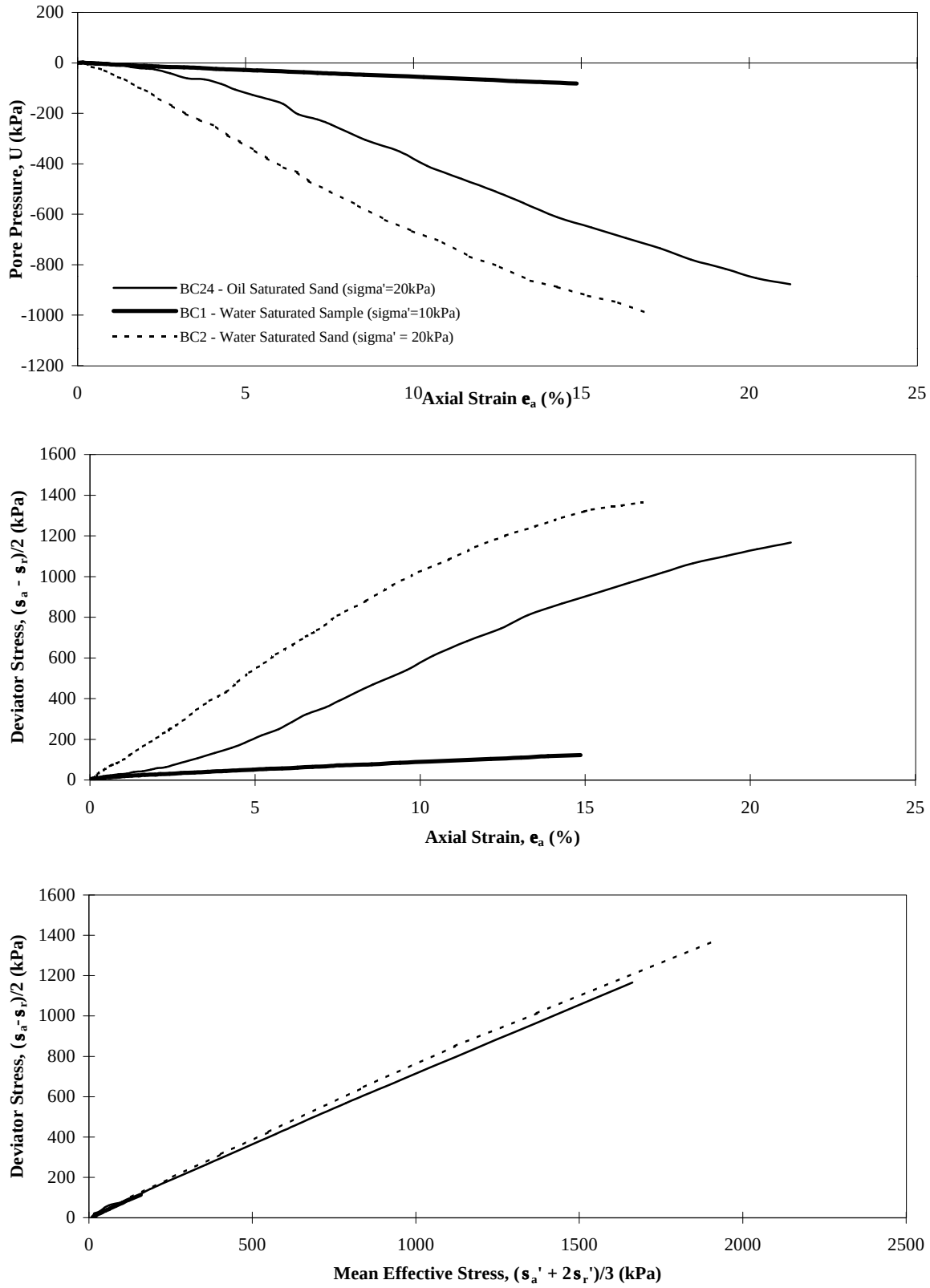

Figure 2.12 - Comparison of CIU triaxial compression tests for Baskarp Cyclone sand prepared at a relative density of 80 % (utilising oil and water as the pore fluid).

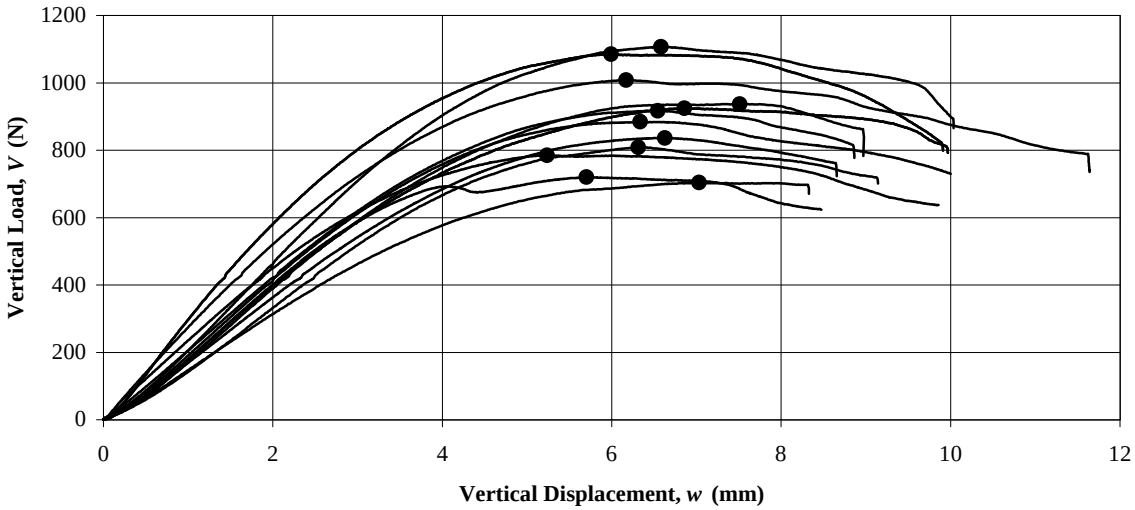

Figure 2.13 - All bearing capacity tests performed during the dry dense sand series of testing.

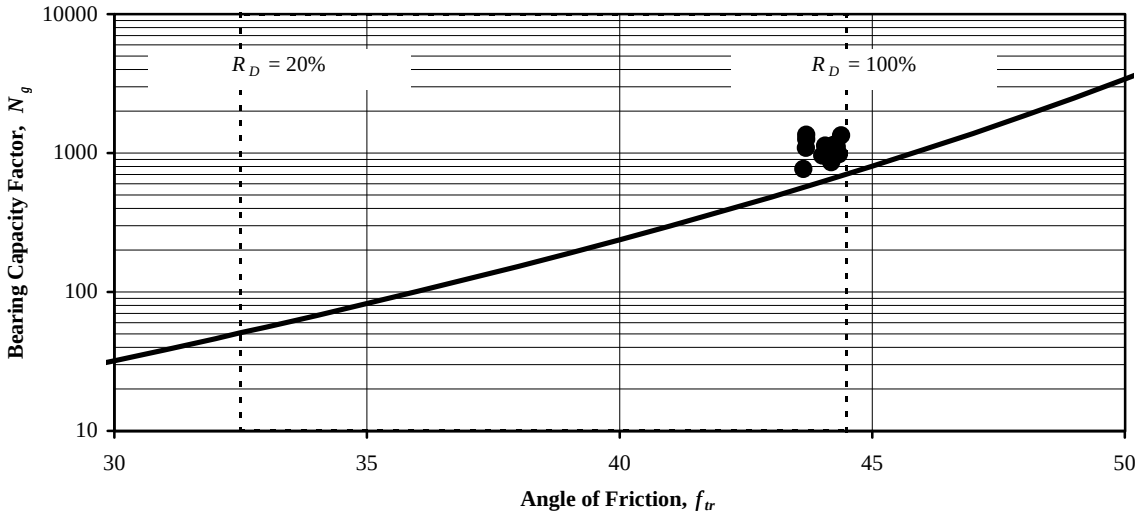

Figure 2.14 - Accumulation of all bearing capacity test results compared to Bolton and Lau (1993).

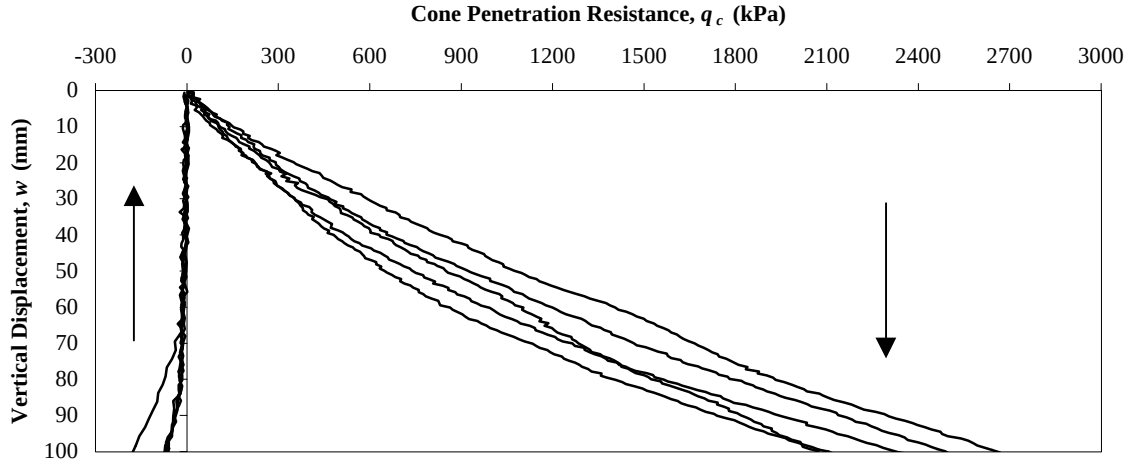

Figure 2.15 - Cone penetration tests performed on dry sand sample DM7.

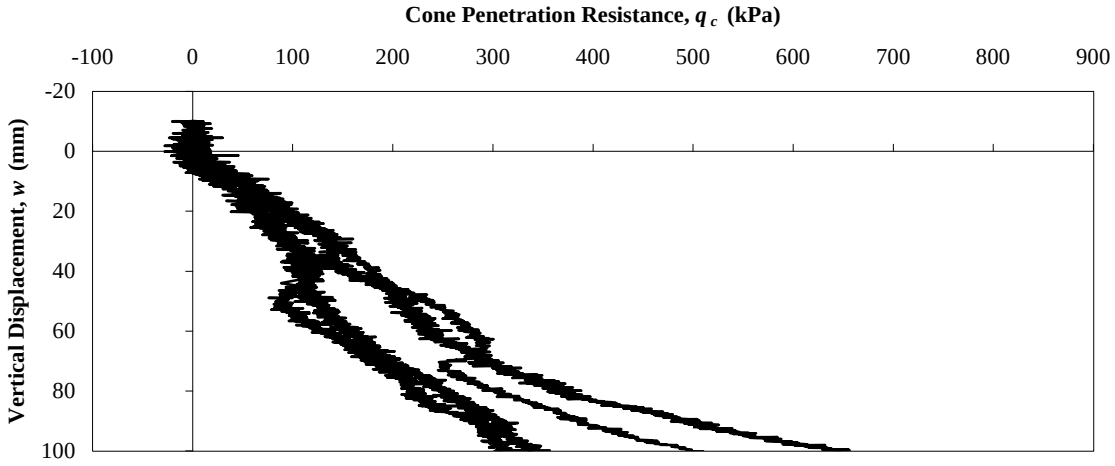

Figure 2.16 - Cone penetration tests performed on the saturated sand sample SM1.

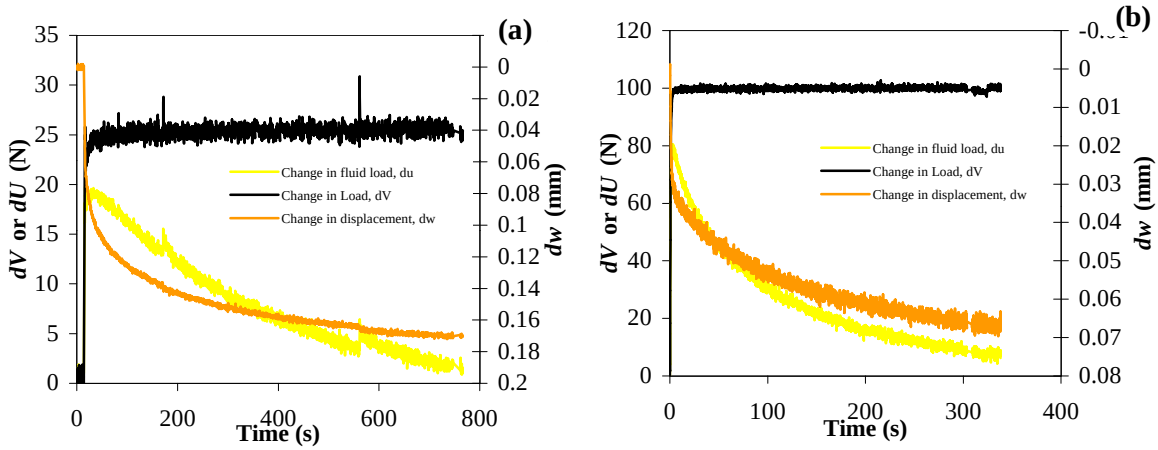

Figure 2.17 - Typical consolidation tests showing vertical load, displacement response and pore fluid response (note that $U = u\ \mathbf{p}D^2/4$) at (a) the beginning of footing test, and (b) towards the end of a footing test.

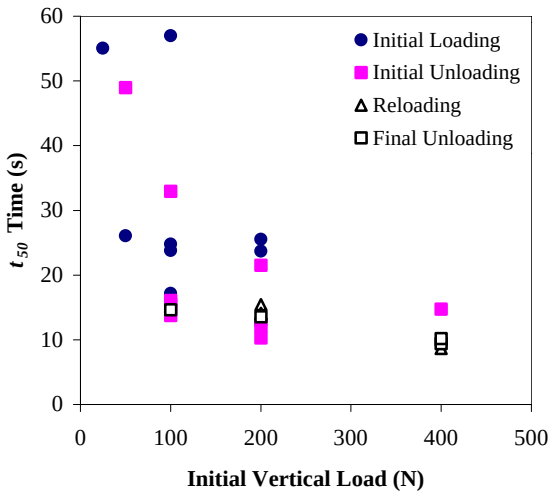

Figure 2.18 - Variation of t_{50} times with initial vertical load.

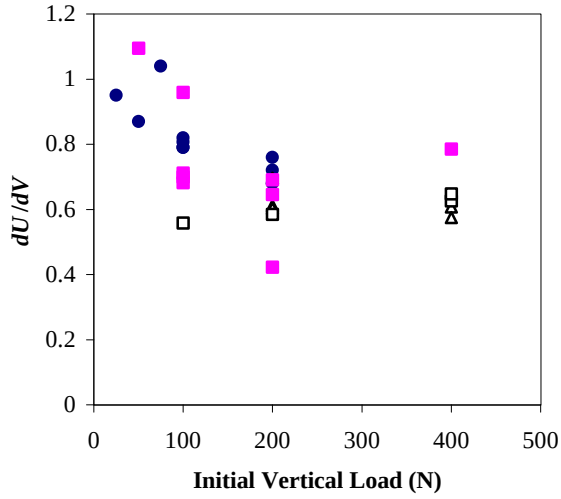

Figure 2.19 - Pore fluid load versus initial vertical load for consolidation tests.

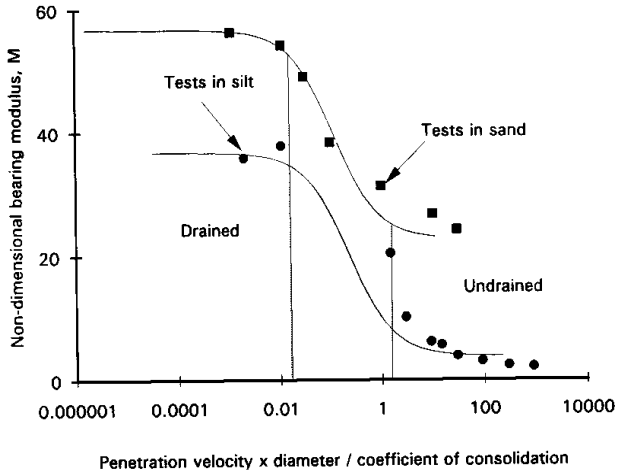

Fig. 6. Effect of loading rate on non-dimensional bearing modulus

Figure 2.20 - Bearing capacity versus penetration rate for foundations on carbonate sand (Finnie, 1993).

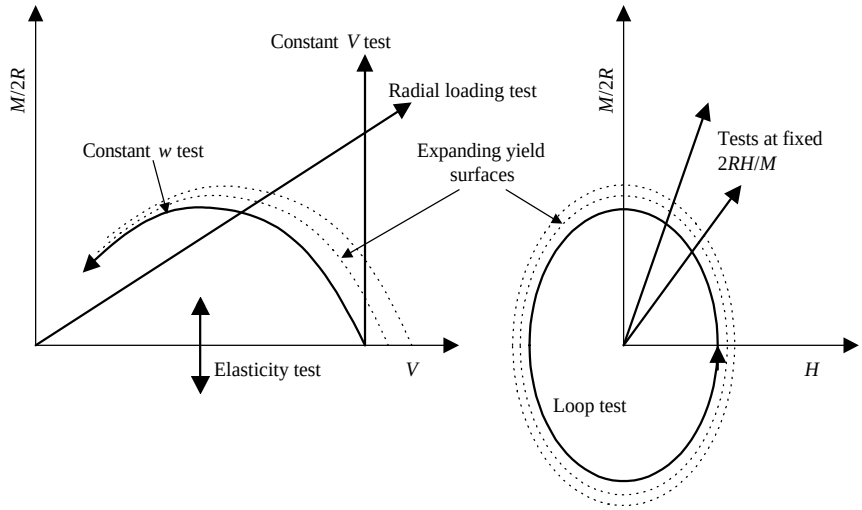

Figure 2.21 - Typical tests that are used to explore plasticity related concepts for foundations.

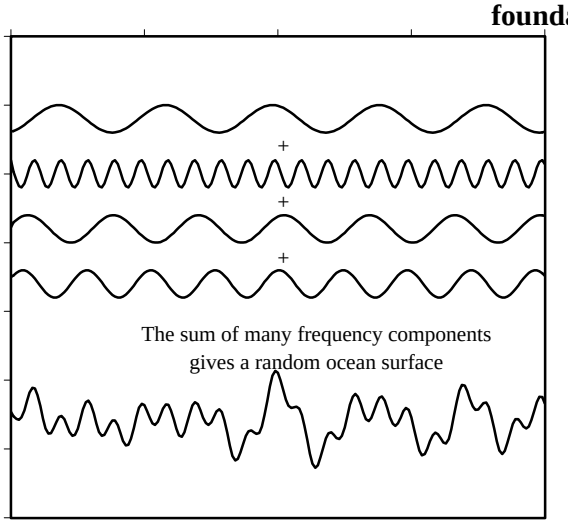

Figure 2.22 - The ocean surface surface viewed as the sum of many different frequency components.

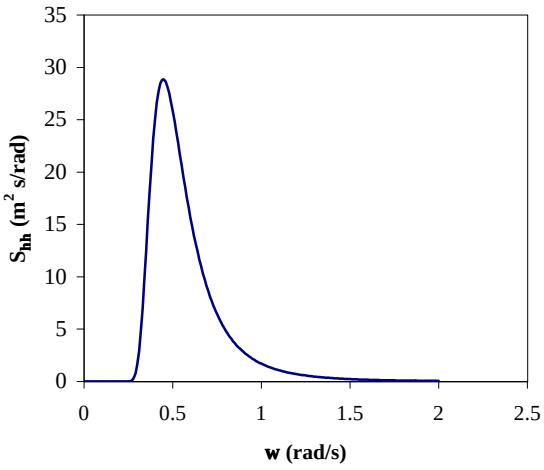

Figure 2.23 - A typical sea elevation spectrum.

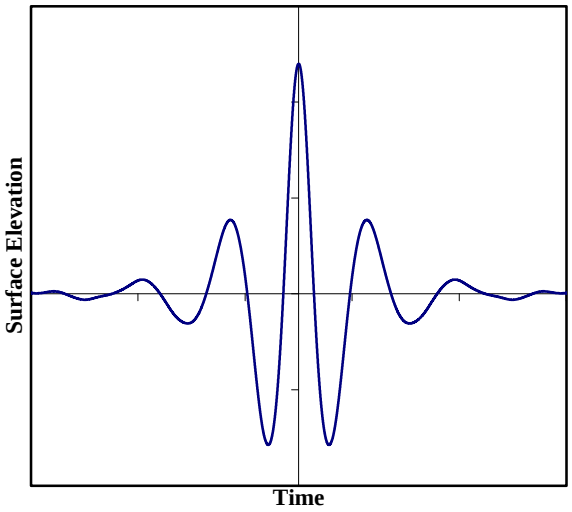

Figure 2.24 - The 'NewWave' shape

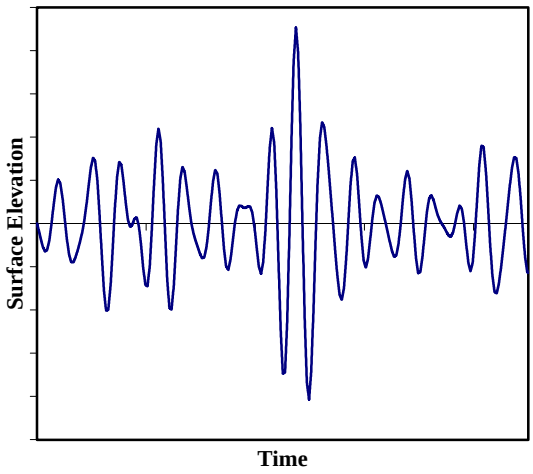

Figure 2.25 - The 'NewWave' constrained within a pseudo-random background

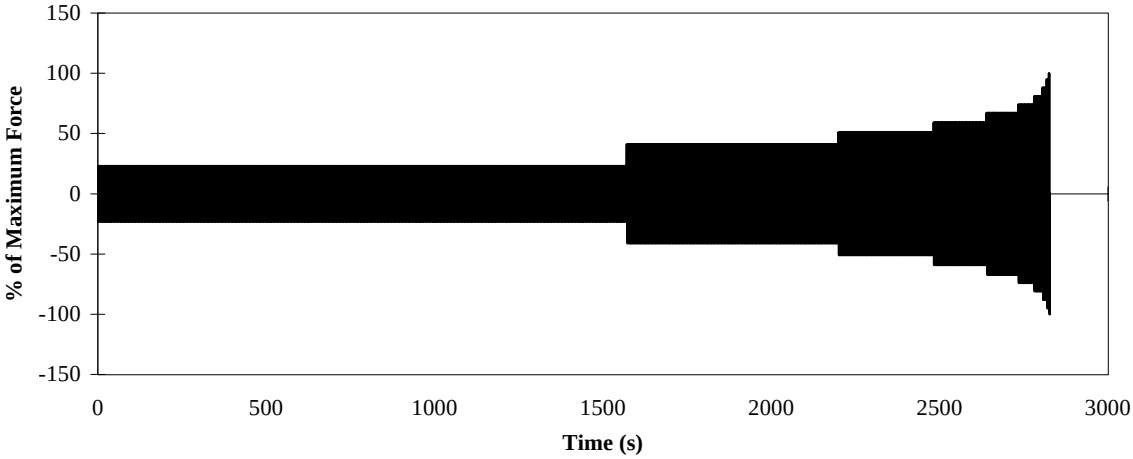

Figure 2.26 - Typical 3 hour storm sequence for use in geotechnical modelling (after Hansteen, 1981).

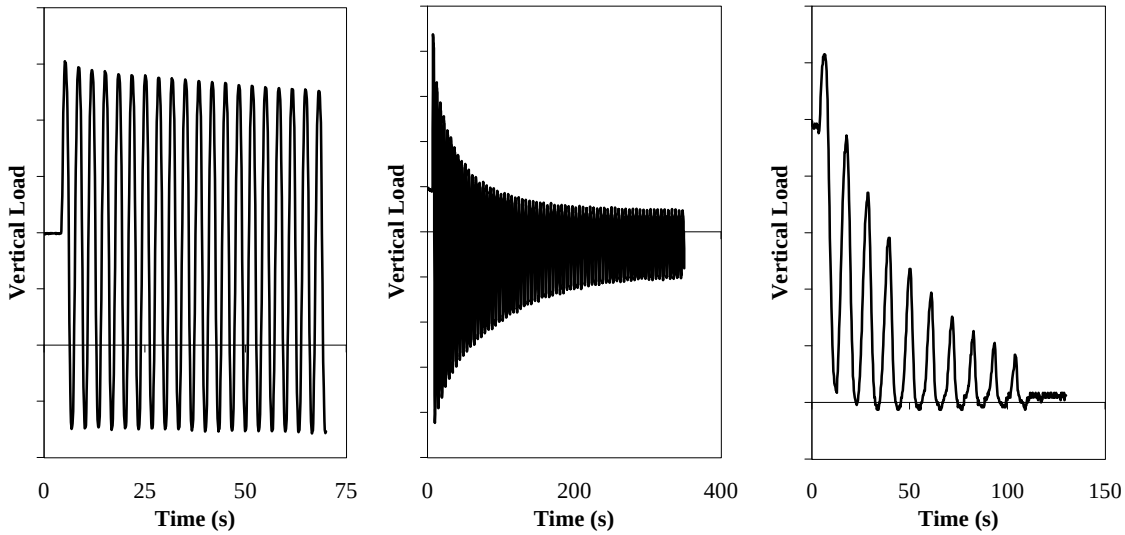

Figure 2.27 - Qualitative results from cyclic testing on suction caissons showing different behaviour.

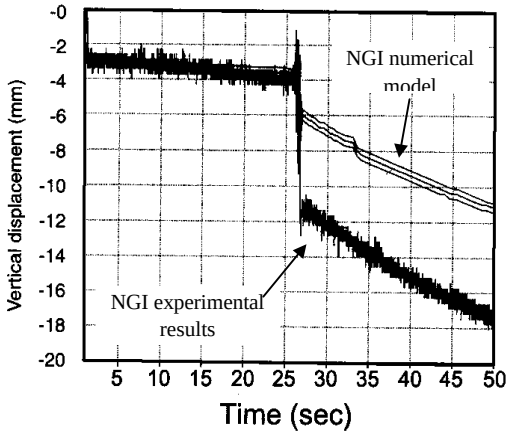

Figure 12: Calculated and measured vertical displacements of the model

Figure 2.28 - Displacement response to extreme events in NGI tests (Jostad *et. al.* , 1997).

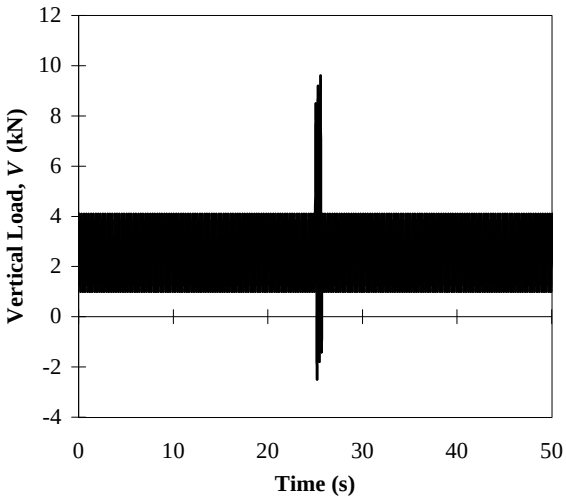

Figure 2.29 - Applied extreme events in NGI testing (Jostad *et. al.* , 1997).

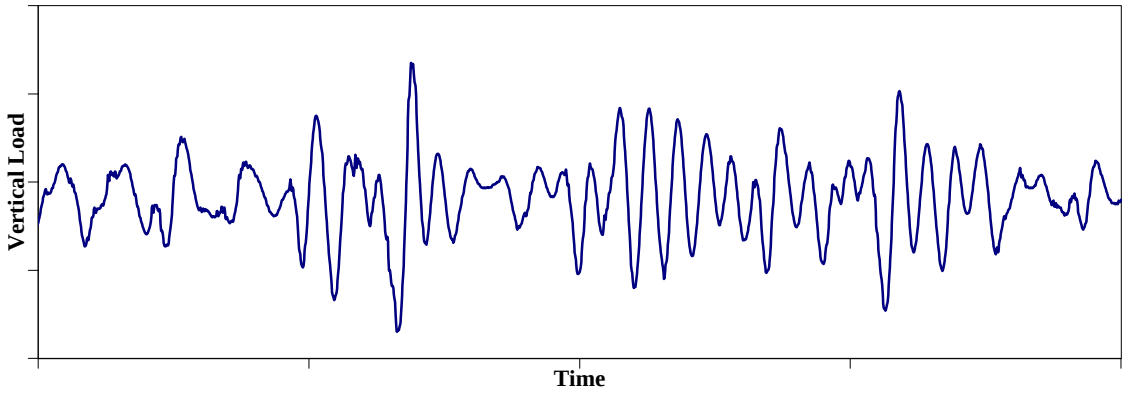

Figure 2.30 - A typical result from a time domain analysis of a jack-up structure using the JAKUP program (Cassidy, 1999).

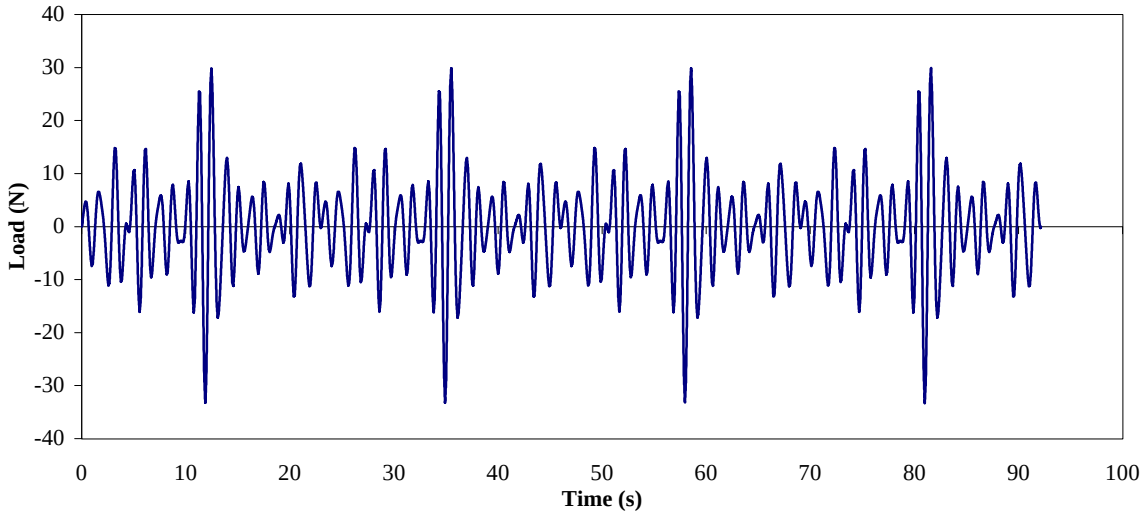

Figure 2.31 - The standard 'NewWave' profile used for the majority of tests.

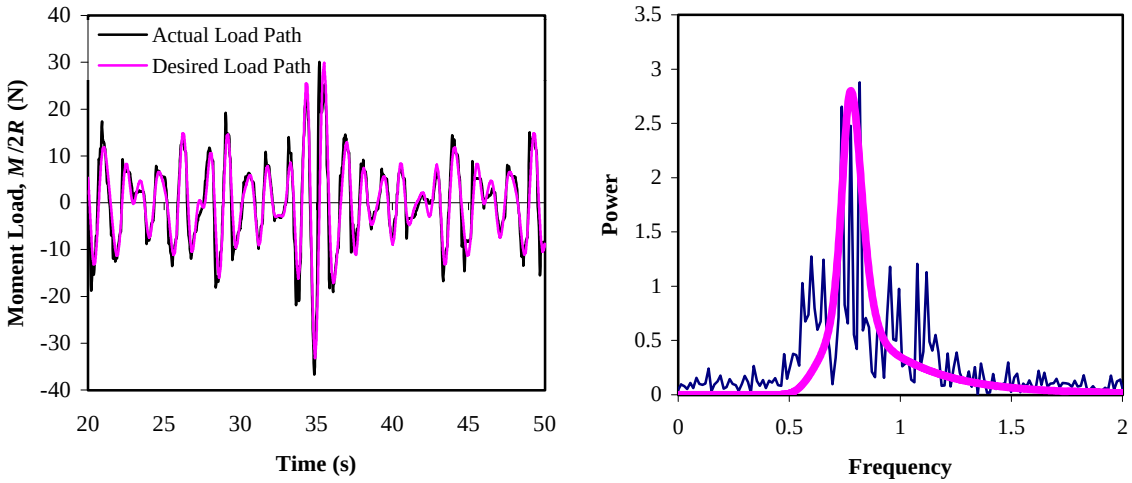

Figure 2.32 - A comparison of desired load path and applied load path (a) visually, and, (b) by a spectral analysis

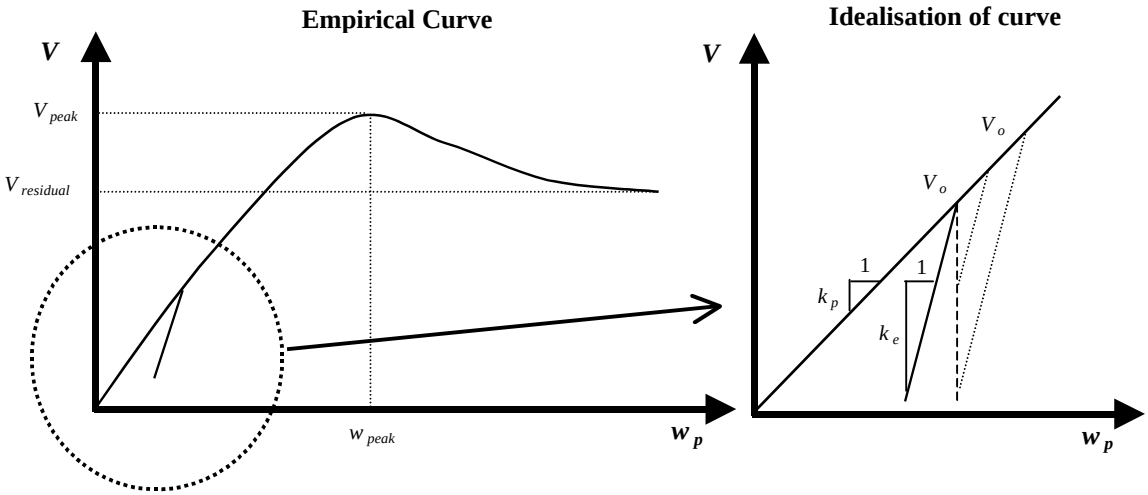

Figure 3.1 - Idealised hardening law for very dense sand (at low values of V/V_{peak}).

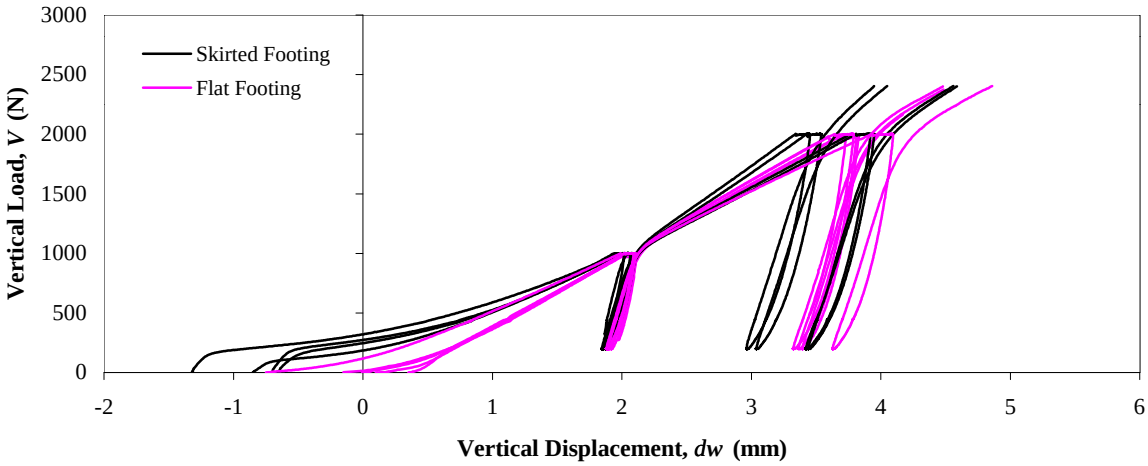

Figure 3.2 - Accumulation of vertical loading tests for flat and skirted footings, of diameter 100mm, undertaken during the testing sequence.

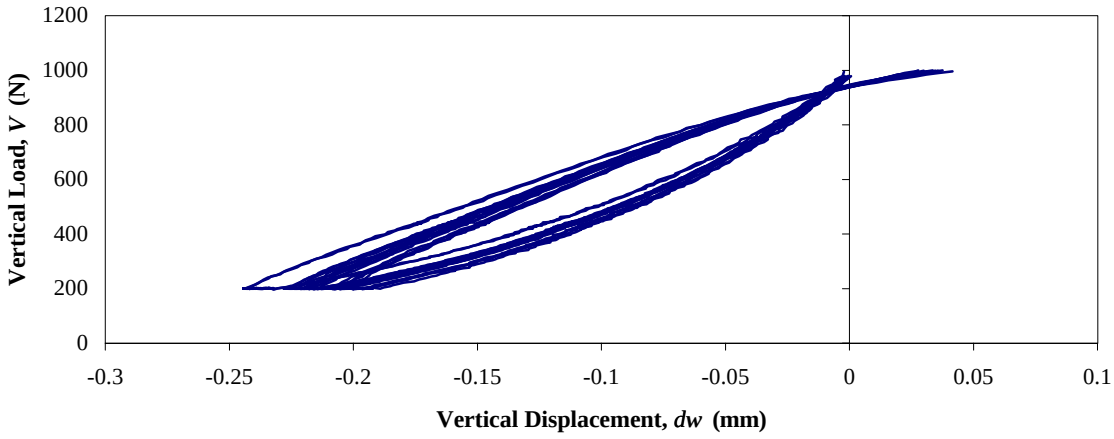

Figure 3.3 - Accumulation of vertical unload-reload loops from flat and skirted footings (diameter 100mm) tests throughout the testing sequence.

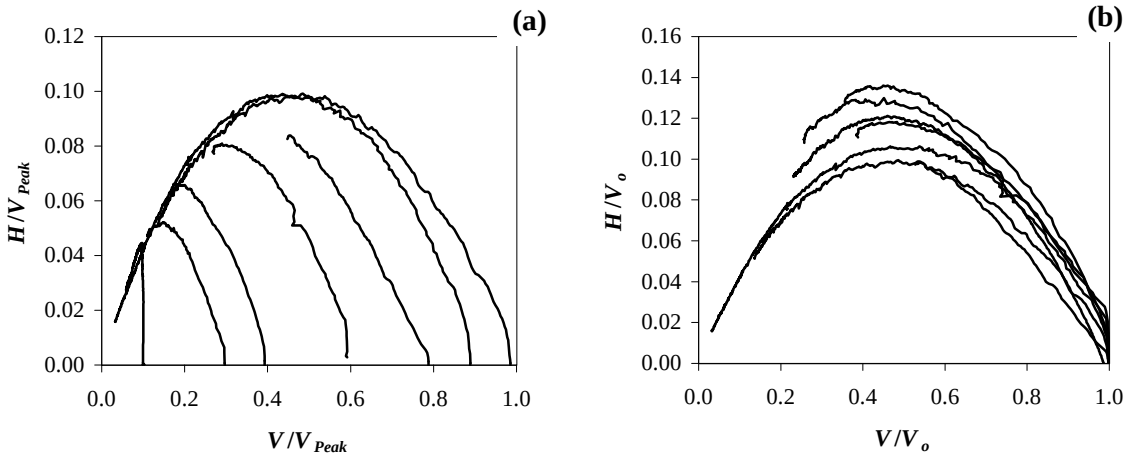

Figure 3.4 - The data from Gottardi and Houlsby (1995) showing the dependence of response on V_{peak}; (a) plotted as a ratio with V_{peak} and (b) plotted as a ratio of V_o.

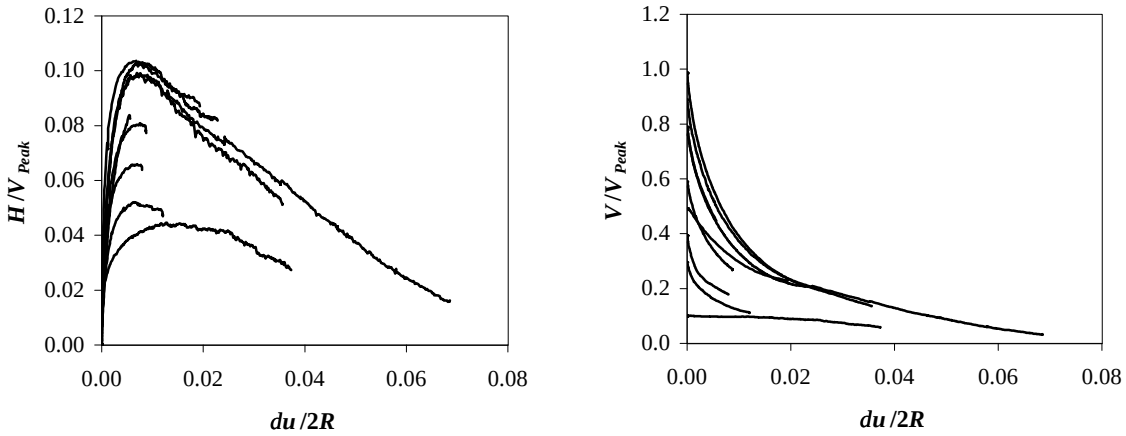

Figure 3.5 - Non-dimensionalised horizontal load-deformation curves suggesting that the parallel point is probably at zero horizontal load.

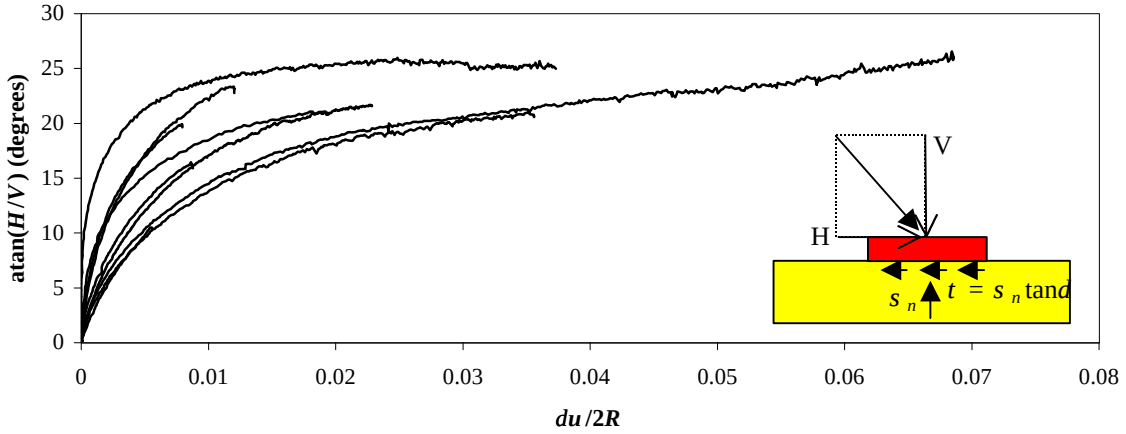

Figure 3.6 - An estimation of the interface friction angle measured during horizontal swipes (tending to approximately 25 degrees at large displacements).

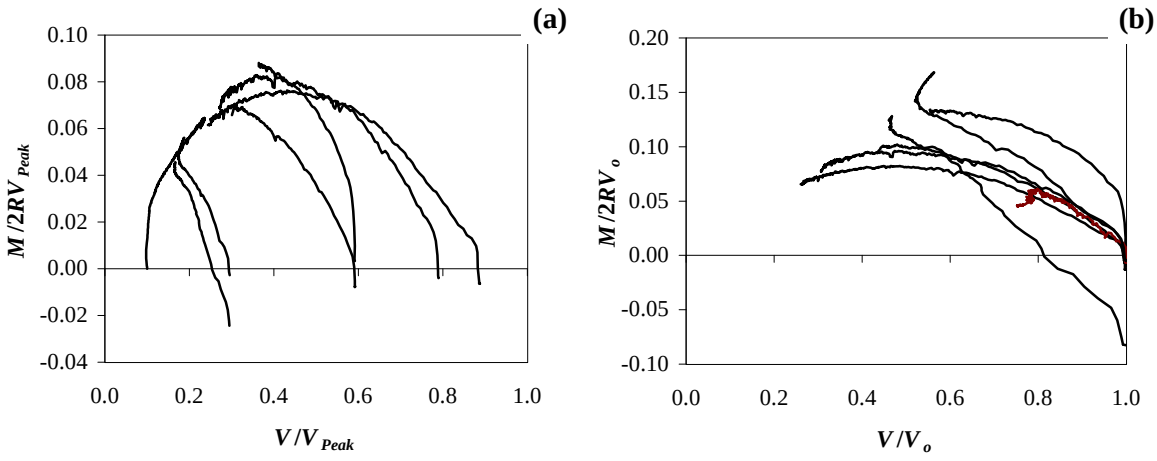

Figure 3.7 - The data from Gottardi and Houlsby (1995) showing the dependence of response on V_{peak}; (a) plotted as a ratio with V_{peak} and (b) plotted as a ratio of V_o.

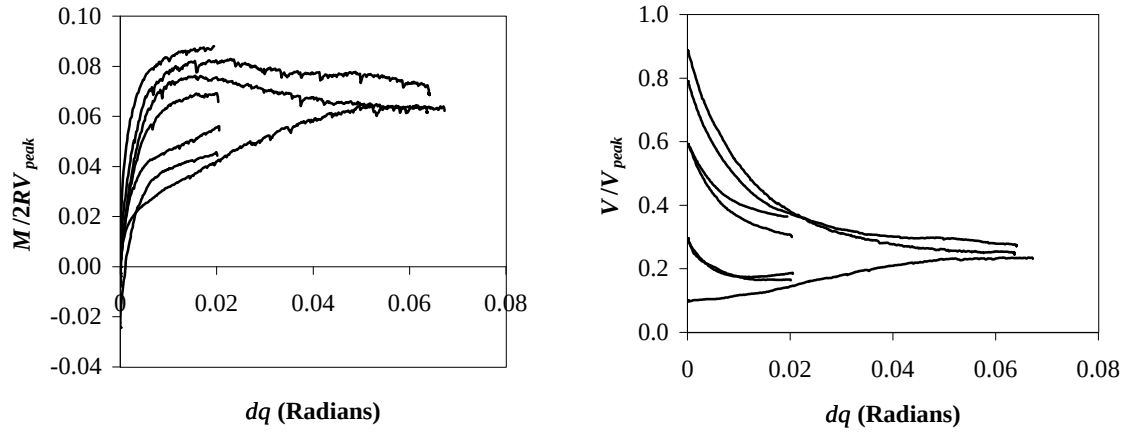

Figure 3.8 - Non-dimensionalised rotational load-deformation curves suggesting that the parallel point is probably at 0.065 non-dimensional load.

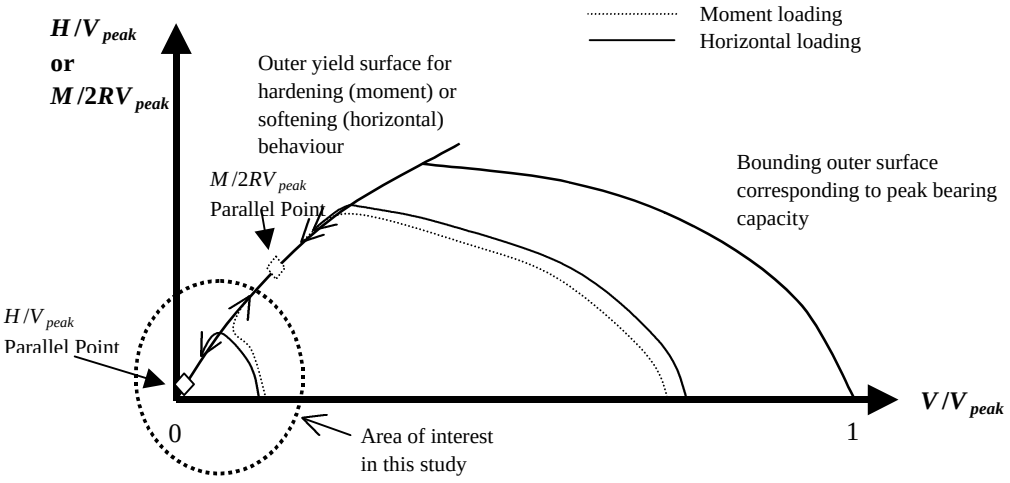

Figure 3.9 - Conceptual yield surface for a footing under horizontal/moment loading.

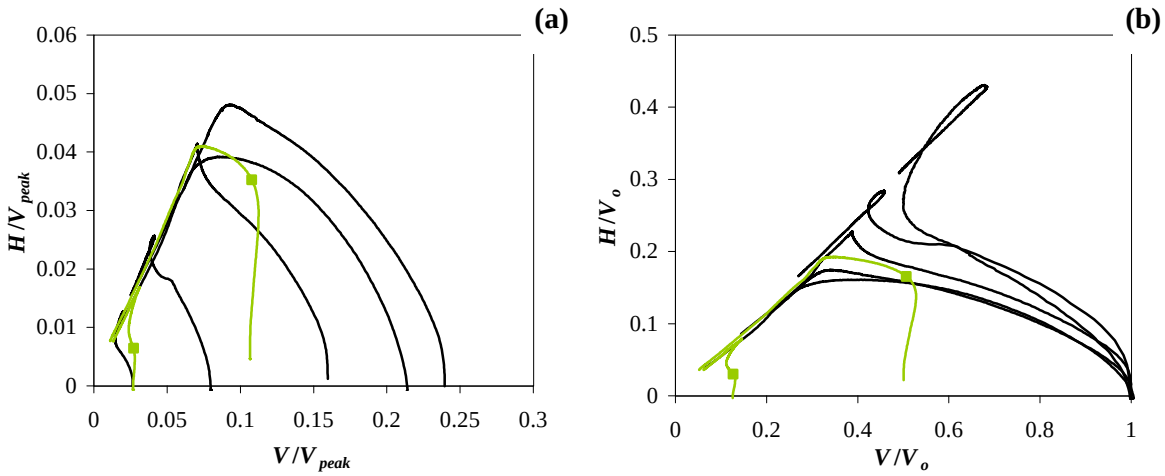

Figure 3.10 - Flat footing behaviour in the $\{V:H\}$ plane; (a) results normalised by V_{peak}, and (b) results normalised by V_o.

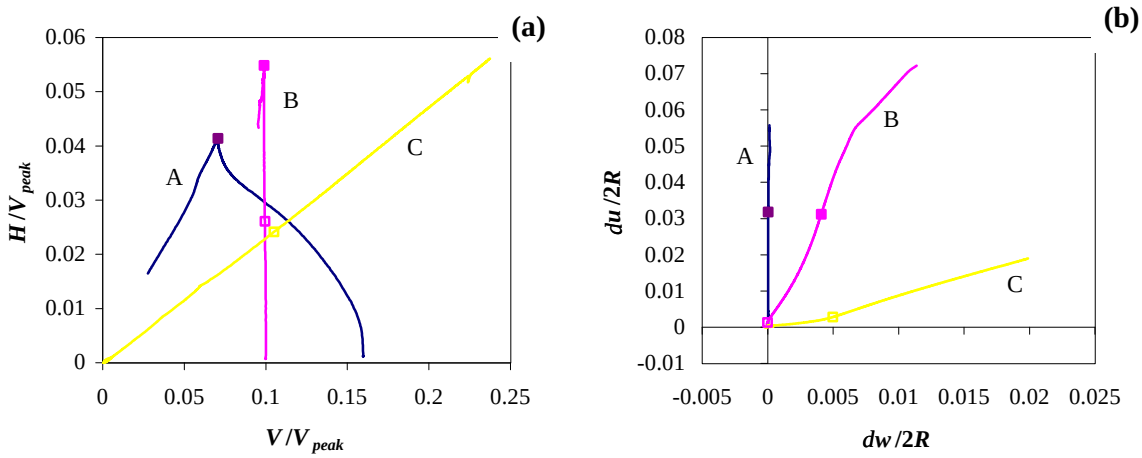

Figure 3.11 - Non-dimensional load deformation curves in (a) load space, and (b) displacement space, indicating the behaviour of three different styles of tests.

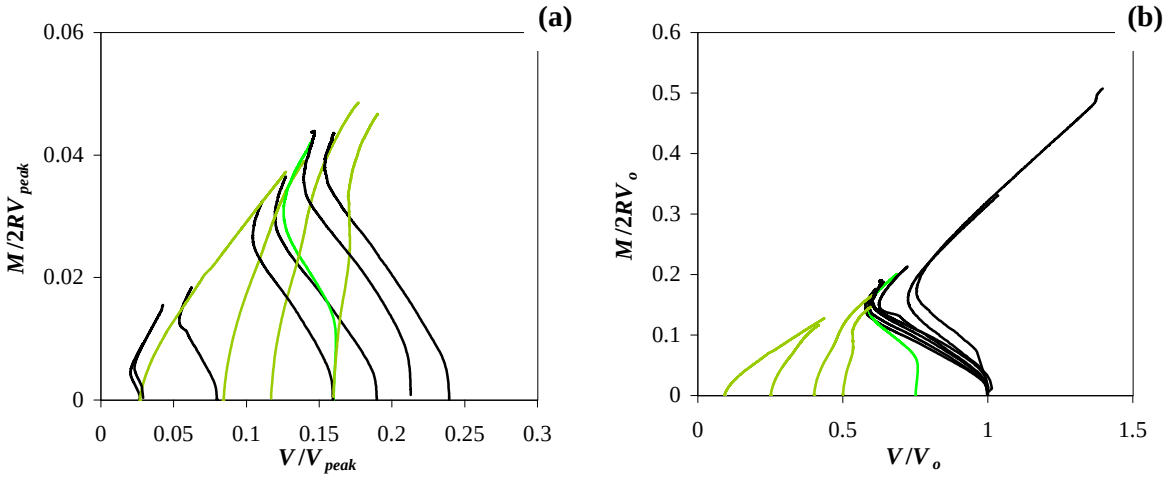

Figure 3.12 - Flat footing behaviour in the $\{V:M/2R\}$ plane; (a) results normalised by V_{peak}, and (b) results normalised by V_o.

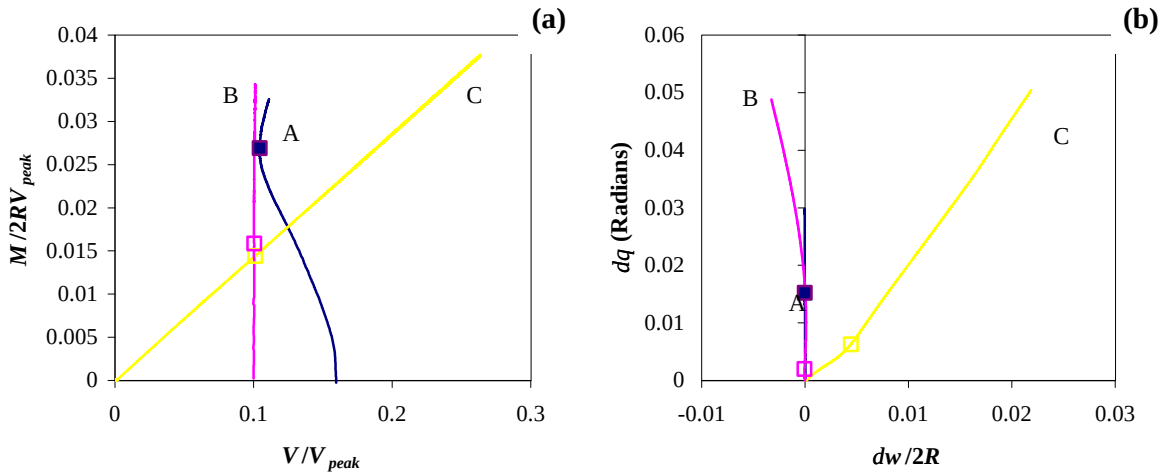

Figure 3.13 - Non-dimensional load deformation curves in (a) load space, and (b) displacement space, indicating the behaviour of three different styles of tests.

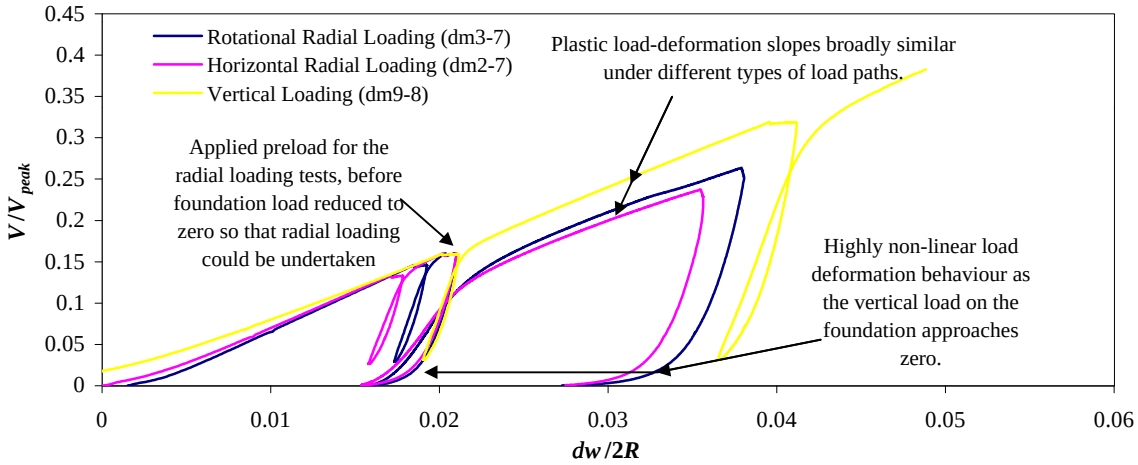

Figure 3.14 - Non-linear behaviour exhibited during unloading to zero vertical load from large vertical loads.

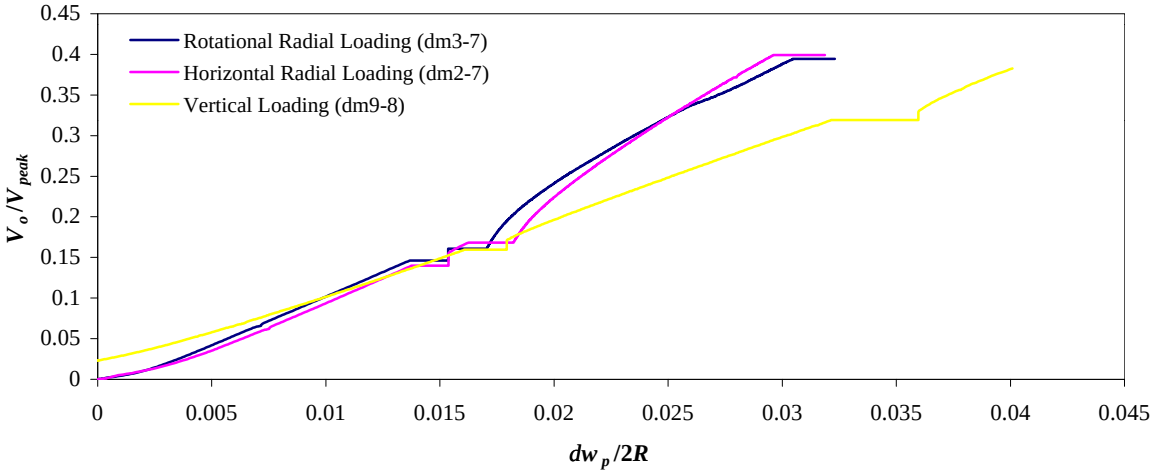

Figure 3.15 - Estimation of the value of V_o for the expanding yield surface tests, compared to the $\{V_o : w_p\}$ behaviour for pure vertical loading.

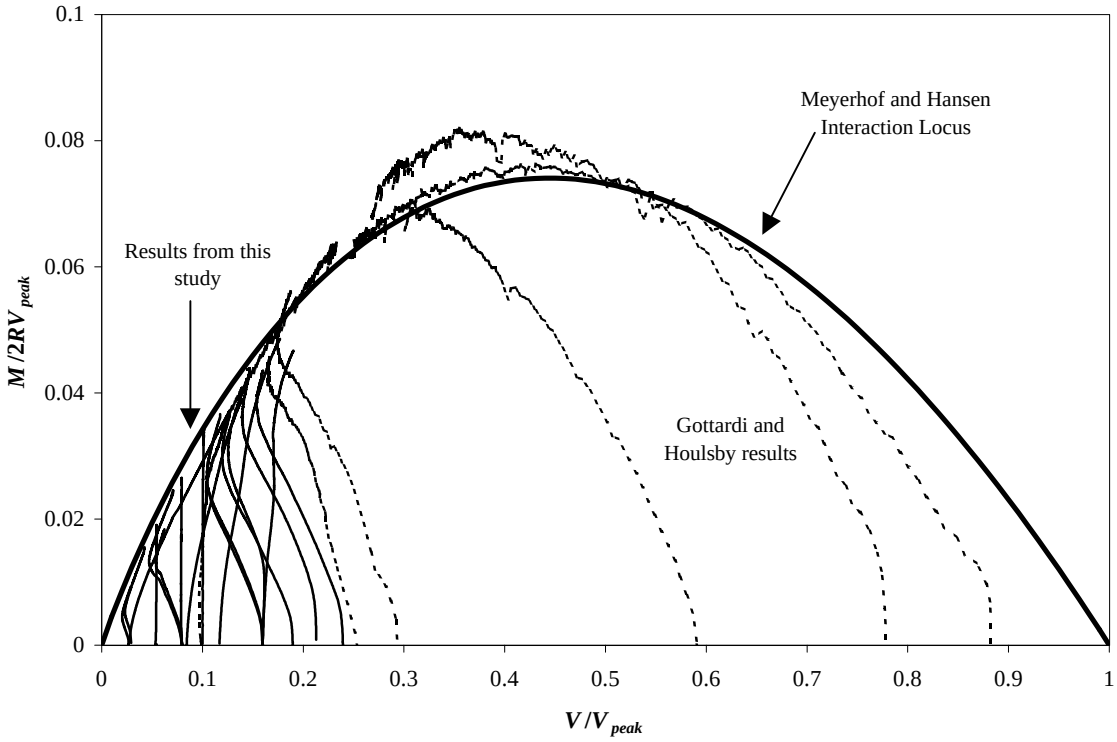

Figure 3.16 - Accumulation of results indicating the applicability of classical theories of bearing capacity for predicting ultimate moment resistance.

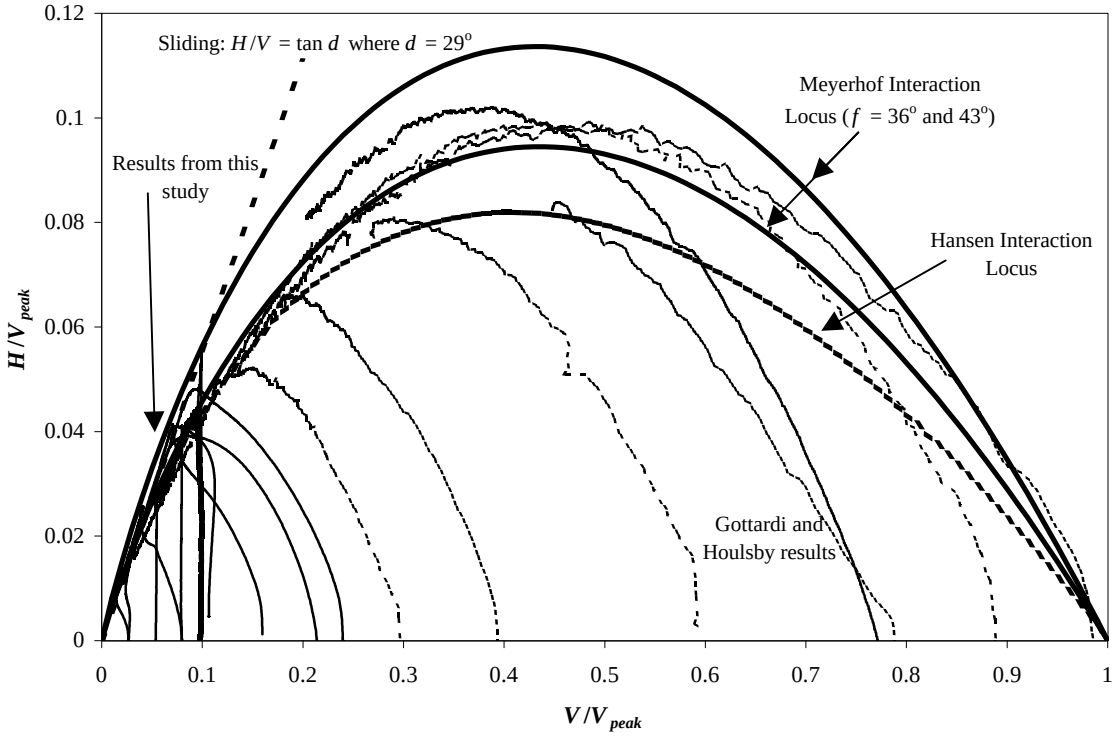

Figure 3.17 - Accumulation of results indicating the applicability of classical theories of bearing capacity for predicting ultimate horizontal resistance.

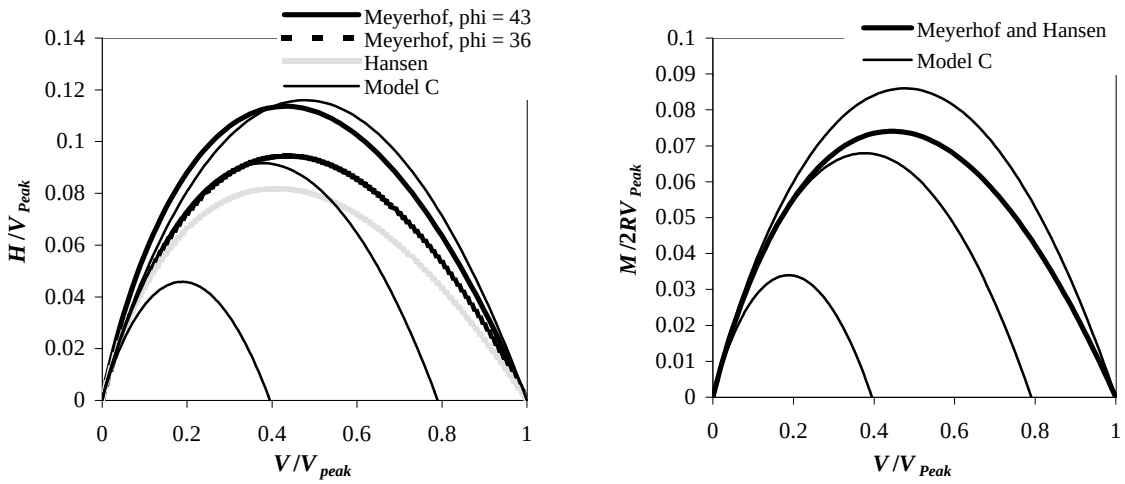

Figure 3.18 - A comparison of the Model C surfaces with classical bearing capacity theory.

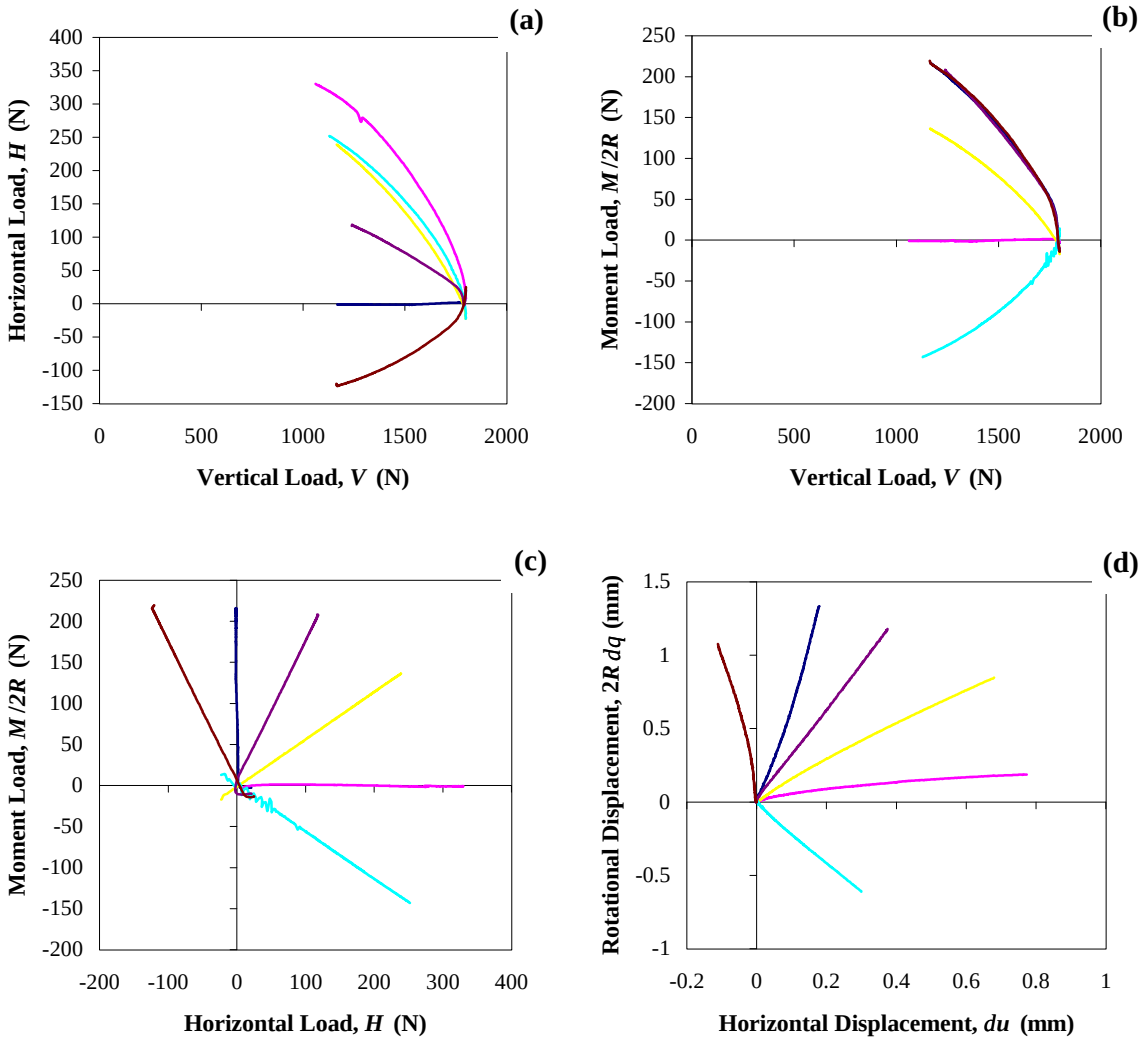

Figure 3.19 - Results from test DM9; small displacement swipe tests from V = 1800N at different ratios of {$2R\,dq$:du} where (a) shows response in {V:H} space, (b) response in {V:$M/2R$} space, (c) response in {$M/2R$:H} space, and, (d) displacement paths in {$2R\,dq$:du} space.

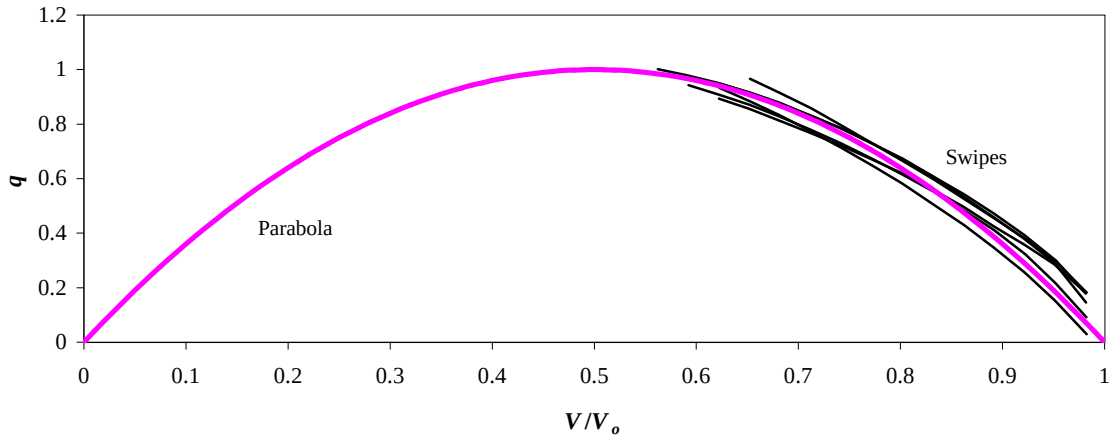

Figure 3.20 - Data from test series DM9 normalised and plotted in $\{V/V_o : q\}$ space.

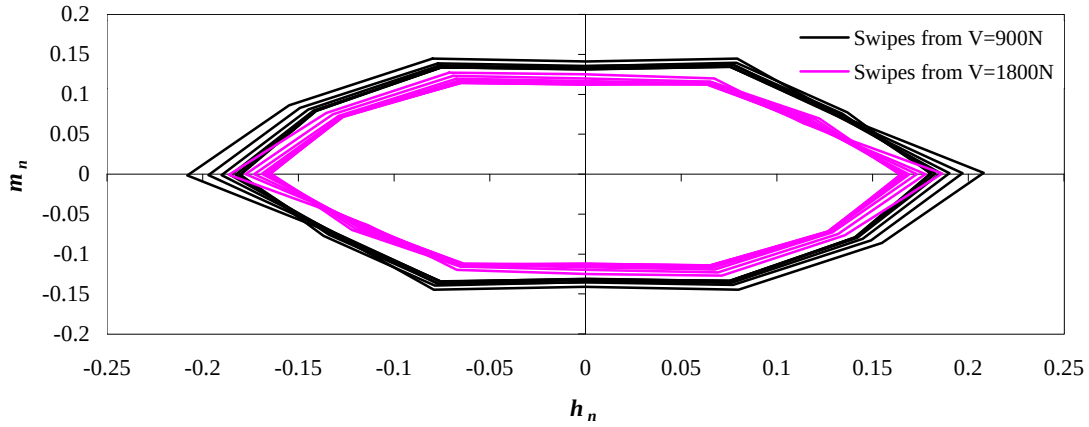

Figure 3.21 - Alternative view of results plotted in normalised $\{M/2R : H\}$ space.

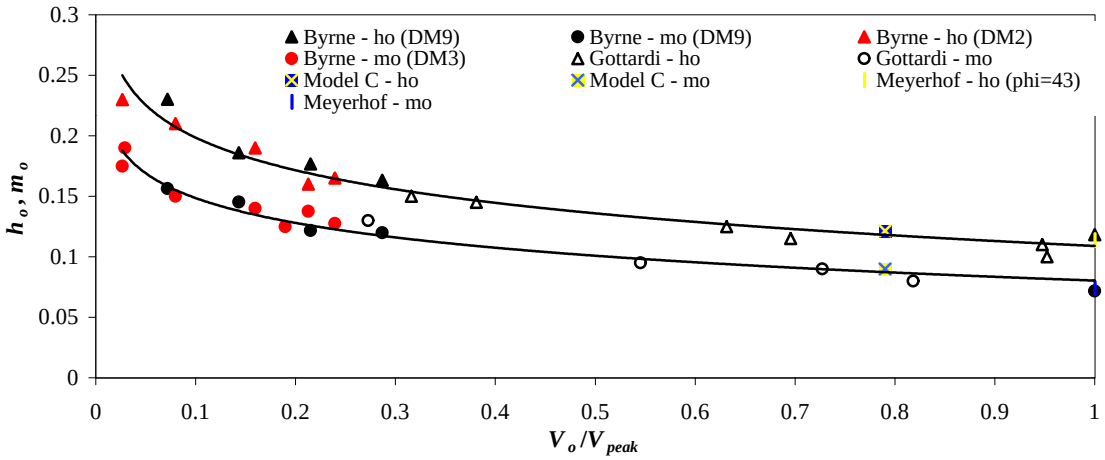

Figure 3.22 - Accumulation of results from various studies of flat footings showing dependence of h_o and m_o on V_o/V_{peak}.

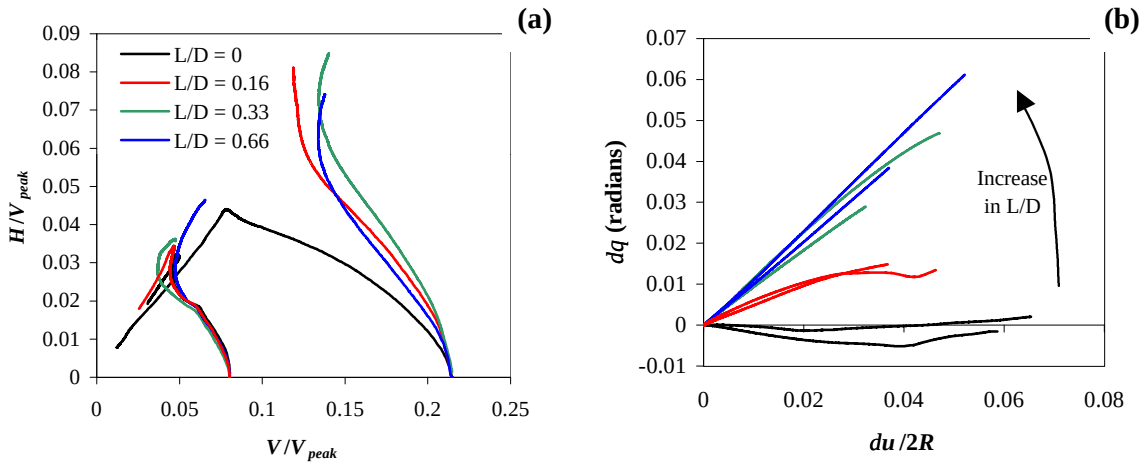

Figure 3.23 - Results from horizontal swipe tests (DM5) showing (a) paths followed in {*V* :*H* } space, and (b) paths followed in {2*R dq*:*du* } space.

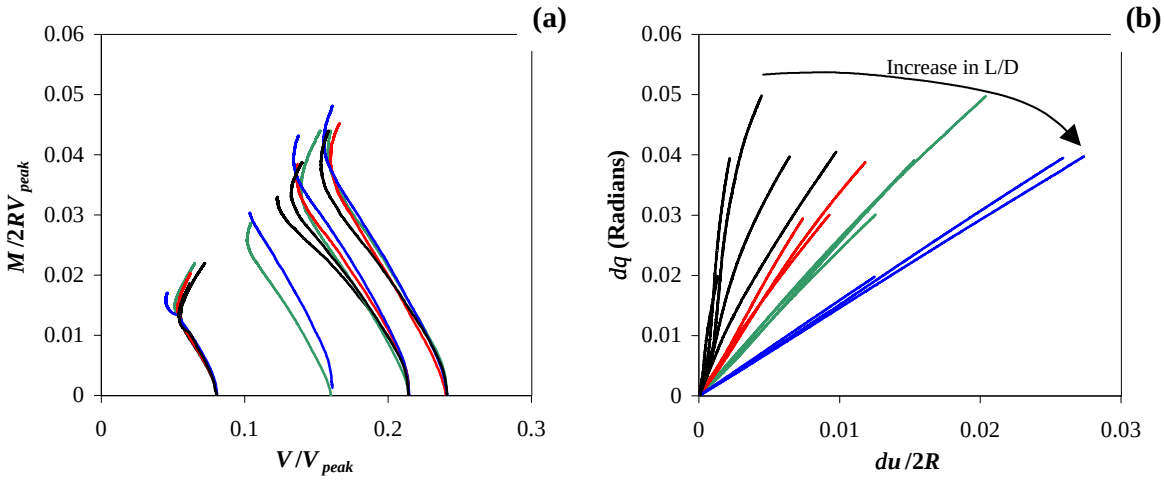

Figure 3.24 - Results from moment swipe tests (DM4) showing (a) paths followed in {*V* :*M* /2*R* } space, and (b) paths followed in {2*R dq*:*du* } space.

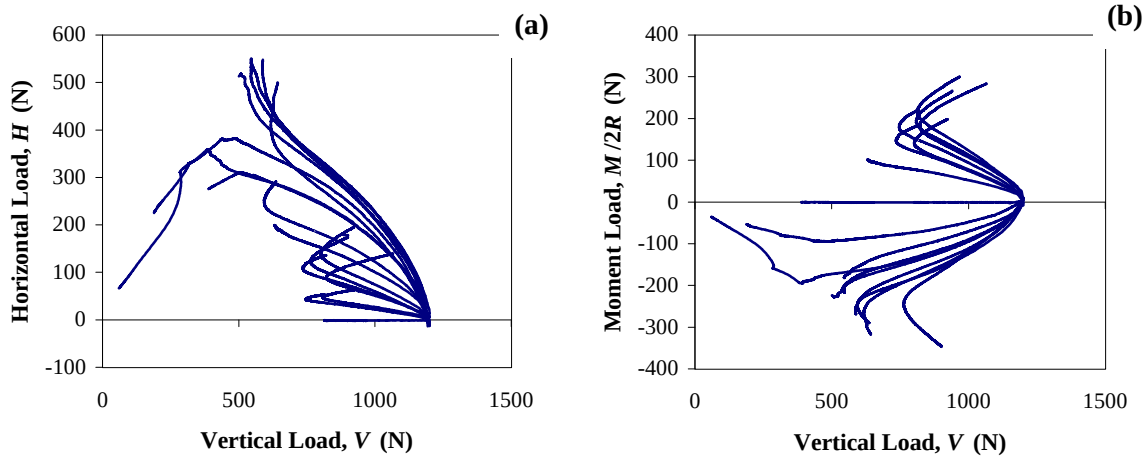

Figure 3.25 - Results from swipe tests (DM6) from $V_o/V_{peak(skirted)}$ = 0.16 at different ratios of $2RH/M$ showing (a) yield paths in {*V* :*H* } space, and, (b) and yield paths in {*V* :*M* /2*R* }

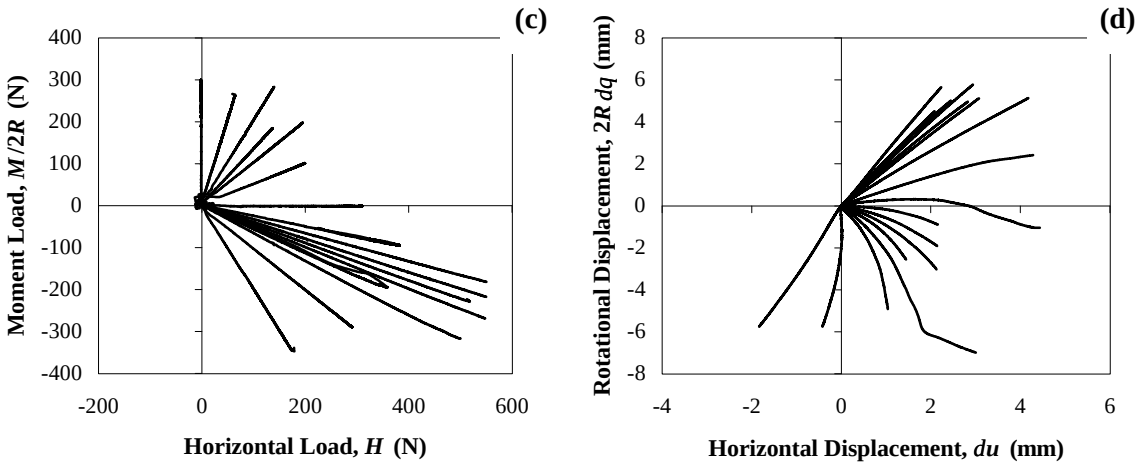

Figure 3.25 - Results from swipe tests (DM6) from $V_o/V_{peak(skirted)}$ = 0.16 at different ratios of $2RH/M$ showing (c) paths in $\{M/2R : H\}$ space, and, (d) and response in $\{2R\,dq : du\}$.

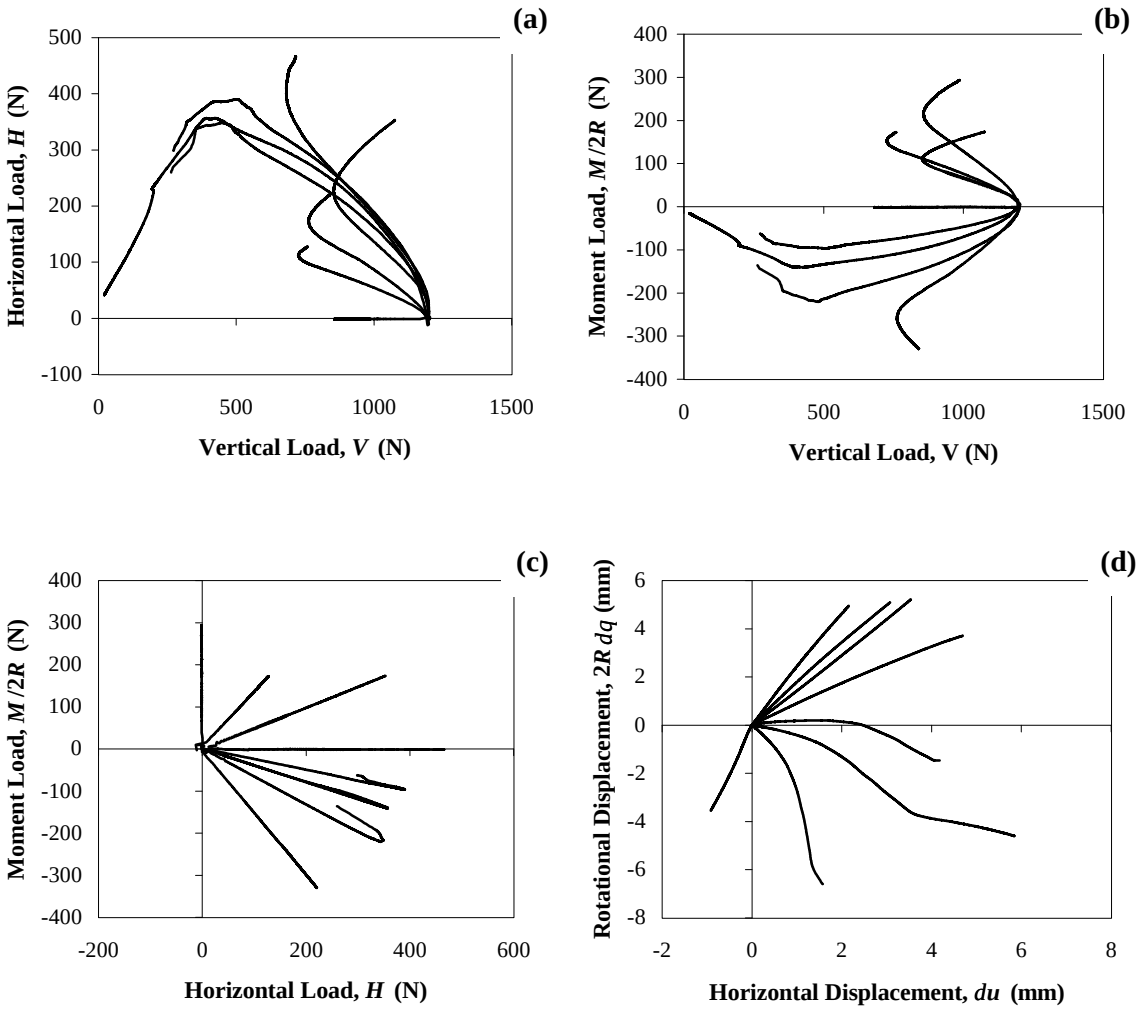

Figure 3.26 - Results from swipe tests (DM7) from $V_o/V_{peak(skirted)}$ = 0.1 at different ratios of $2RH/M$ showing (a) yield paths in $\{V : H\}$ space, (b) yield paths in $\{V : M/2R\}$ space, (c) paths in $\{M/2R : H\}$ space, and, (d) and response in $\{2R\,dq : du\}$.

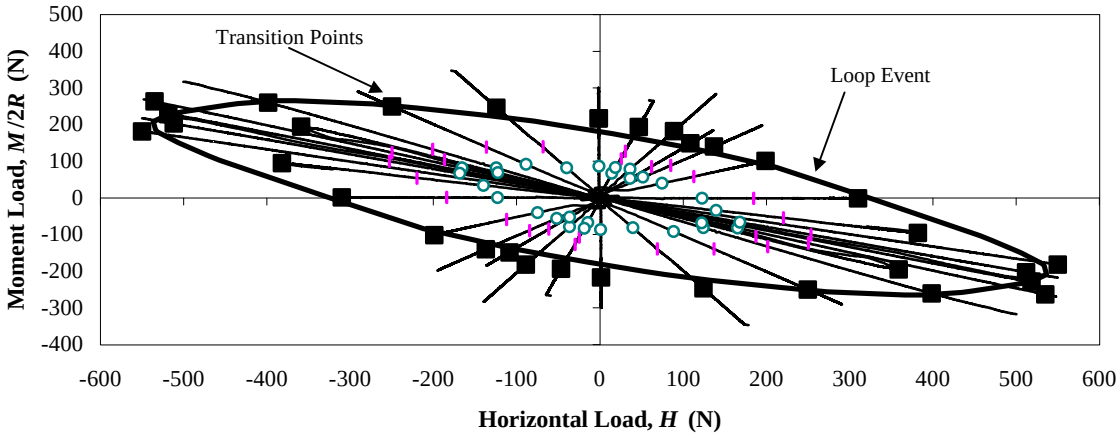

Figure 3.27 - Accumulation of normally consolidated swipes for series DM6 (y = 0.33).

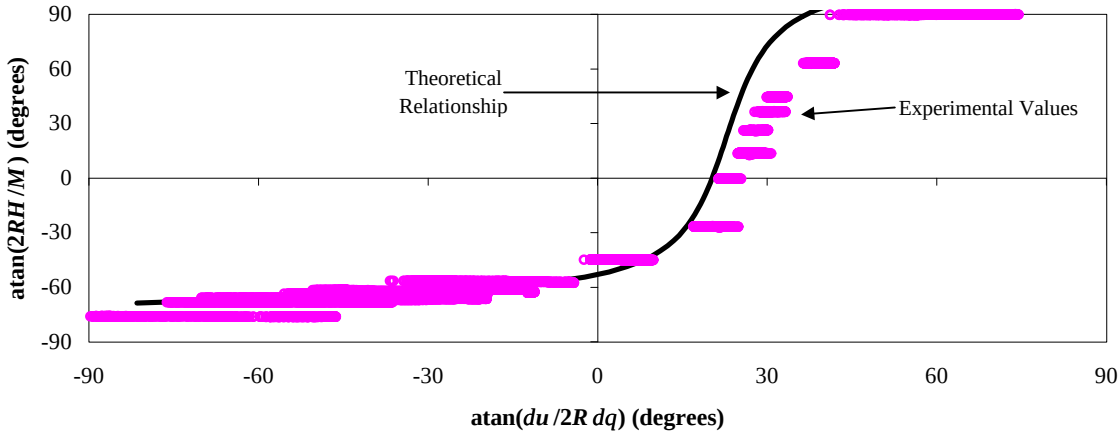

Figure 3.28 - Assessment of associated flow rule in the deviatoric plane for series DM6.

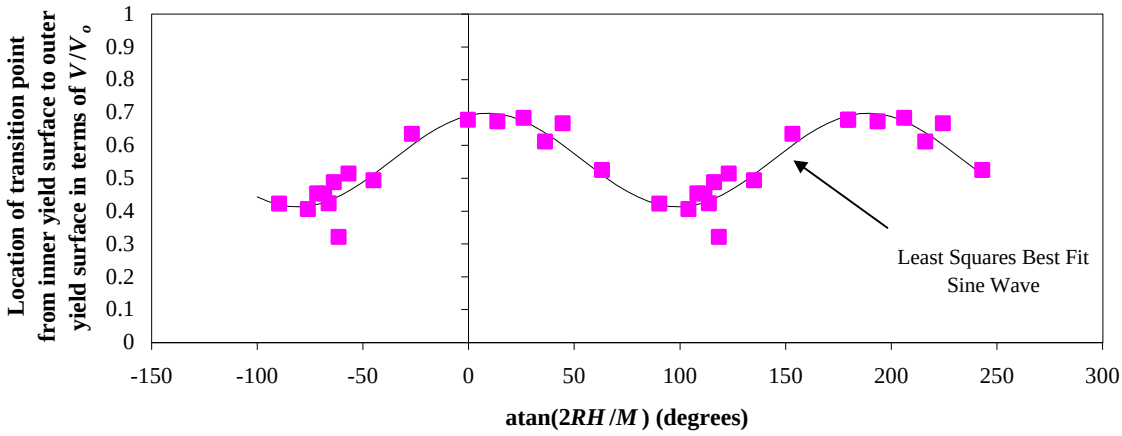

Figure 3.29 - Variation of transition point with load ratio in the deviatoric plane.

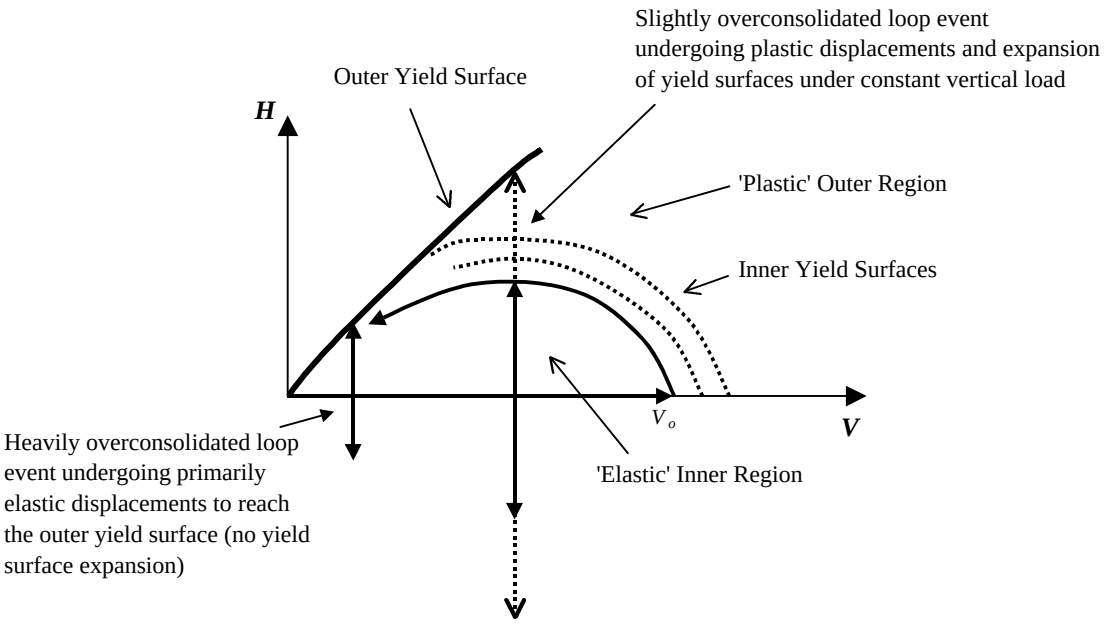

Figure 3.30 - Effects of overconsolidation on the load path followed during a loop event.

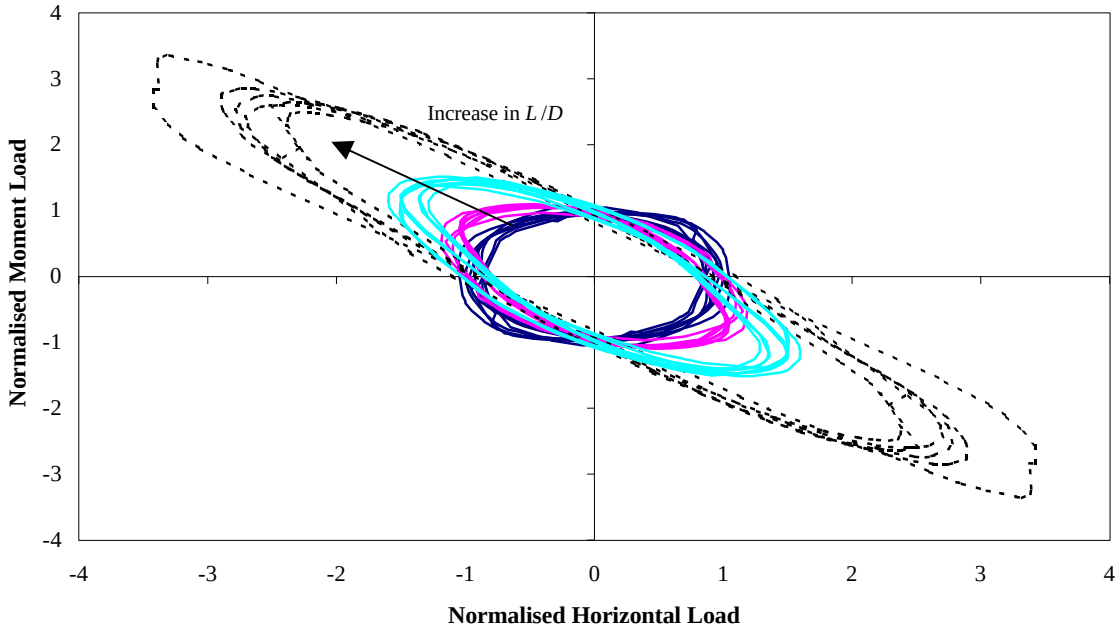

Figure 3.31 - Accumulation of results for loop events at high overconsolidation ratios for different skirt depths.

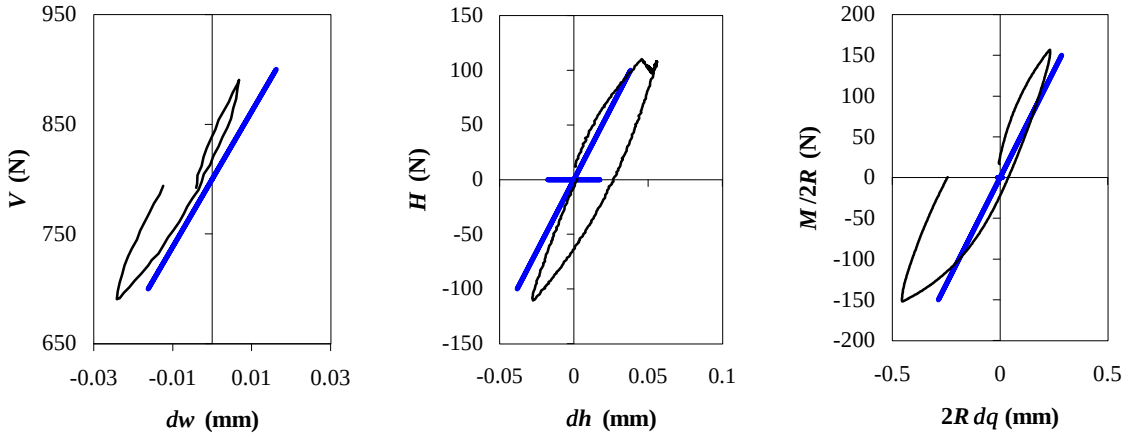

Figure 3.32 - Elastic stiffness excursions for a flat footing, with values predicted using an elastic stiffness matrix method.

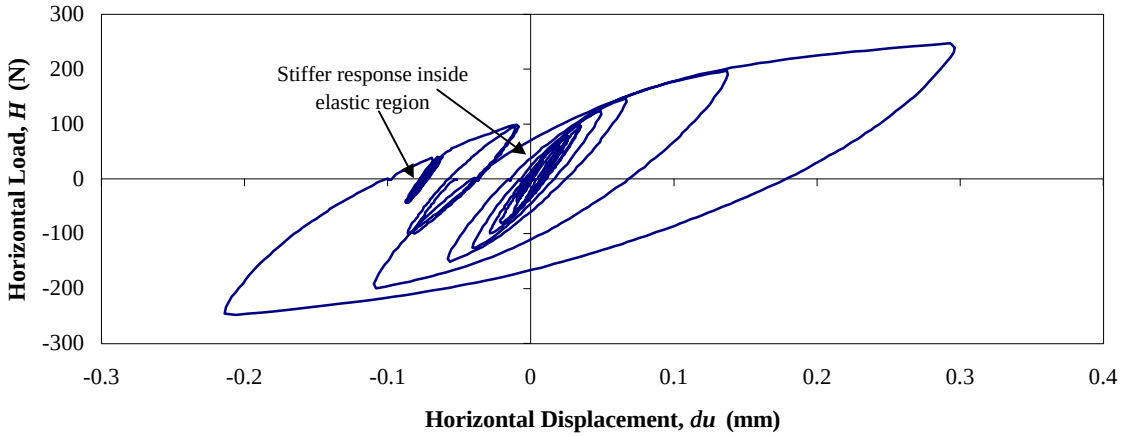

Figure 3.33 - Elastic horizontal load deformation behaviour for a flat footing (V/V_o = 0.33).

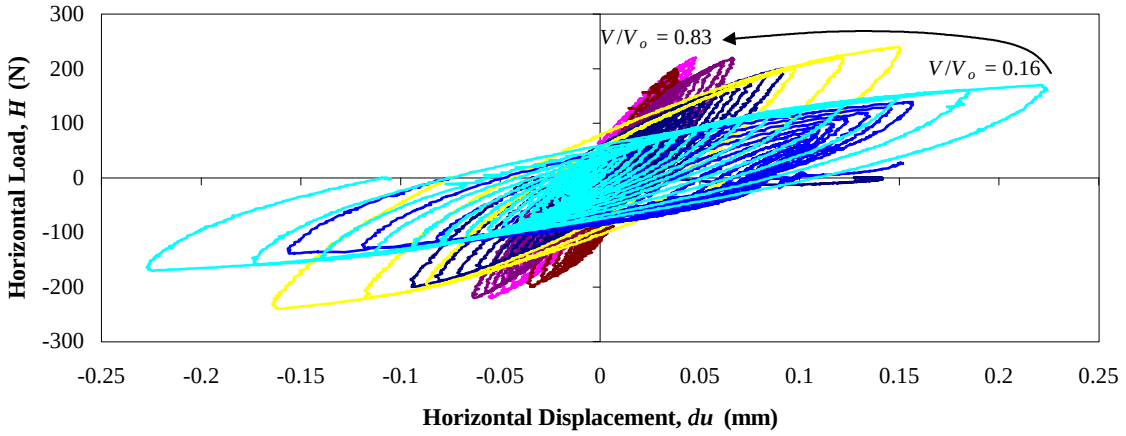

Figure 3.34 - Elastic horizontal load deformation behaviour for a flat footing as a function of V/V_o.

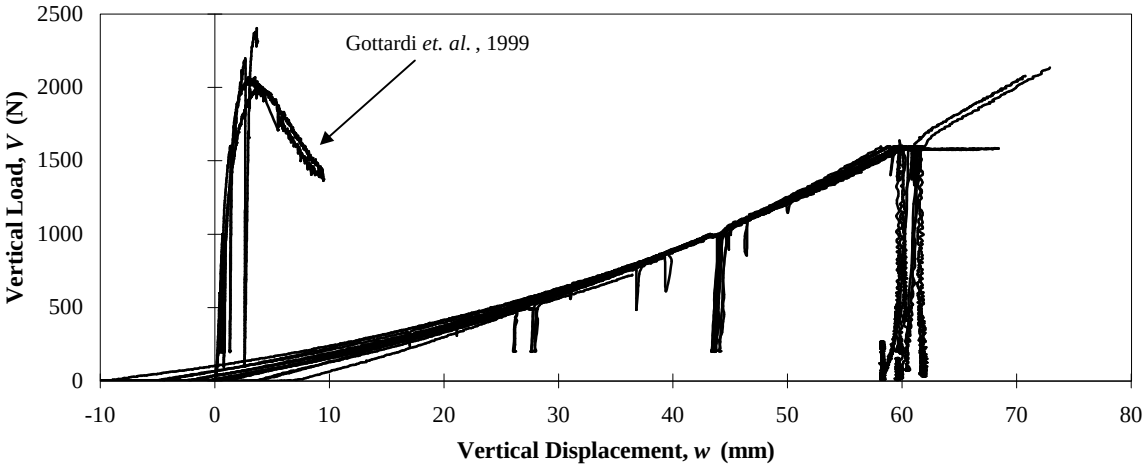

Figure 3.35 - Assembly of carbonate sand vertical loading curves.

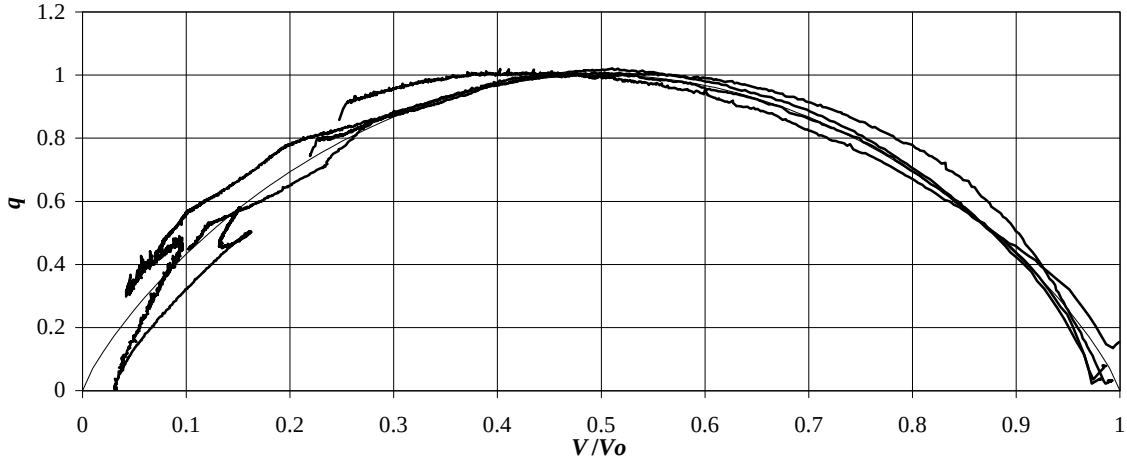

Figure 3.36 - The swipe tests plotted in $\{v:q\}$ space.

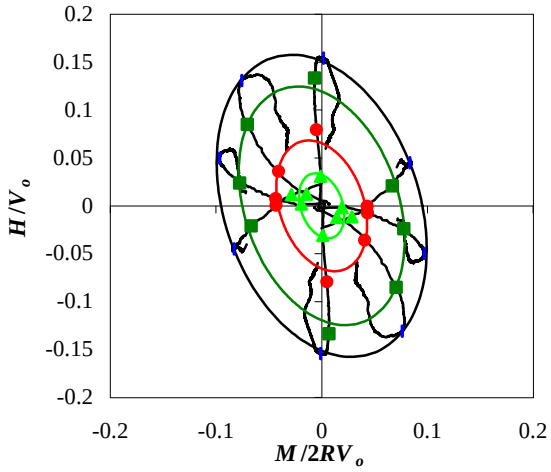

Figure 3.37 - An alternative view of the data in the $\{H/V_o : M/2RV_o\}$ plane.

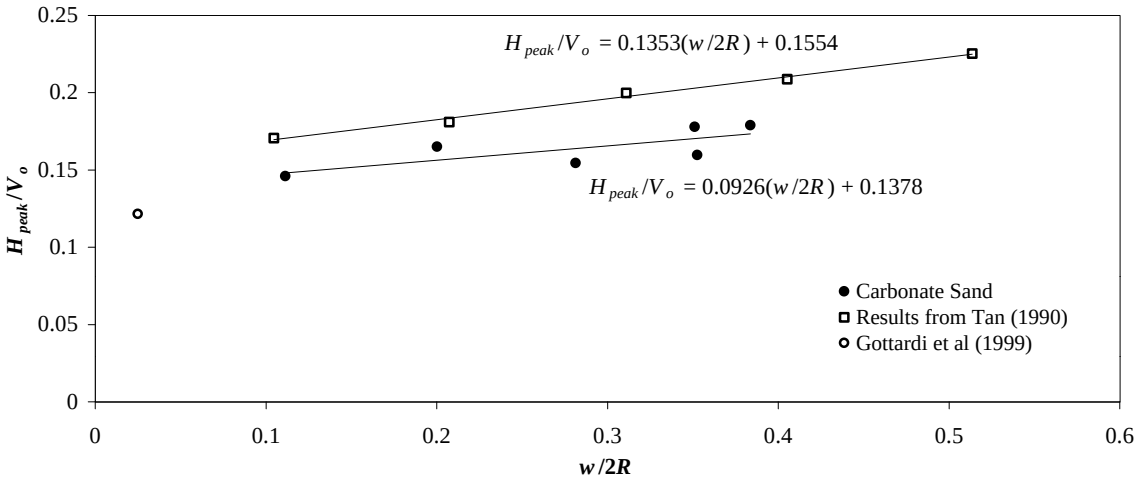

Figure 3.38 - Increase in H_{peak}/V_o with embedment depth for circular footings on carbonate sand.

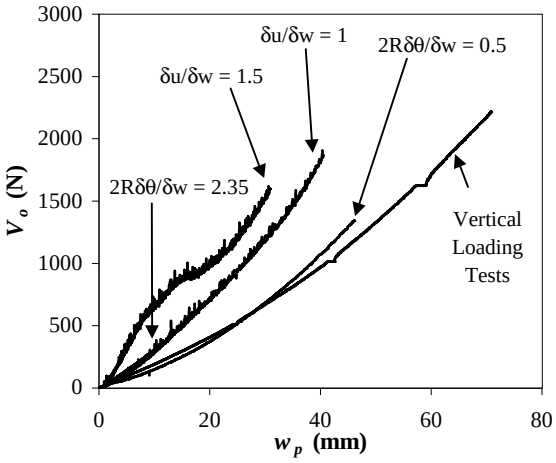

Figure 3.39 - Additional hardening observed in expanding yield surface tests.

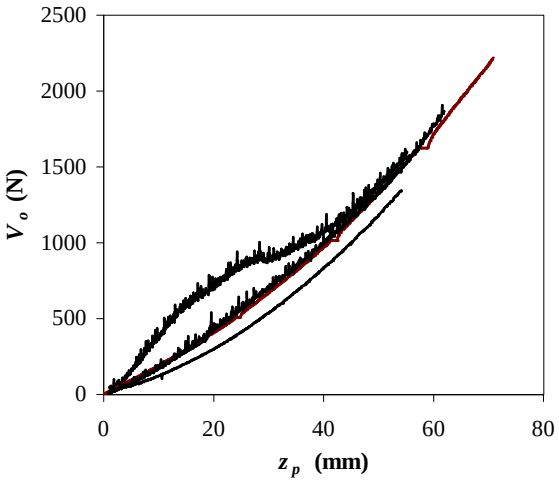

Figure 3.40 - Data from expanding yield surface tests with the new formulation for hardening.

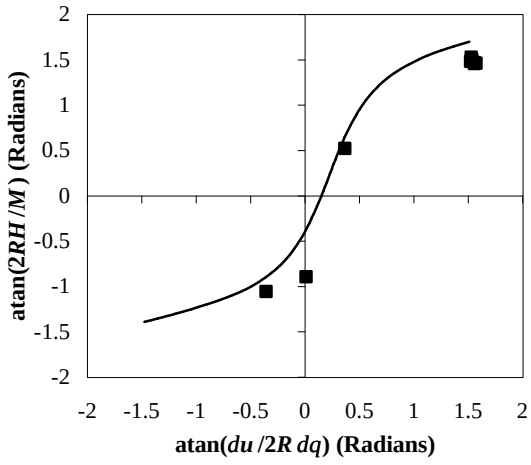

Figure 3.41 - Normality of flow in the {*h* :*m* } plane.

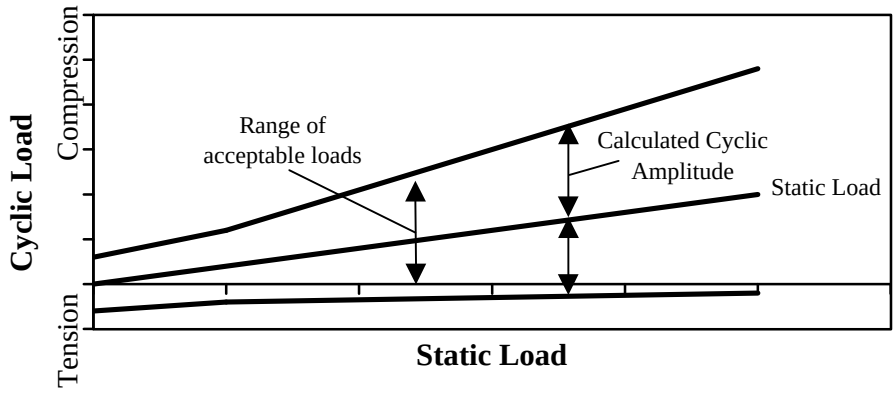

Figure 4.1 - Understanding of the cyclic capacity of suction caissons as set out by Bye *et. al.* (1995)

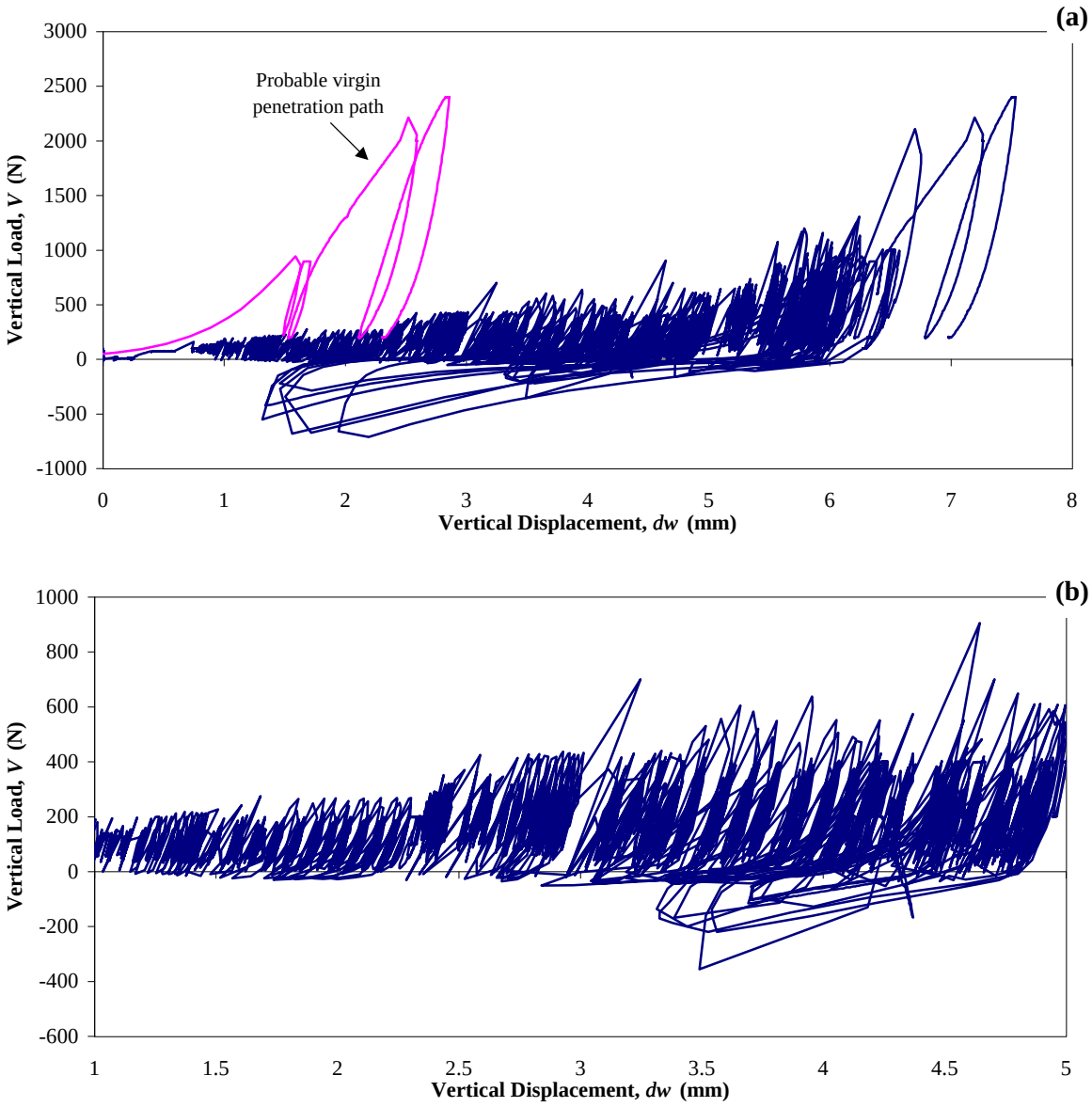

Figure 4.2 - Typical vertical cyclic load sequence showing (a) the total testing sequence including monotonic pull out tests, (b) highlighting initial cyclic loading.

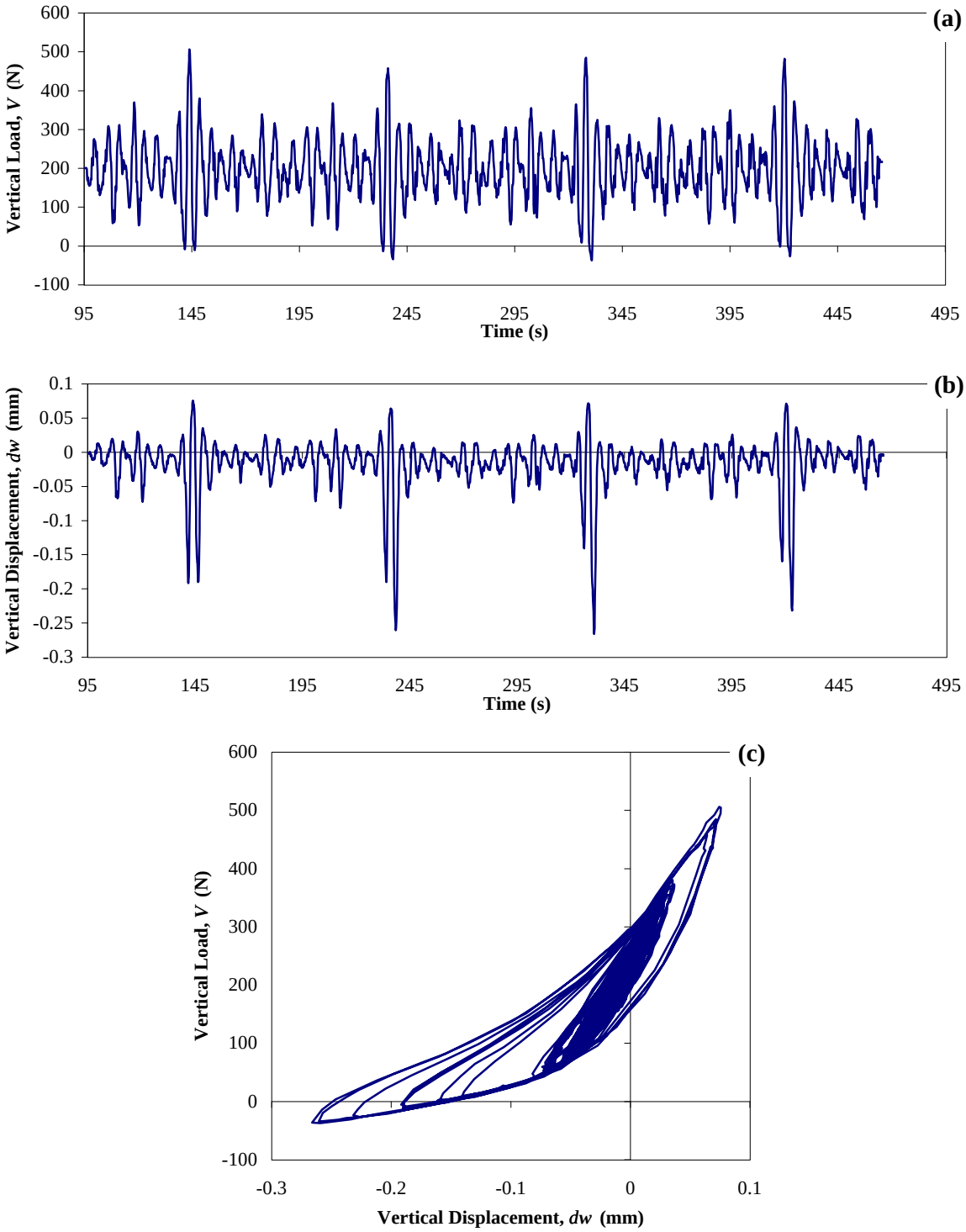

Figure 4.3 - A typical cyclic loading test which incorporates extreme events within a random background with (a) the load time history showing four extreme events, (b) the resulting displacement response, and (c) the asymmetric load displacement behaviour.

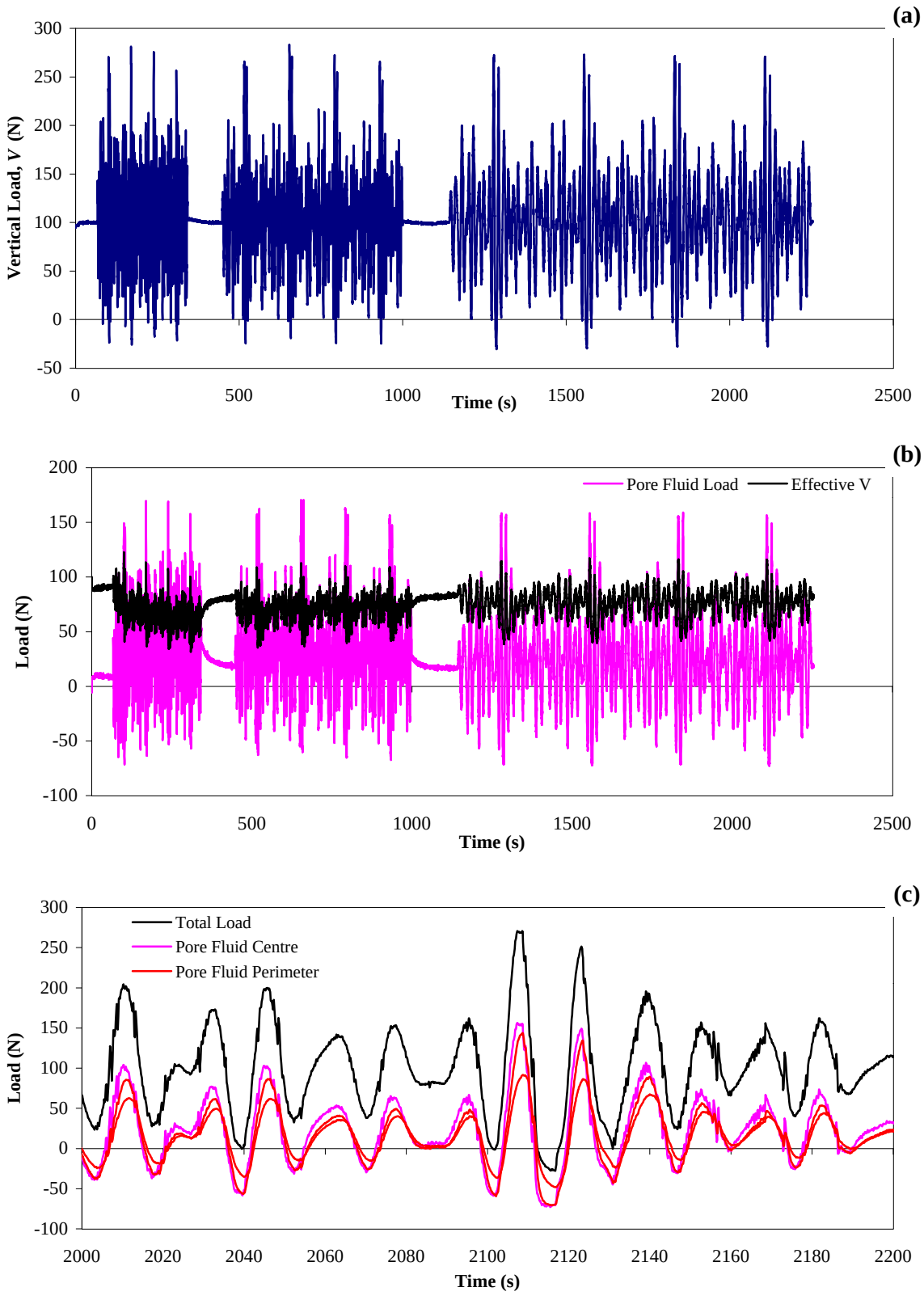

Figure 4.4 - A test which included (a) three sequences of pseudo-random load time histories, (b) the measure of pore fluid response and thus an estimate of the effective vertical load (in this case total load minus pore fluid load), and, (c) the different response of the pressure transducer comparing the centre measurement to the perimeter measurements.

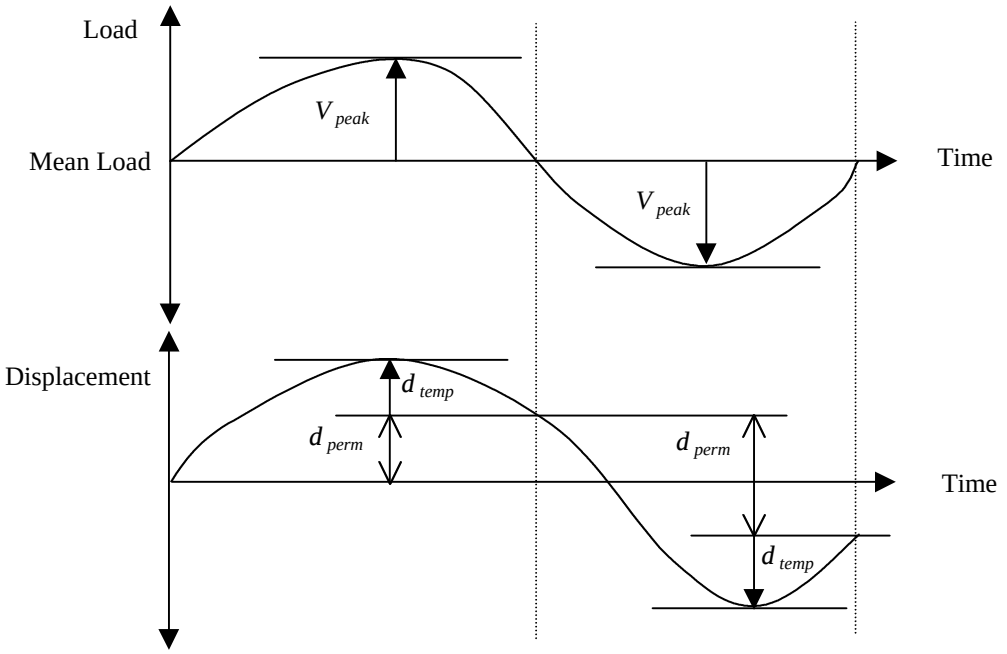

Figure 4.5 - Methodology utilised for reduction of cyclic data.

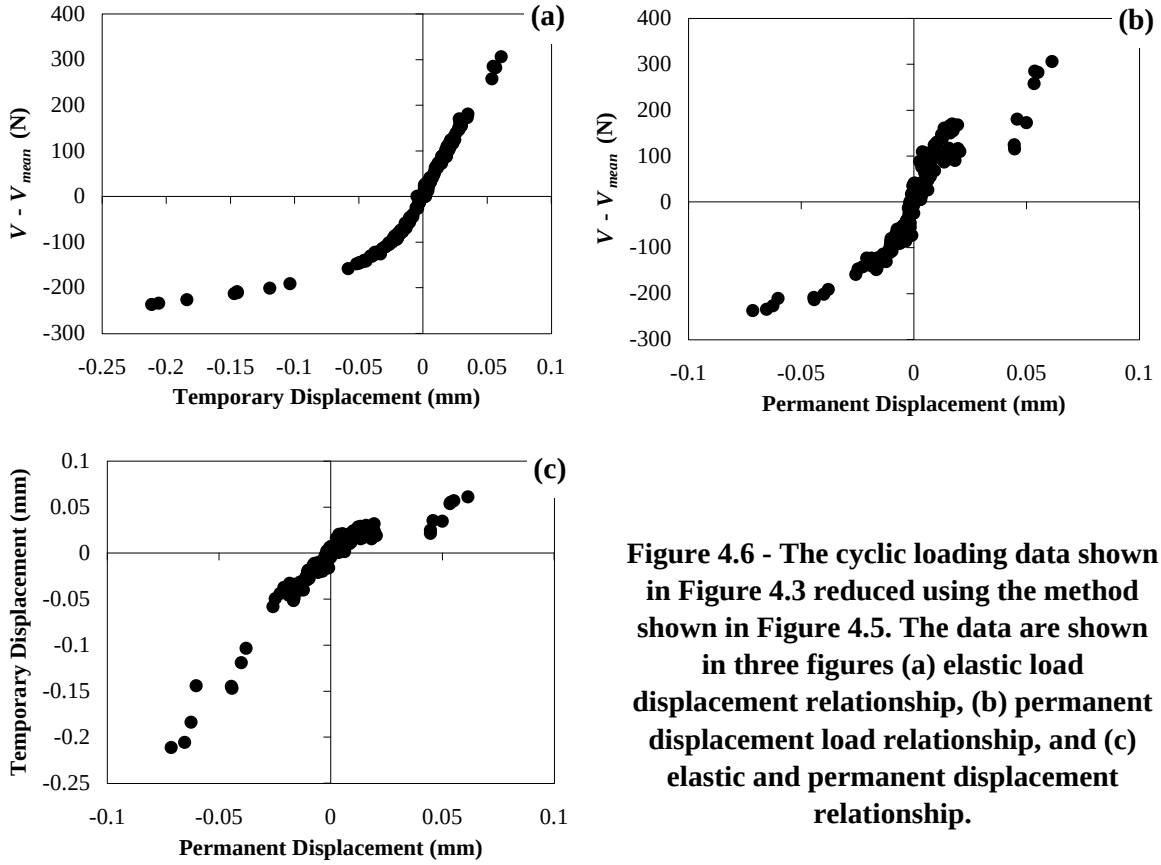

Figure 4.6 - The cyclic loading data shown in Figure 4.3 reduced using the method shown in Figure 4.5. The data are shown in three figures (a) elastic load displacement relationship, (b) permanent displacement load relationship, and (c) elastic and permanent displacement relationship.

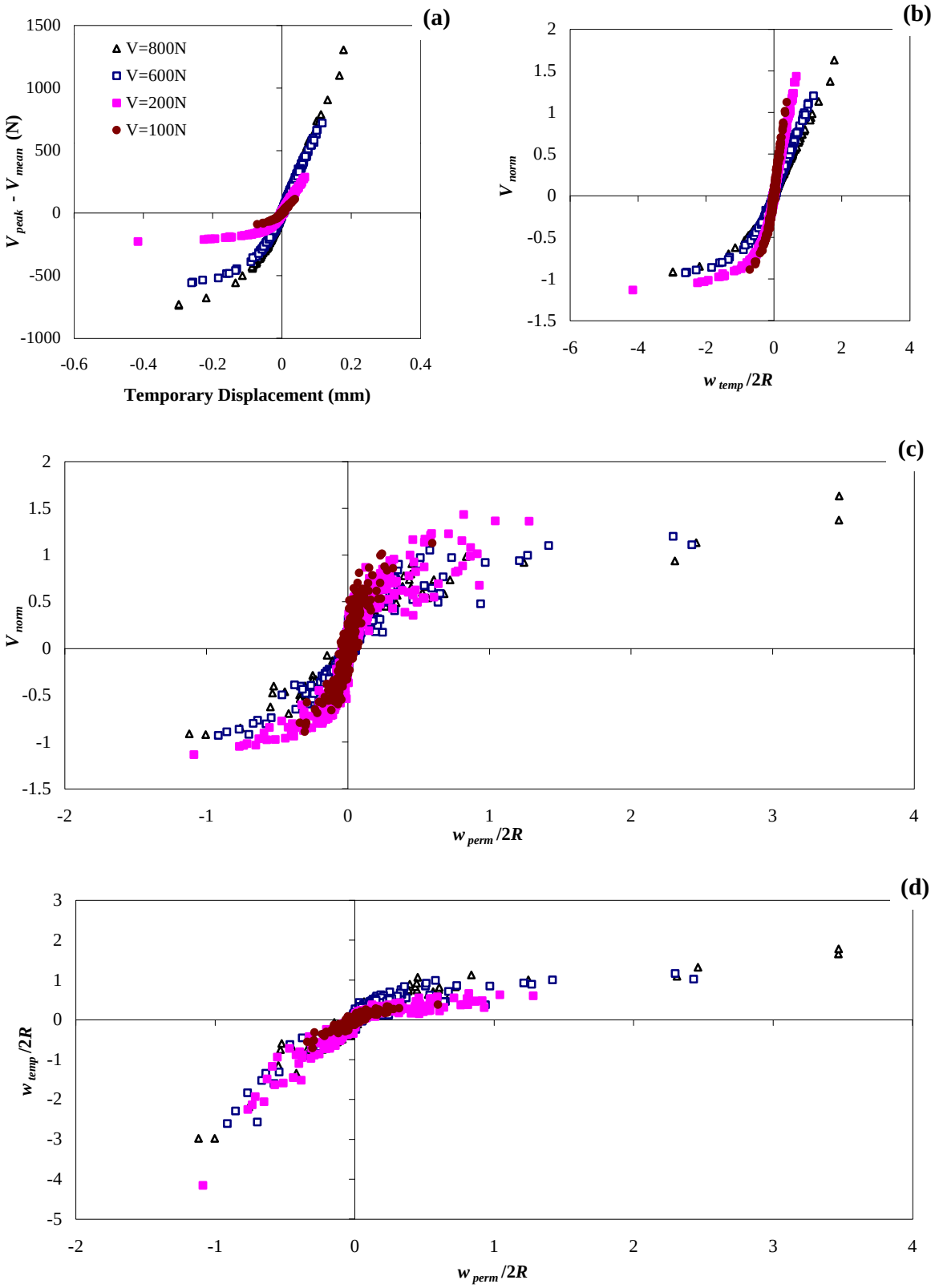

Figure 4.7 - Reduced data from several tests conducted at different mean vertical loads showing (a) difference in load against elastic displacement, (b) difference in load normalised to mean load against elastic displacement, (c) normalised load against permanent displacement, and, (d) the displacement responses plotted against each other.

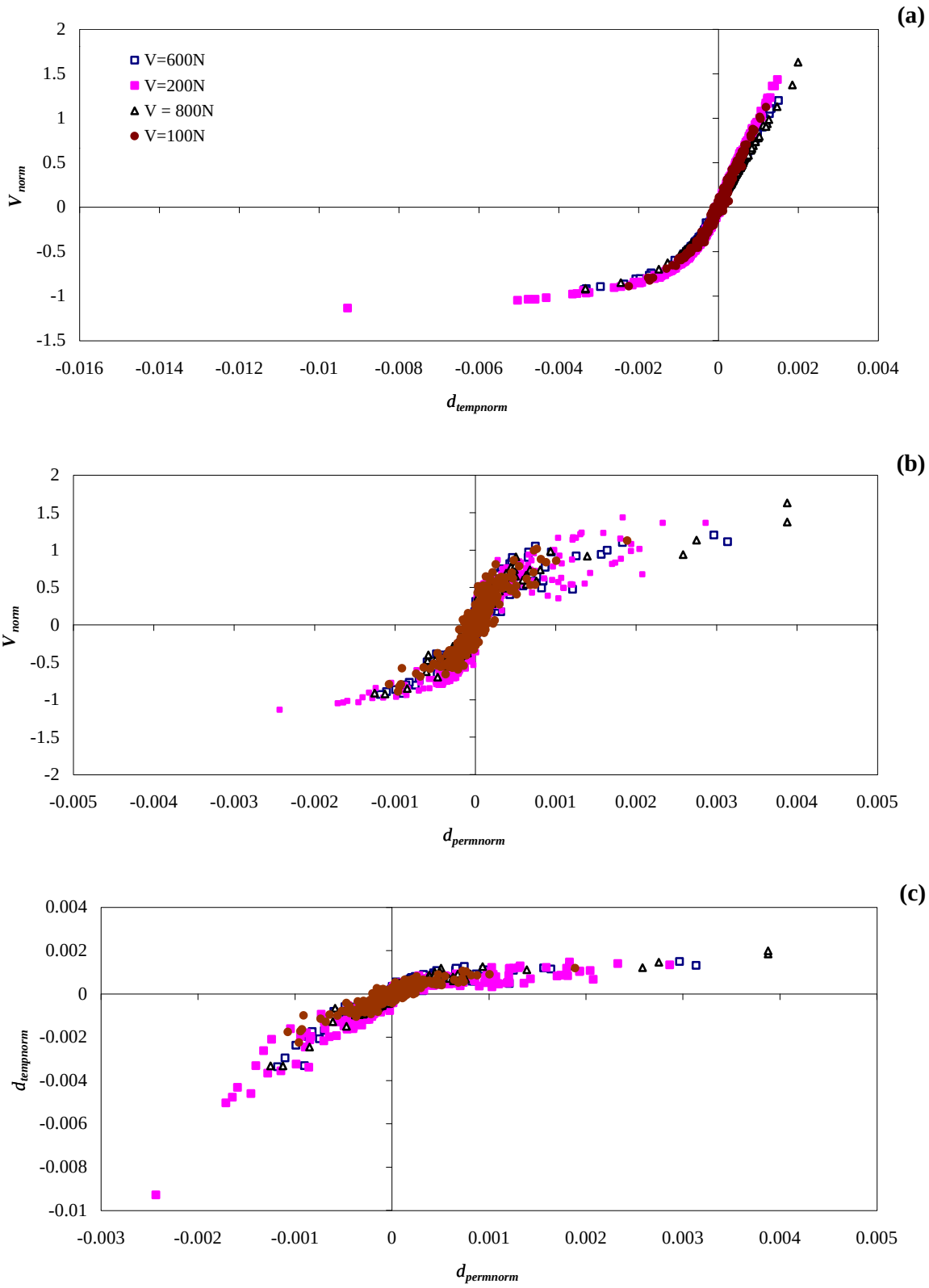

Figure 4.8 - Reduced cyclic loading data normalised using the dimensional analysis group. The results are shown for four different mean vertical loads on the same footing of diameter 150mm.

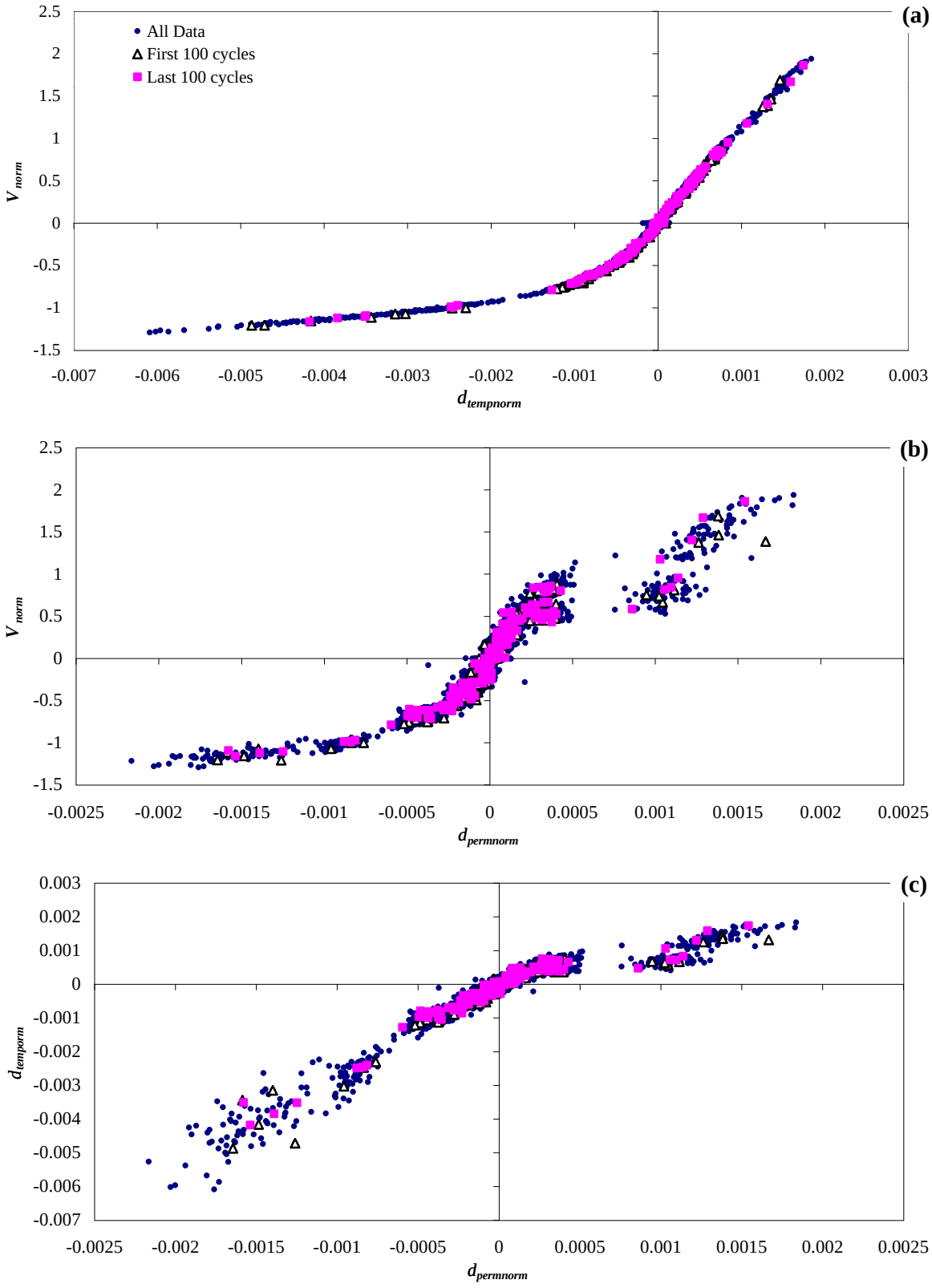

Figure 4.9 - Reduced data from the sequence of 2000 cycles of pseudo-random cycling showing little effect of degradation between the first 100 cycles and the last 100 cycles.

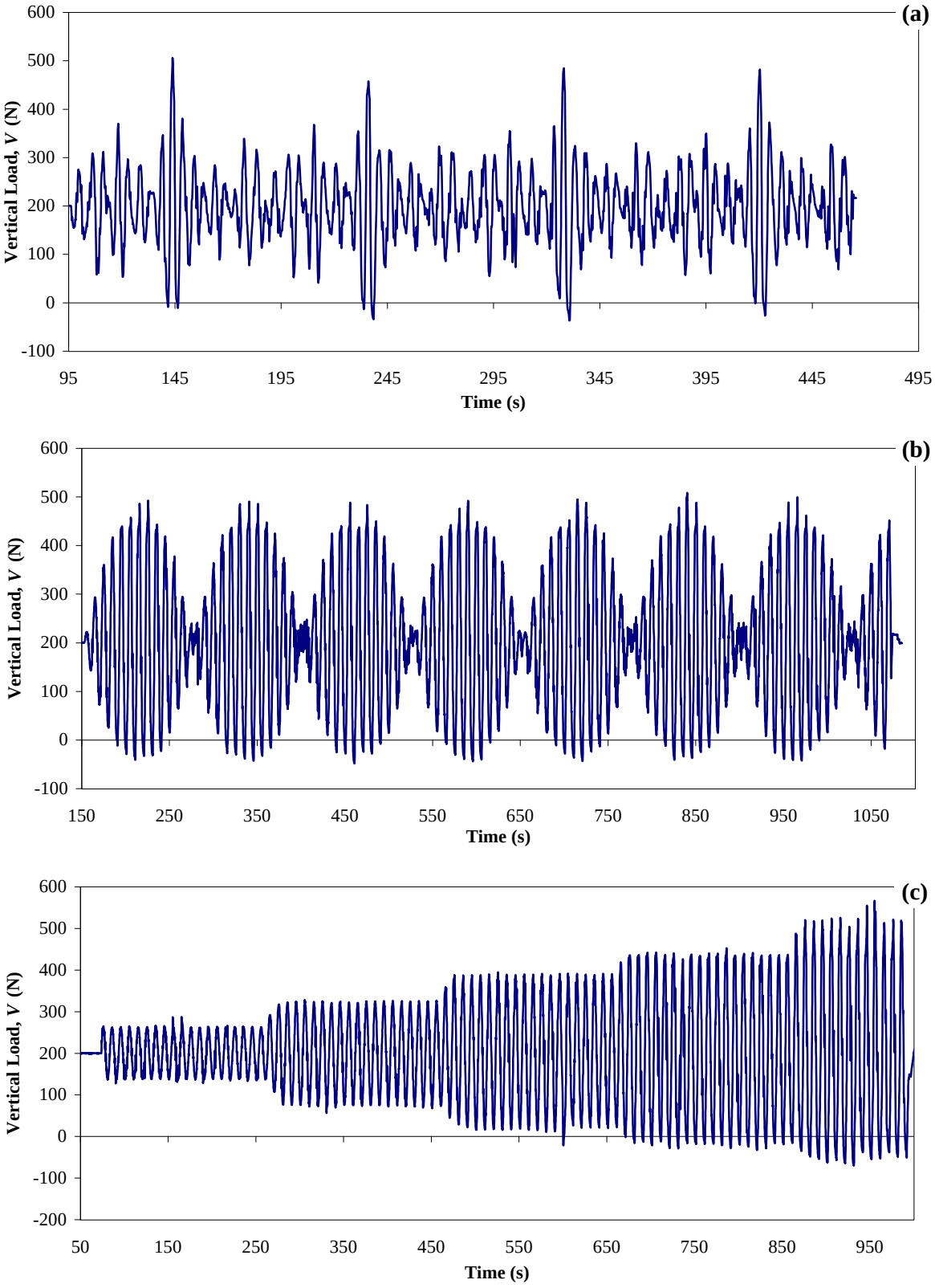

Figure 4.10 - The different loading time histories employed during the testing, (a) 'constrained NewWave' approach, (b) modulated sine wave, and, (c) stepped sine wave.

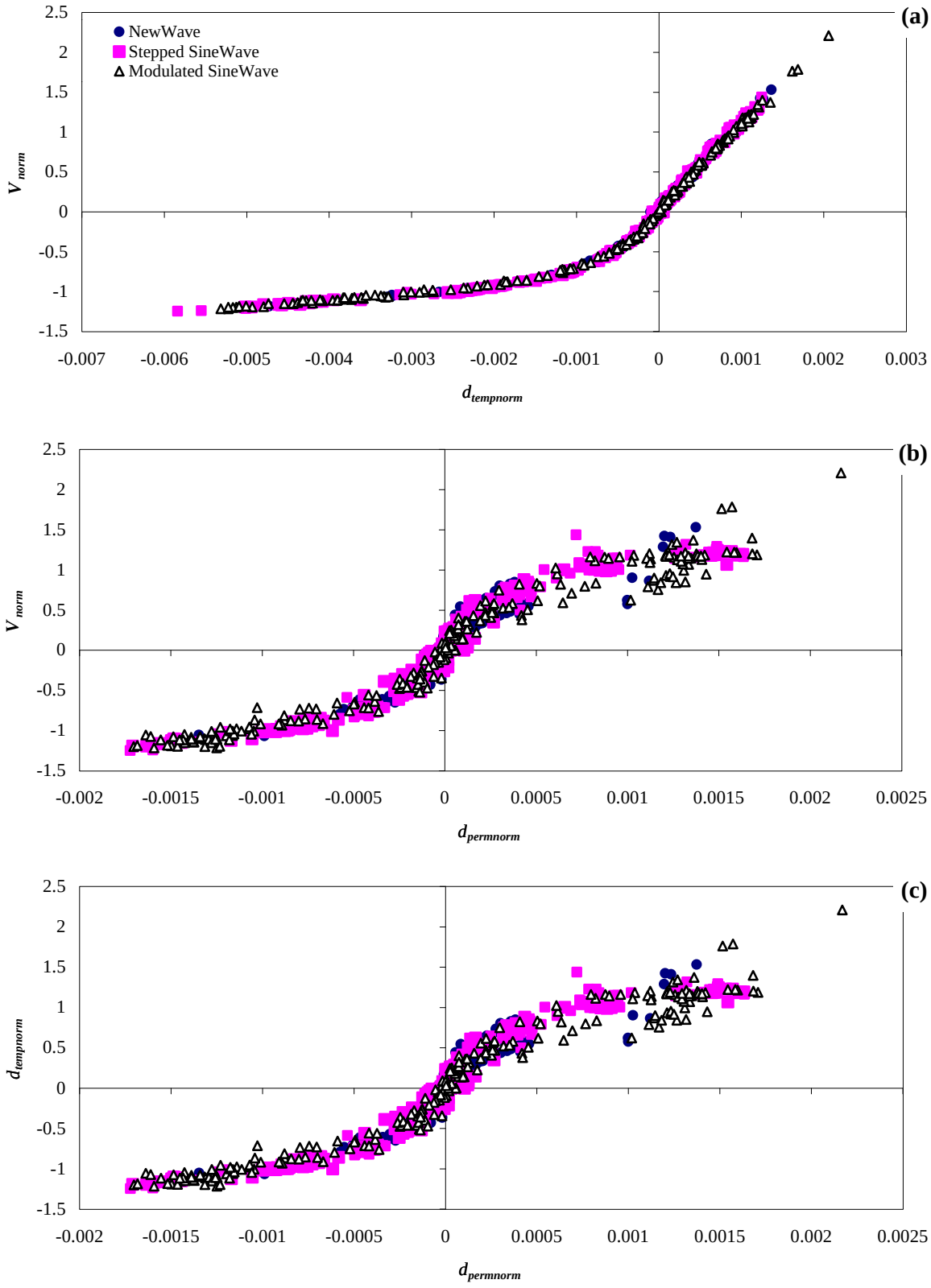

Figure 4.11 - The reduced data from the different loading time histories shown in Figure 4.10

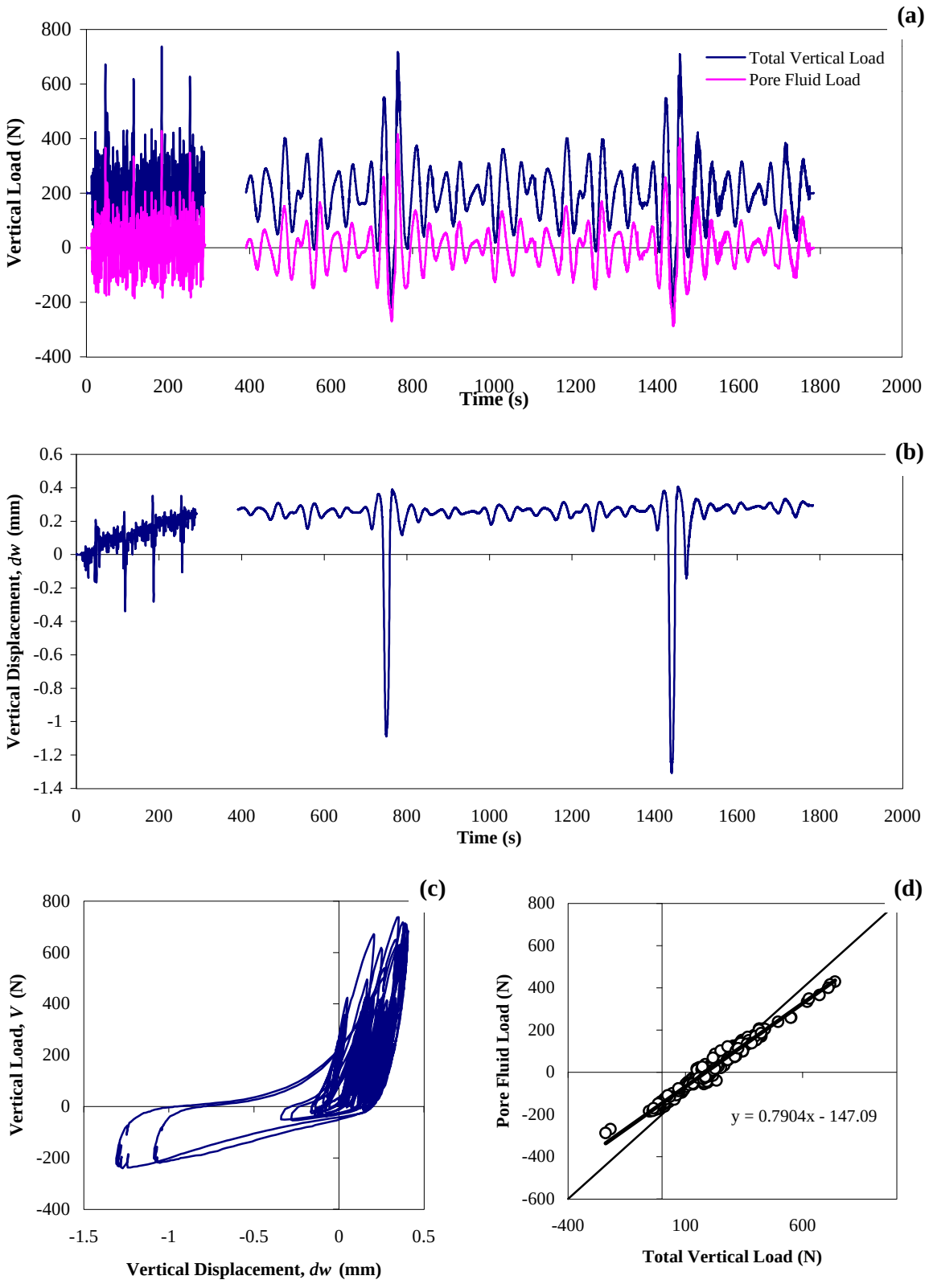

Figure 4.12 - Data from cyclic test where two different loading rates were used to investigate the effect of rate on load displacement response (a, b and c), and fluid load response (d).

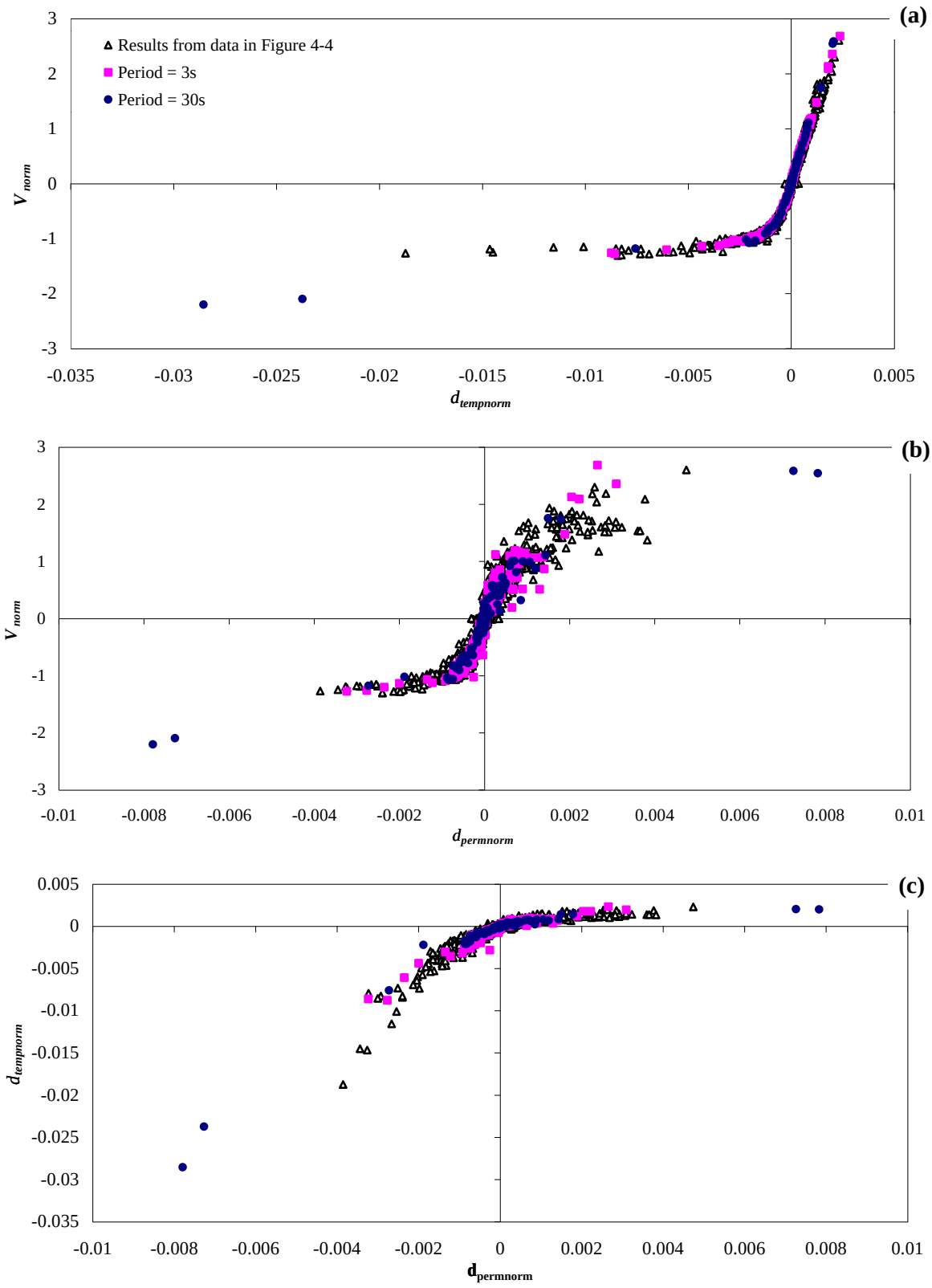

Figure 4.13 - Reduced data from different loading rate tests showing (a) load elastic displacement response, (b) load permanent displacement response, and, (c) displacement

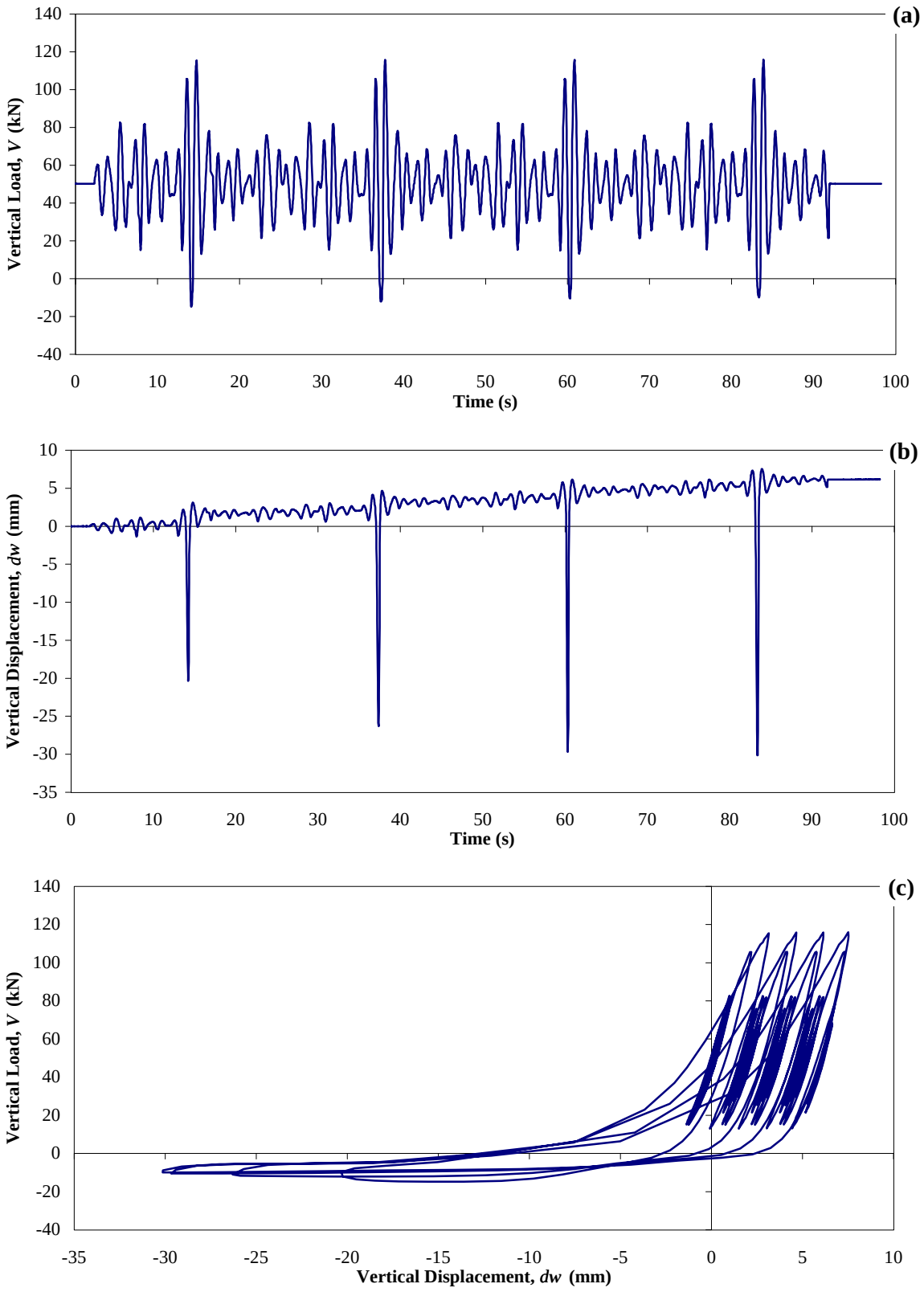

Figure 4.14 - Results from axial loading experiments on a 300mm footing in the Structural Dynamics Laboratory (Johnson, 1999) showing (a) load time history, (b) displacement time history, and, (c) load displacement response.

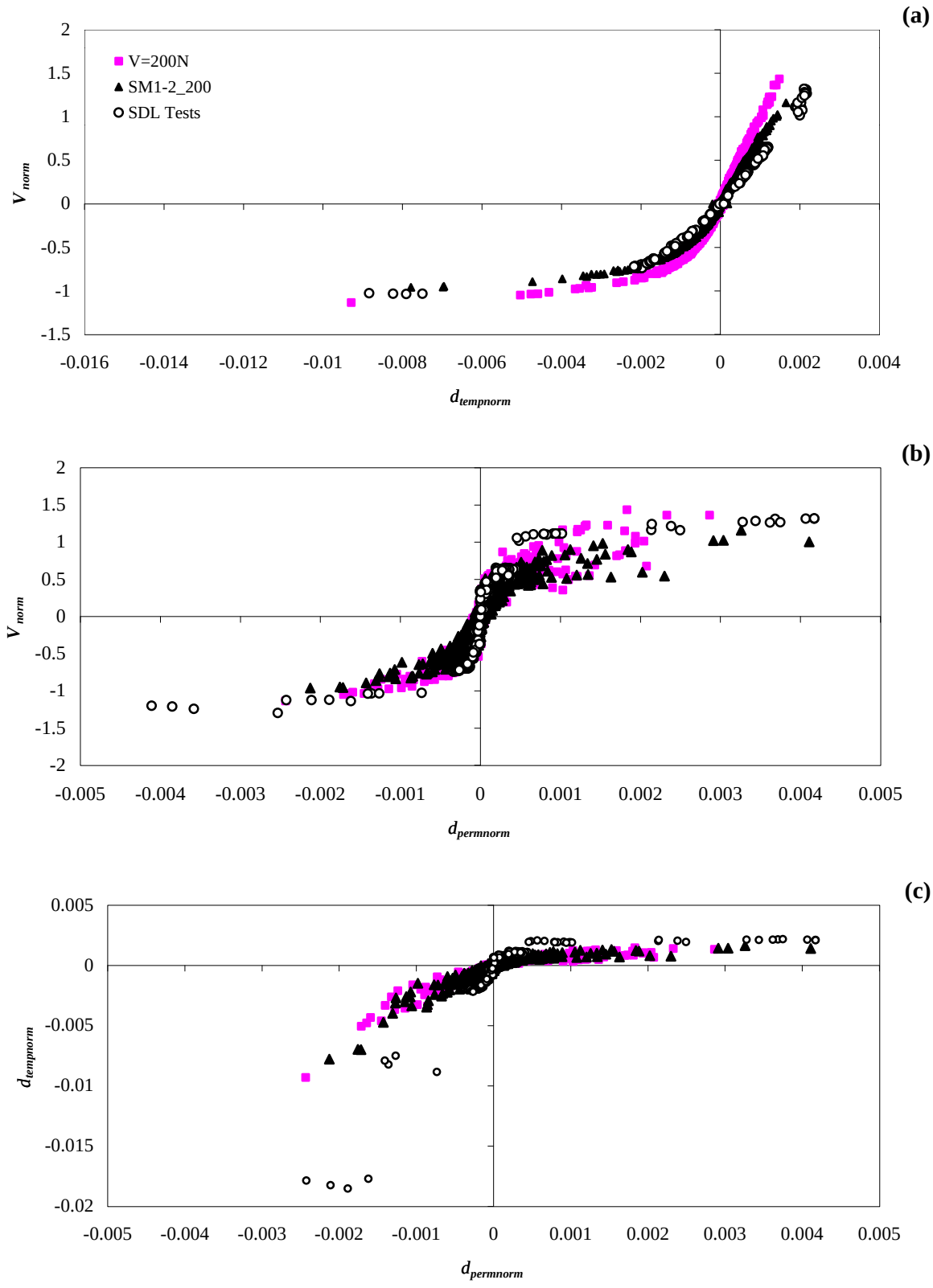

Figure 4.15 - Comparison of normalised vertical cyclic loading tests for three different footing sizes 100mm (SM1-2_200), 150mm (V=200N) and 300mm (SDL Tests) displayed as (a) elastic displacements, (b) permanent displacements, and (c) displacements relationship.

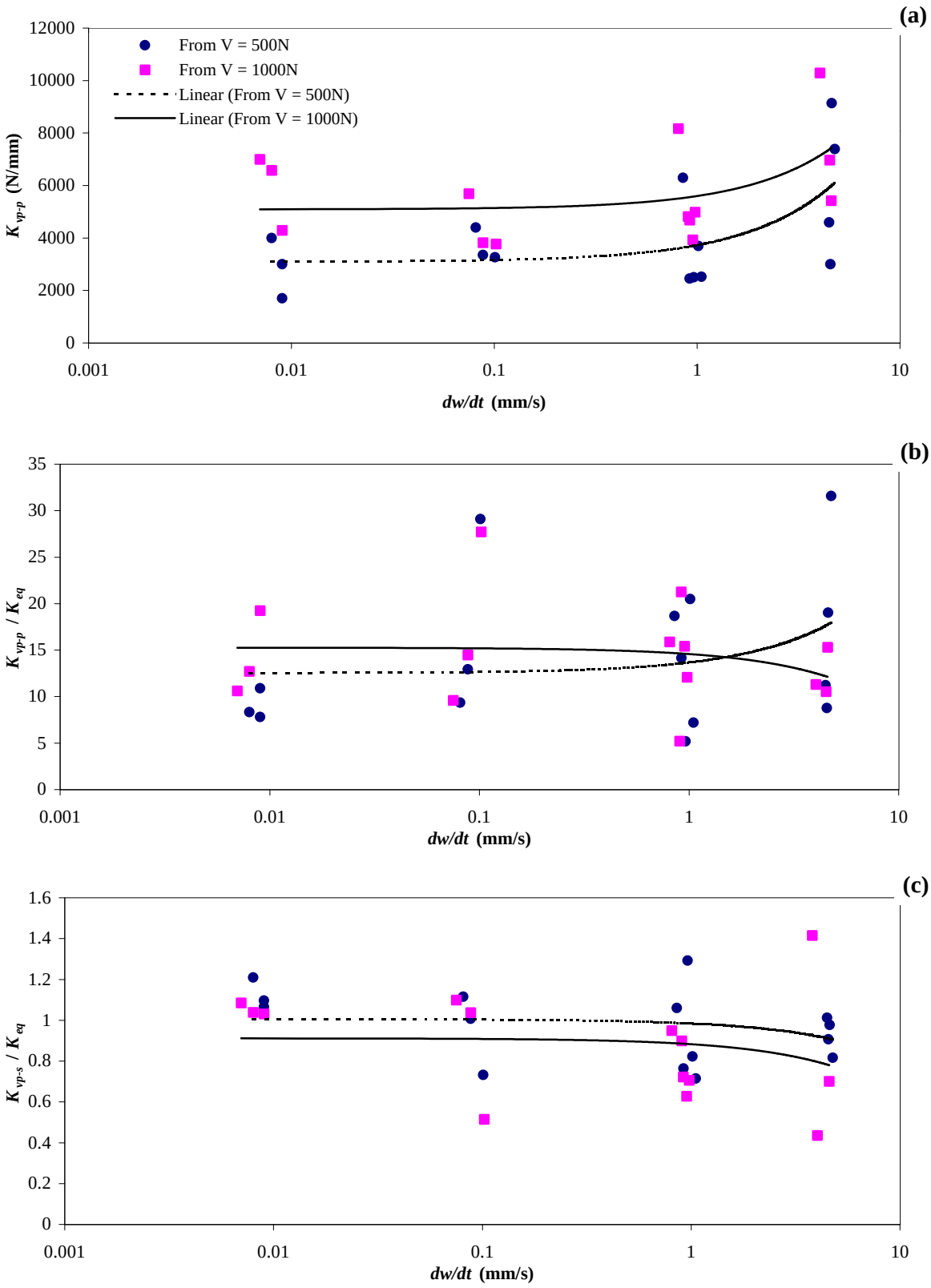

Figure 4.16 - Results from Mangal (1999) who examined the partially drained behaviour of flat footings where (a) shows 'primary' stiffness against load rate, (b) shows the primary stiffness normalised to the equivalent stiffness, and, (c) shows the secondary stiffness also normalised to the equivalent stiffness.

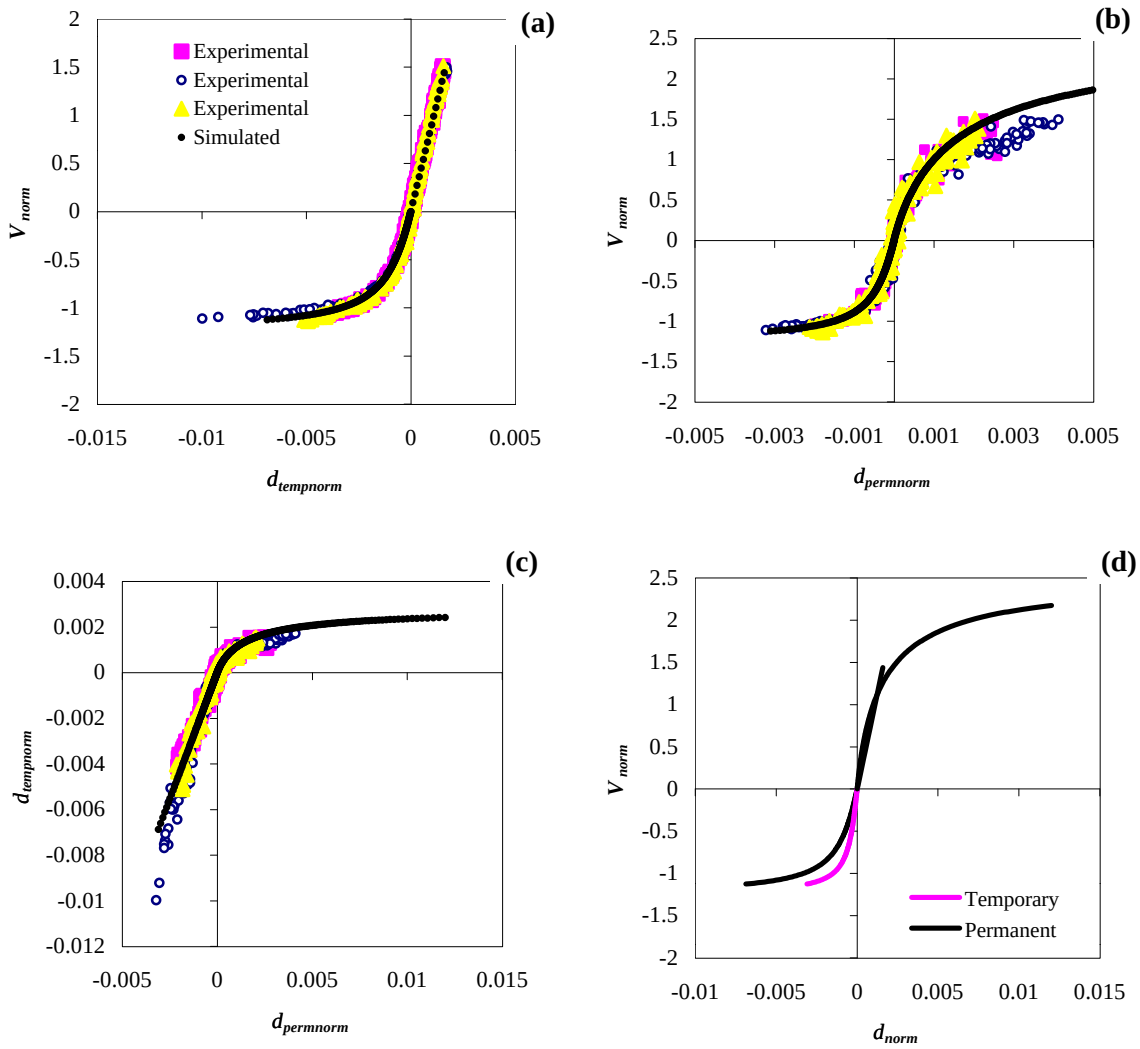

Figure 4.17 - Empirical curve fits using a hyperbolic function showing fits for (a) elastic response, (b) plastic response, (c) comparing displacements, and, (d) comparing elastic and plastic responses.

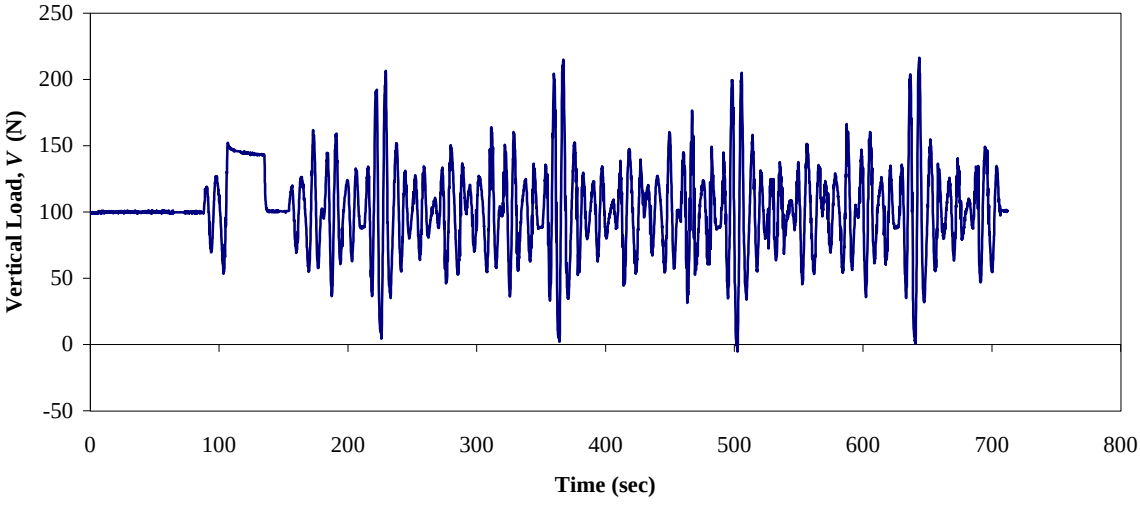

Figure 4.18 - Pseudo random load-time history from which the above curve fits have been produced.

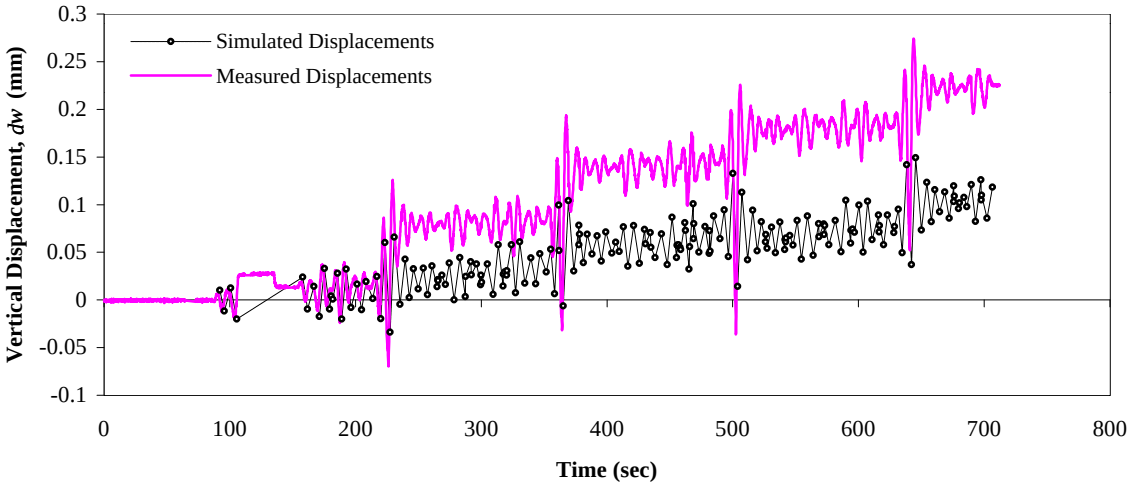

Figure 4.19 - Displacement response to load path shown in Figure 4.18 and predicted response using empirical curve fits.

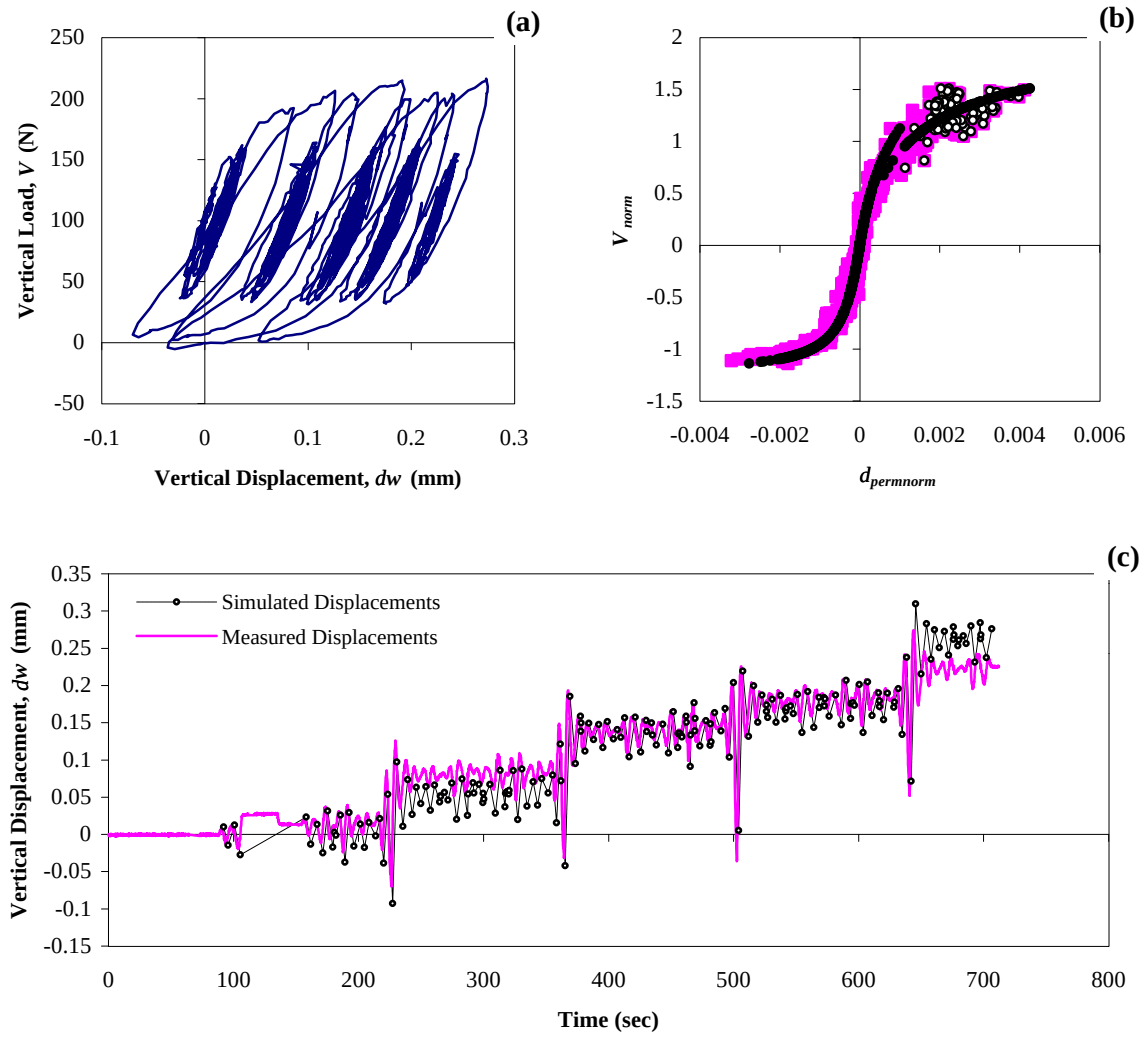

Figure 4.20 - (a) Actual load displacement response showing penetrations after tensile pull, (b) correction to empirical curve fit, and, (c) resulting prediction.

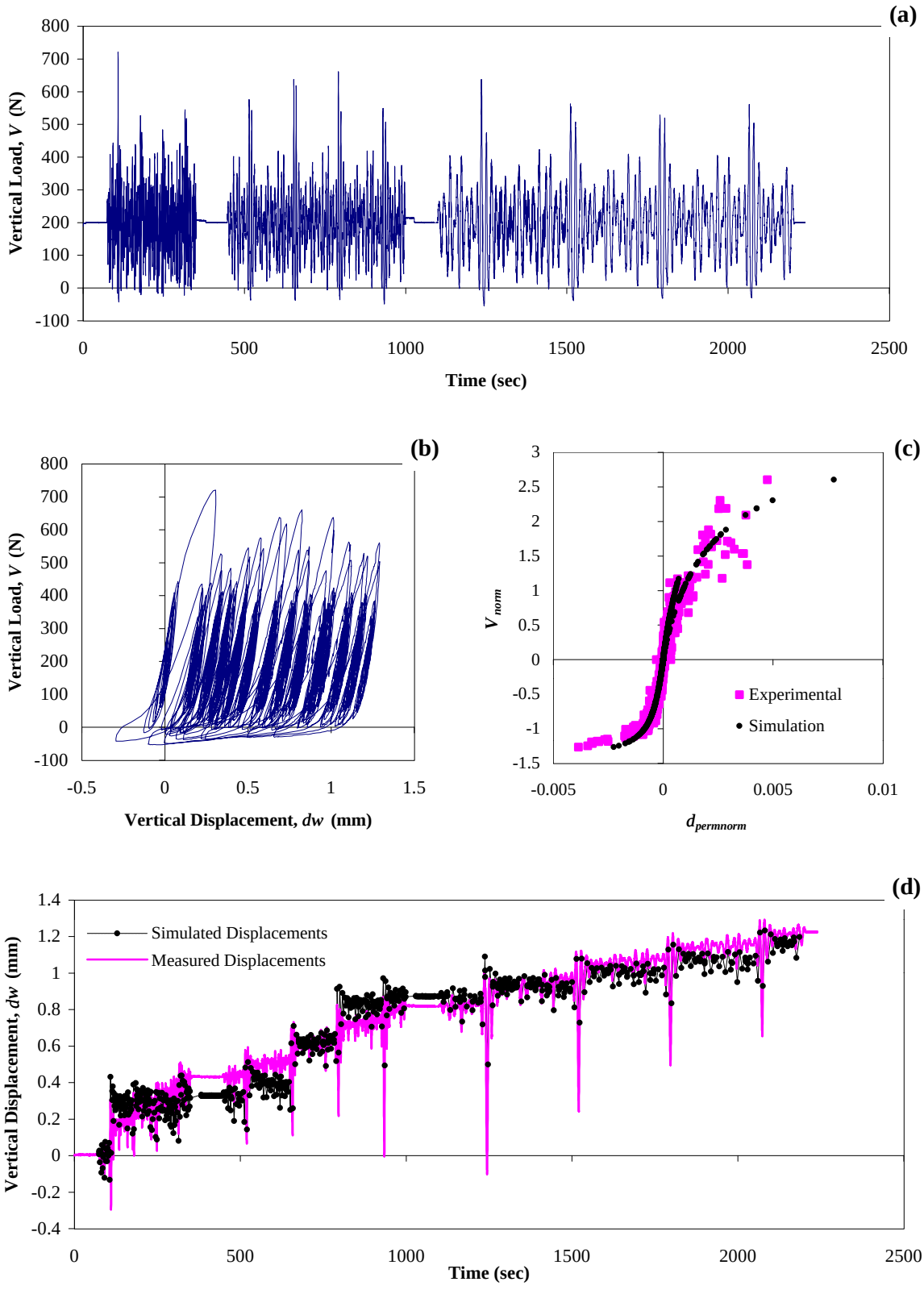

Figure 4.21 - Results of empirical prediction of displacements where (a) shows the load time history which includes three different periods of loading, (b) shows the load displacement response measured experimentally, (c) shows the empirical fit through the permanent displacement data, and, (d) the resulting prediction of displacements.

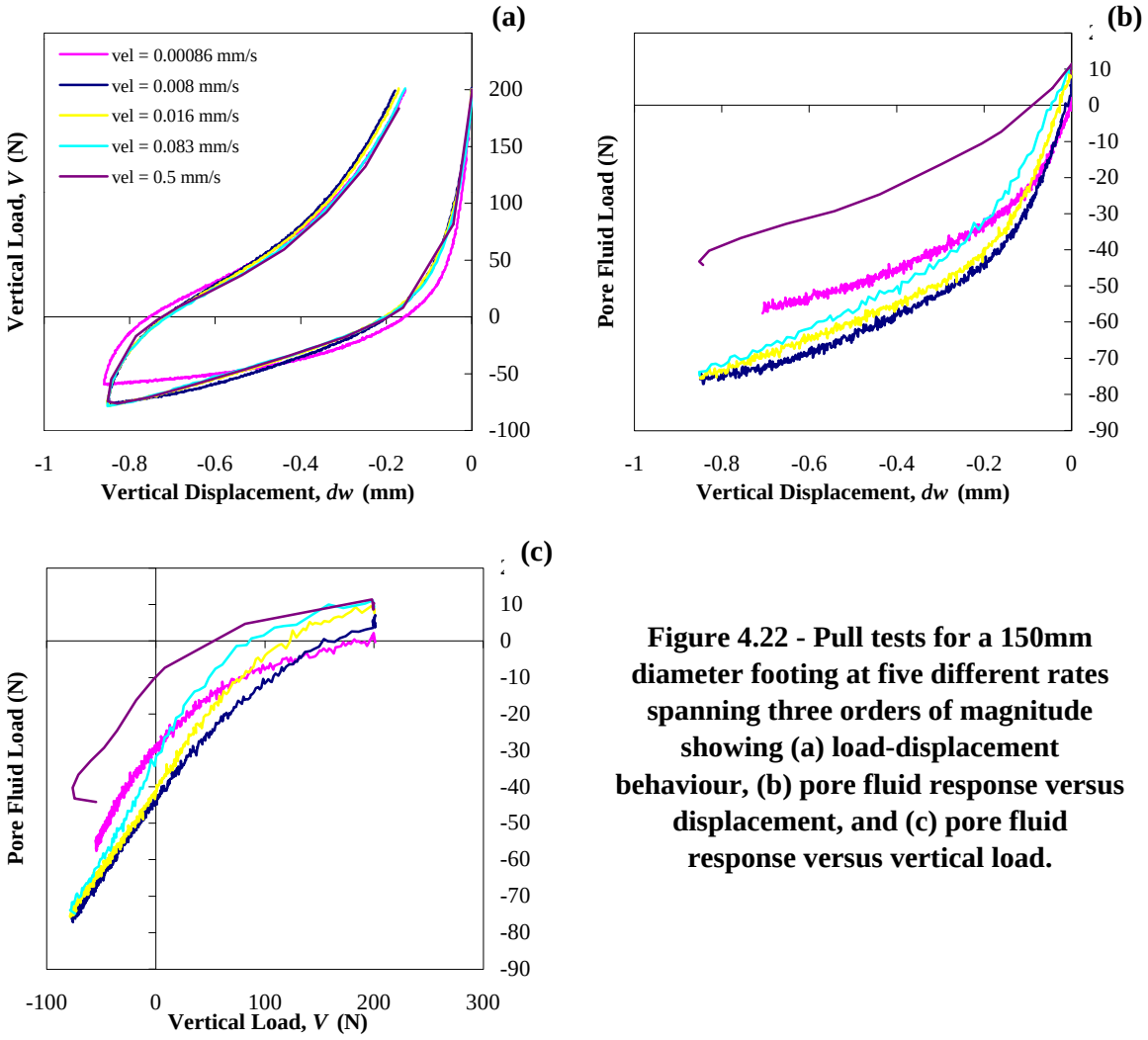

Figure 4.22 - Pull tests for a 150mm diameter footing at five different rates spanning three orders of magnitude showing (a) load-displacement behaviour, (b) pore fluid response versus displacement, and (c) pore fluid response versus vertical load.

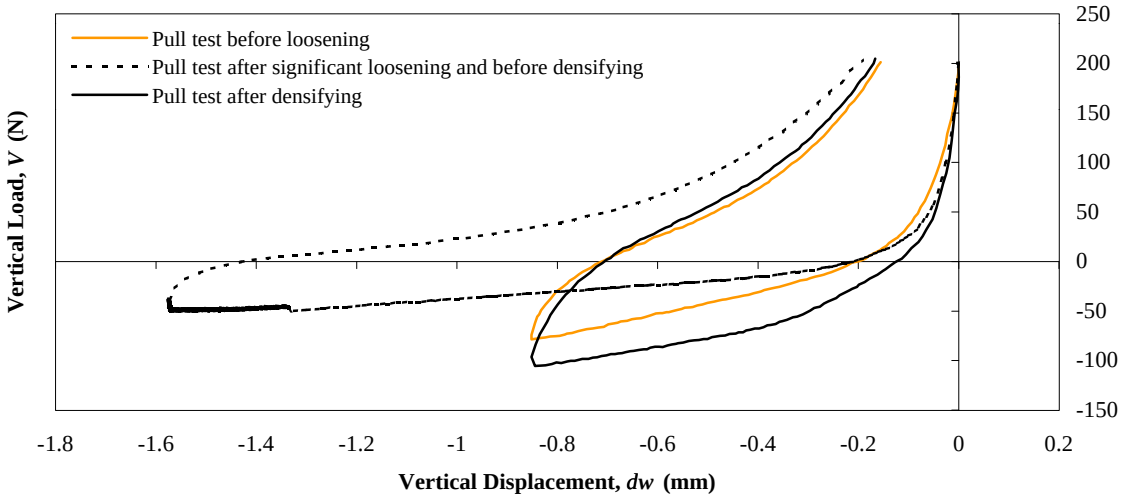

Figure 4.23 - Comparison of three different pull tests performed at the same rate on the same footing after differing degrees of loading history showing the effect of local density.

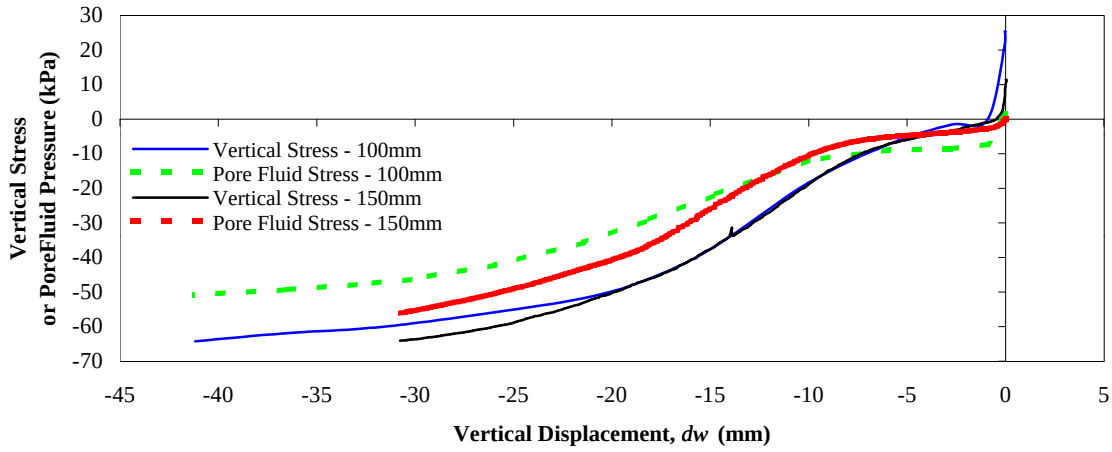

Figure 4.24 - Comparison of two different pull tests undertaken on different diameter footings taken to very large displacements.

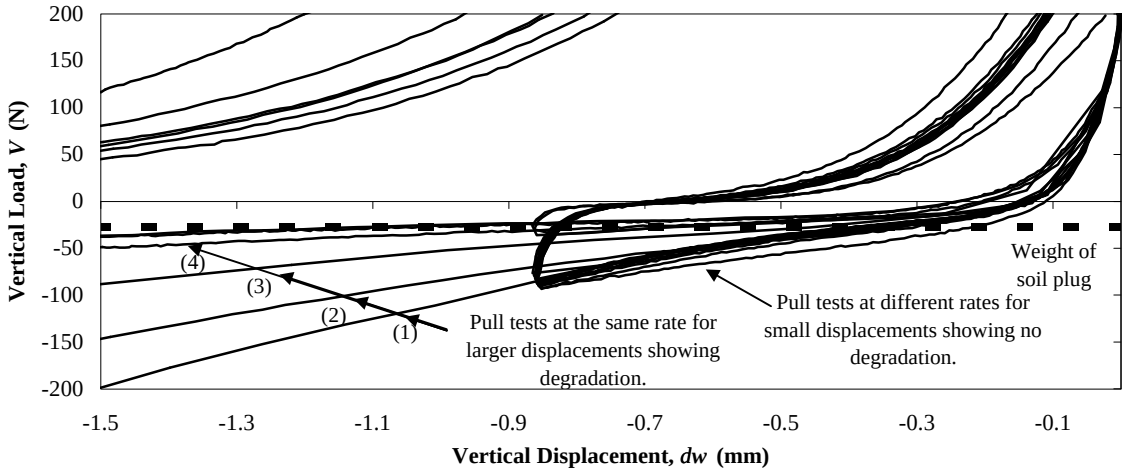

Figure 4.25 - Multiple pull tests showing degradation of response upon repeated application.

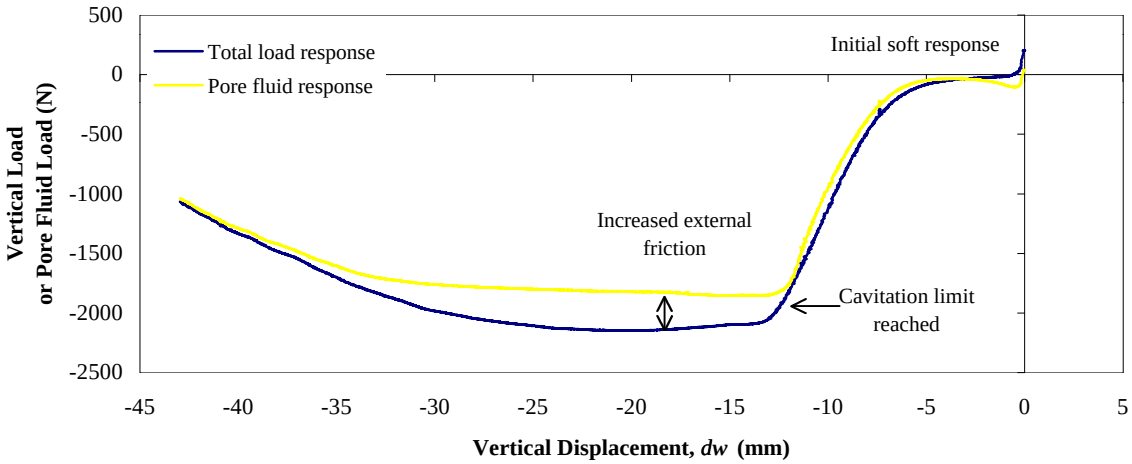

Figure 4.26 - Pull test taken to the cavitation limit on a denser sand (150mm diameter footing).

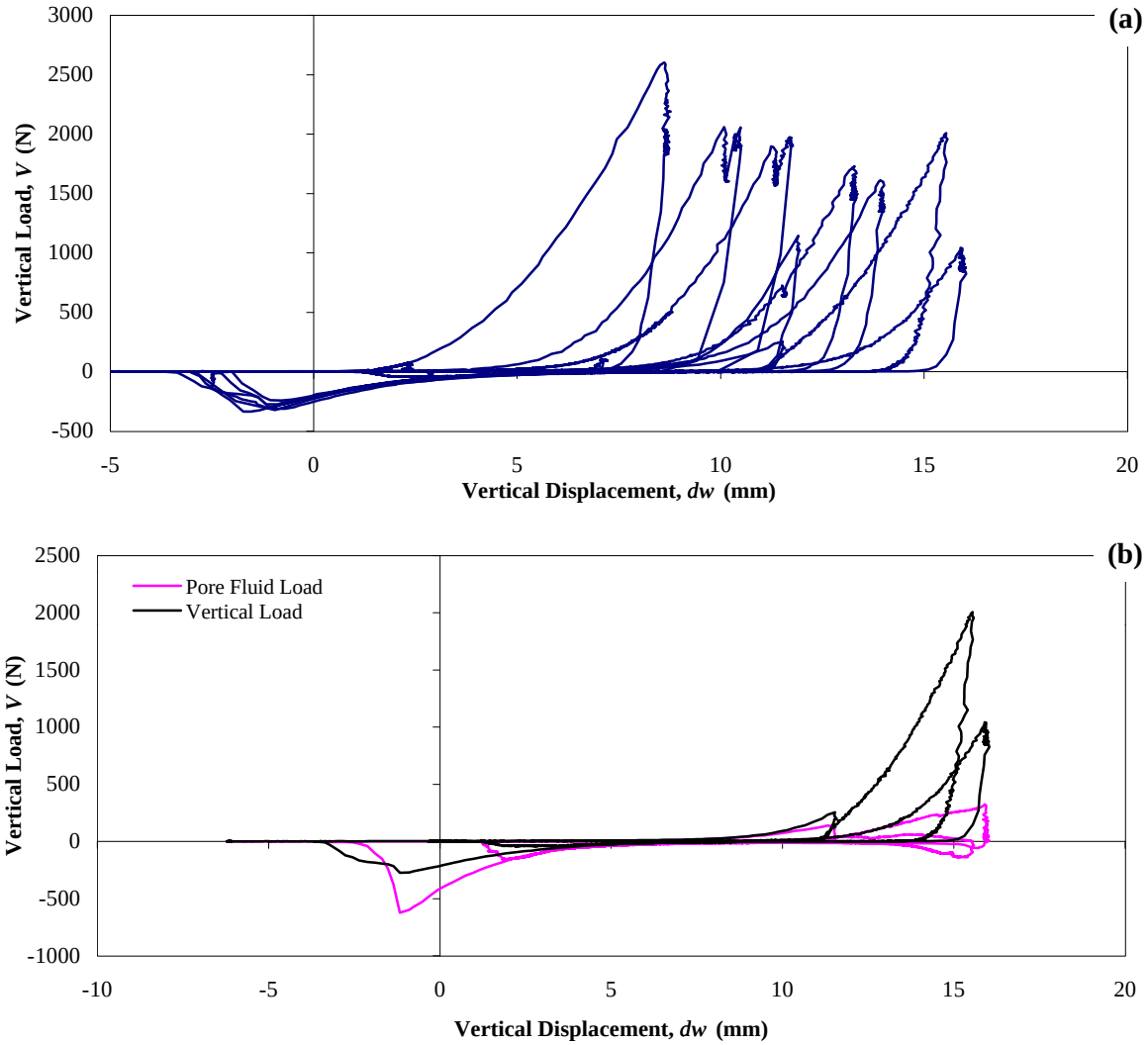

Figure 4.27 - Results from monotonic penetration and pull tests for a 100mm flat footing where (a) the load displacement paths of successive penetrations and pulls, and, (b) the pore fluid response.

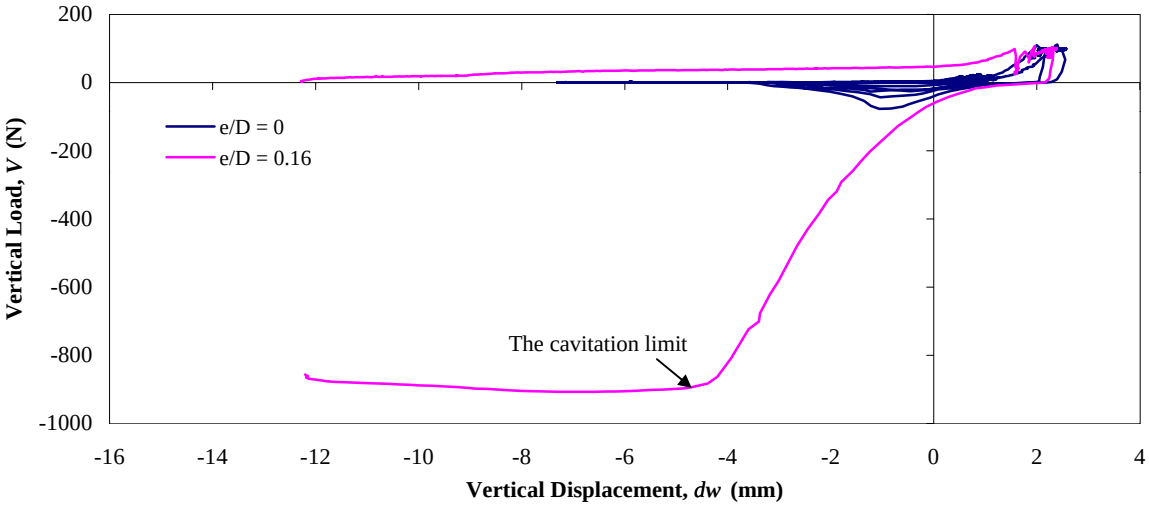

Figure 4.28 - The comparison of the load displacement response of a flat footing and a skirted footing with an embedment ratio of 0.16.

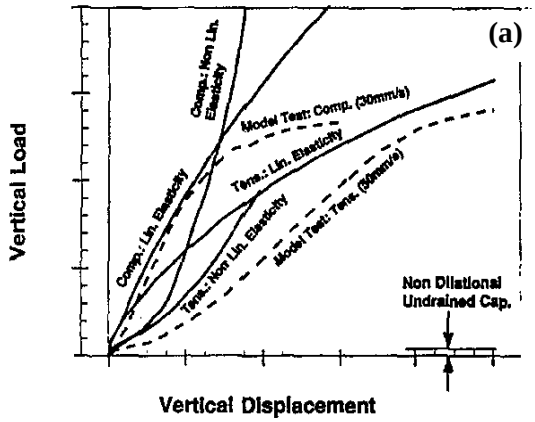

FIGURE 2.6
UNDRAINED COMPRESSION & TENSION

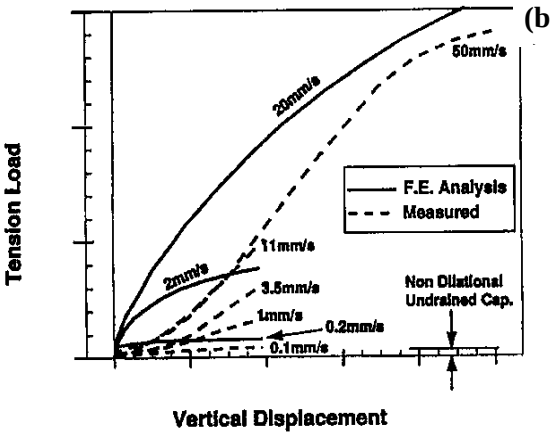

FIGURE 2.7
TENSION CAPACITY: EFFECT OF LOAD RATE

Figure 4.29 - Monotonic pull test results from Bye *et. al.* (1995) indicating softened response at low displacements

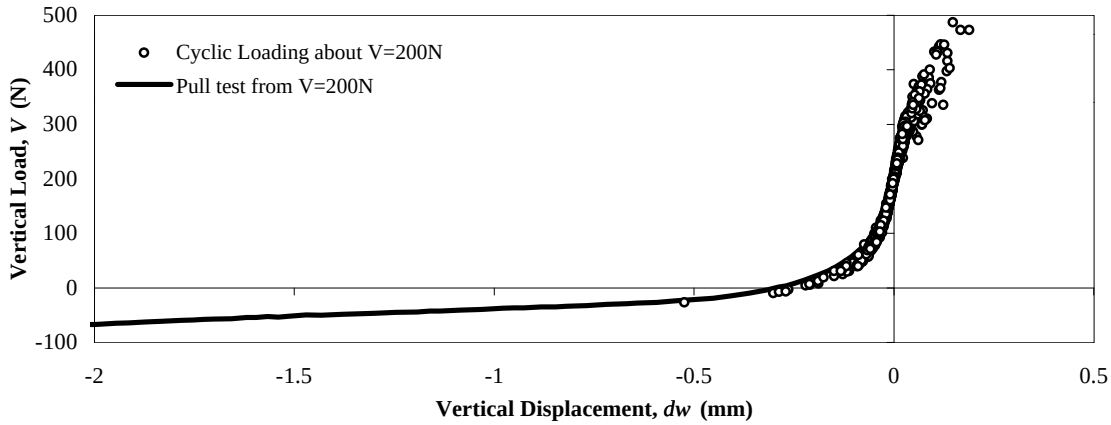

Figure 4.30 - Comparison of a pull test with the results from a vertical cyclic load test.

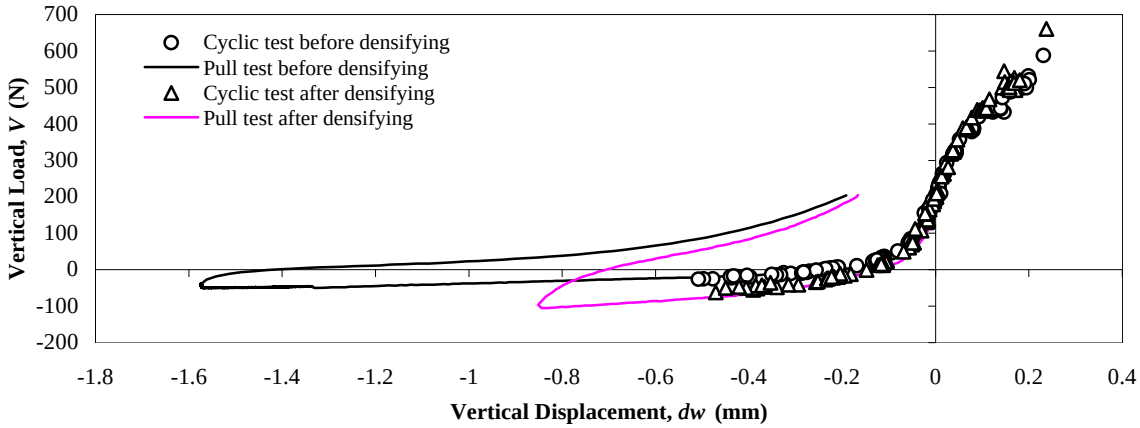

Figure 4.31 - Comparison of pull tests and cyclic load tests performed before and after densifying showing excellent agreement.

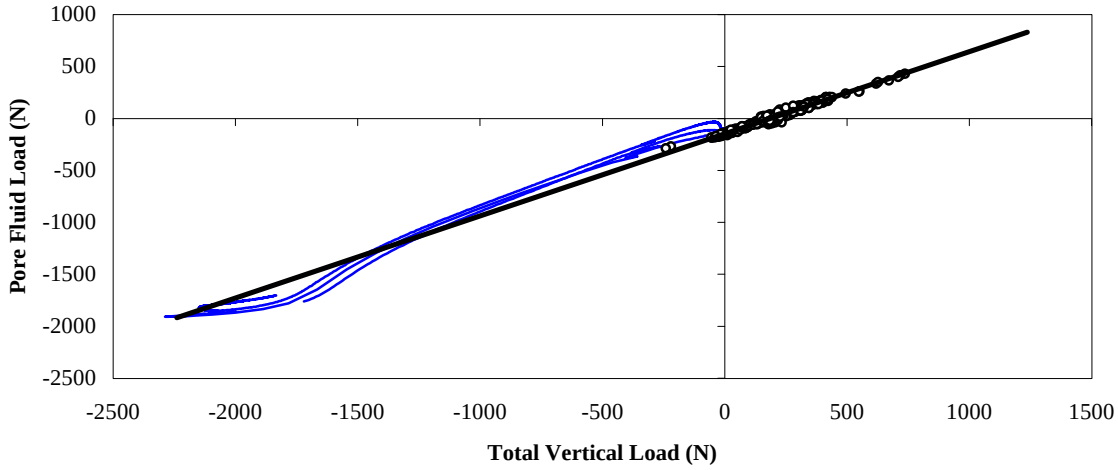

Figure 4.32 - Accumulation of pore fluid load response against total load for cyclic loading tests and monotonic pull tests. Best fit trend line shown pore fluid load ~ 80% total load.

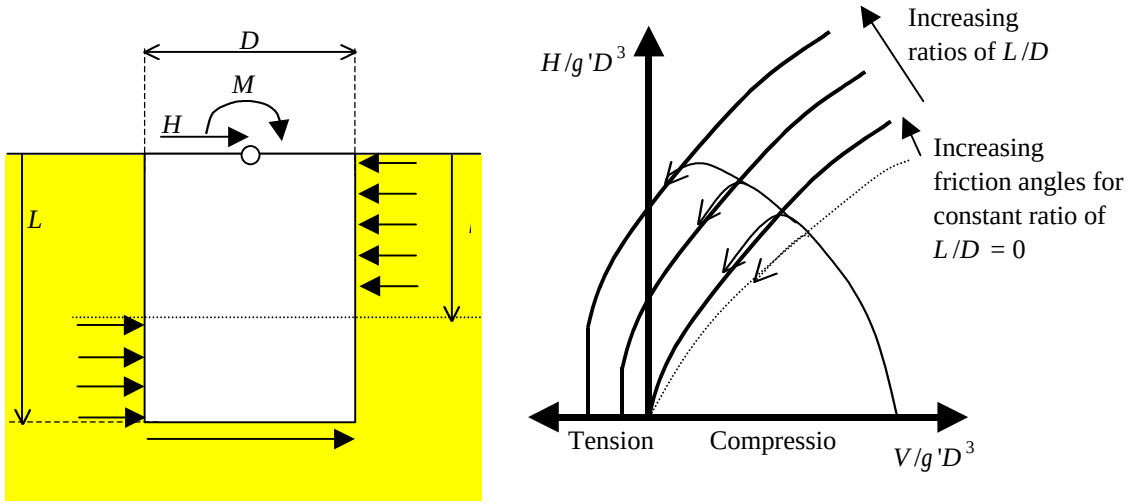

Figure 5.1 - Simplified mechanism of load transfer for a caisson under zero vertical load and the effects of skirt depth and friction angle on the horizontal response.

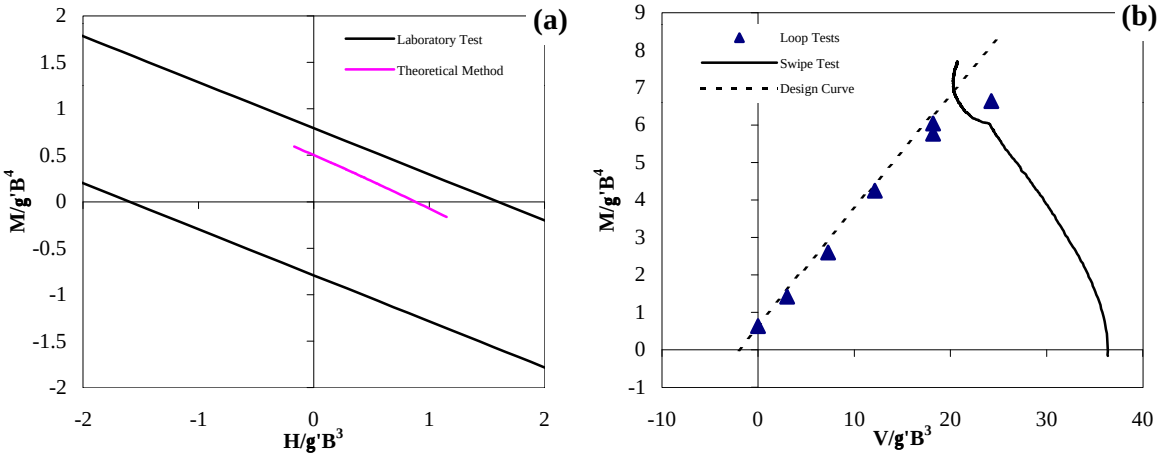

Figure 5.2 - Observed experimental response for a caisson (a) under small vertical loads in {M:H} space, and, (b) the increase in moment capacity as the vertical load increases.

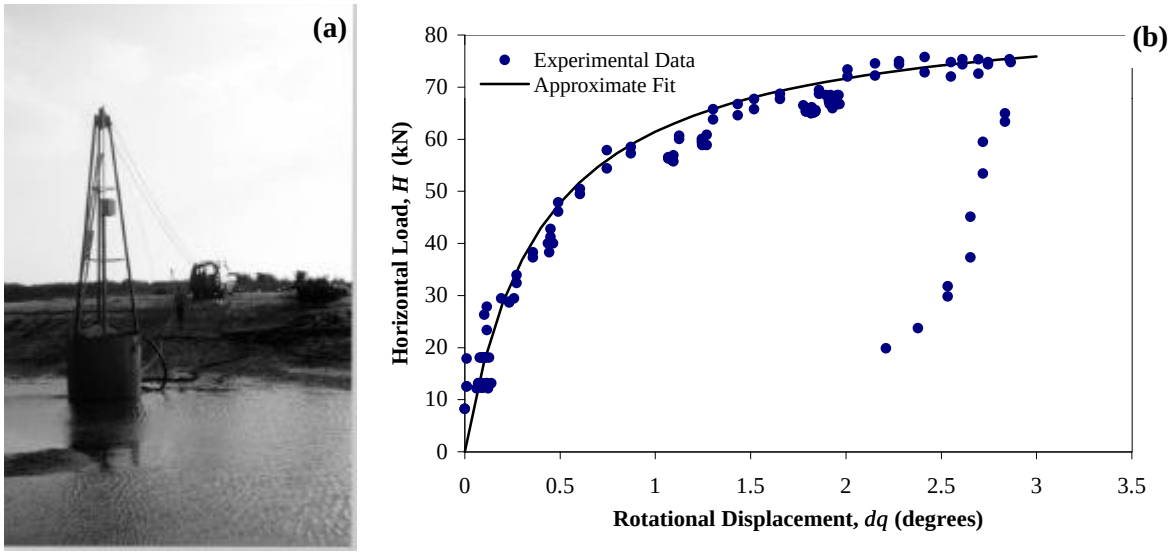

Figure 5.3 - Field scale tests of caisson subjected to overturning moments (a) field set-up prior to caisson installation, and, (b) hyperbolic load displacement response.

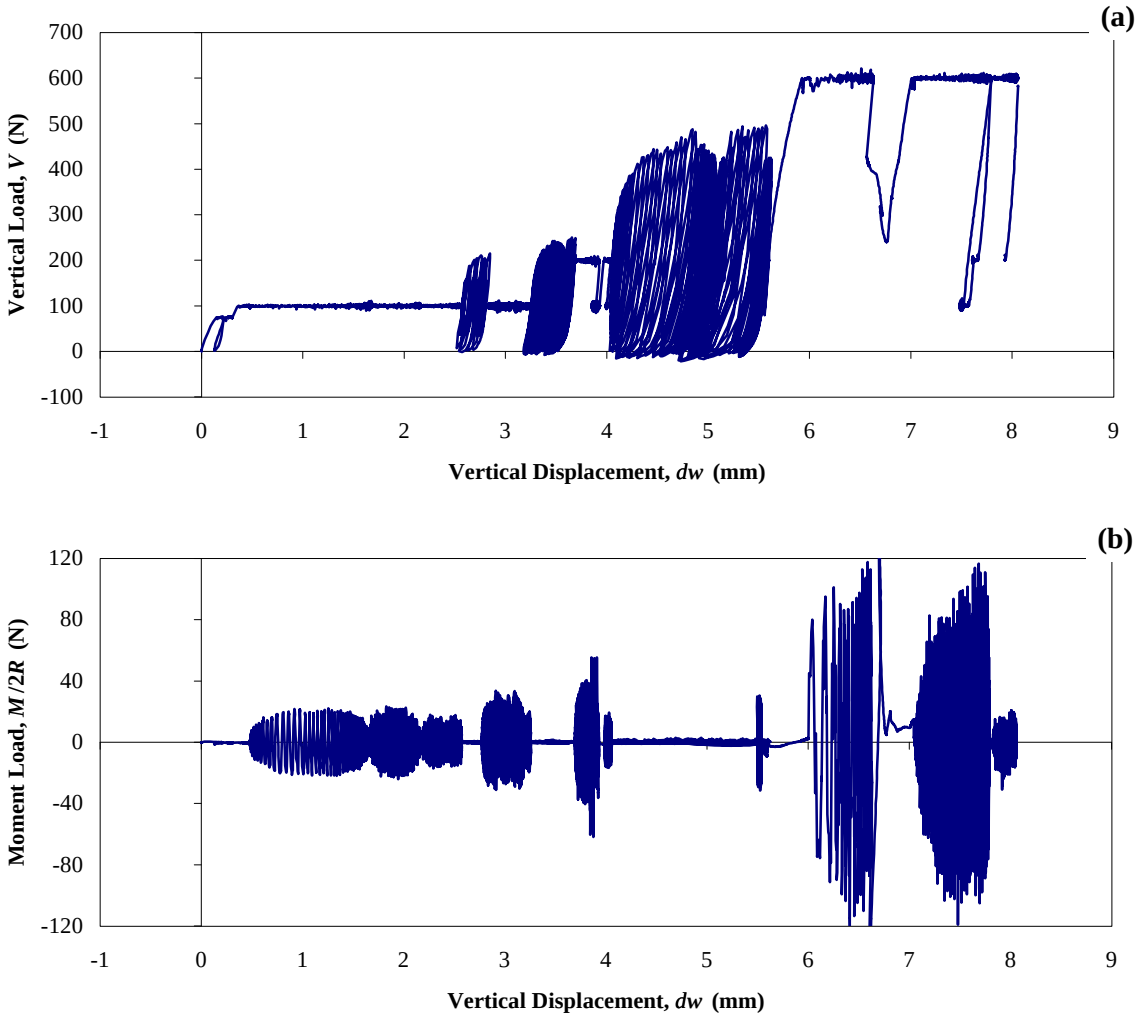

Figure 5.4 - A typical test sequence which includes (a) vertical cyclic loading, and, (b) moment cyclic loading, both plotted against vertical displacement.

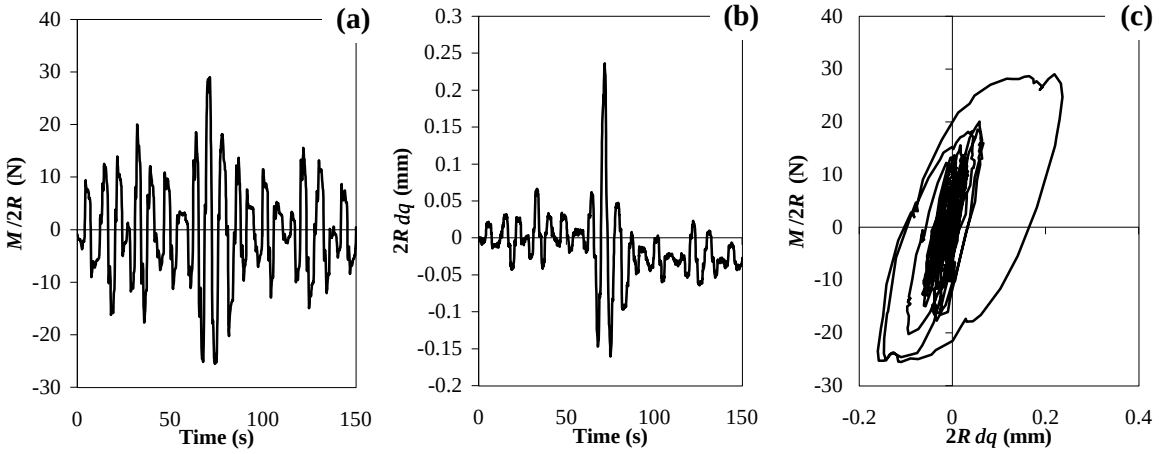

Figure 5.5 - A typical pseudo random (a) loading time history, (b) corresponding displacement response, and, (c) the load displacement behaviour showing increasing hysteresis for large cycles.

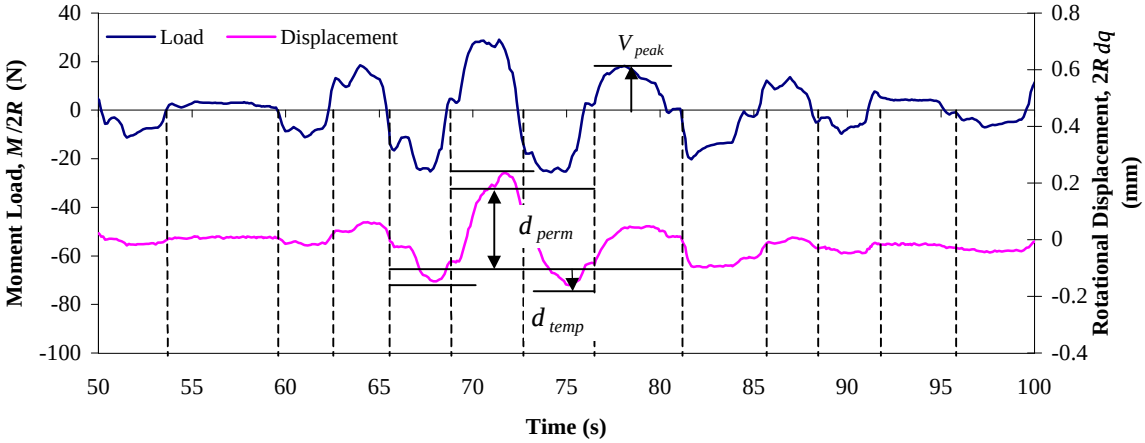

Figure 5.6 - Methodology used for reduction of cyclic data.

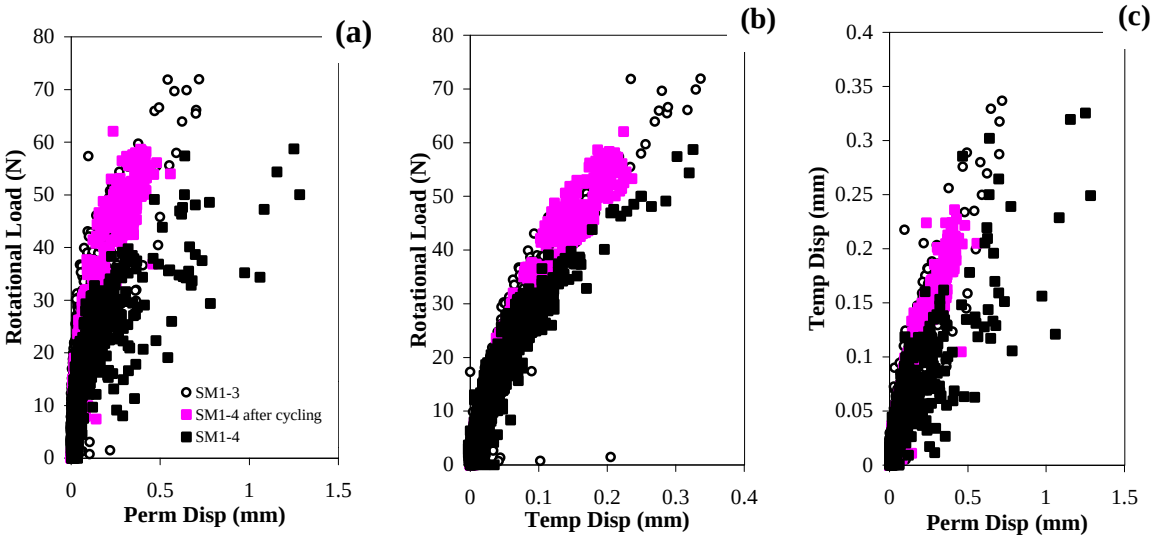

Figure 5.7 - Reduced data from several cyclic loading tests showing (a) permanent displacements, (b) temporary displacements, and (c) displacement relationship.

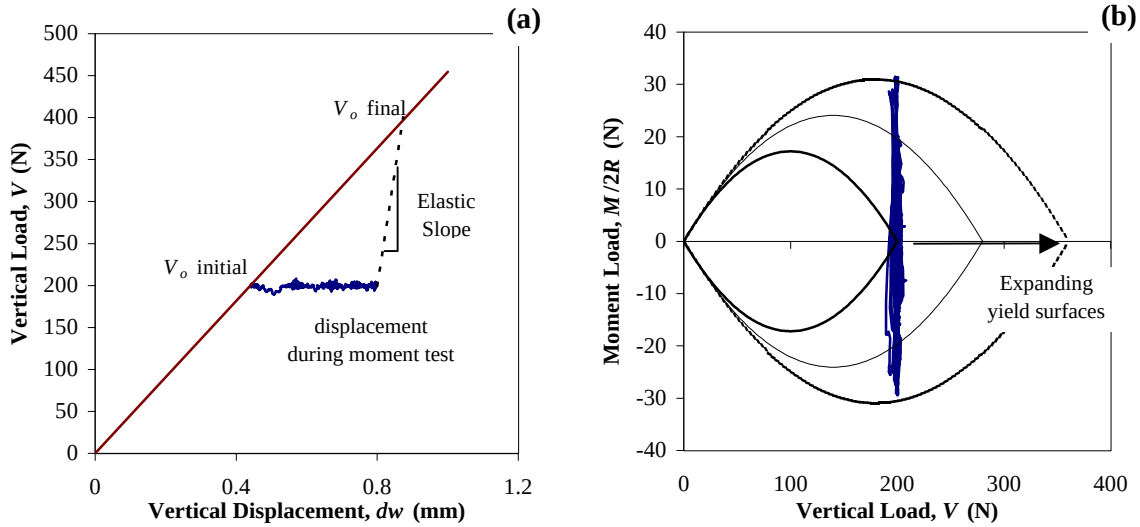

Figure 5.8 - Initial moment loading showing (a) vertical displacement during test, and, (b) interpretation of behaviour with yield surface framework.

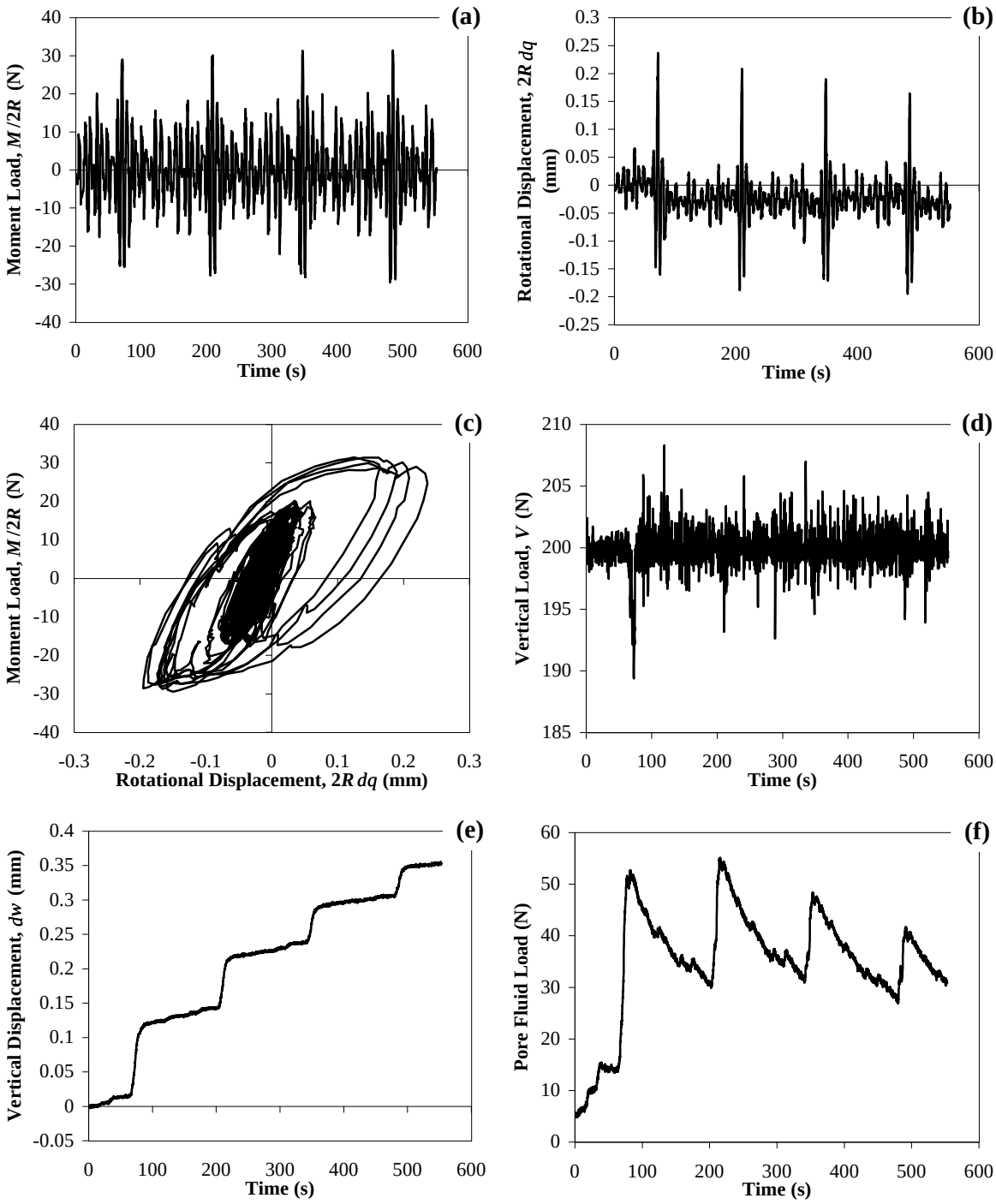

Figure 5.9 - Initial moment loading showing (a) moments applied to foundation, (b) resulting displacement path, (c) the load displacement response, (d) the applied "constant" vertical load, (e) resulting vertical displacement, and, (f) pore fluid load.

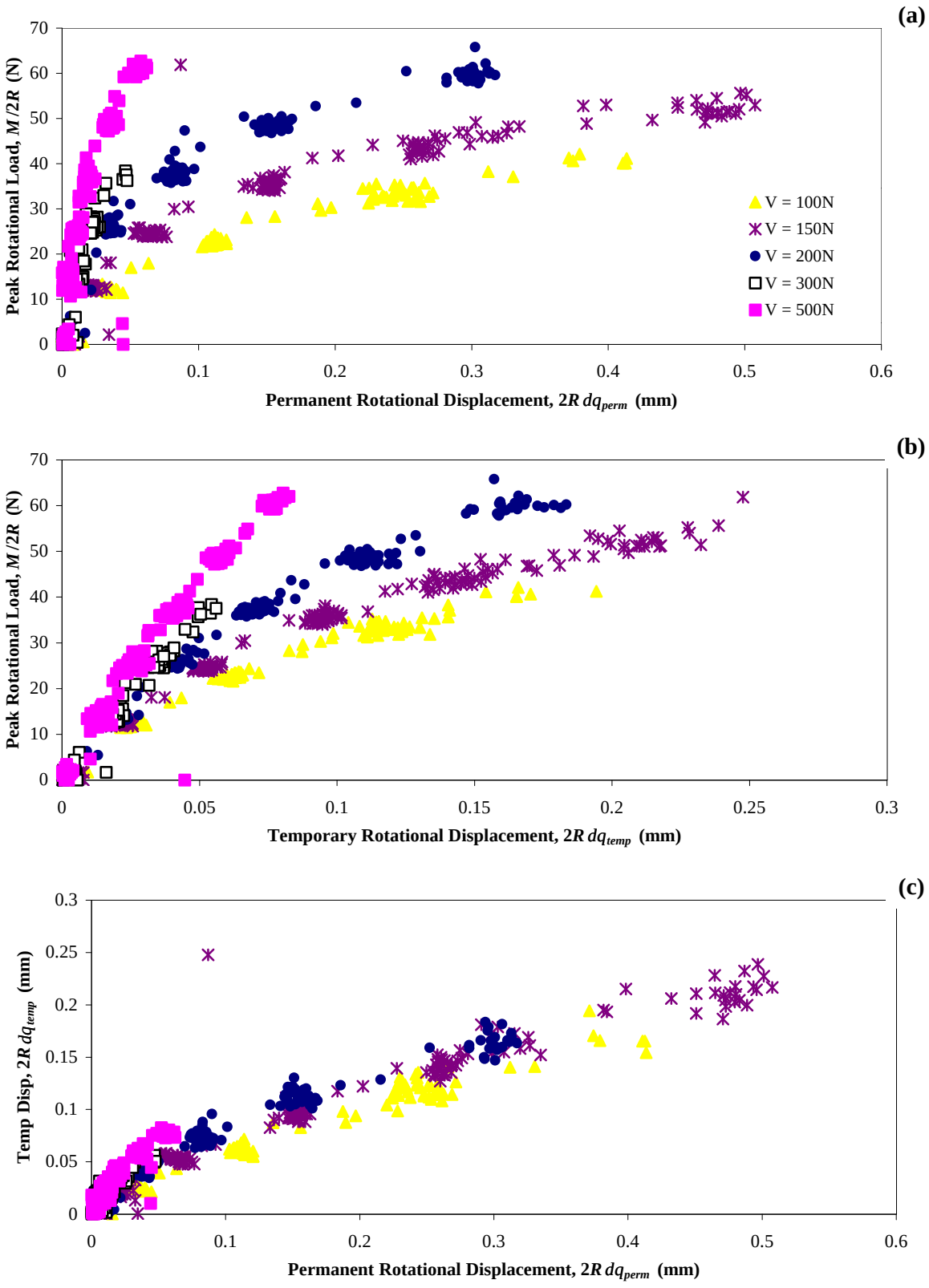

Figure 5.10 - Results from tests conducted at different values of overconsolidation ratio showing the effect of vertical load on rotational response, (a) permanent displacements, (b) temporary displacements, and, (c) displacement relationship.

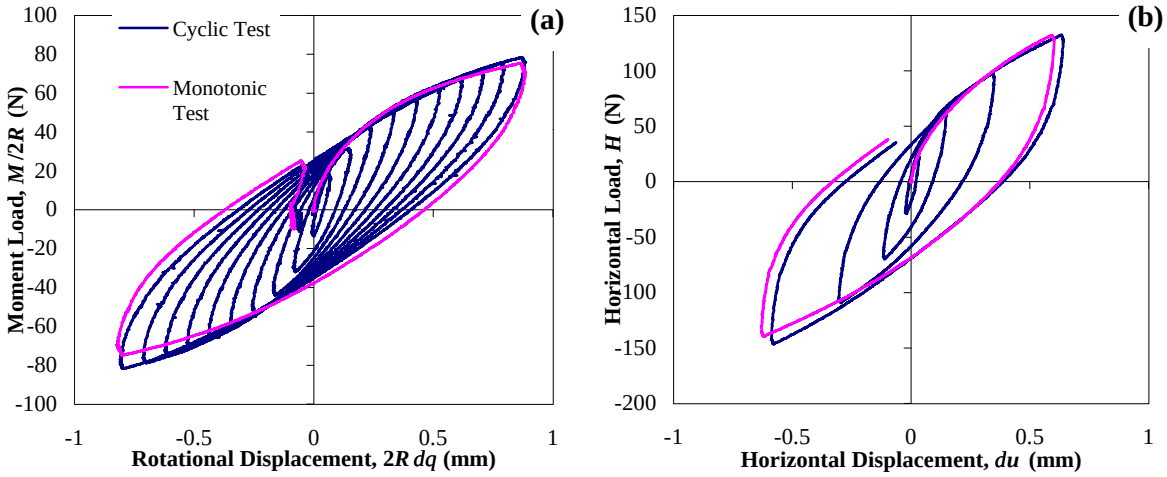

Figure 5.11 - Comparison of monotonic and cyclic tests for both (a) moment loading, and, (b) horizontal loading.

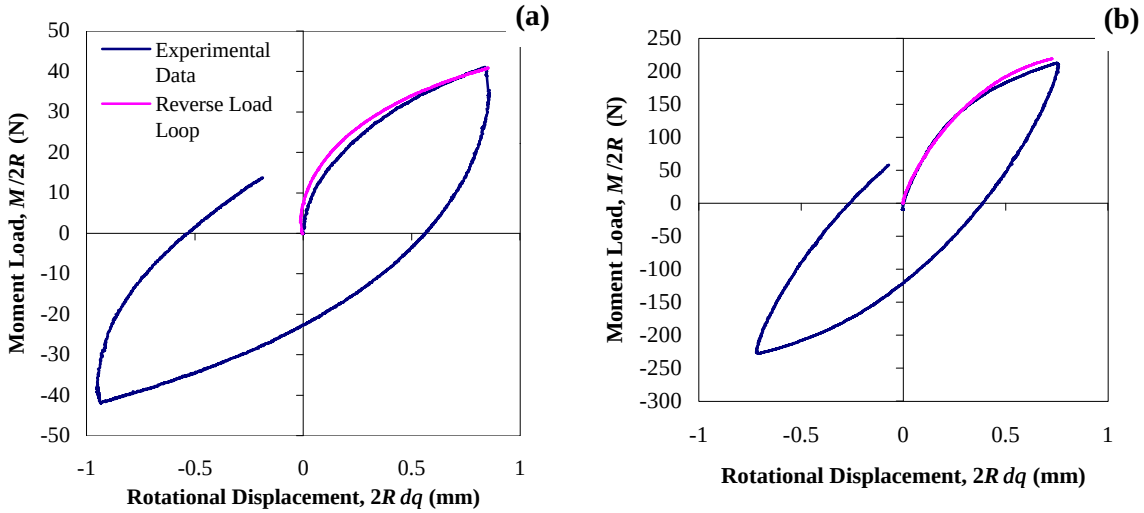

Figure 5.12 - Comparison of the reverse loading loop with the initial loading for moment loading as a check for Masing behaviour

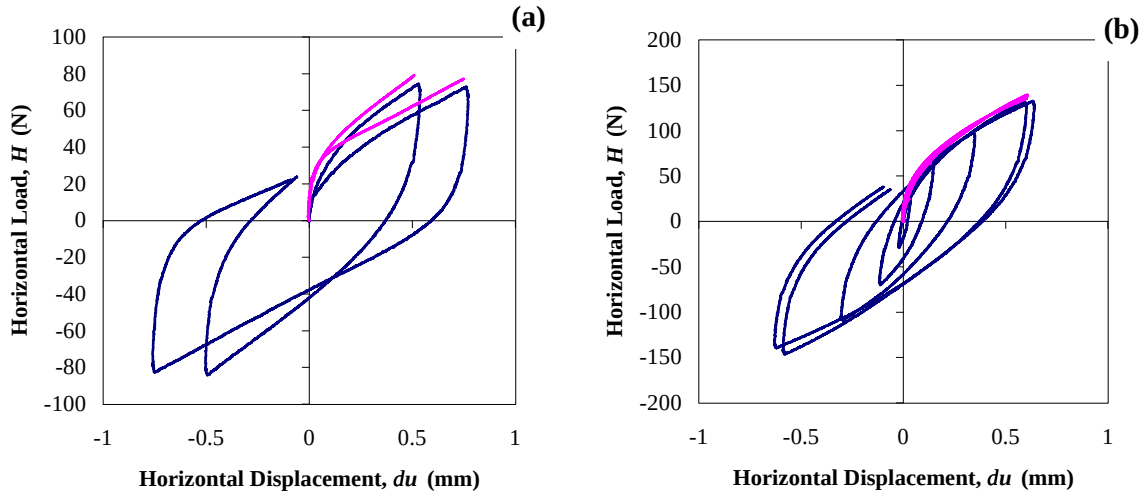

Figure 5.13 - Comparison of the reverse loading loop with the initial loading for horizontal loading as a check for Masing behaviour

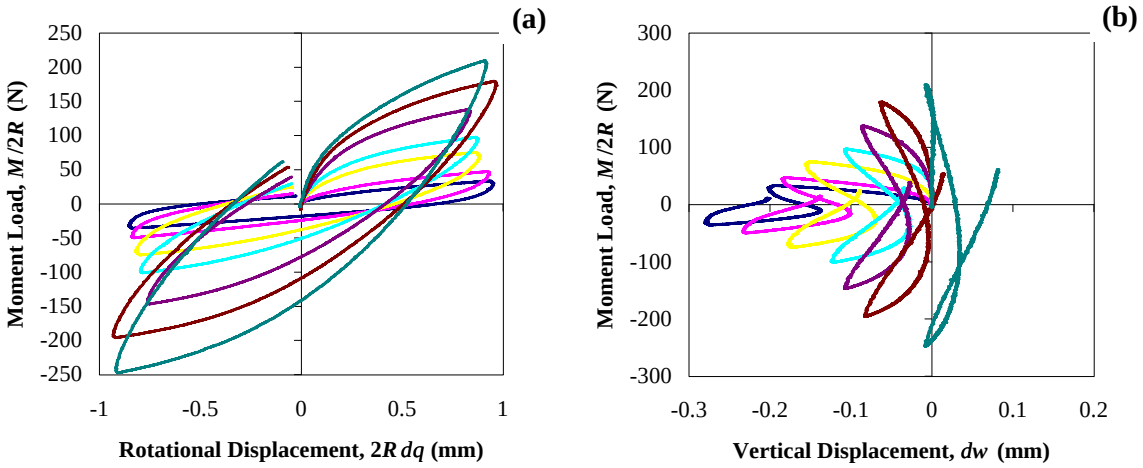

Figure 5.14 - Results from monotonic moment rotation tests under different constant vertical loads. As the vertical load level increases (a) the stiffness of response increases, and (b) the heave of the footing decreases.

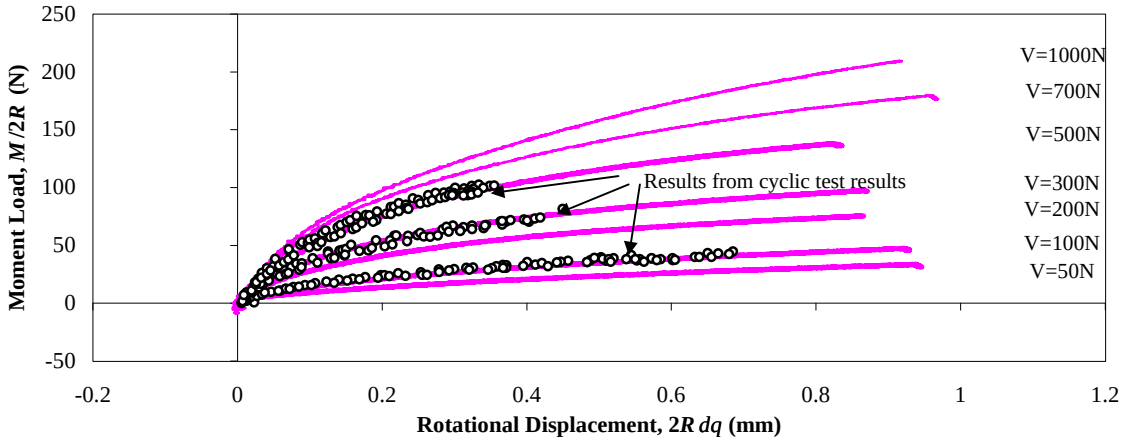

Figure 5.15 - Results from moment rotation tests at different constant vertical loads comparing to the results from cyclic tests.

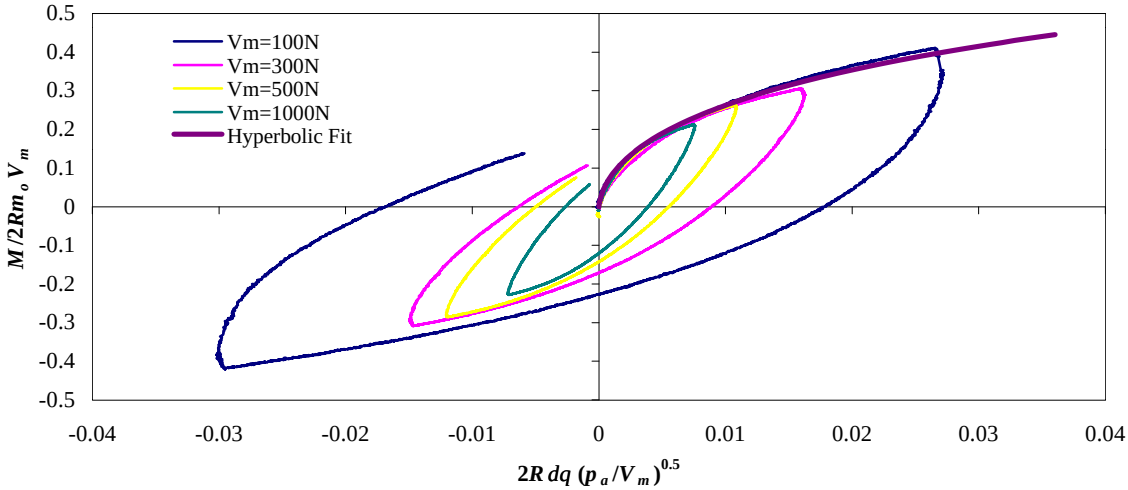

Figure 5.16 - Results from moment rotation tests at different constant vertical loads compared using an appropriate normalisation. A hyperbolic is fitted through the common backbone curve.

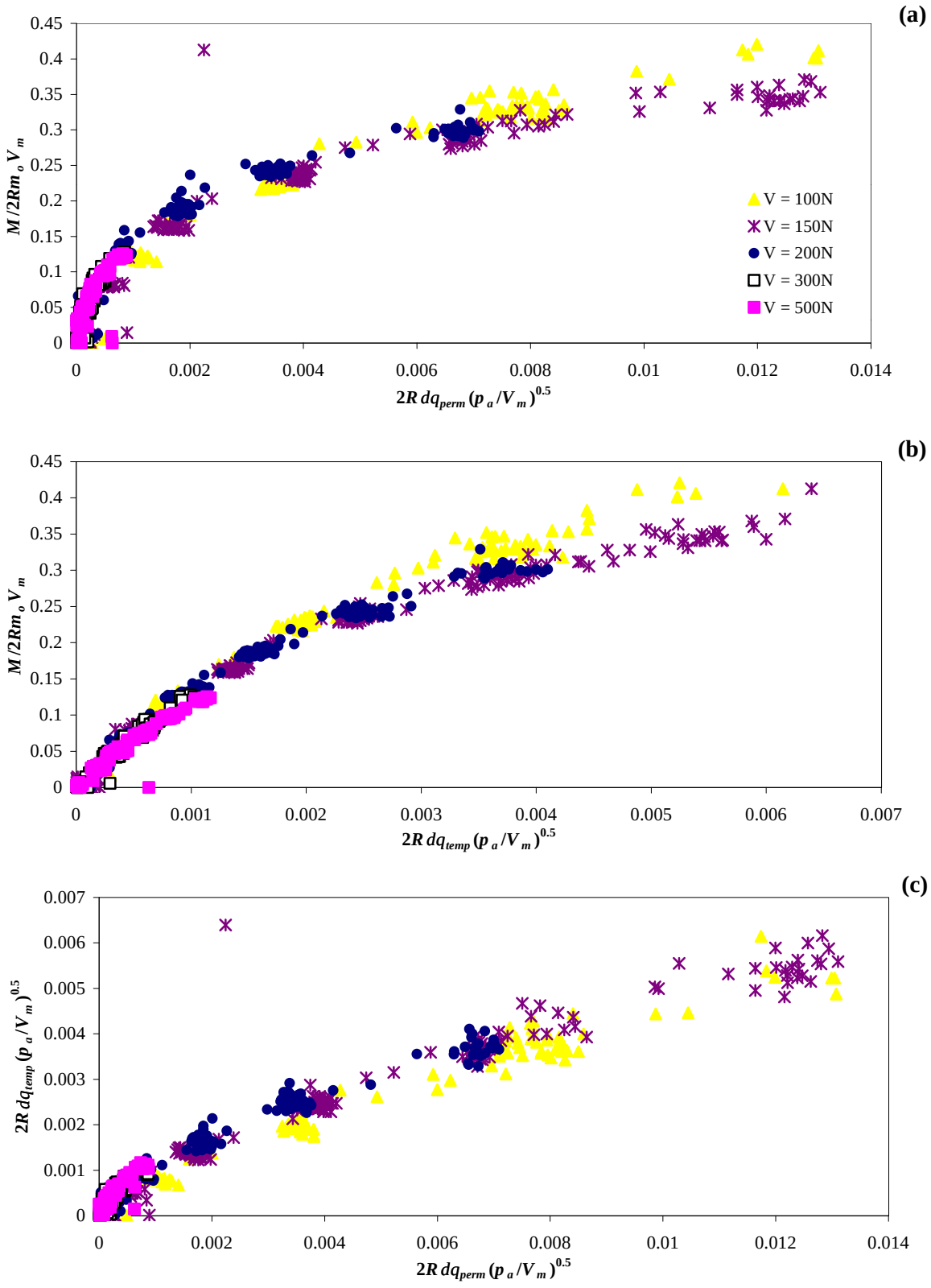

Figure 5.17 - The results shown in Figure 5.10 with the appropriate normalisation

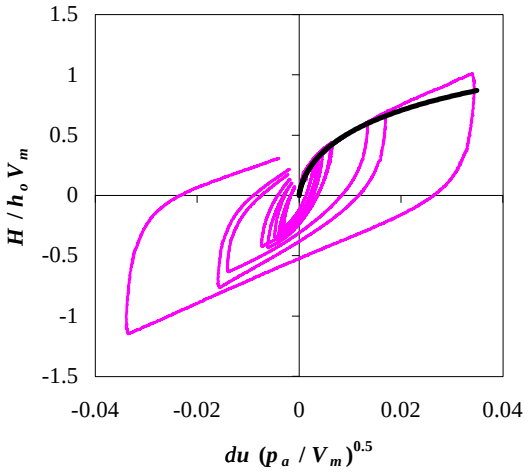

Figure 5.18 - Similar normalisations work for horizontal loading.

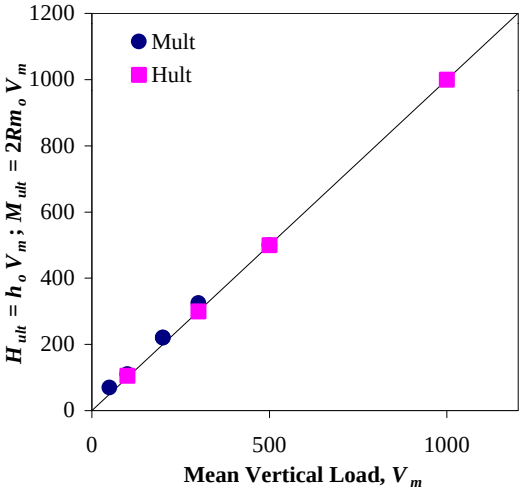

Figure 5.19 - Comparison of ultimate deviatoric loads to the mean load.

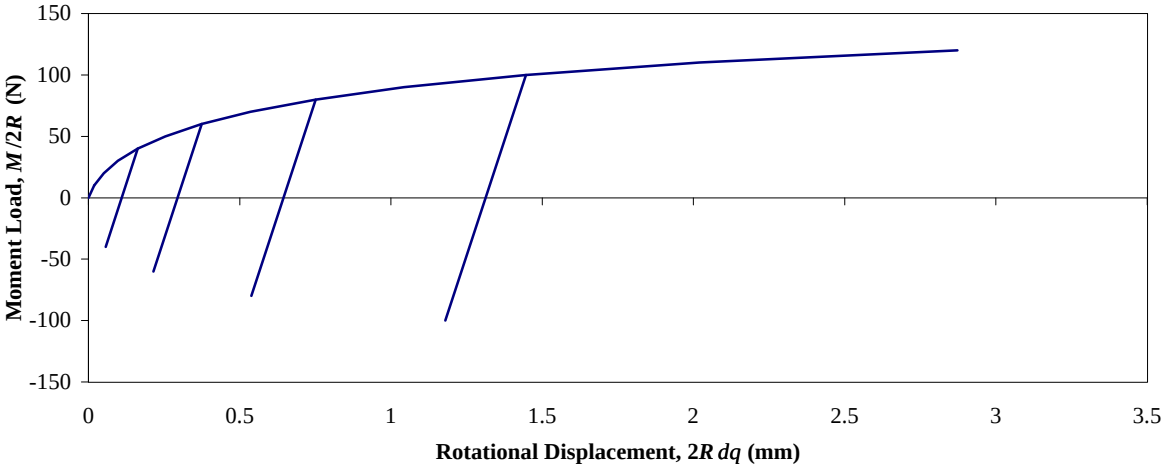

Figure 5.20 - A typical response from a typical plasticity theory for load reversals.

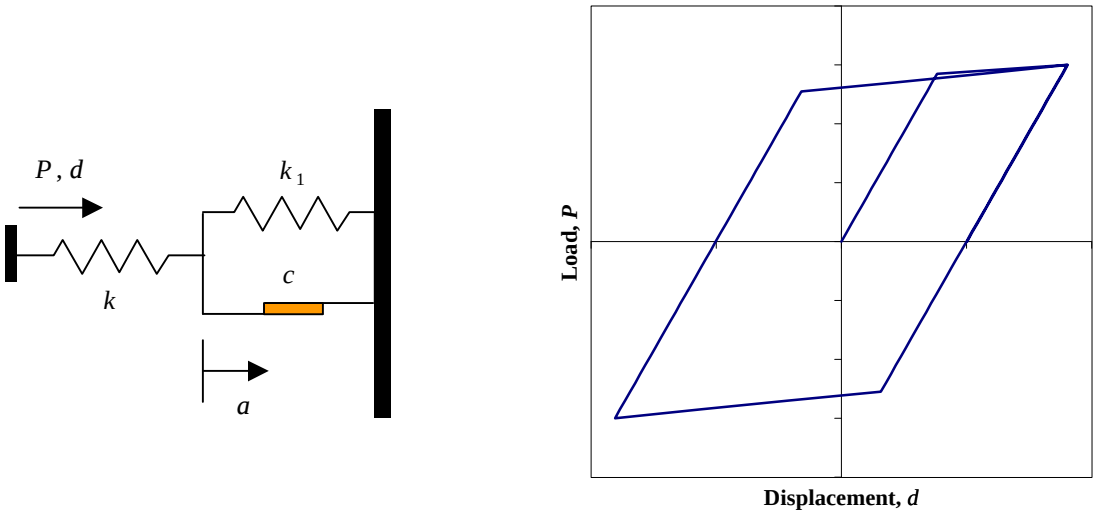

Figure 5.21 - The St Venant model and appropriate load displacement response.

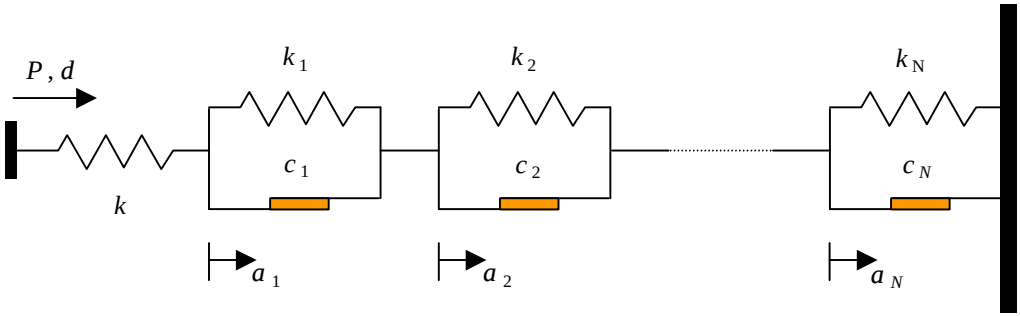

Figure 5.22 - Schematic layout of the spring-slider system of Iwan (1967).

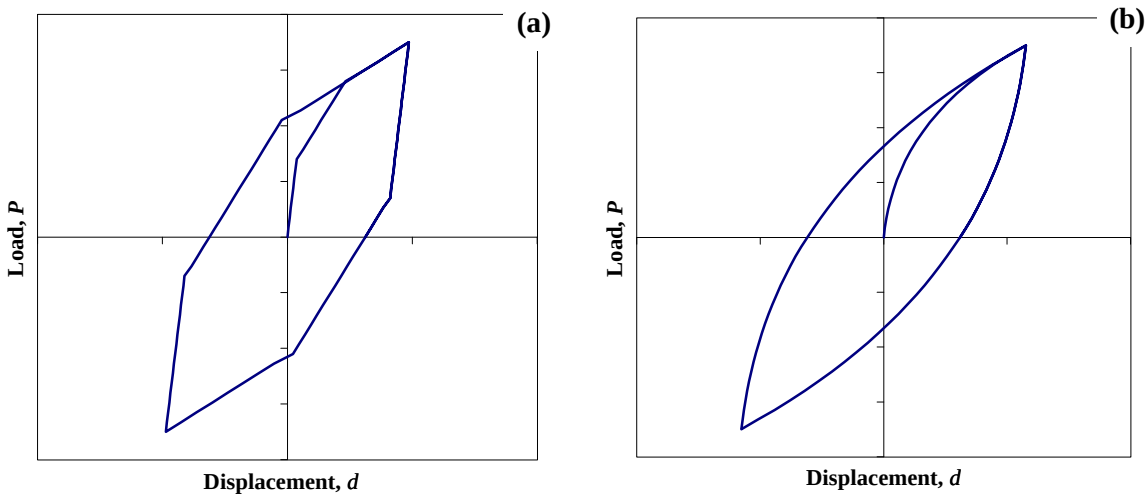

Figure 5.23 - The response of the functional model (a) for a small number of yield surfaces, and, (b) as the number of yield surfaces increases.

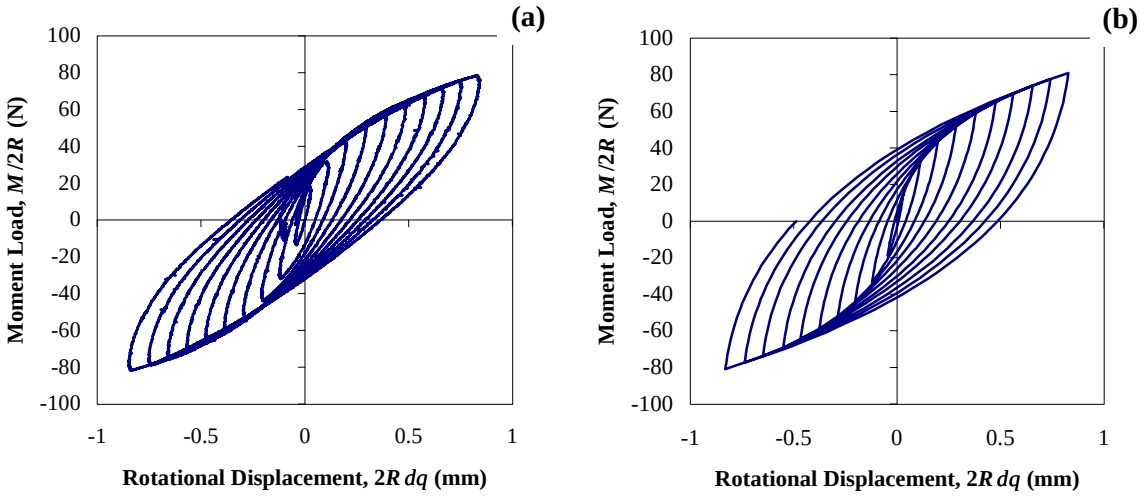

Figure 5.24 - (a) An experiment carried out where increasing cycles of stress have been applied to the foundation, and, (b) the response of the theoretical model to the same cycles of stress.

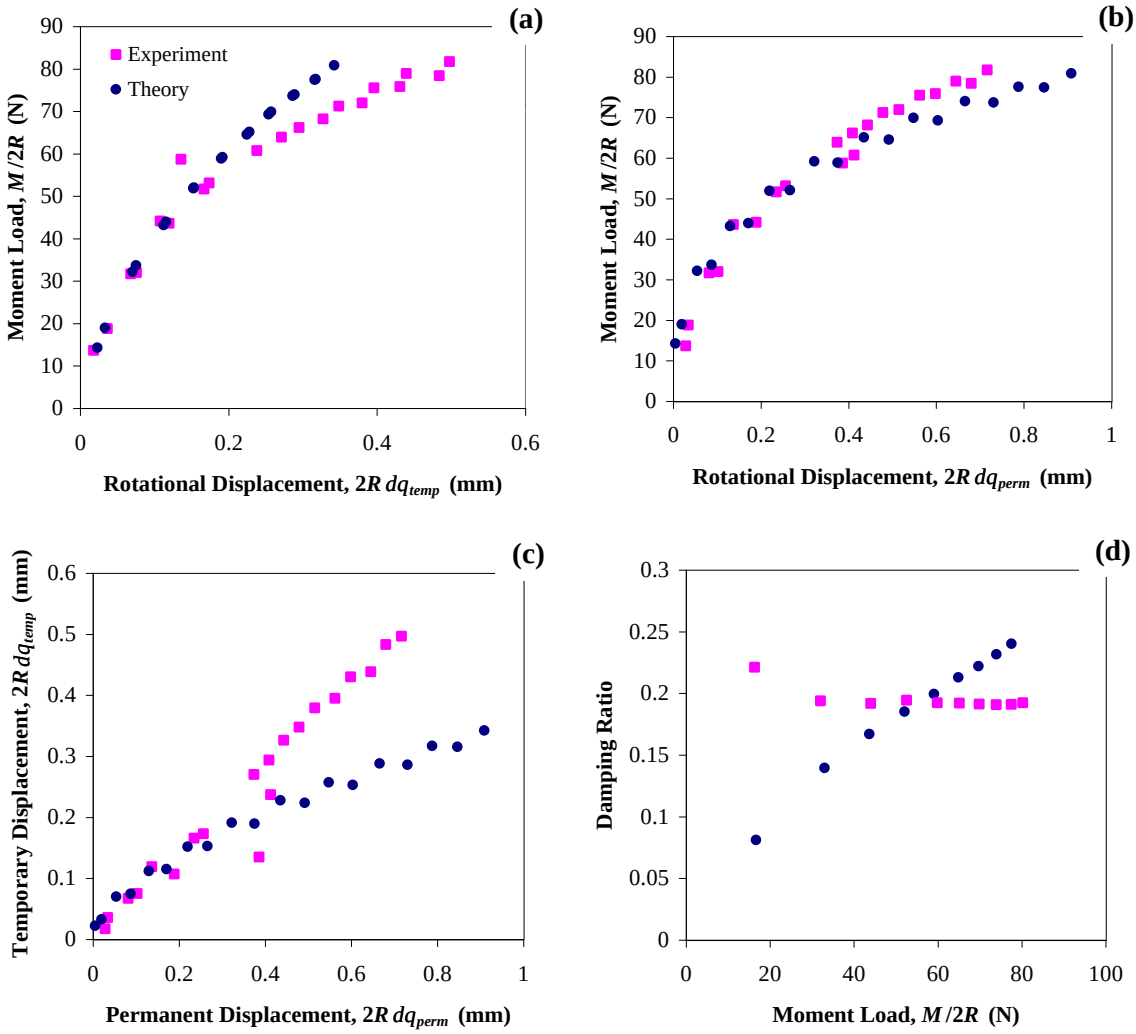

Figure 5.25 - Quantitative assessment of the performance of the functional model for the stress cycles shown in Figure 5.24; (a) the elastic response, (b) the plastic response, (c) comparing displacement responses, and, (d) the damping ratio.

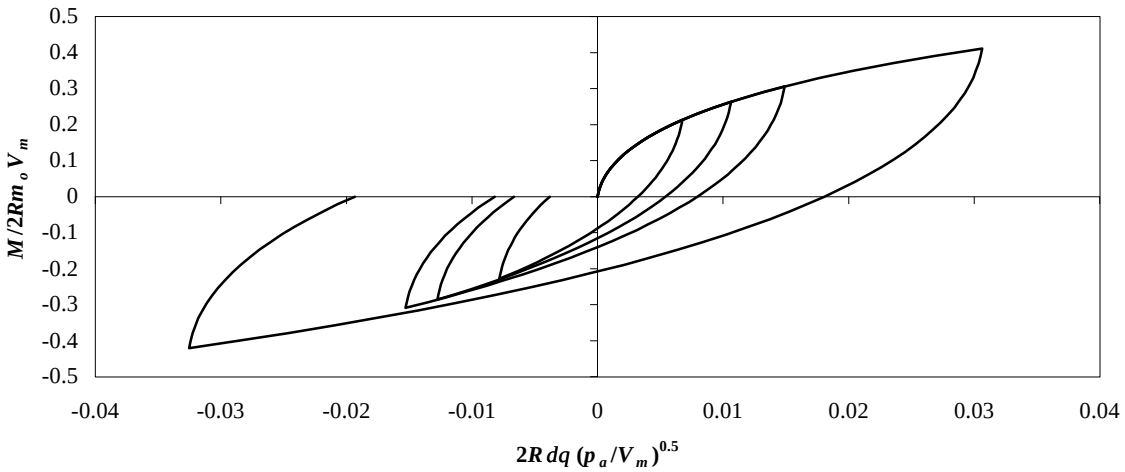

Figure 5.26 - The prediction of the functional model in normalised moment space of monotonic loops at different vertical loads.

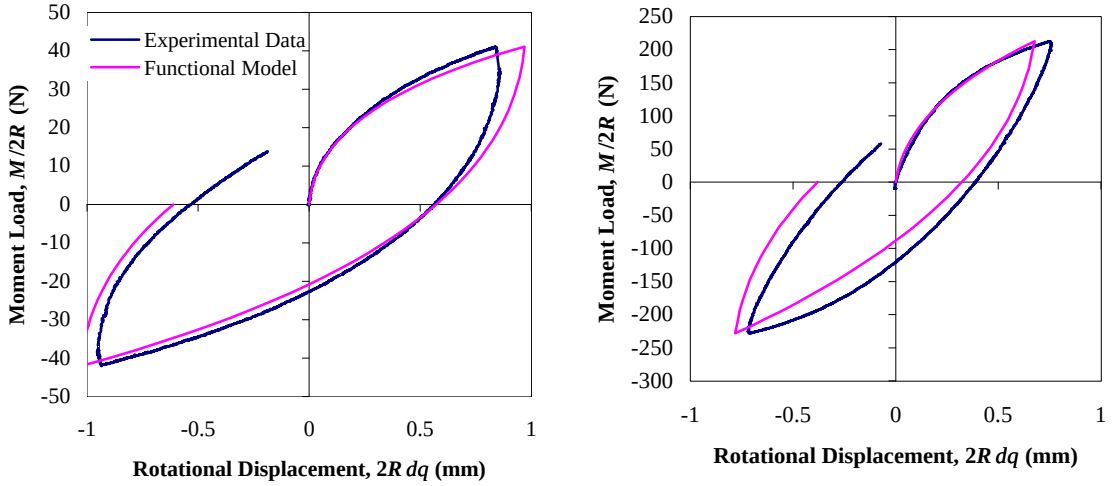

Figure 5.27 - Comparisons of scaled up moment rotation tests at different vertical load levels with the actual experimental data.

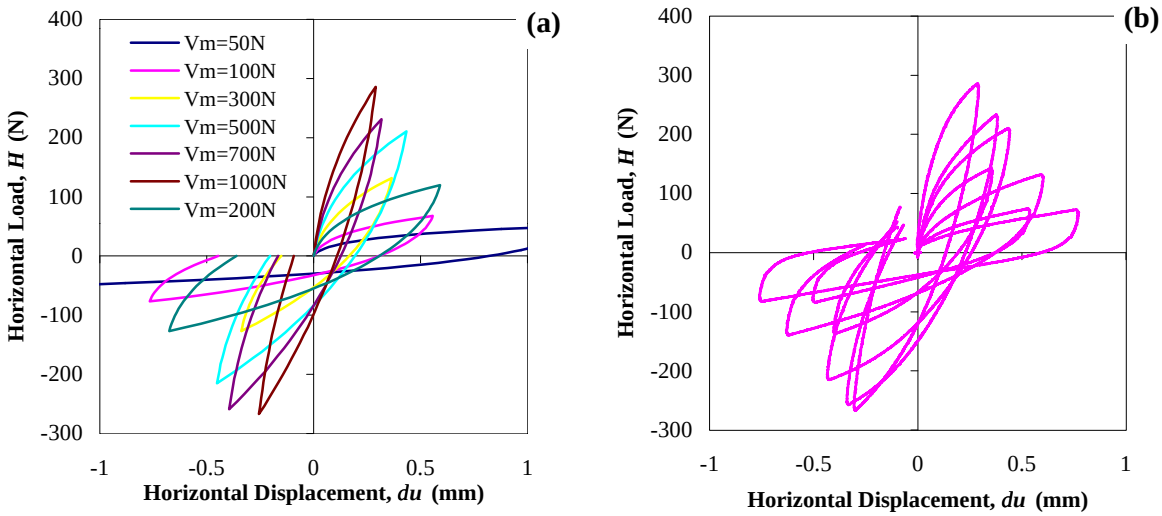

Figure 5.28 - Comparisons of (a) scaled up horizontal loading results using the hyperbolic curve shown in Figure 5.18 (b) the actual experimental data.

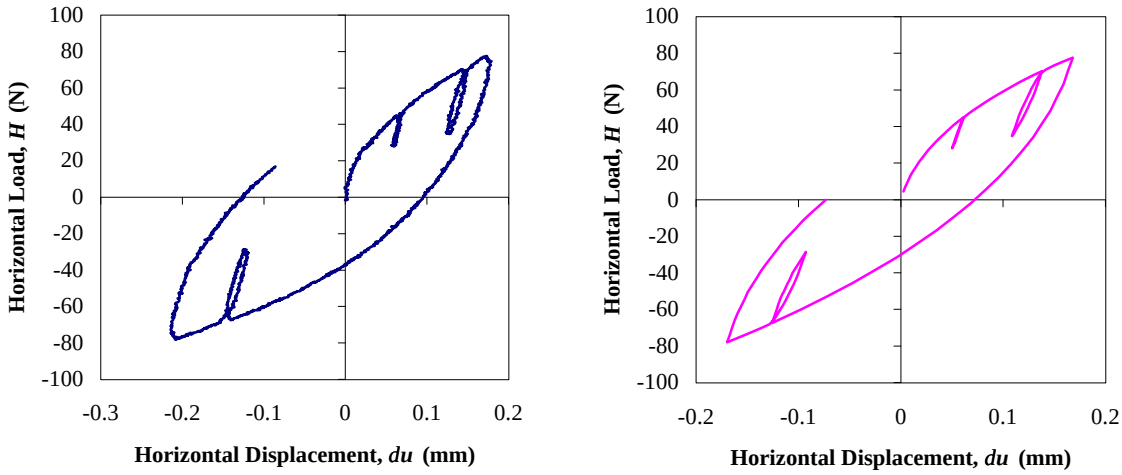

Figure 5.29 - A comparison of a horizontal loading test with small stiff unloading and reloading paths.

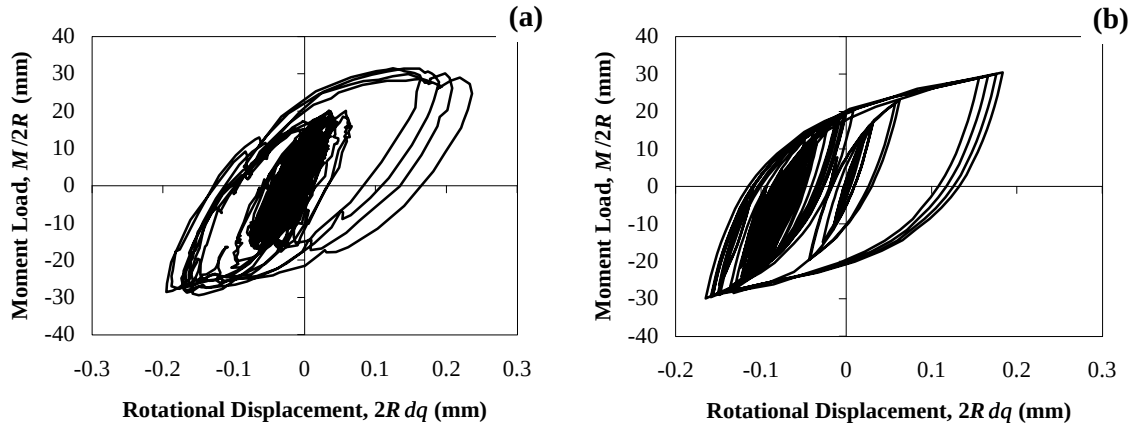

Figure 5.30 - Typical experimental load displacement response (a) and corresponding functional model response to the same stress cycles (b).

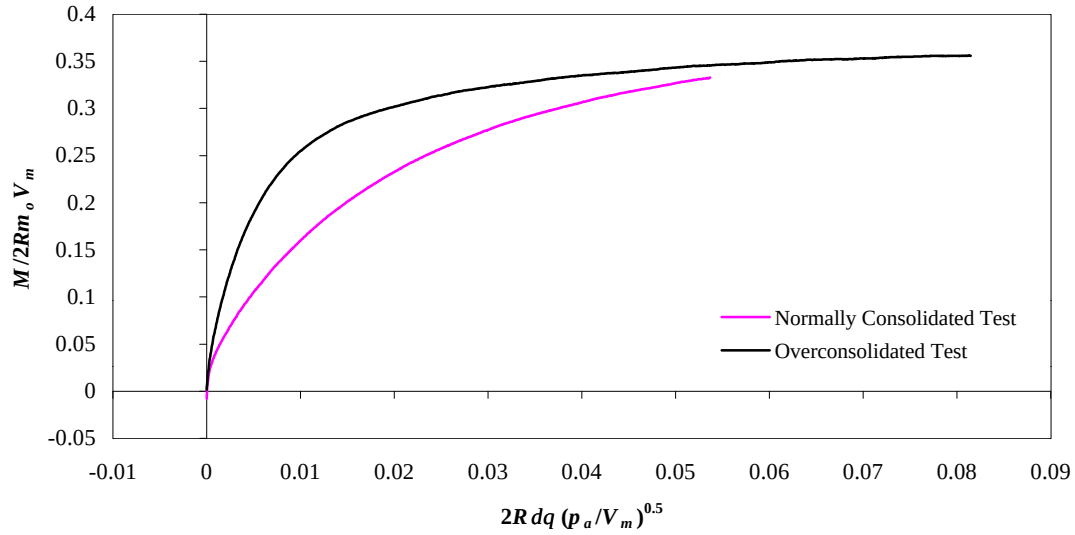

Figure 5.31 - Comparison of normally consolidated and overconsolidated constant load tests.

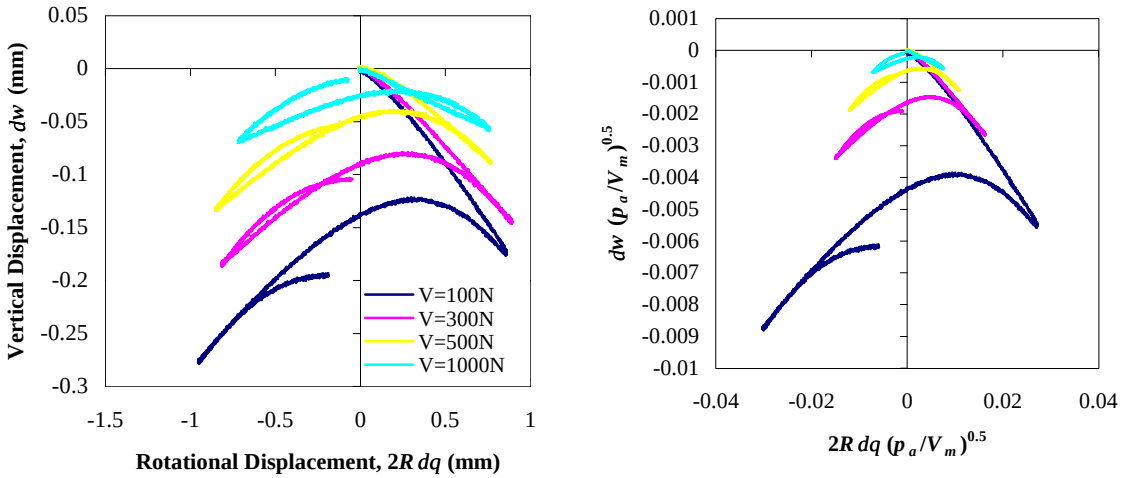

Figure 5.32 - Raw experimental results and normalised results in displacement space for moment rotation tests under constant vertical loads.

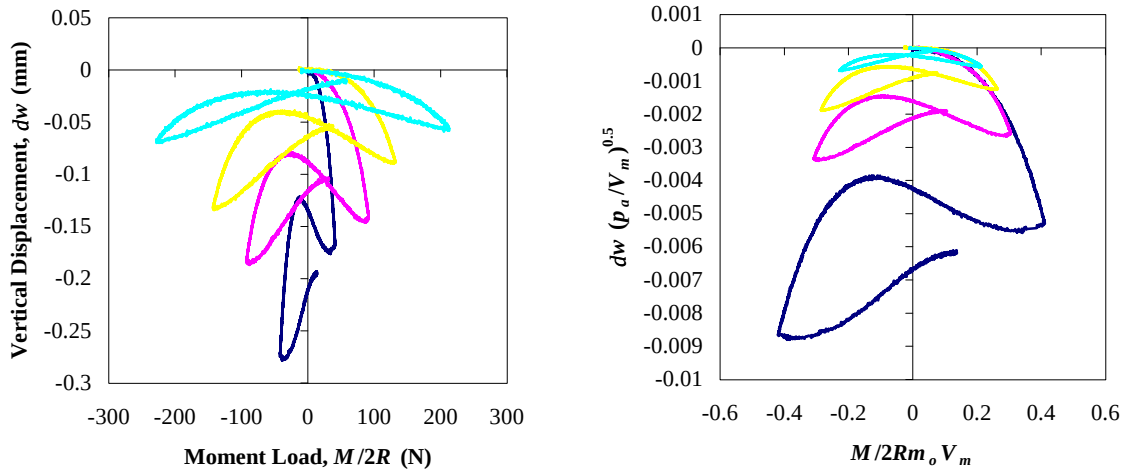

Figure 5.33 - Raw experimental results and normalised results for the vertical displacement during a moment rotation test at constant vertical load.

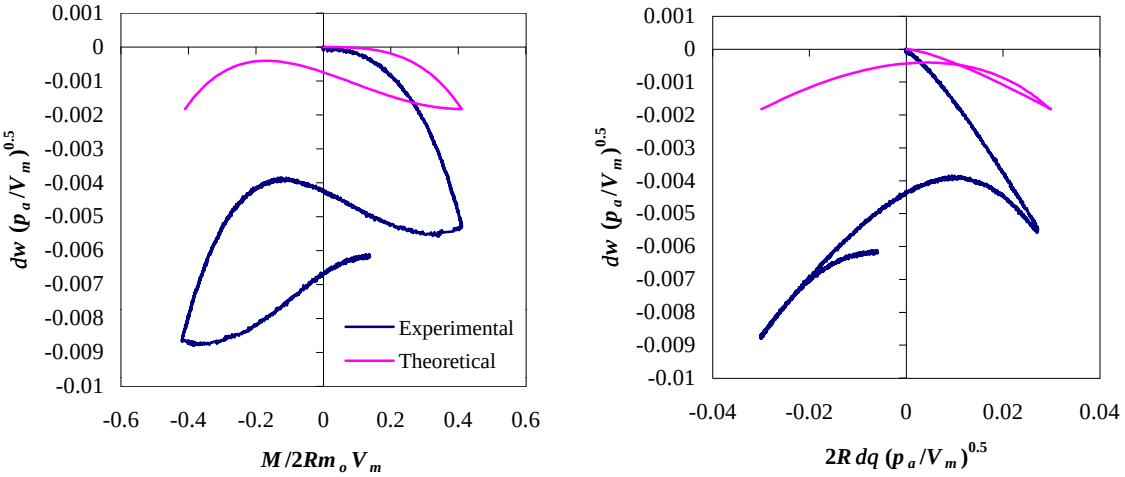

Figure 5.34 - The theoretical predictions of vertical movement from a hyperplasticity formulation of the footing problem compared to the observed experimental response.

APPENDIX A - COLLECTION OF PAPERS RELEVANT TO SUCTION CAISSONS

Aas, P.M. and Andersen, K.H. (1992). Skirted foundations for offshore structures. *Proceedings of the 9th Offshore South East Asia Conference*, Singapore.

Alhayari, S. (1998). Innovative developments in suction pile technology. *Offshore Technology Conference*, Houston, Texas. Paper 8836.

Andreasson, B., Christophersen, H.P. and Kvalstad, T.J. (1988). Field model tests and analyses of suction installed long skirted foundations. *Proceedings of the International Conference on the Behaviour of Offshore Structures*, BOSS 88. Trondheim, Norway.

Barbour, R.J. and Erbrich, C.T. (1995). Analysis of soil-skirt interaction during installation of bucket foundations using ABAQUS. *Proceedings of the International ABAQUS Users Conference*, Paris, France.

Bransby, M.F. and Randolph, M.F. (1997). Finite element modelling of skirted strip footings subject to combined loading, *Proc. 7th International Offshore and Polar Engineering Conference*, ISOPE-97, Honolulu, Hawaii, **2**, pp. 791-796. ISOPE.

Bransby, M.F. and Randolph, M.F. (1997). Shallow foundations subject to combined loadings, *Proc. 9th International Conference of the International Association for Computer Methods and Advances in Geomechanics*, Wuhan, China, **3**, pp. 1947-1952.

Burgess, I.W. and Hird, C.C. (1983). Stability of installation of marine caisson anchors in clay. *Canadian Geotechnical Journal* **20**, pp. 385-393.

Chimisso, C., Tagher, H., Biss, N.C., and Stani, G. (1998). Deepwater FPSO for Aquila field development in the Adriatic. *Offshore Technology Conference*, Houston, Texas. Paper 8808.

Christensen, N.H. and Haahr, F. (1992). A computer program to analyse suction effects. *Offshore Technology Conference*, Houston, Texas. Paper 6845.

Christophersen, H.P., Bysveen, S. and Stove, O.J. (1992). Innovative foundation systems selected for the Snorre field development. *Proceedings of the International Conference on the Behaviour of Offshore Structures*, BOSS 92. London, United Kingdom.

Colliat, J.L., Boisard, P., Andersen, K.H., and Schroeder, K. (1995). Caisson foundations as alternative anchors for permanent mooring of a process barge offshore Congo. *Offshore Technology Conference*, Houston, Texas. Paper 7797.

Colliat, J.L., Boisard, P., Gramet, J.C. and Sparrevik, P. (1996). Design and installation of suction anchor piles at a soft clay site in the Gulf of Guinea. *Offshore Technology Conference*, Houston, Texas. Paper 8150.

Colliat, J.L., Boisard, P., Gramet, J.C. and Sparrevik, P. (1997). Geotechnical design and installation behaviour of suction anchor piles - comparison with drag anchors. *Proceedings of the International Conference on the Behaviour of Offshore Structures*, BOSS 97. Delft, Netherlands.

Cuckson, J. (1981). The suction pile finds its place. *Offshore Engineer*. April, pp. 80-81.

Eide, A., Tuen, K.A., and Baerheim, M. (1996). The YME jack-up with skirt foundation. *Offshore Technology Conference*, Houston, Texas. Paper 8158.

El-Gharbawy, S.L. and Olsen, R. (1998). Laboratory modelling of suction caisson foundations. *Proceedings of the International Offshore and Polar Engineering Conference* **1**, pp. 537-542.

El-Gharbawy, S.L., Iskander, M.G. and Olsen, R. (1997). Application of suction caisson foundations in the Gulf of Mexico. *Offshore Technology Conference*, Houston, Texas. Paper 8832.

Erbrich, C. (1994). Modelling of a novel fondation for offshore structures. *Proc. 9th UK ABAQUS Users Conference*, London.

Erbrich, C. (1996). Bucket Foundations. Australian Centre for Geomechanics Newsletter, Perth, Australia.

Fines, S., Stove, O.V. and Guldberg, F. (1991). Snorre TLP tethers and foundation. *Offshore Technology Conference*, Houston, Texas. Paper 6623.

Hagen, D., Andenaes, E. and Korstad, G.M. (1998). Innovative suction anchor design and installation. *Offshore Technology Conference*, Houston, Texas. Paper 8833.

Hjortnes-Pedersen, A.G.I. and Bezuijen, A. (1992). Offshore skirt penetration in clay in the geo-centrifuge. *Proceedings of the International Conference on the Behaviour of Offshore Structures*, BOSS 92. London, United Kingdom.

Hogervorst, J.R. (1980). Field trials with large diameter suction piles. *Offshore Technology Conference*, Houston, Texas. Paper 3817.

Hu, Y. and Randolph, M.F. (1998). H-adaptive FE analysis of bearing capacity of skirted foundations, *8th International Offshore and Polar Engineering Conference*, Colorado, USA, International Society of Offshore and Polar Engineers (ISOPE), **1**, pp. 549-556.

Jones, W.C., Iskander, M.G., Olsen, R.E. and Goldberg, A.D. (1994). Axial capacity of suction piles in sand. *Proceedings of the International Conference on the Behaviour of Offshore Structures*, BOSS 94. Massuchusetts Institute of Technology, Cambridge, USA.

Jonsrud, R. and Finnesand, G. (1992). Instrumentation for monitoring the installation and performance of the concrete foundation templates for the Snorre tension leg platform. *Proceedings of the International Conference on the Behaviour of Offshore Structures*, BOSS 92. London, United Kingdom.

Karal, K., Hermstad, J., Nedrebo, O. and Keaveny, J.M. (1993). Concrete anchors for offshore mooring systems. *Proceedings of the 3rd International Offshore and Polar Engineering Conference*, Singapore.

Keaveny, J.M., Hansen, S.B., Madshus, C. and Dyvik, R. (1994). Horizontal capacity of large-scale model anchors. *Proceedings of the 8th International Conference on Soil Mechanics and Foundation Engineering*, New Delhi, India.

Larsen, P. (1989). Suction anchors as an anchoring system for floating offshore constructions. *Offshore Technology Conference*, Houston, Texas. Paper 6029.

Mitcha, J.L., Morrison, C.E. and de Oliviera, J.G. (1996). The Heidrun field - development overview. *Offshore Technology Conference*, Houston, Texas. Paper 8084.

Morrison, M.J., Clukey, E.C. and Garnier, J. (1994). Behaviour of suction caissons under static uplift loading. *Proceedings of the International Conference on Centrifuge*, Singapore.

Myrvoll, F. (1992). Instrumentation of the skirt piled Gullfaks C gravity platform for performance monitoring. *Proceedings of the International Conference on the Behaviour of Offshore Structures*, BOSS 92. London, United Kingdom.

Olberg, T.S., Guttormsen, T., Molland, G. and Andersen, J. (1997). Full scale field trial of taut leg mooring using fibre rope and suction anchor attached to a semi-submersible drilling unit. *Offshore Technology Conference*, Houston, Texas. Paper 8357.

Olberg, T.S., Guttormsen, T., Molland, G. and Andersen, J. (1997). Field trial for taut leg moorings. *Journal of Offshore Technology* **5**, N^{o} 2, pp. 35-37.

Randolph, M.F., O'Neill, M.P., Stewart, D.P. and Erbrich, C.T. (1998). Performance of suction anchors in fine-grained calcareous soils, *Offshore Technology Conference*, Houston, Texas. Paper 8831.

Rao, N.S., Ravi, R. and Prasad, B.S. (1997). Pullout behaviour of suction anchors in soft marine clays. *Marine Georesources and Geotechnology* **15**, N^{o} 2, pp. 95-114.

Rao, S.N., Ravi, R. and Ganapathy, C. (1997). Behaviour of suction anchors in marine clays under TLP loading. *Proceedings of the International Conference on Offshore Mechanics and Arctic Engineering*, Vol 1, pp 151-155.

Rao, S.N., Ravi, R. and Ganapathy, C. (1997). Pullout behaviour of model suction anchors in soft marine clays. *Proceedings of the International Offshore and Polar Engineering Conference*, Vol 1, pp 740-744.

Renzi, R. and Maggioni, W. (1994). Modelling the behaviour of skirt piles. *Proceedings of the International Conference on the Behaviour of Offshore Structures*, BOSS 94. Massuchusetts Institute of Technology, Cambridge, USA.

Rusaas, P., Giske, S.R., Aas-Jakobsen, A., Barrett, G., Christiansen, P.E., and Baerheim, M. (1995). Design, Operations Planning and experience from the marine operations for the Europipe jacket with bucket foundations. *Offshore Technology Conference*, Houston, Texas. Paper 7794.

Solhjell, E., Sparrevik, P., Haldorsen, K., and Karlsen, V. (1998). Comparison and back-calculation of penetration resistance from suction anchor installation in soft to stiff clay at the Njord and Visund

fields in the North Sea. *Proceedings of the International Conference on Offshore Site Investigation and Foundation Behaviour - New Frontiers*, London, United Kingdom.

Sparrevik, P. (1998). Suction anchors - a versatile foundation concept finding its place in the offshore market. *Proceedings of the International Conference on Offshore Mechanics and Arctic Engineering*.

Stϕve, O.J., Bysveen, S. and Christopherson, H.P. (1992). New Foundation Systems for the Snorre Development. *Offshore Technology Conference*, Houston, Texas. Paper 6882.

Steensen-Bach, J.O. (1992). Recent model tests with suction piles in clay and sand. *Offshore Technology Conference*, Houston, Texas. Paper 6844.

Svano, G., Eiksund, G., Kavli, A., Lango, H., Karunakaran, D. and Tjelta, T.I. (1997). Soil-structure interaction of the Draupner E bucket foundation during storm conditions. *Proceedings of the International Conference on the Behaviour of Offshore Structures*, BOSS 97. Delft, Netherlands.

Tjelta, T.I., Janbu, N. and Grande, L. (1992). Observations on drainage control on Gullfaks C gravity structure. *Proceedings of the International Conference on the Behaviour of Offshore Structures*, BOSS 92. London, United Kingdom.

Tjelta, T.I., Skotheim, A.A. and Svano, G. (1988). Foundation design for deepwater gravity base structure with long skirts on soft soils. *Proceedings of the International Conference on the Behaviour of Offshore Structures*, BOSS 88. Trondheim, Norway.

Wang, M.C. and Demars, K.R. (1978). Applications of suction anchors in offshore technology. Offshore Technology Conference, Houston, Texas. Paper 3203.

Wang, M.C., Demars, K.R. and Nacci, V.A. (1977). Breakout capacity of model suction anchors in soil. *Canadian Geotechnical Journal* **14**, pp. 246-257.

Watson, P.G. and Randolph, M.F. (1997). A yield envelope design approach for caisson foundations in calcareous sediments, *Proc. 8th International Conference on the Behaviour of Offshore Structures*, Delft, The Netherlands **2**, pp. 259-272, Elsevier Science, Amsterdam.

Watson, P.G. and Randolph, M.F. (1997). *V*ertical capacity of caisson foundations in calcareous sediments, *Proc. 7th Int. Offshore and Polar Engineering Conference* ISOPE-97, Honolulu, Hawaii, **II**, pp. 784-790, International Society of Offshore and Polar Engineers.

Watson, P.G. and Randolph, M.F. (1998). Failure envelopes for caisson foundations in calcareous sediments, *Applied Ocean Research* **20**, pp. 83-94.

Whittle, A.J., Germaine, J.T. and Cauble, D.F. (1998). Behaviour of miniature suction caissons in clay. *Proceedings of the International Conference on Offshore Site Investigation and Foundation Behaviour - New Frontiers*, London, United Kingdom.

Zdravkovic, L., Potts, D.M., and Jardine, R.J. (1998). Pull-out behaviour of bucket foundations in soft clay. *Proceedings of the International Conference on Offshore Site Investigation and Foundation Behaviour - New Frontiers*, London, United Kingdom.

APPENDIX B - DETERMINATION OF {*dw*:*du*:2*Rdq*) FROM THE SMALL LVDTS (TAKEN FROM MANGAL, 1999)

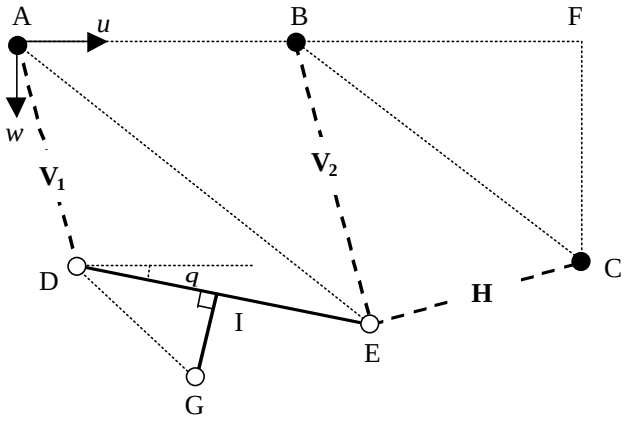

Key

A, B, C	Point fixed relative to speciment tank
D, E	Point moves with footing displacement
DE, IG	Length fixed
V_1, V_2, H	Length changes with footing displacement (LVDTs)
G	Displacement reference point on footing

Chapter 2 outlines the experimental techniques pursued during the investigation of the footing response. On the dense sand the footing displacements are very small, so it is not possible to obtain accurate estimates of the displacements using the long LVDT system. It is necessary to use a system of small LVDTs, bolted to the specimen tank, to measure accurately the footing deflections, relative to the tank. In the above diagram A, B and C are points which are fixed relative to the specimen tank, and to which the LVDTs (shown by V_1, V_2 and H) are attached. Points D and E represent the attachment of the LVDTs to the footing. Length IG represents the distance from the LVDT attachment point to the load reference point of the footing, taken to be at the centre of the base of the footing. As the footing moves the LVDTs change length accordingly. It is necessary to determine trigonometrically, the movements of G, with respect to the co-ordinate axes, from the change in lengths of the LVDTs. All fixed lengths (AB = 120mm, BF=135mm, FC = 99mm, DE = 120mm, IG = 43mm, DI = 60mm) are known from the geometry of the equipment and the co-ordinates of A, B and C are known (A is taken as the origin).

Point E

From triangle BCE:

$$\angle BCE = \cos^{-1}\left(\frac{(BC)^2 + (H)^2 - (V_2)^2}{2(BC)(H)}\right) \quad \text{B1}$$

This angle can be used to determine the co-ordinates of point E:

$$u_E = u_c - H\sin(\pi - \angle BCE - \angle BCF) \quad \text{B2a}$$

$$w_E = w_c + H\cos(\pi - \angle BCE - \angle BCF) \quad \text{B2b}$$

Point D

The length of AE can be found:

$$AE = \sqrt{u_E^2 + w_E^2} \quad \text{B3}$$

This can be used to find the angle of DAB which is equal to the sum of BAE and DAE:

$$\angle DAB = \cos^{-1}\left(\frac{(AB)^2 + (AE)^2 - (V_2)^2}{2(AB)(AE)}\right) + \cos^{-1}\left(\frac{(V_1)^2 + (AE)^2 - (DE)^2}{2(V_1)(AE)}\right) \quad \text{B4}$$

This angle is used to deduce the co-ordinates of point D:

$$u_D = (V_1)\cos(\angle DAB) \quad \text{B5a}$$

$$w_D = (V_1)\sin(\angle DAB) \quad \text{B5b}$$

Point G (the load reference point)

The footing rotation (q) is given by:

$$q = \tan^{-1}\left(\frac{w_E - w_D}{u_E - u_D}\right) \quad \text{B6}$$

Whilst the vertical and horizontal movements are given by:

$$u_G = u_D + (DG)\sin\left(\frac{p}{2} - \angle GDI - q\right) \quad \text{B7a}$$

$$w_G = w_D + (DG)\cos\left(\frac{p}{2} - \angle GDI - q\right) \quad \text{B7b}$$

These trigonometric manipulations are easily programmed into the computer control program so that the footing displacements are known as the tests proceed. The LVDT system was zeroed by ensuring that the footing was level (i.e. q = 0) and the vertical LVDTs (V_1 and V_2) were vertical. During the testing both processed and raw values were recorded for the footing displacements, so that data could be reprocessed if necessary.